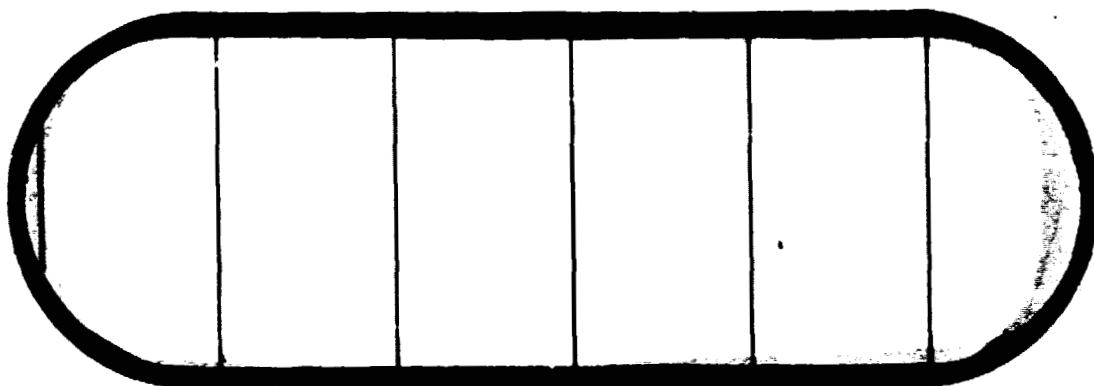


NASA CR-151993

BOEING



(NASA-CE-151993) GROUND EFFECTS AND CONTROL
EFFECTIVENESS TESTS OF A .095 SCALE FLOWRED
MODEL OF A MODIFIED T-39 LIFT/CRUISE FAN
V/STOL RESEARCH AIRPLANE (Boeing Aerospace
Co., Seattle, Wash.) 221 P HC A10/MF A01 N77-21084
Uncias G3/05 25384



CR 151993

THE **BOEING** COMPANY
CODE IDENT. NO. 81205

THIS DOCUMENT IS:

CONTROLLED BY

ALL REVISIONS TO THIS DOCUMENT SHALL BE APPROVED
BY THE ABOVE ORGANIZATION PRIOR TO RELEASE.

PREPARED UNDER

- CONTRACT NO.
 IR&D
 OTHER

DOCUMENT NO. D180-20391-1

MODEL AX-1355

TITLE GROUND EFFECTS AND CONTROL EFFECTIVENESS TESTS OF A .095
SCALE POWERED MODEL OF A MODIFIED T-39 LIFT/CRUISE FAN V/STOL
RESEARCH AIRPLANE

ORIGINAL RELEASE DATE 2 22 77

ISSUE NO. 10

ADDITIONAL LIMITATIONS IMPOSED ON THIS DOCUMENT
WILL BE FOUND ON A SEPARATE LIMITATIONS PAGE

PREPARED BY *C. R. Dawson*

(2-15-77)

SUPERVISED BY *C. R. Dawson*

APPROVED BY *M. E. Omar*

(2-15-77)

APPROVED BY *I. H. Rettie*

(2-21-77)

GROUND EFFECTS AND CONTROL EFFECTIVENESS
TESTS OF A .094 SCALE POWERED MODEL
OF A MODIFIED T-39 LIFT/CRUISE FAN
V/STOL RESEARCH AIRPLANE

BY C. Dawson and E. Omar

D180-20391-1

January 1977

THE BOEING AEROSPACE COMPANY
BOEING MILITARY AIRPLANE DEVELOPMENT
P. O. Box 3999
Seattle Washington 98124

FOREWORD

Presented herein are the results of wind tunnel tests of a .094 scale model of a modified T-39 Lift/Cruise Fan V/STOL research airplane. The tests were conducted by the Boeing Military Airplane Development organization of the Boeing Aerospace Company to define the general aerodynamic characteristics of the modified T-39 in ground effects and to determine the effectiveness of the ailerons, rudder and yaw control vanes. The model was powered by three 13.97 (5.5 inch) diameter tip driven turbopowered simulators. It was tested in four configurations, namely VTOL, STOL, CTOL and loiter. Test variables included: Thrust level, forward speed, model pitch and sideslip angle, and ground height. Static tests were conducted in the Boeing Static Checkout Facilities while forward speed tests were conducted in the Boeing 9' Lowspeed Wind Tunnel.

TABLE OF CONTENTS

	<u>PAGE</u>
SUMMARY	1
1.0 INTRODUCTION	4
2.0 NOMENCLATURE	6
3.0 TEST PROGRAM	8
3.1 Model Description	8
3.2 Test Facilities	15
3.3 Test Conditions and Procedures	17
3.4 Data Acquisition and Reduction	26
4.0 TEST RESULTS	29
4.1 VTOL Configuration in Ground Effect	30
4.1.1 Static Hover Characteristics	30
4.1.2 Effects of Forward Speed	34
4.1.3 Effect of Horizontal Tail	36

	PAGE
4.1.4 Effect of Engine Tilt Angle	37
4.1.5 Yaw Vane Control Effectiveness	38
4.2 STOL Configuration in Ground Effects	40
4.2.1 Effect of Angle of Attack	40
4.2.2 Effects of the Horizontal Tail	41
4.3 STOL Lateral and Directional Control Effectiveness	44
4.3.1 Aileron effectiveness	44
4.3.2 Rudder effectiveness	45
4.3.3 Vertical tail effectiveness	46
4.4 Configuration Characteristics with L/C Fan	48
Nacelles Removed	
4.4.1 Effect of horizontal tail	48
4.4.2 Effect of sideslip	49
5.0 CONCLUSIONS	50
6.0 REFERENCES	53

	PAGE
FIGURES	55
APPENDIX	101

Wind Tunnel Test Data

SUMMARY

Wind tunnel tests of a .094 scale powered model of a modified T-39 Lift/Cruise Fan V/STOL research airplane have been conducted. The tests were run concurrently with a similar test program completed under a NASA contract (Reference 1) using the model developed under that contract. The model was powered by three 14cm (5.5 inch) turbopowered simulators. It was tested primarily in two configurations: a VTOL configuration with flaps deployed, gear down, and lift/cruise fan nacelles tilted to 80°, 90° and 95°; and in an STOL configuration which differed from the VTOL configuration primarily in that the lift/cruise fans were tilted to 50°. Additional tests were conducted with the basic wing-body-tail combination (nacelles-off).

The tests were principally to determine the ground effects upon the VTOL and STOL configurations at forward speeds and to determine the effectiveness of the aerodynamic controls. Tests were conducted from zero forward speeds to 31 m/sec (50 knots) with the VTOL configuration and from 33 m/sec (65 knots) to 46 m/sec (90 knots) with the STOL configuration. Other test variables included model pitch, yaw, ground height and thrust.

The following characteristics of the VTOL configuration in ground effect were determined:

- Differential thrust (side-to-side), simulating roll control during hover produced induced rolling moments which opposed the thrust control power at model heights of 1.4 wing chords and above, and augmented the thrust control near the ground.
- The landing gear produced a 1% lift-loss.
- When the horizontal tail was set to zero degrees, a down load on the tail was produced. Removing the tail resulted in a 2% lift increase.
- The yaw vanes produced only 50% of the desired yawing moment during hover which remained constant up to 15.44 msec (30 knots) but diminished with increased speed at ground heights above 1.5 chords.

The STO configuration during ground roll conditions exhibited longitudinal stability which was degraded by height (up to four chord lengths). The lift at gear contact and at a height of four chords compared well with free air data but dropped off approximately 20% at a height of one chord. Horizontal tail

effectiveness was comparable with free-air data at a height of four chord lengths but was reduced 50% at gear contact.

When out of ground effect the STOL configuration ($\lambda = 50^\circ$) exhibited aileron effectiveness which produced adequate rolling moments for the desired angular acceleration. The rudder, however, did not produce an adequate yawing moment.

1.0 INTRODUCTION

Wind tunnel tests have been conducted using a .094 scale powered model of a modified T-39 V/STOL research airplane, which was designed to provide a technology base for a Navy type 'A' V/STOL airplane. The tests were primarily to determine ground effects and the effectiveness of the aerodynamic control surfaces.

STO lift-off speeds and hence the length of the takeoff ground roll are impacted by ground effects; also impacted is the stability during hover over a moving ship's deck. Control effectiveness is of particular interest for V/STOL development because of the diminishing dynamic pressure as the configuration utilizes more propulsive lift.

The tests were conducted concurrently with another program: NASA contract NAS2-9178, titled "Design and Fabrication of a Lift/Cruise Fan V/STOL Model for Wind Tunnel Tests", and used the model developed under that contract.

Static ground tests were conducted in the Boeing Static Checkout Facilities while tests at forward speeds were conducted in the Boeing 9' Low Speed Wind Tunnel.

Three 14CM (5.5 inch) turbopowered simulators were used to power the model which was tested primarily in two configurations:

- VTOL with flaps deployed, gear down, and engines tilted to 80°, 90° and 95°.
- STOL with flap & gear down and engines tilted to 50°.
- Loiter with flaps and gear up and L/C nacelles off.

Data acquired during the tests are included as an appendix to this report while the report itself focuses on data analysis. Results of the contract test program which was run concurrently are presented in Reference 1.

2.0 NOMENCLATURE

Capital letters are generally used for symbols to be compatible with the computer plotted results of the Appendix. The stability axis coefficients and ratios in the following list are related to aerodynamic forces and moments, where the direct thrust and ram forces and moments have been removed; a detailed description of the data reduction procedure is given in Reference 1.

A	aerodynamic (direct thrust and ram removed)
CLA	aerodynamic lift coefficient = LA/QS
CDA	aerodynamic drag coefficient = DA/QS
CPMA	aerodynamic pitching moment coefficient = PMA/QS
CSFA	aerodynamic side force coefficient = SFA/QS
CYMA	aerodynamic yawing moment coefficient = YMA/QS
CRMA	aerodynamic rolling moment coefficient = RMA/QS
LA/FGT	aerodynamic lift ratio
DA/FGT	aerodynamic drag ratio
PMA/FGTXC	aerodynamic pitching moment ratio
SFA/FGT	aerodynamic side force ratio
YMA/FGTXB	aerodynamic yawing moment ratio
RMA/FGTXB	aerodynamic rolling moment ratio
C	aerodynamic mean chord
CJ	thrust coefficient = FG/QS

D	drag, Newtons (pounds)
FGT	total gross thrust of all three propulsion units. FGA, FGB and FGC represent the gross thrust of each individual propulsion unit, Newtons (pounds)
HGT	height of model reference point above ground plane (see Figure 1), meters (inches)
HGT/C	model ground height-to-chord ratio
L	lift, Newtons (pounds)
PM	pitching moment, Newton meters (ft-lbs)
Q	wind tunnel test section dynamic pressure, Newton/meters ² (psf)
RM	rolling moments, Newton meters (ft-lbs)
S	wing reference area, meters ² (ft ²)
SF	side force, Newtons (pounds)
V/V	ratio of freestream velocity to fan efflux velocity
YM	yawing moment, Newton meters (ft-lbs)
α , ALPHA	angle of attack of body axis, degrees
β , BETA	angle of sideslip of body axis, degrees
λ , LAMDA	lift/cruise fan tilt angle relative to body axis
δA	aileron angle (positive: T/E up)
δ	horizontal tail angle (positive: L/E up)
δR	rudder angle (positive: left rudder, T/E to port)

3.0 TEST PROGRAM

3.1 Model Description

The .094 scale model represented a V/STOL technology demonstrator airplane based on a modified T-39 (Model 1041-135-2R of Reference 2). The modifications included:

- Expanding the forebody to house a lift fan
- Replacing the T-39 engine pods with tilting lift/cruise fan pods
- Raising the stabilizer to a T-tail position
- Replacing the gear with A-4 gear
- Adding a flap door to provide clearance for the lift/cruise fan efflux when the nacelles are tilted to the hover position.

A photograph, Figure 1, gives a general view of the model in VTOL configuration ($\lambda = 90^\circ$) mounted in the static test facility. Figure 2 shows the model in STOL configuration ($\lambda = 50^\circ$) mounted in the Propulsion Low Speed Wind Tunnel. The model was supported

on a six-component, strain-gauged "flow through" balance which is illustrated on Figure 3 and discussed in Reference 3.

Figure 4 shows the model in its various configurations and gives the principal dimensions. The top view depicts the CTOL configuration, with the nacelles at $\lambda = 0^\circ$ and the front fan doors open; the side view depicts a VTOL configuration, showing the nacelles at $\lambda = 90^\circ$. The flaps and flap doors are shown extended in the VTOL configuration.

Three "Technology Development Inc." 14 cm (5.5 inch) diameter tip driven fans were used to simulate the propulsion system. One of these units is shown, disassembled, in Figure 5 and a description is found in Reference 4. The units were furnished by NASA for this test program.

Each fan was rated at 35000 RPM with a design fan pressure ratio of 1.25. At this rating each had a fan airflow of 2.5 kg/sec (5.55 lbs/sec) and used .5 kg/sec (1.1 lbs/sec) of drive air. For the purpose of this test, they were operated up to a maximum of 30000 RPM. The drive air was supplied to the model at 41.4 bars (600 psig) and heated to 71°C (160°F) to prevent icing at the turbine exit. Remotely controlled valves and critical-

flow venturi meters located within the model were used to control and monitor the airflow to each individual fan (Figure 6).

The high pressure air supplied to the L/C nacelles was divided into two portions, one part for driving the fan and the other for simulating the primary exhaust efflux. Since both portions were always choked the simulated primary weight flow varied in direct proportion to the fan supply weight flow. The primary air was passed through a choke plate and screens, to obtain a uniform total pressure distribution and representative pressure ratio, before exhausting from the primary nozzles. Figure 7 shows details of the lift/cruise nacelle assembly. Each nacelle can be pre-set to various tilt positions, representing various flight configurations. A serrated interconnection allowed angular settings in increments of 5° . The limits of angular rotation were determined by instrumentation cables and tubes which were routed out of the nacelle around the periphery of this connection. This allowed rotation from $\lambda = 0^\circ$ (aligned with the model axis) to $\lambda = 105^\circ$, about a pivot point located at fuselage station 82.93 cm (32.65 inches) and water line 30.53 cm (12.02 inches).

The external lines of the nacelle were generated to represent those of the technology demonstrator having Allison PD 370-16

engines installed. The model scale was determined by the fan exit area; the scale factor (.094) being the square root of the ratio of model fan to full scale fan exit area. A more complete description of the design process is included in Appendix "B" of Reference 1, which describes how the inlet contours were chosen and gives details of the nacelle ordinates. The external cross-section of the core engine nozzle cowl was elliptical as indicated by the shading in Figure 7. This was done on the assumption that the engine accessories could be distributed between the top and bottom of the core engine.

Each nacelle was instrumented with total pressure rakes aft of the fans and near the exits of the core engine simulator as well as total temperature probes and static pressure orifices. The nacelles were also instrumented with inlet total pressure probes and static orifices. The locations of the pressure and temperature instrumentation are illustrated in Figure 7, and described in further detail in Reference 1.

Yaw vanes were located at the fan nozzle exit for thrust deflection and are shown in their undeflected position in Figure 7. The vane chord was 35.56 cm (14 in) full scale and its section was that of a NACA 0012 airfoil. The pivot point was at 10% of vane chord with the vane leading edge located at the fan

exhaust plane. Deflection angles of $\pm 10^\circ$, and $\pm 20^\circ$ were provided.

Fairings were used to cover the Lift/Cruise Fan nacelle pivots, instrumentation connections and air supply lines. These fairings were not completely representative of the full scale airplane. Part of each fairing was attached to, and rotated with, the nacelle and part was attached to the fuselage. These fairings are shown detailed in Figure 8. In order to determine the aerodynamic effect of the fairing attached to the nacelle, it was removed for one test and the leading edges of the nacelle fittings were faired with modelling clay as shown in Figure 8. Results of this comparison was reported in Reference 1.

Details of the nose fan installation are given in Figure 9. The nose fan was located as low in the fuselage as possible in order to allow length for development of the inlet contours. The fuselage forebody was hand-worked to provide the desired inlet shape. Sections of the inlet are presented in Appendix "B" of Reference 1.

The nose fan inlet doors, which when closed form the upper surface of the airplane nose, are shown diagrammatically on Figure 9 in the open and closed positions. When the doors were

in the open position, they were stowed at the sides of the fuselage as shown. Parts were provided to test both open and closed configurations.

The nose fan exit doors which, when open, could be deflected to provide thrust vectoring for yaw control are shown in the open position in Figure 9. The outboard doors opened towards the airplane plane of symmetry and the inboard doors opened from the plane outwards to form the projections shown. A disc was provided to fair and seal the exit when a "door-closed" configuration was tested.

The basic T-39 model airframe was defined in accordance with the Saberliner Specifications Document (Reference 5) with additional consideration of measurements taken from a full scale T-39. Wing and tail planforms and section definitions are presented in Figures 10 and 11. The model wing was positioned .38 cm (.15 inches) lower relative to the fuselage than full scale airplane definitions indicated. This had the effect of increasing the body depth in the vicinity of the wing and was done to provide more space within the model for structure and instrumentation. The wing dihedral was 3.15° . The wing was twisted linearly from zero incidence at the root to -2.9° at the construction tip. The tip of the vertical fin was modified to

support the horizontal stabilizer. A NACA-0010 airfoil section was used for the vertical fin. The airfoil section of the all new horizontal stabilizer varied linearly from a NACA-0010 airfoil at the tip to a NACA-0015 airfoil at the root. The stabilizer had an anhedral of 9°.

The basic high lift system (i.e., slats and flaps) were positioned in accordance with measurements of a full scale airplane in their fully deployed position. The slats and flaps were unchanged throughout the test with the exception of tests of the loiter configuration at which time the slats and flaps were nested. The flap doors, designed to provide clearance for the lift/cruise fan efflux, were deflected for tests of the hover configuration when λ was 90° or greater and retracted for all other tests. Details of the flap and slat geometry are shown on Figure 11.

The model was equipped with ailerons and rudder. The aileron hinge line of the T-39 is such as to provide aerodynamic balance as shown in Figure 11. The rudder hinge line was located at the center of its leading edge radius.

No transition grit was used on the model for any of the tests reported herein.

3.2 Test Facilities

- **Flight Simulation Chamber (FSC)**

Preliminary calibrations of the model fans were conducted in the Boeing Wind Tunnel Flight Simulation Chamber. The facility includes thrust and mass flow measuring systems and allows for variation of back pressure by means of evacuating the chamber into which the thrust simulator discharges. A schematic of the chamber is shown in Figure 12. A detailed description of the facility is presented in Reference 6.

- **Static Checkout Area**

All of the static hover tests were conducted in this facility. The primary use of this area is for checkout of models being prepared for tests in the Boeing Transonic Wind Tunnel. This facility is essentially a 8.5m X 12.2m by 4.0m high room (28 ft X 40 ft X 13 ft), as shown in Figure 13, equipped with a model support system providing for pitch and vertical translation of sting mounted models. The model is controlled from an adjacent control room with visibility provided by both a window and closed circuit television. Instrumentation outputs are carried to the Boeing Supersonic Wind Tunnel Data System by means of a permanent hardwired interconnect. Both on-line and final data reduction are accomplished by the wind tunnel central computing system. The model was installed in approximately the center of the room

with the model axis aligned with the longer (12.2m) room dimension. The room floor served as the ground plane.

- 9' X 9' Propulsion Low Speed Wind Tunnel-B

The wind tunnel testing was conducted in the Low Speed Wind Tunnel located at the Propulsion Laboratories' North Boeing Field Test Complex. The 9' X 9' LSWT-B is an open circuit wind tunnel which draws air directly from the atmosphere through a test section 2.591 meters (102 inches) high by 2.667 meters (105 inches) wide. A schematic of the tunnel is shown on Figure 14. The tunnel is powered by an Allison model 501-D13 gas turbine engine using a variable pitch propellor. Flow straighteners and screens are located in the tunnel inlet to minimize the effect that atmospheric wind conditions have on the tunnel flow profile. Tunnel velocities can be varied from 0 to approximately 180 knots. The tunnel is equipped with a sting support system mounted in the aft portion of the constant area section of tunnel. The motion of the support system is in the horizontal plane such that the model lateral axis was in the vertical plane as shown in Figure 2.

A ground plane was installed in the tunnel working section for VTO and STC testing which provided a surface with minimal boundary layer growth, and this boundary layer was minimized by

suction at a perforated surface upstream of the model location. Schematic details of the geometry of the ground plane and bleed system is shown on Figure 15. Views of the flow passages above and below the ground plane are presented in Figure 16.

The effects of the ground plane and its suction system upon the test section static pressure gradient were determined using the static probe shown in Figure 15. A description and results of the flow calibration are presented in Reference 7.

The 9' x 9' LSWT-B Data System was used for recording the data on magnetic disc. The Acquisition System is a software controlled, Boeing designed, Standard Digital Data System (SDDS). A PDP-8 computer is used for system control and on line "quick-look" data calculation with CRT output. A PDP-8/I is used for on/off-line final data calculation.

3.3 Test Conditions and Procedures

The model was tested in four basic configurations, which are defined as follows:

- VTOL with flaps deployed, gear down, and engines tilted to 80°, 90°, and 95°.

- STOL with flaps and gear down and engines tilted to 50°.
- Loiter with flaps and gear retracted and nacelles off.

The conditions under which each was wind tunnel tested are summarized in Figure 17. Test variables included lift/cruise fan tilt angle, forward speed, thrust, pitch and sideslip angle, stabilator angle as well as component effects. In addition, the VTOL configuration was tested statically. Test conditions for the static test included: effects of landing gear, horizontal tail, yaw vanes and the effect of differential thrust with the main gear doors on and off. Height of the model reference point above the ground was varied from .0025 meters (0.1 inch) to 1.83 meters (72 inches).

The model fans were supplied with high pressure air from a plenum inside the model. This plenum is essentially part of the internal balance and the pressure level in the plenum has some effect on the balance outputs. The balance plenum pressure was always set and maintained at a level of 41.4 bars (600 psig) for all tests, fan calibrations, and balance calibrations. This procedure is standard with this type of balance and ensures that the measured force levels are not influenced by balance pressure tares. Since the individual fan control valves are downstream of

this plenum there is still complete control of fan thrust without varying the balance plenum pressure.

The high pressure air used to drive the fans was pre-heated to eliminate icing problems. During the initial calibration it was determined by observation of the fans that the minimum supply air temperatures at which visible ice would not form was about 71°C (160°F) as measured in the balance plenum. This temperature was used for all further testing. In the colder environment of the open circuit wind tunnel, it was occasionally observed that under some conditions ice could be seen on the fan shroud between stator blades. This condition would only last for a few minutes then the ice would fall off.

Since warmed air was being carried across the internal balance it was necessary to establish procedures to minimize balance zero drift. During the static test it was found that by pre-warming the balance to about 54°C (130°F) prior to recording zeros, the problem of balance output drift was minimized. However, during the wind tunnel test, it was not possible to maintain the balance at this temperature during a run because the heat input from the warmed air was not adequate in the presence of the large heat transfer from the model to the tunnel stream. This resulted in greater thermal gradients and consequently

somewhat greater balance output drift than those occurring during the static tests.

A serious problem in measuring fan exit total and static pressures occurred during the static test: erratic readings were observed and were eventually traced to an accumulation of fan lubricating oil in the pressure measuring lines. This problem was apparently related to the large quantity of oil-mist which had to be supplied to the fan bearings. The oil-mist was blown into the bearing cavity and subsequently flowed out into the fan air-stream ahead of the pressure instrumentation.

Because of this problem, RPM rather than pressures was used to reduce the static data. For the wind tunnel data it was not considered adequate to rely on RPM in the presence of the substantial levels of fan flow distortion and back pressure variation expected during forward speed operation at large nacelle tilt angles. The pressure measuring problem was eliminated, for the wind tunnel tests, by replumbing the model to utilize external rather than internal pressure scanning valves. This allowed the use of an existing system which was designed to blow dry nitrogen from the pressure-scanner back through the pressure lines to remove any foreign matter. This was accomplished by using an automated system during the off-shift

which scavenged every pressure measuring line after each day's testing. The procedure was adequate to solve the problem, since some time was required to accumulate sufficient oil to affect measurements.

During both the static and wind tunnel tests, the fans were calibrated in place: in the static test facility the calibration consisted of positioning the complete model at about 1.8 meters (72 inches) above the floor and at an angle of pitch of 15° to minimize the ground effects within the constraints of the support system. Each fan was then run separately (lift cruise fans tilted to their 90° position) to determine the relationships between RPM and thrust as measured by the internal force balance. (Thrust was also computed from fan pressure instrumentation but due to the instrumentation difficulties mentioned above, this data was not utilized for the static test data reduction.) The fans were run at thrust levels up to about 400 Newton's (90 lbs).

In the wind tunnel similar calibrations were run, except that the fan efflux was directed outside the test section by means of a scavenging pipe. This prevented re-circulation of the fan-flow around the model and also avoided inducing a flow velocity through the wind tunnel by the ejector action of the fans. The pressure instrumentation difficulties of the static test had been

solved as mentioned previously, by utilizing the permanent tunnel scan-i-valve system, and the calibrations were used to relate the forces measured by the internal balance to those computed from the fan exit pressure instrumentation.

The above calibrations established the basis for determining thrust during actual tests. In addition, a variation of thrust coefficient with back pressure was included in the data reduction. This relationship had been established during the initial calibration of each fan in the Flight Simulation Chamber.

The calibrations are described in greater detail in Appendix B of Reference 1.

For static testing the model was initially positioned with the landing gear clear of the ground plane by about .25 cm (.1 inch). Each fan was set at a specified RPM value, selected to give the desired thrust level. The lift/cruise fans were generally set to give about 350 Newton's (79 lb) thrust each and the nose fan was set to give an approximate pitching moment trim about the moment reference center. This value was computed from geometric considerations and varied with nacelle tilt angle as shown in Figure 18. Certain runs were also made with the thrust intentionally unbalanced, either side to side or fore and aft.

The model was then traversed away from the floor with periodic stops for pressure stabilization and data recording. Constant angle of attack was held throughout a height traverse. Due to ground effects the thrust levels (especially of the nose fan) tended to change somewhat with height above the floor. No attempt was made to maintain the original thrust levels. The control parameter was tip turbine supply pressure which was maintained constant during height traverses.

During "ground effects" testing (in the 9' x 9' LSWT-B with the ground plane installed) the model support system was used in the translation mode. The model was translated from: wheels approximately 0.1 inch from the ground plane to 40 inches from the ground plane. Data was taken at fixed increments above the ground plane after translation was stopped to allow for pressure and temperature stabilization. Any attitude changes such as pitch or yaw was accomplished by pre-setting points in the sting support.

VTOL testing, in ground effect, was made at tunnel velocities of 15.443 m/sec (30K) and 30.886 m/sec (60K) to simulate heavy gusts while the STOL ground effects tests were made between 33.44 m/sec (65 KTS) to 61.77 m/sec (120 KTS). This resulted in thrust

coefficients as high as 22 for the VTOL configuration and as high as 5.5 for the STOL configuration during ground effects testing.

Before the tunnel was brought up to speed, the vacuum pump controlling ground-plane suction was activated and generally a suction of .5588 m (22") Hg was established in the tunnel exit manifold.

Tests conducted without the ground plane installed (i.e., out of ground effects) utilized the pitch mechanism which provided continuously variable model pitch angles from -8° to $+14^{\circ}$, while maintaining the model pitch center approximately in the center of the tunnel flow.

As with the ground effects tests, the desired variations in thrust coefficient (CJ) were obtained primarily by changing the tunnel speed at a constant fan thrust setting. The predominant thrust setting used corresponded to a fan pressure ratio of about 1.14. The tunnel speeds were in the range 33 to 62 m/sec (65-120 KTS) giving a CJ range of about 1.8 to 5.5 and corresponding to a Reynolds number range from .6 million to 1.2 million based on the model reference chord. However, partway through the test a model structural problem was discovered which required limiting the tunnel speed to about 46.33 m/sec (90 KTS) compared to the

previously selected maximum of 61.77 m/sec (120 KTS). Thereafter the lowest CJ value (CJ = 1.8) was run at a fan pressure ratio of about 1.10 while for all higher CJ values the $\lambda PR = 1.14$ setting was maintained.

The upper CJ limit of 5.5 was selected based on considerations of tunnel flow breakdown. While time did not permit a detailed study of that limitation, observations were made of tufts on the tunnel walls at several fixed angles of attack as CJ was gradually increased. These runs were made with the nacelle tilt angle set at 90° . It was observed that as CJ increased, the flow on the tunnel wall beneath and behind the model became increasingly rough. At $V = 33.46$ m/sec (65 KTS, CJ = 5.5) the region of rough flow had moved forward to a position under the model tail but there were no significant areas of reversed flow. However, when the speed was lowered to about 31 m/sec there were large areas under the model where the flow was actually reversed. This was interpreted as a "flow breakdown" situation representing a region where valid free air testing was not possible. In no case was the tunnel flow observed to "climb the sidewalls" as has been observed during similar tests on other models for flow breakdown situations. It is worth noting that the test limit determined by this method is in good agreement with a detailed study presented in Reference 8.

The thrust balance among the three fans was generally set to provide approximate trim about the moment reference center for the static case. No attempt was made to readjust the initial static supply pressure values to allow for thrust changes or aerodynamic moments resulting from forward speed.

In general, an angle of attack series was taken with angle increasing from -8° to $+30^{\circ}$. It was noted that some hystereses existed and that for certain configurations this effect was appreciable. This phenomenon was not explored in any detail and in general the data presented are all on the same side of the hystereses loop.

3.4 Data Acquisition and Reduction

The data acquired during the wind tunnel test program included:

- Model force and moment measurements (axial force, normal force, side force, and moments about the pitch, yaw and roll axis) from an internal, flow-thru, strain gauge balance.
- Balance temperature as well as the temperature and pressure within the balance plenum.

- Jet efflux total pressure, static pressure and total temperature.
- Pressure and temperature of the individual air supplies to power the three turbo-powered simulators.
- Fan inlet total and static pressures.
- Simulator RPM and bearing temperature. The bearing temperature was monitored but not recorded.
- Test section conditions including static and total pressure and total temperature.
- Model pitch and side-slip angles and ground height during wind tunnel tests; pitch and roll angle and ground height during static ground tests.

The data was reduced both directly (thrust components included) and also with the direct thrust components of forces and moments, and ram forces and moments subtracted. A full description of the method and equations used are given in Appendix 'C' of Reference 1. The forces and moments presented in

this report are the aerodynamic forces which include only the "induced" aerodynamic effect of the propulsion system.

Corrections were made for tunnel wall constraints based on Heyson's Interference Theory and this is also described in Appendix 'C' of Reference 1.

4.0 TEST RESULTS

The data presented in this section is in the form of summarized graphs comparing those forces and moments mostly influenced by the test configuration and which are pertinent to the discussion. The appendix includes all test data available, in the form of machine plots, these are listed at the front of the appendix and each figure includes an identification of the test conditions.

As mentioned in Section 3.4, the data presented in this report have had the direct thrust and ram forces removed. The resulting force coefficients are given the subscript "A" (e.g., CLA) meaning aerodynamic. The relationship of the aerodynamic forces to the total model forces is illustrated in Figure 19 for a forward speed case representing a typical V/STOL lift-off condition. It shows that the aerodynamic forces are small relative to the total model forces. The aerodynamic data therefore represents the difference between two large numbers (total force minus thrust and ram forces). This has an effect on the accuracy which can be achieved in the aerodynamic data.

In using the data to predict airplane performance, the "thrust-drag" bookkeeping system must be taken into account and it should be noted that there is a difference between the systems

used for static data compared to that used for wind tunnel data. In using the static data, the full scale thrust out of ground effect should be applied since the backpressure effect on thrust is already included in the data. However, in using the wind tunnel data, any effects of backpressure on the full scale fan performance must be taken into account in the propulsion data used, since the thrust removed from the wind tunnel data was based on actual measured backpressure.

Static data and low forward speed data (30.886 m/sec 60 kts and below) in ground effect are presented in the form of non-dimensionalized forces and moments, plotted against the height of the model reference point above the ground as a fraction of mean chord (HGT/C). The data was non-dimensionalized in terms of total gross thrust.

The data presented for cases out of ground effect are in the usual aerodynamic coefficient form (see nomenclature).

4.1 VTOL Configuration in Ground Effect

4.1.1 Static hover characteristics.

The characteristics of the basic VTOL configuration in the hover mode ($\lambda = 90^\circ$), at zero forward speed, are discussed in

detail in Reference 1. In summary, the significant findings reported in Reference 1 were that: with the model out of ground effect, a lift loss of approximately 2% occurred. This loss represented the difference between the lift with all three fans operating versus the sum of the lifts produced by the individual fans. As the model moved into ground effects at a level attitude, no further lift loss occurred and in fact, ground effect was found to be favorable as shown in Figure 20 for the basic model. As pitch angle was increased beyond 5° , a lift loss due to ground effect of 2% was found to occur. As the model was pitched nose down to -5° , a 7% lift increase occurred. The greatest lift loss measured during the static tests amounted to 5% and occurred at a combination of 10° of pitch and 10° of roll.

Further static ground tests were conducted to assess the effects of the landing gear in ground effect and the effects of thrust variations. The results of those tests are presented herein.

The location of the landing gear is shown on Figure 4, which indicates the proximity of the gear to the jet efflux in the VTOL mode. A test was completed to determine the effect of the landing gear on the induced aerodynamics during static VTOL operation.

Figure 20 presents plots of LA/F; DA/F and PMA/FXC versus non-dimensionalized height above the ground plane. Since there was no forward speed, the forces and moments are referred to total gross thrust of the fans. It is evident that small changes of these induced forces occurred when the landing gear was removed.

The effect of removing the gear on drag (longitudinal force) was to increase it (rearward force) by 1.5% to 2.5% of gross thrust over most of the ground height range for which data were obtained. A lift increase of approximately 1% occurred due to removal of the gear. It should be noted that repeat tests with the basic configuration: one made at the beginning of the series and one near the end did indicate a shift in the absolute level of measured lift of about 2% of thrust (Reference 1). Most of the test data presented in this section was obtained close to the latter test run which has been used for comparison. The gear off case was tested between the two repeatability tests, it is possible, therefore, that the difference between the curves CLA vs HGI/C for gear on and gear off could be greater by 2% of thrust - the basic case moving more negative by that amount.

The effect on pitching moment was to introduce a nose down moment when the gear was removed, but again, the effect was not significant.

The effects of applying differential thrust (reducing fan 'A' thrust to represent roll control) on the induced aerodynamics of the airplane at zero forward speed are shown on Figure 21. A slight increase in induced lift is apparent at HGT/C = 1.4 and 2.26 as fan 'A' thrust was reduced. There was a negligible effect on pitching moment (approximately 3% of control power), but induced rolling moment was adversely affected at these heights (20% of roll control power). Close to the ground the induced moments augmented the thrust moment.

The induced yawing moment (YMA/FXB) resulting from roll control by thrust indicates a significant coupling. The maximum side-to-side thrust variation available could produce yawing moments of up to 20% of the available yaw control power. Changes of side force were not significant however.

To determine how the main landing gear center doors influenced the VTOL induced aerodynamics, tests were conducted with the doors removed while fan 'A' thrust was varied. These results are also presented on Figure 21 (solid symbols), and show

that the doors produced a negative rolling moment ($\Delta CRMA = -.001$) at maximum thrust, combined with a small positive yawing moment ($\Delta CYMA = +.0007$).

To look at the effect of variations of total thrust, data was taken at various heights and at thrust levels of 73%; 86% and 100%. These results are presented on Figure 22 which shows that at $HGT/C = 7.2$, there was a negligible effect of changes in total thrust. At the two lower heights ground effect did have some influence but the variations in induced lift, drag and pitching moment with total thrust were small.

4.1.2 Effects of Forward Speed

Variations of asymmetric thrust were also tested at forward speeds of 30.886 m/sec (60 knots) and 15.443 m/sec (30 knots). Fan 'B' was varied at $\beta = 0^\circ$ and the effect on lift, drag and pitching moment is shown on Figure 23. The data indicates some change in induced pitching moment only (at 30.886 m/sec (60 knots)). The induced lift increased slightly as was the case during the static tests. Changes in induced lift and drag due to asymmetric thrust at 15.443 m/sec (30 knots) were negligible.

A similar test was conducted at $\beta = 10^\circ$; the rolling moment variations with differential thrust are compared for $V = 30.886$

m/sec (60 knots) at $\beta = 0^\circ$ & 10° on Figure 24(a) and the yawing moment variations are compared on Figure 24(b). When $\beta = 0^\circ$ the effect of reducing fan 'B' thrust on induced rolling moment was negligible except at heights below 1.5C (Figure 24(a)) where an induced opposing moment of up to 23% of the estimated available rolling moment occurs. The thrust variation had little effect on yawing moment, Figure 24(b).

At $\beta = 10^\circ$ it was again at heights below 1.5C that the induced effect was most significant. Applying negative roll by reducing fan '2' thrust at HGT/C = 1.0 resulted in an induced positive rolling moment equivalent to 16% of the available roll power. Reducing fan 'A' thrust also gave an opposing induced moment equivalent to 27% of the roll capability. When HGT/C = 4.0 the maximum induced unfavorable rolling moment was equivalent to 16% of that available.

The effect on yawing moment is favorable in that the reduction of thrust of fan 'A' or 'B' tends to restore some of the yaw stability as the model approaches the ground. At heights above 2.0C the effect was not significant.

Side force changes due to differential thrust were negligible at 30.886 m/sec (60 KTS).

Data taken at 15.443 m/sec (30 KTS);, $\beta = 10^\circ$ was questionable due to large balance zero shifts, and because visual observations indicated a possibility of tunnel flow breakdown at this speed. The data is included in the appendix.

4.1.3 Effect of Horizontal Tail

The effect of the horizontal tail was investigated in the VTOL mode with no forward speed. The model was tested with horizontal tail settings: $\Delta = 0^\circ$ and -19° and also with the horizontal tail removed. The results shown on Figure 25 indicate small changes in the induced effects of lift, drag and pitching moment. As the model was translated from ground contact an increase in induced lift occurred which reached a maximum of 3% gross thrust above the ground contact value at a height/chord = 2.5 for the deflected tail condition ($\Delta = -19^\circ$), but as the height increased further, lift equalized for all three conditions before HGT/C = 4.0, finally settling out with an induced lift loss equal to 2% of total gross thrust. Neither drag or pitching moment showed dramatic changes.

At 15.443 m/sec (30 knots) and 30.886 m/sec (60 knots), the VTOL configuration was tested with the horizontal tail on at zero degrees deflection and tail-off. At 30.886 m/sec (60 knots)

these cases were tested at model angles of attack of 0° and 5° , and at 15.443 m/sec (30 knots) they were tested at $\alpha = 5^\circ$.

Figure 26 shows that at 15.443 m/sec (30 knots) a large induced lift occurred as the airplane moved away from the ground reaching 12.5% of total thrust when $HGT/C = 1.8$, but this collapsed rapidly until at $HGT/C = 2.75$ the aerodynamic lift was only 2.5%. The tail effect was insignificant at this tunnel speed.

At 30.866 m/sec (60 knots); (Figure 27) the aerodynamic lift did not show abrupt changes as occurred at 15.443 m/sec (30 knots), the lift increased steadily until $HGT/C = 2.75$ where it reached a maximum. With the horizontal tail off the maximum aerodynamic lift amounted to 17% of the gross thrust; when the tail was fitted ($\delta = 0^\circ$) a reduction of lift occurred amounting to 3% of gross thrust. This indicated a down load on the tail which is also indicated by the positive increase in pitching moment (Figure 27(b)). When the model angle of attack was set to 5° , the lift curves and pitching moment curves were similar, indicating approximately 5° downwash at the tail.

4.1.4 Effect of Engine Tilt Angle

Engine tilt angles of 60°, 90°, 95° were tested at both 15.443 m/sec (30 knots) and 30.883 m/sec (60 knots) with the horizontal tail off. These results are summarized in Figures 28 (15.443 m/sec (30 knots)) and 29 (30.886 m/sec (60 knots)). A reduction in lift was found to occur when the tilt angle was changed from 90° to 95°. This probably resulted from the fan efflux impinging on the wing and flap system at $\lambda = 95^\circ$. Associated with the lift reduction was a general reduction in drag for $\lambda = 95^\circ$ and more positive pitching moment. A unique feature of lift in ground effects at a forward speed of 15.443 m/sec (30 KTS) is the large induced lift at one and a half chord heights. This characteristic persisted at $\lambda = 95^\circ$ but did not occur at $\lambda = 80^\circ$.

4.1.5 Yaw Vane Control Effectiveness

Yaw control in the VTOL configuration at low forward speed is achieved by yaw vanes mounted in the fan exhaust stream of the lift/cruise fans (A & B) and by varying the angle of the lift fan (C) exit doors. These devices are shown fitted in the undeflected position on Figures 7 and 9.

A comparison is made at zero forward speed on Figure 30 between cases with the yaw vanes undeflected and when deflected by 20°. At the higher ground heights the yaw vanes produced

yawing moments amounting to only half the desired value, that being $\Delta YMA/FX_3 = -.028$. An associated lift loss of 4% occurred at ground heights of 3 model chords due to yaw vane deflection. A similar comparison is made on Figure 31 at forward speeds of 15.443 m/sec (30 knots) and 30.886 m/sec (60 knots); which shows that at 15.443 m/sec (30 knots) the yaw vane effectiveness is similar to the static case, but as the velocity increased to 30.886 m/sec (60 knots), degradation of the yaw vane effectiveness occurred above heights of $HGT/C = 1.5$.

4.2 STOI Configuration in Ground Effect

4.2.1 Effect of Angle of Attack

Figure 32 presents the angle of attack effect on lift, drag and pitching moment at $CJ = 5.5$ (typical at STO lift-off speed) with the horizontal tail at zero degrees. Cross plots of the lift, drag and pitching moment at ground heights relating to gear contact, one and four model chords are compared with free air data in Figure 33. The lift at gear contact and at a height of four model chords compares well with the free air data. The lift drops off rapidly as the model was moved away from the ground plane reaching a minimum at a height of one model chord. The lift loss represents approximately a 3% loss in the total aerodynamic plus propulsion lift at typical lift-off conditions. The drag which was similar to free-air levels at lift-off conditions reduced significantly at heights from gear contact to four chord lengths as angle of attack decreased.

Although the lift change with increased ground height was small at $\alpha = 0^\circ$, a significant change in pitching moment occurred ($\Delta CPMA = -0.49$) between gear contact and 1.05 model chords. The effect of ground height on pitching moment at 8° and 14° angle of attack was smaller than at $\alpha = 0^\circ$ but showed similar trends. The curves of CPMA versus α in Figure 33 show that the configuration

has longitudinal stability during the ground roll with a gradual degradation of stability with ground height.

4.2.2 Effects of the Horizontal Tail

The effects of the horizontal tail upon the lift, drag and pitching moments of the STOL configuration in ground effect are presented in Figures 34, 35 and 36 for thrust coefficients of 5.5 (33.46 m/sec (65 knots)), 3.7 (41.18 m/sec (80 knots)) and 1.8 (46.33 n/sec (90 knots)). The results indicate, as shown earlier for the VTOL case, that the effect of the horizontal tail at $\Delta = 0^\circ$ was to reduce the lift and provide a nose-up change in pitching moment. The largest lift loss ($\Delta CL_A = 0.2$) occurred at the highest thrust value as did the smallest amount of pitch-up.

The horizontal tail effectiveness for the STOL configuration was investigated at airplane angles of attack of 8° and 14° for CJ values of 1.8, 3.7 and 5.5. Figure 37 compares tail setting angles of $s = 0^\circ$ and $s = 10^\circ$ for the three CJ values. The aerodynamic pitching moment is plotted versus height of the airplane reference point above the ground plane (CPMA vs HGT/C). It can be seen that at $CJ = 5.5$ and $\alpha = 8^\circ$, a significant negative pitching moment change occurred when $\Delta = 10^\circ$ compared to $\Delta = 0^\circ$: at $HGT/C = 4.0 \Delta CPMA = -.34$. At $\alpha = 14^\circ$, however, a slight positive change in pitching moment occurred.

Large variations in pitching moment are indicated as the model moved away from the ground plane, first increasing negatively (nose-down) then positively (nose-up). The tail off case shows similar changes suggesting that it is a wing/body effect rather than a phenomenon associated with the horizontal tail.

At $CJ = 3.7$, a similar trend occurred but the incremental changes for $\alpha = 14^\circ$ were smaller, then as CJ decreased further to $CJ = 1.8$, changes in the trend are apparent: at $\alpha = 8^\circ$, $\Delta = 0^\circ$, an increase in negative pitching moment is shown until $HGT/C = 1.5$ where $CPMA = -0.8$; as the model moved further from the ground plane a relatively small decrease in negative pitching moment is indicated. At $\alpha = 8^\circ$, $\Delta = 10^\circ$ the tail contribution was $\Delta CPMA = -.2$ giving $CPMA = -1.0$ when the model height/chord ratio was 1.5 which then remained virtually constant as the model height increased to 4.26. The tail effectiveness was less at $\alpha = 14^\circ$ and the tail contribution to pitching moment decreased to zero when $HGT/C = 4.5$.

The effect of thrust on horizontal tail effectiveness is summarized on Figure 38, which compares the free air data with ground effect data. This shows that at $\alpha = 8^\circ$ and a model height/chord ratio of approximately 4.0, the tail control

effectiveness was similar to free-air data but when the model height was reduced to "gear contact" the tail effectiveness was reduced by 50%. At $\alpha = 14^\circ$, the tail control effectiveness was virtually zero.

4.3 STOL Lateral and Directional Control Effectiveness

Out of Ground Effect

4.3.1 Aileron Effectiveness

Two aileron deflections: $\delta A = 15^\circ$ and 25° , were tested on the STOL configuration ($\lambda = 50^\circ$: gear, flaps and slats deployed; $A = 10^\circ$) at a tunnel velocity of 41.18 m/sec (80 knots); and CJT = 3.64. In both cases, they were deflected through equal angles with the portside aileron deflected down and the starboard side aileron up, to give positive rolling moment.

The aileron effectiveness is summarized by Figure 39, which compares the rolling moment coefficient of the three conditions: $\delta A = 0^\circ$, 15° and 25° . The data at $\delta A = 0^\circ$ indicates the model has a residual rolling moment of about -.012 over most of the angle of attack range. The data at $\delta A = 15^\circ$ is questionable because of a large balance zero shift on rolling moment which occurred during the run. The data at $\delta A = 0^\circ$ & 25° did not have a significant zero shift. Also plotted on Figure 39, is the variation of rolling moment with speed for the 25° aileron deflection which shows the speed, above which augmentation from the propulsion system is not required is 46.84 m/sec (91 KTS). The rolling moments were not significantly affected by increasing

angle of attack except near CLMAX. It appears that the right wing consistently stalls before the left.

The value of the rolling moment achieved was less than would be predicted by using plain flap effectiveness for this NACA section.

4.3.2 Rudder Effectiveness

The STOL configuration ($\lambda = 50^\circ$, flaps, slats and gear deployed) with horizontal tail $\Delta = 10^\circ$, was tested at 41.18 m/sec (80 kncts); with CJ = 3.7 to determine the effectiveness of the rudder. Three runs were made: a basic condition ($\beta = 0^\circ$; $\delta R = 0^\circ$); then $\beta = 10^\circ$, $\delta R = 0^\circ$; and $\beta = 10^\circ$, $\delta R = 15^\circ$. These results are summarized on Figure 40 which presents the airplane aerodynamic moment coefficients versus angle of attack.

The effect of sideslip was directionally destabilizing for this configuration, particularly at low angles of attack; at $\alpha = 0^\circ$ $\Delta CYMA = -.022$ for an application of $\beta = 10^\circ$. The destabilizing effect reduced as angle of attack increased and the configuration became neutrally stable at $\alpha = 9^\circ$; further increase in angle of attack produced stabilizing yawing moments.

The effect of sideslip on rolling moment was favorable producing $\Delta CRMA = -.068$ at $\alpha = 8^\circ$.

A positive change in pitching moment resulted from positive sideslip at low angles of attack; ($\Delta CPMA = +.25$ at $\alpha = 0^\circ$), but the effect reduced as angle of attack increased, reaching a negligible amount at $\alpha = 10^\circ$.

With the application of rudder: $\delta R = -15^\circ$ (trailing edge to starboard) a small positive change in yawing moment can be seen at positive angle of attack reaching a maximum $\Delta CYMA = +.008$. Rolling moment was pushed further negative ($\Delta CRMA = -.02$ for $\delta R = -15^\circ$ at $\alpha = 0^\circ$) and pitching moment increased further in a positive direction ($\Delta CPMA = .015$). The required yawing moment of 27341 Nm (20,166 lbs/ft) to achieve a desired angular acceleration of 0.2 radians/sec², would be developed at 113.76 m/sec (221 knots) using the rudder effect shown. It should be noted that the rudder effectiveness may well have been diminished by the non-representative nacelle fairings discussed in Section 3.1.

4.3.3 Vertical Tail Effectiveness

The yawing moment and rolling moment characteristics versus angle of attack for vertical tail-on and vertical tail-off are

shown in Figure 41 (when the vertical tail was on, the horizontal tail was also fitted at $\Delta = 10^\circ$). A restoring yawing moment was produced by the tail of approximately $\Delta CYMA = .007$ in the range of $\alpha = 0$ to 10° , whereas a change in yawing moment coefficient based on the tail alone, at a control surface angle of attack of 10° , is calculated at approximately .05.

Oil-flow visualization of the STOL configuration indicated that the large region of separated flow behind the nacelles produced vortices which swept a significant portion of the vertical tail (Figure 42) making it largely ineffective. The non-representative fairings attached to the nacelle were a major factor in the poor flow quality in this region.

4.4 Configuration Characteristics with L/C Fan Nacelles Removed

4.4.1 Effect of Horizontal Tail

The basic wing-body-tail configuration (flaps, slats and gear stowed, lift-fan doors closed) was tested at (61.77 m/sec (120 knots)); with two horizontal tail settings; $\Delta = 0^\circ$ and $+10^\circ$. The tail contribution to lift can be seen on Figure 43; at $\alpha = 0^\circ$ the increment of lift due to the tail ($\Delta = 10^\circ$) was $\Delta CLA = .12$; this represented a change in $CL(tail) = 0.988$ which agreed closely with the theoretical value based on a NACA 0012 airfoil. The horizontal tail had a tip contour of NACA 0010 and root contour of NACA 0015 (Figure 10).

The tail lift (at $\Delta = 10^\circ$) produced a nose down pitching moment equivalent to $\Delta CPMA = -.225$ which was consistent with a calculated value based on the horizontal tail moment arm.

As the airplane angle of attack was increased, the horizontal tail lift increment ($\Delta = 10^\circ$) remained virtually constant until $\alpha = 7^\circ$ after which the tail became progressively more ineffective as angle of attack increased apparently due to the tail stalling. At CL_{MAX} there was practically no effect of tail angle between $\Delta = 0^\circ + 10^\circ$.

A comparison of the horizontal tail off condition and $\beta = 0^\circ$ (Figure 41) indicates that the tail was stabilizing up to CLMAX.

The effect of the horizontal tail angle on other airplane aerodynamic components was not significant.

4.4.2 Effect of Sideslip

The basic configuration with nacelles removed was tested for the effect of sideslip with the horizontal tail set to $\delta = +10^\circ$. Figure 44 compares $\beta = 0^\circ$ with $\beta = 10^\circ$ and shows the effect of angle of attack on CYMA. A stabilizing yawing moment resulted when positive sideslip was applied and the value $\Delta CYMA = 0.13$ remained fairly constant over the range of angle of attack up to CLMAX. Rolling moment was also stabilizing as angle of attack increased, Figure 44 indicates an increasing negative value of CRMA with angle of attack for $\beta = 10^\circ$ from CRMA = -.003 ($\alpha = 0^\circ$) to CRMA = -.024 ($\alpha = 16^\circ$).

A slight nose down pitching moment ($\Delta CPMA = -.05$ at $\alpha = 8^\circ$) resulted from the application of positive sideslip which was almost constant with angle of attack (Figure 44). This probably resulted from a change of wing pressure distribution since the change in total lift was not significant.

5.0 CONCLUSIONS

Ground tests of the VTOL configuration showed:

- Differential thrust (side-to-side) simulating roll control during hover, induced rolling moments which opposed the thrust control power at ground heights of 1.4 model chords and above, and augmented the thrust control near the ground. The induced moments ranged up to 20% of the available thrust control power about the roll axis.
- Presence of the landing gear produced a 1% lift loss with the model hovering in ground effects.
- The horizontal tail produced a down load when set at zero incidence during hover. Removing the horizontal tail or setting it at an incidence of -20° resulted in a 2% lift increase.
- The yaw vanes located in the efflux of the three fans were found to produce only half of the desired moments ($\Delta YMA/F*B = .028$) during hover. The vane effectiveness was unchanged by forward speed to 15.44 m/sec (30 knots) but diminished with increased speed at ground heights above 1.5 model chords.

Tests of the STO configuration in ground effects showed:

- At typical lift-off conditions the lift at gear contact and at a height of four model chords compares well with free air data but the lift dropped off approximately 20% as the model moved away from the ground plane, reaching a minimum at a height of one model chord.
- The configuration had longitudinal stability during ground roll with a degradation of stability as height increased to 4.0 chord lengths.
- H-tail effectiveness was similar to free-air data at a height of 4.0 chord lengths but was reduced by 50% at gear contact.
- Aileron and rudder effectiveness were determined with the STOL configuration out of ground effect. The aileron effectiveness continually increased to aileron deflections of 25°. The ailerons can produce adequate rolling moment for a desired angular acceleration of .6 radians/sec² about the roll axis.

With the L/C nacelles tilted to 50° for STO operation, the rudder produced a yawing moment of only .005 with 15° of

deflection. Only one deflection angle was tested. This yawing moment is inadequate to produce a desired angular acceleration of .2 radians/sec² in yaw.

6.0 REFERENCES

1. Wind Tunnel and Ground Static Tests of a .094 Scale Powered Model of a Modified T-39 Lift/Cruise Fan V/STOL Research Airplane NASA CR-151923, D. Hunt, J. Clingen, V. Salemann, and E. Omar, January 1977.
2. Follow-on Studies for Design Definition of a Lift/Cruise Fan Technology V/STOL Airplane, Boeing Military V/STOL Group, NASA CR-137976, January 1976.
3. Multi-Component Force Data Reduction, Equations, T. M. Curry presented at 3rd SESA International Congress, May 14, 1973.
4. Lowe, W. H., and Sanger, R. W., Static Performance of a 13.97 cm (5.5 inch) Diameter Model VTOL Lift-Fan, NASA CR-2051, May 1972.
5. Saberliner Twin-Jet Executive Aircraft Specifications. Airplanes; Ser. No. 292-91 and Subsequent NA-62-768-2, June 20, 1966.

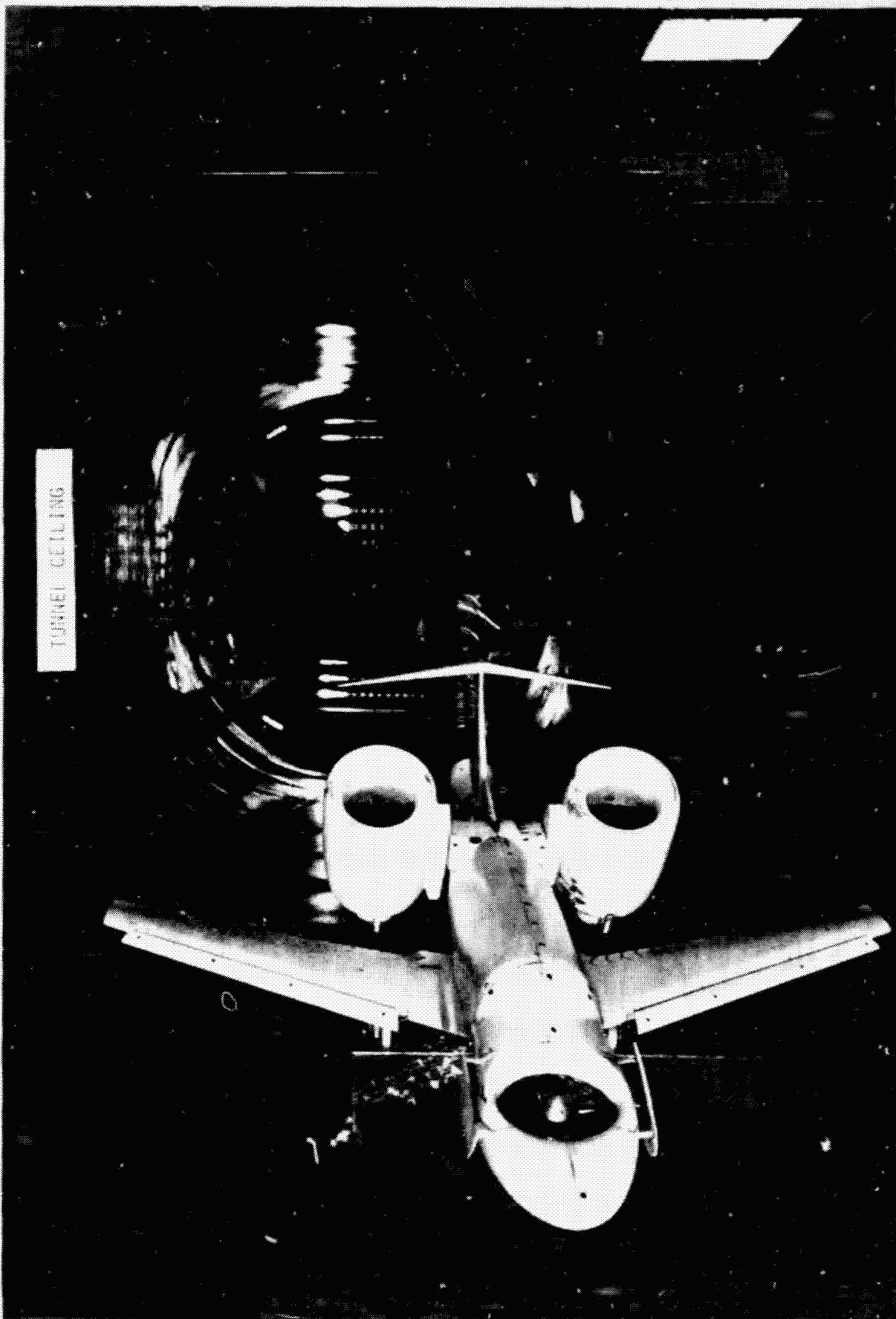
6. The Boeing Flight Simulation Chamber for Static Calibrations of Engine Simulators, presented at 45th Meeting of the Supersonic Tunnel Association, E. K. Fromm, April 1976.
7. 9 X 9 B LSWT Centerline Static Pressure Distribution with and without Ground Plane, Boeing Document D6-45005, R. P. Doerzbacher.
8. Cull, M. J., V/STOL Wind Tunnel Model Test and Experimental Assessment of Flow Breakdown Using Multiple Fan Model, AGARD-CPP-174.



FIGURE 1 TENTH SCALE POWERED WIND TUNNEL MODEL OF RTA

REPRODUCIBILITY OF THIS
ORIGINAL PAGE IS POOR

REPRODUCIBILITY OF THE
ORIGINAL PAGE IS POOR

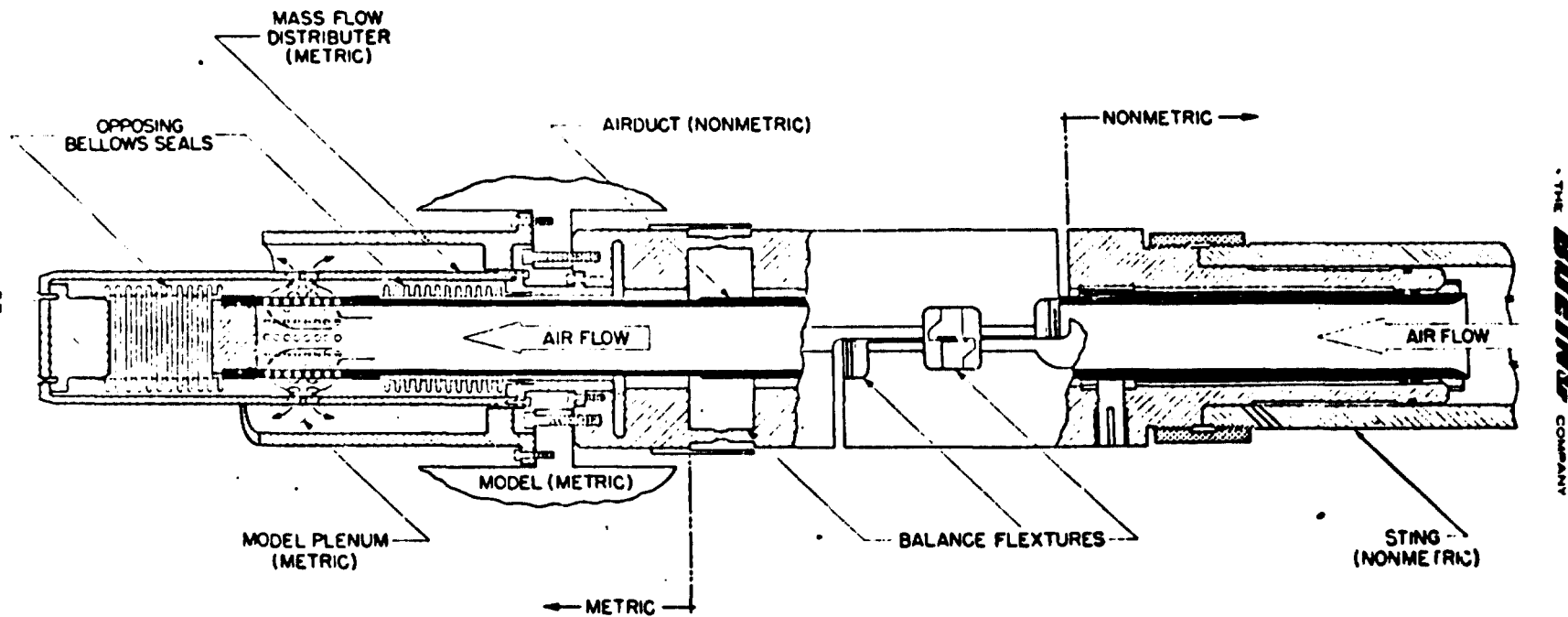


A.D. 15413

REV SYM

FIGURE 2 MODEL INSTALLED IN THE BOEING 9' LOW SPEED WIND TUNNEL

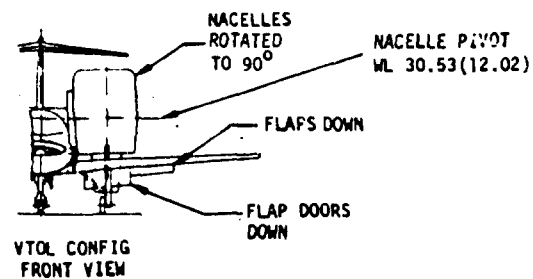
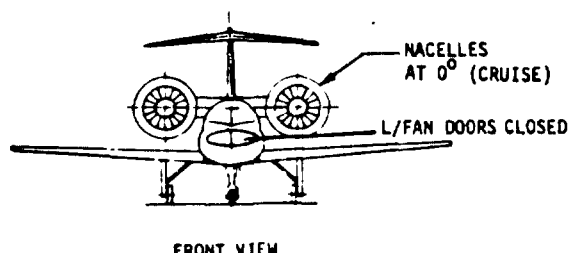
57



THE BOEING COMPANY

FIGURE 3 SCHEMATIC OF "FLOW-THRU" INTERNAL BALANCE

	WING	H. TAIL	V. TAIL
REFERENCE AREA CM ² (IN ²)	2808(435.17)	523 (81.07)	341(52.85)
SPAN CM (IN)	127.3(50.11)	51.26(20.18)	23.32(9.18)
MAC CM(IN)	24.02(9.46)	10.24(4.03)	14.62(5.76)
ASPECT RATIO	5.77	4.998	1.59
TAPER RATIO	.325	.35	.387
SWEEP, 25% LINE	28.55°	30°	30°



DIMENSIONS: CM (INS)

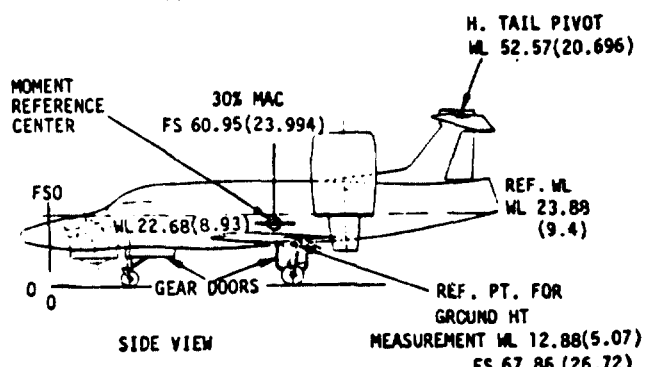
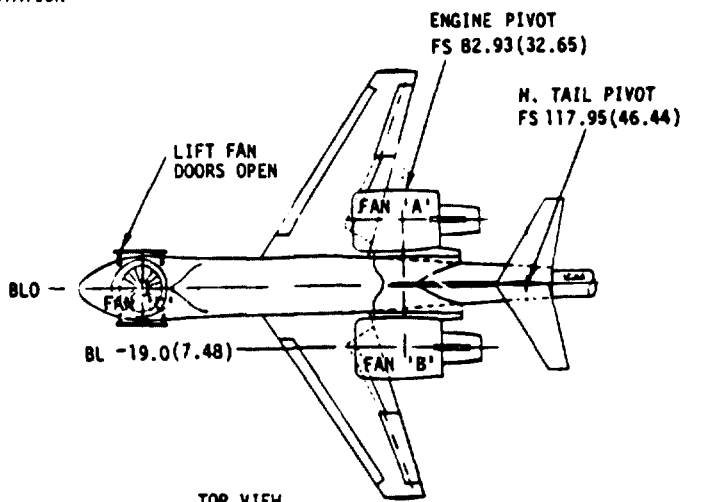
MODEL SCALE • .094

REF. WL 23.88 IS T-39 REFERENCE WATER LINE (FULL SCALE WL 100)

BL = BUTT LINE

FS = FUSELAGE STATION

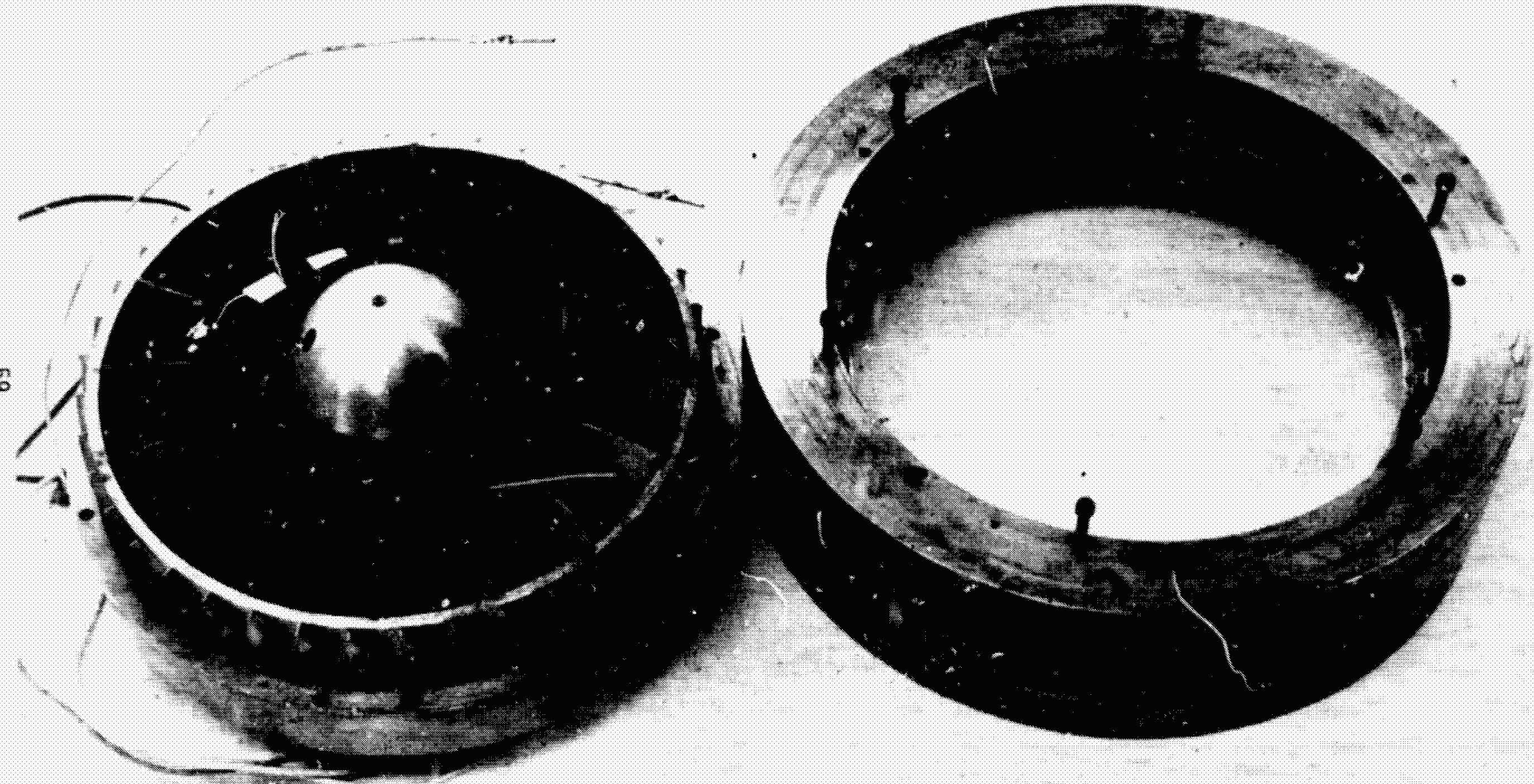
WL = WATER LINE



THE BOEING COMPANY

FIGURE 4 MODIFIED T-39 LIFT/CRUISE FAN AIRPLANE MODEL

REPRODUCIBILITY OF THE
ORIGINAL PAGE IS POOR



59

FIGURE 5 MODEL TD-457 TIP DRIVEN FAN AND DRIVE PLENUM

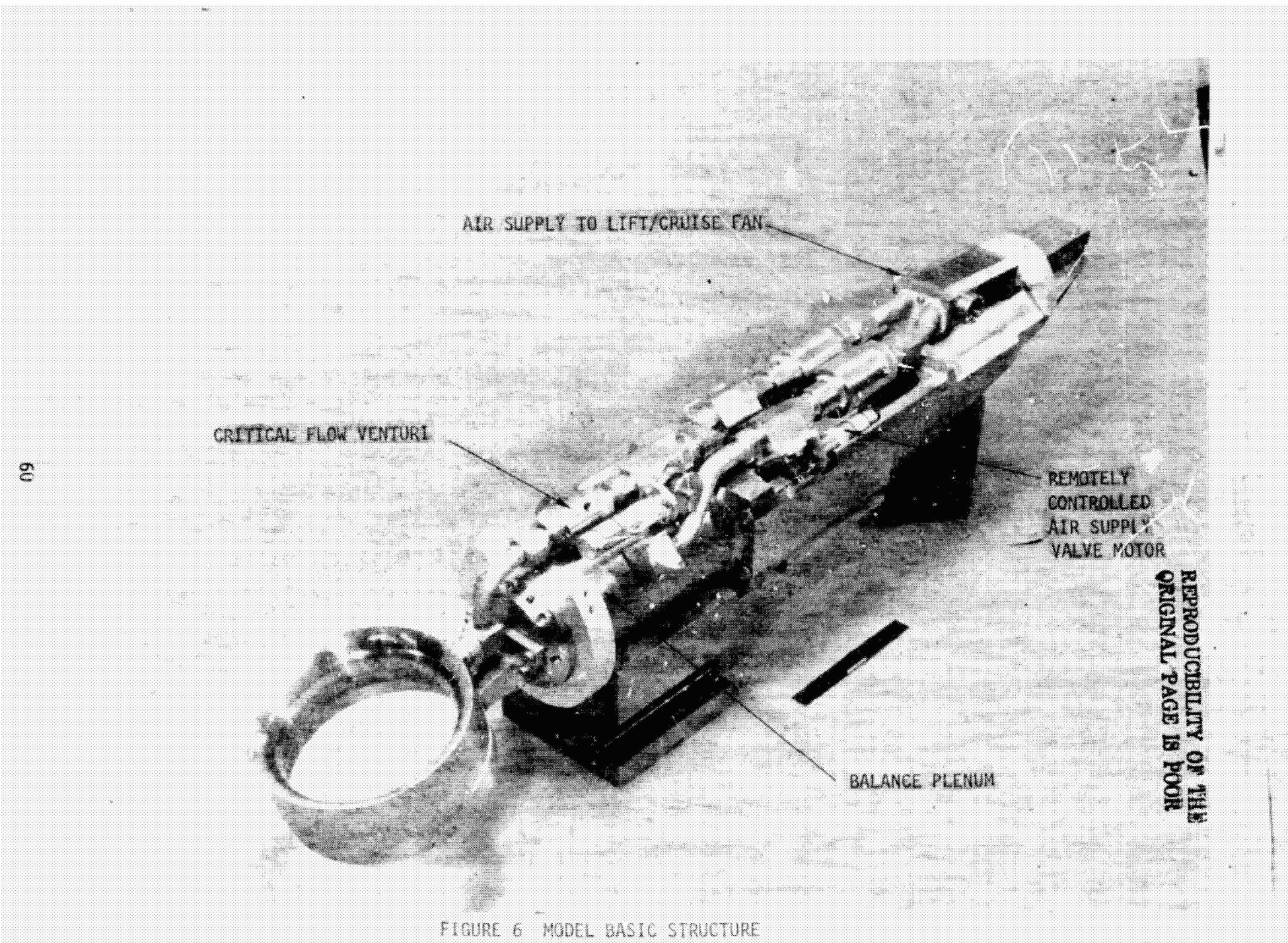


FIGURE 6 MODEL BASIC STRUCTURE

61

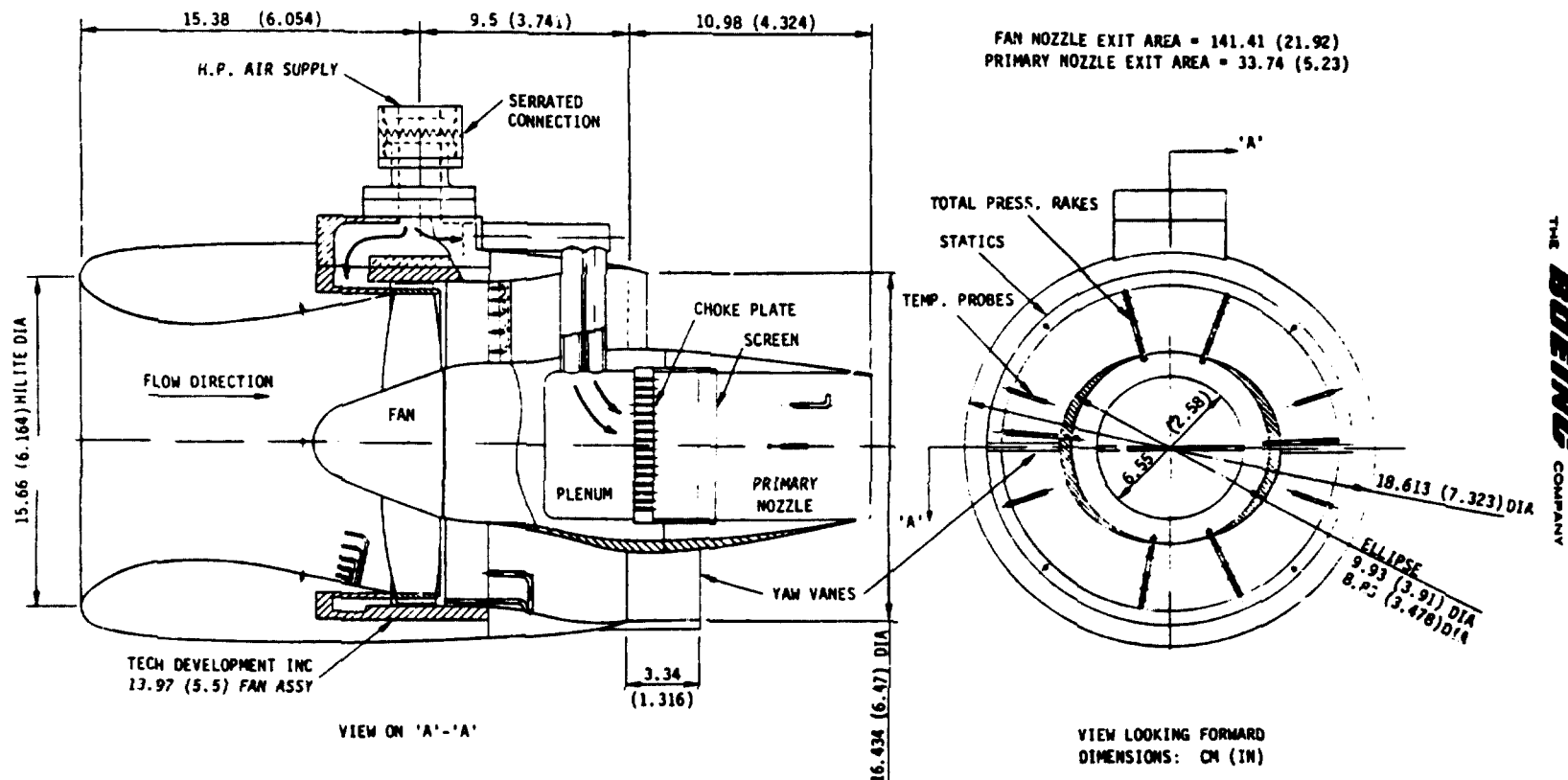


FIGURE 7 ASSEMBLY OF L/C FAN NACELLE

THE **BOEING** COMPANY

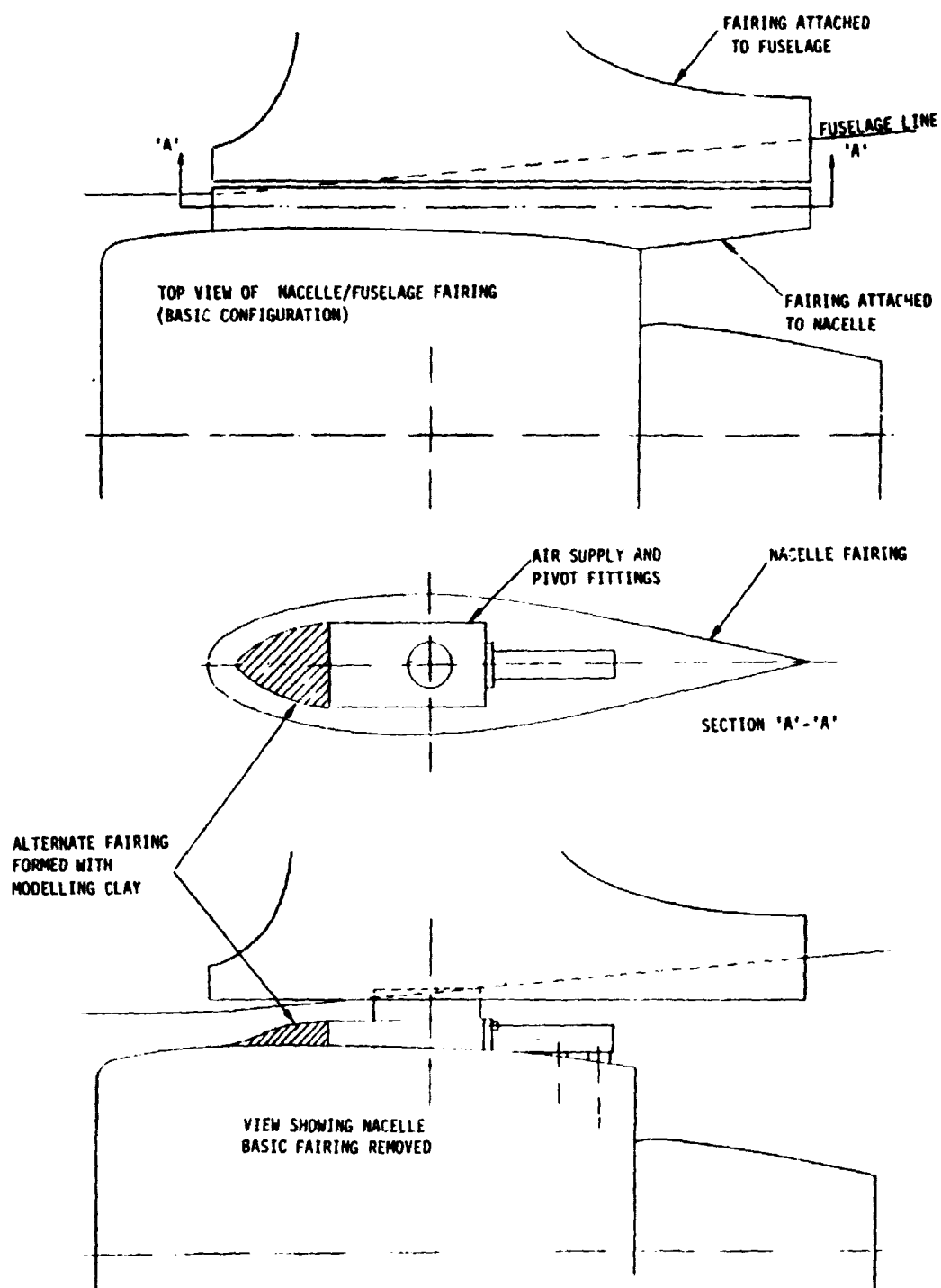
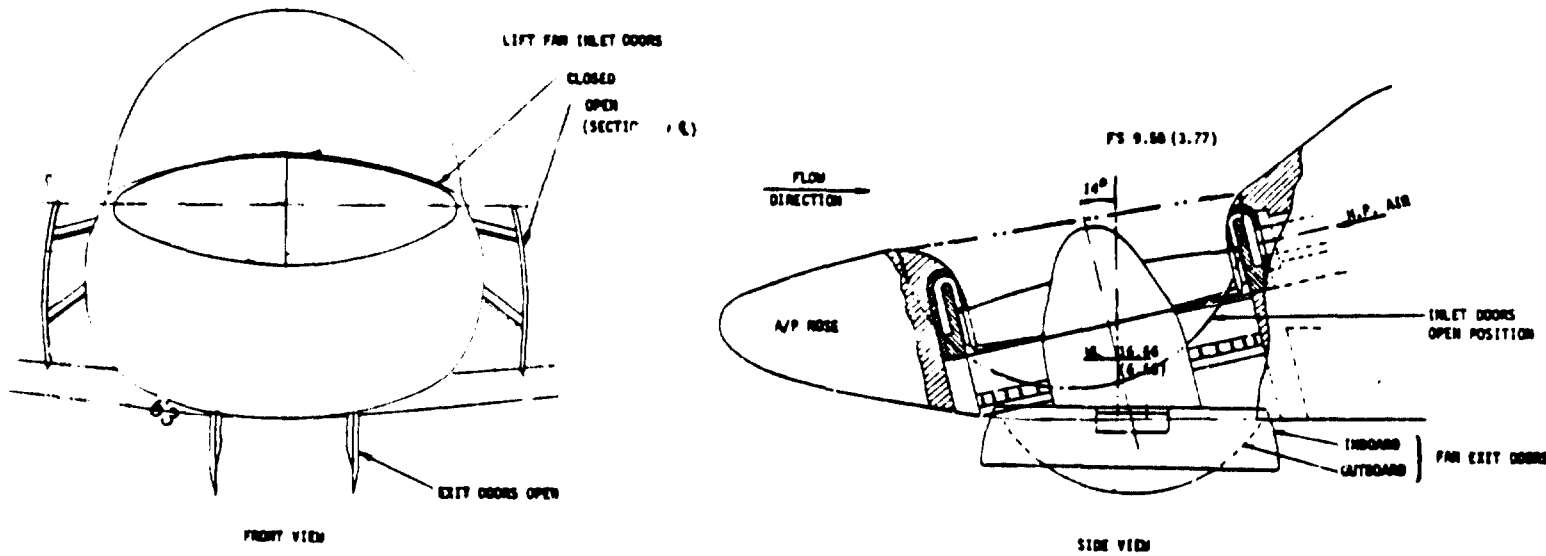


FIGURE 8 DETAILS OF NACELLE/FUSELAGE FAIRING

63



DRAWING NO.: CR (200)

FIGURE 9 ASSEMBLY OF LIFT FAN

REPRODUCTION OF THE
ORIGINAL PAGE IS PROHIBITED

THE BOEING COMPANY

THE **BOEING** COMPANY

WING

- DIMS IN WING REF SYSTEM
 - 0.25 MAC AT FS 59.752 (23.524)
 - REF PLANE INTERSECTS PLANE OF SYMMETRY
@ ML 15.635 (6.155)
 - REF PLAN = WING CHORD PLANE @ BL = 0
 - DIHEDRAL: 3.15°
 - SECTION: NACA 64, A212 (MOD) AT WBL = 15.021 (5.91)
NACA 64, A012 (MOD) AT WBL = 60.87 (23.96)

DIMENSIONS: CM (INS)

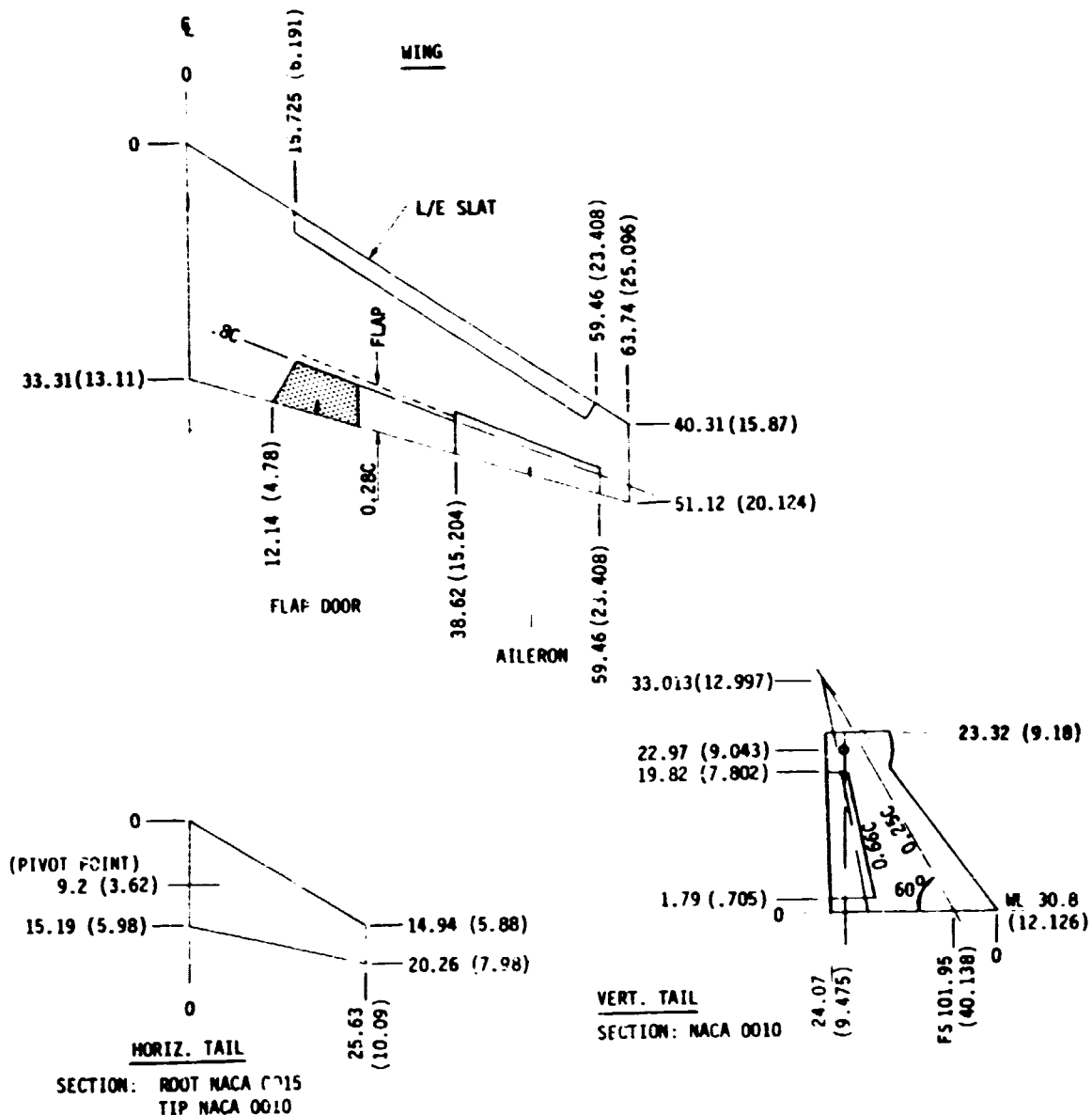
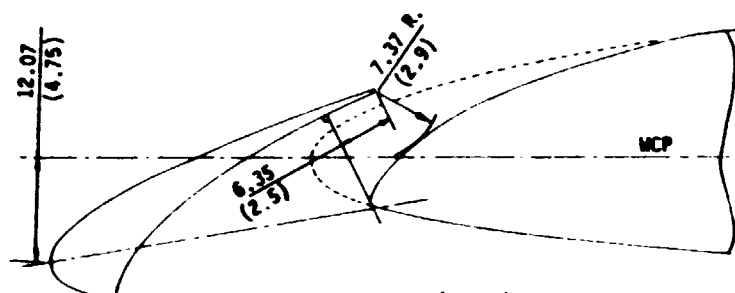


FIGURE 10 MODEL PLANFORM DETAILS

THE **BOEING** COMPANY



BL 167.28 (65.86)
INBOARD EDGE OF L.E. SLAT

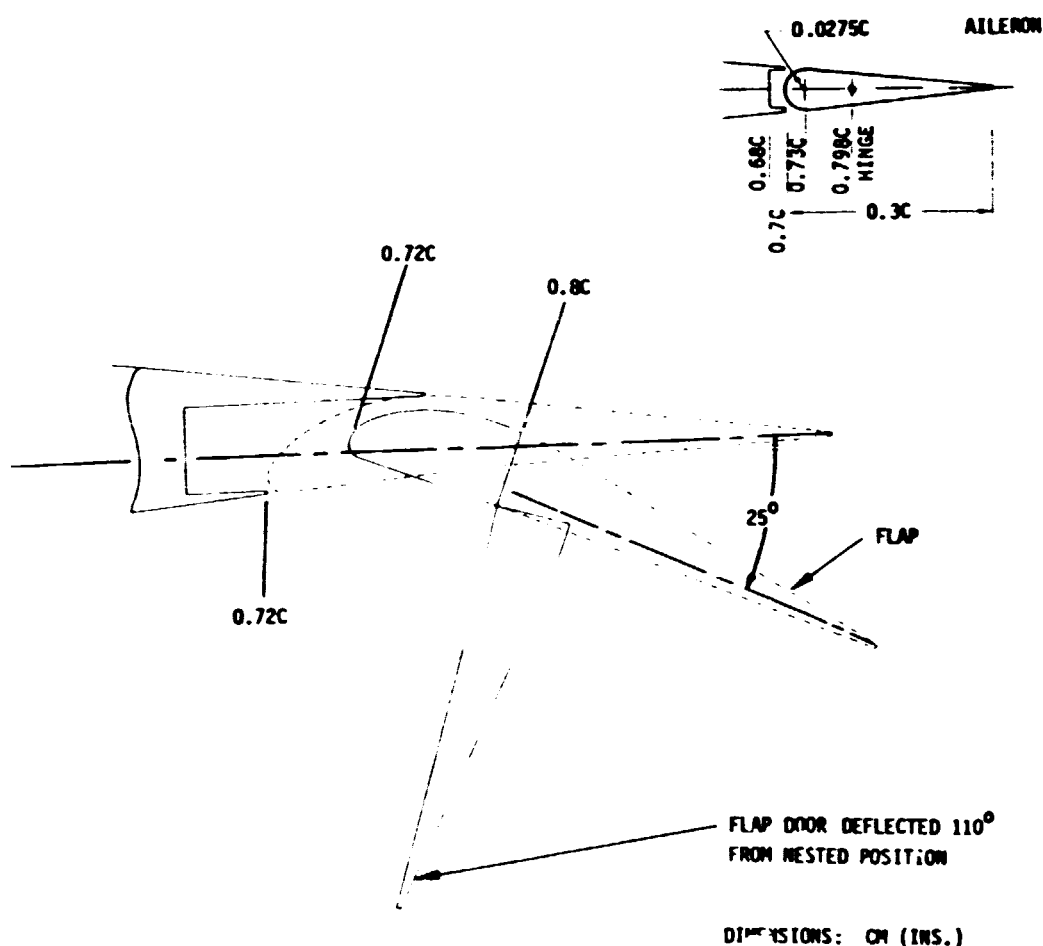


FIGURE 11 MODEL SECTION DETAILS

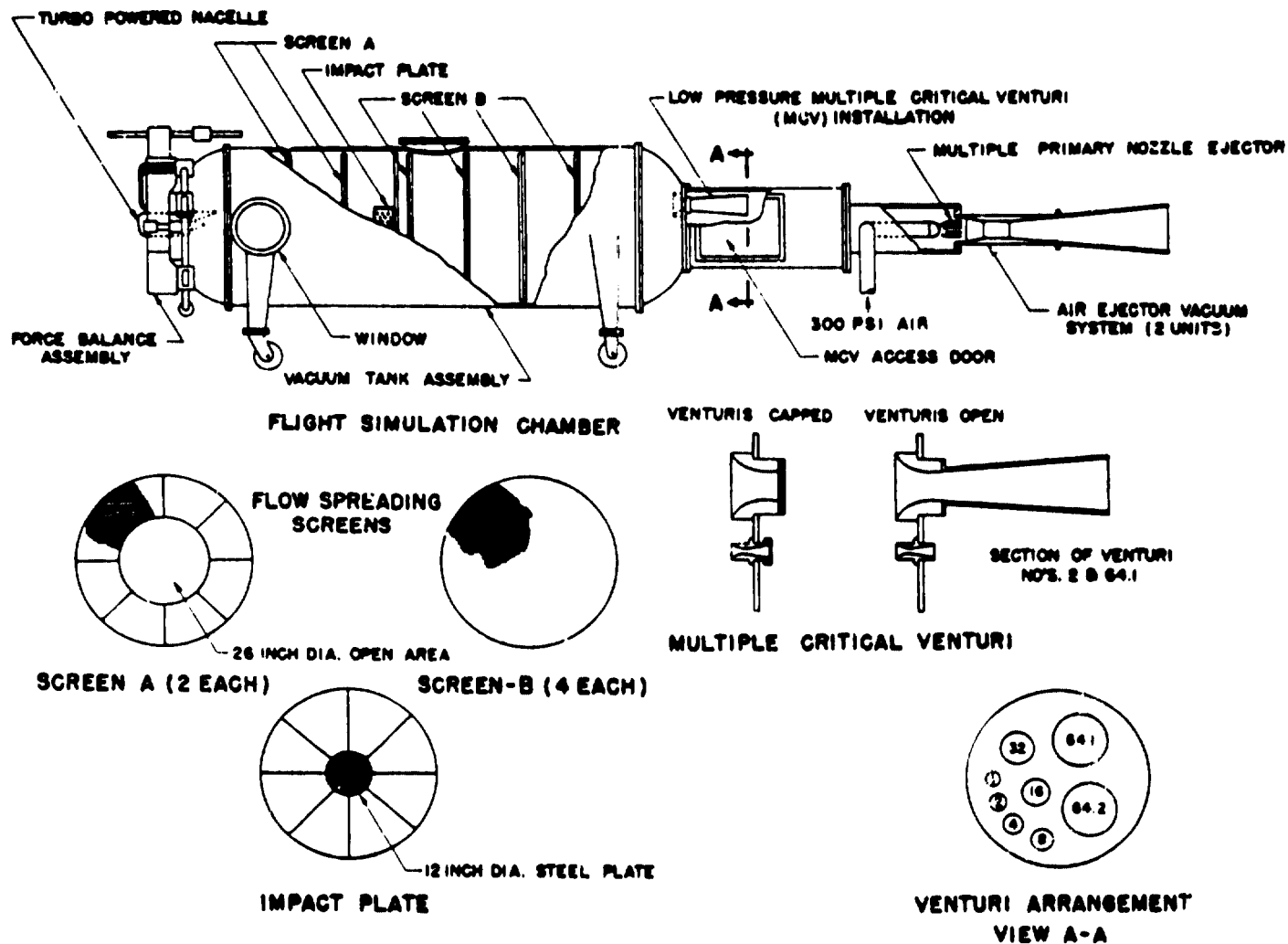


FIGURE 12 FLIGHT SIMULATION CHAMBER

67

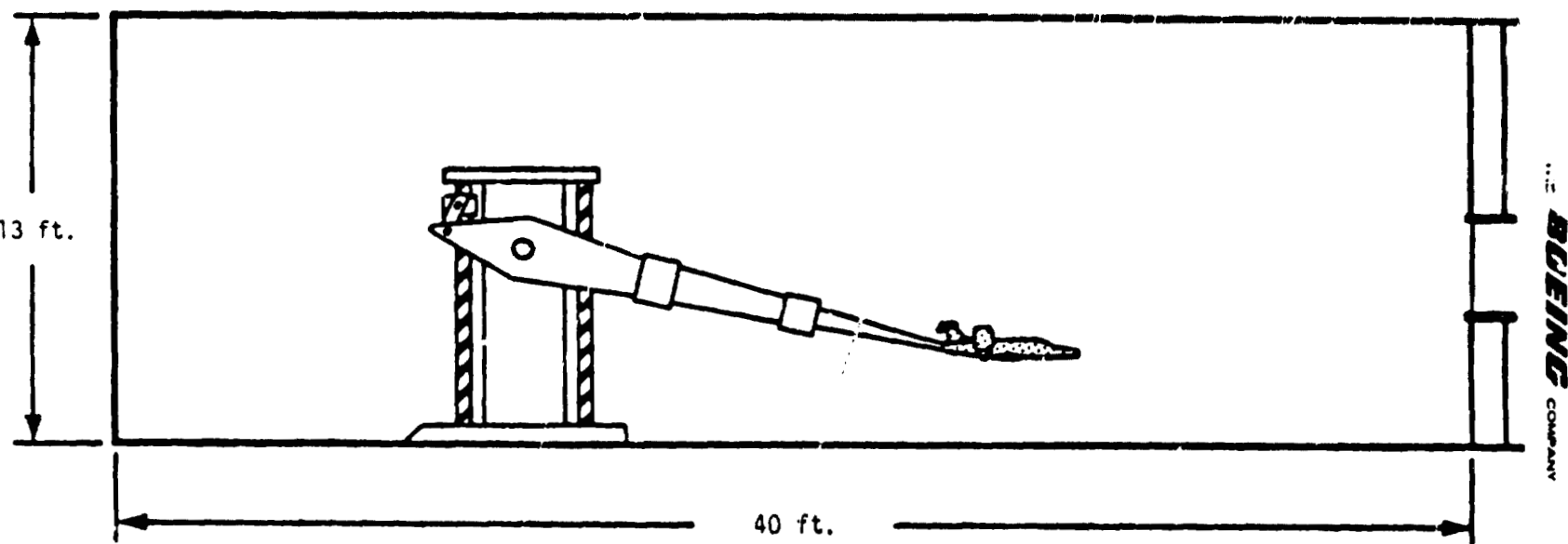


FIGURE 13 BOEING STATIC CHECKOUT FACILITIES

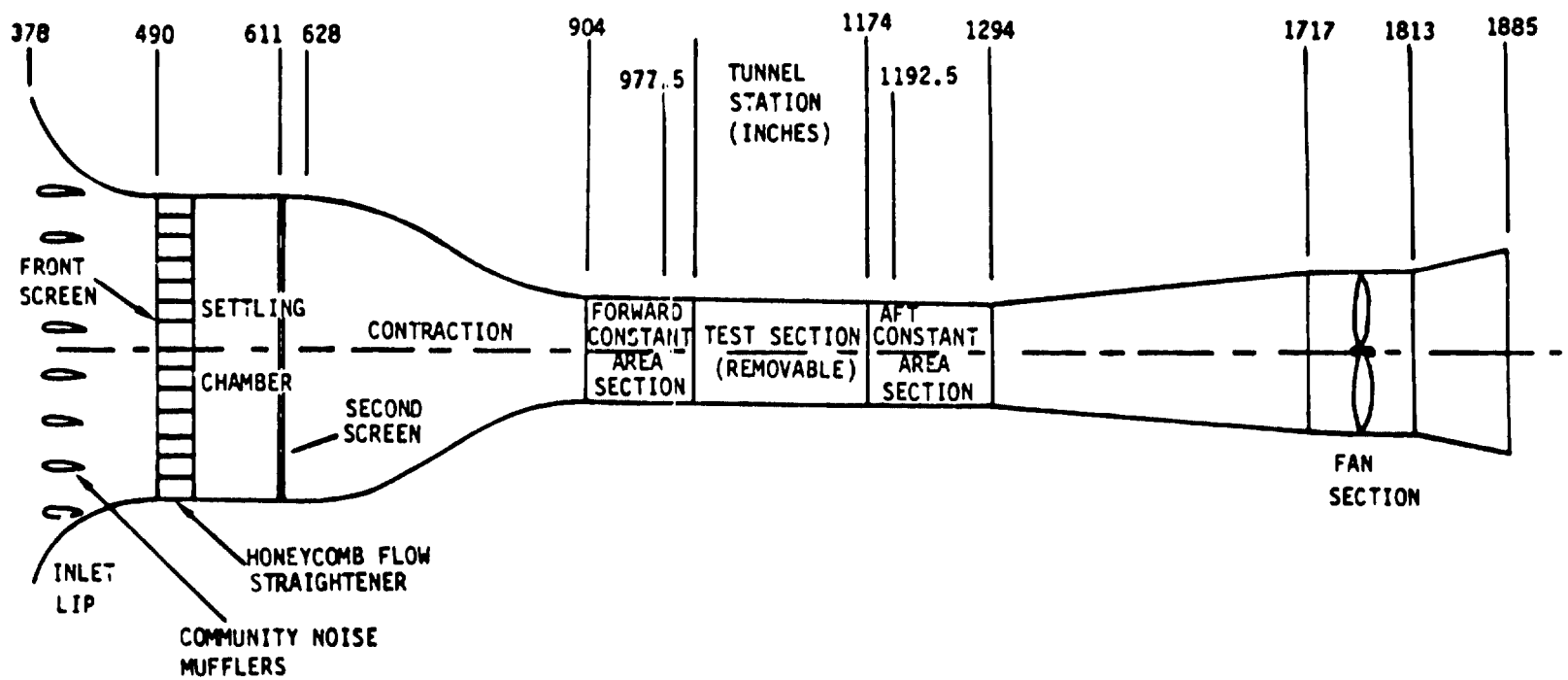


FIGURE 14 GENERAL ARRANGEMENT OF BOEING 9' X 9' WIND TUNNEL

69

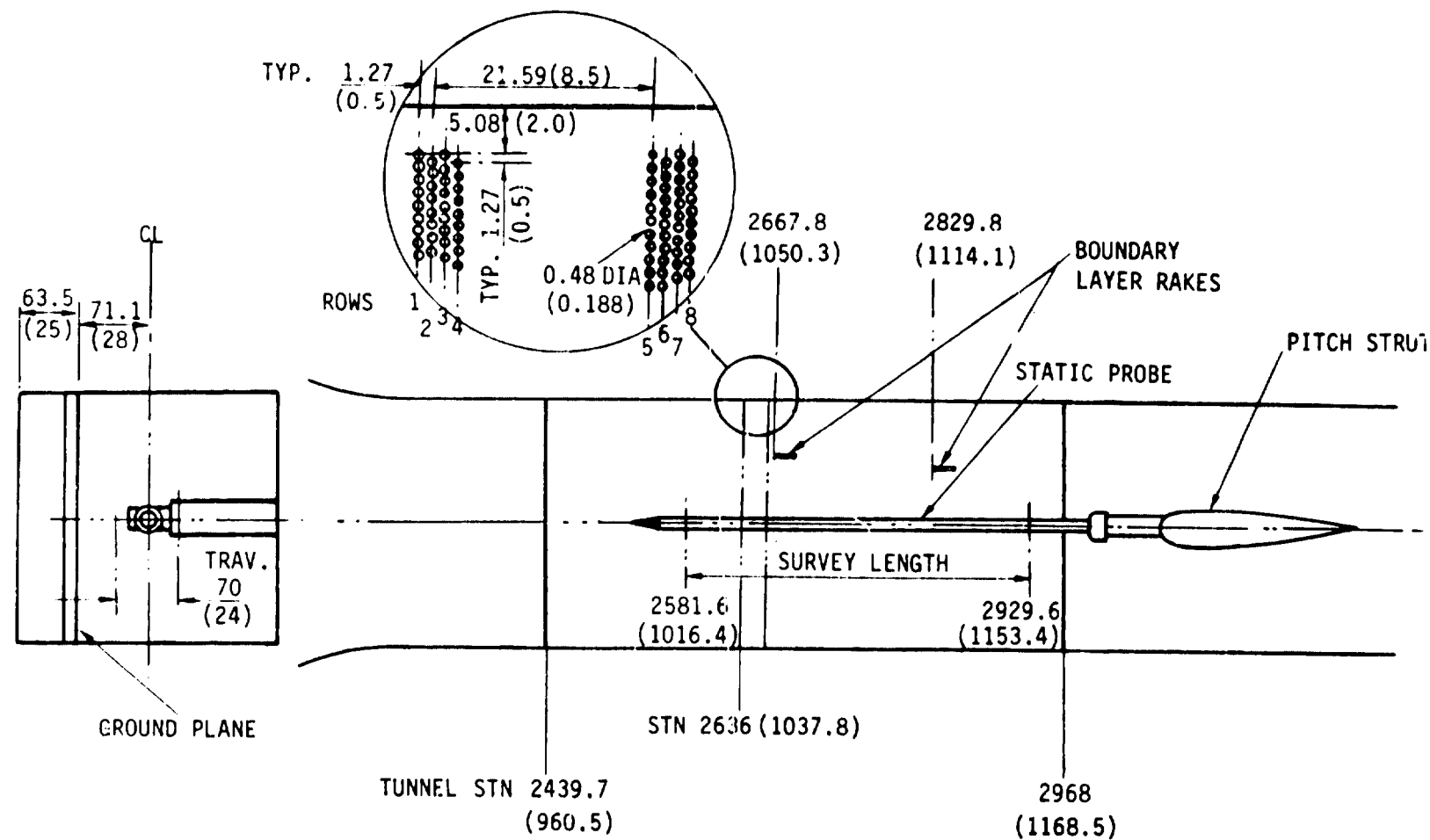
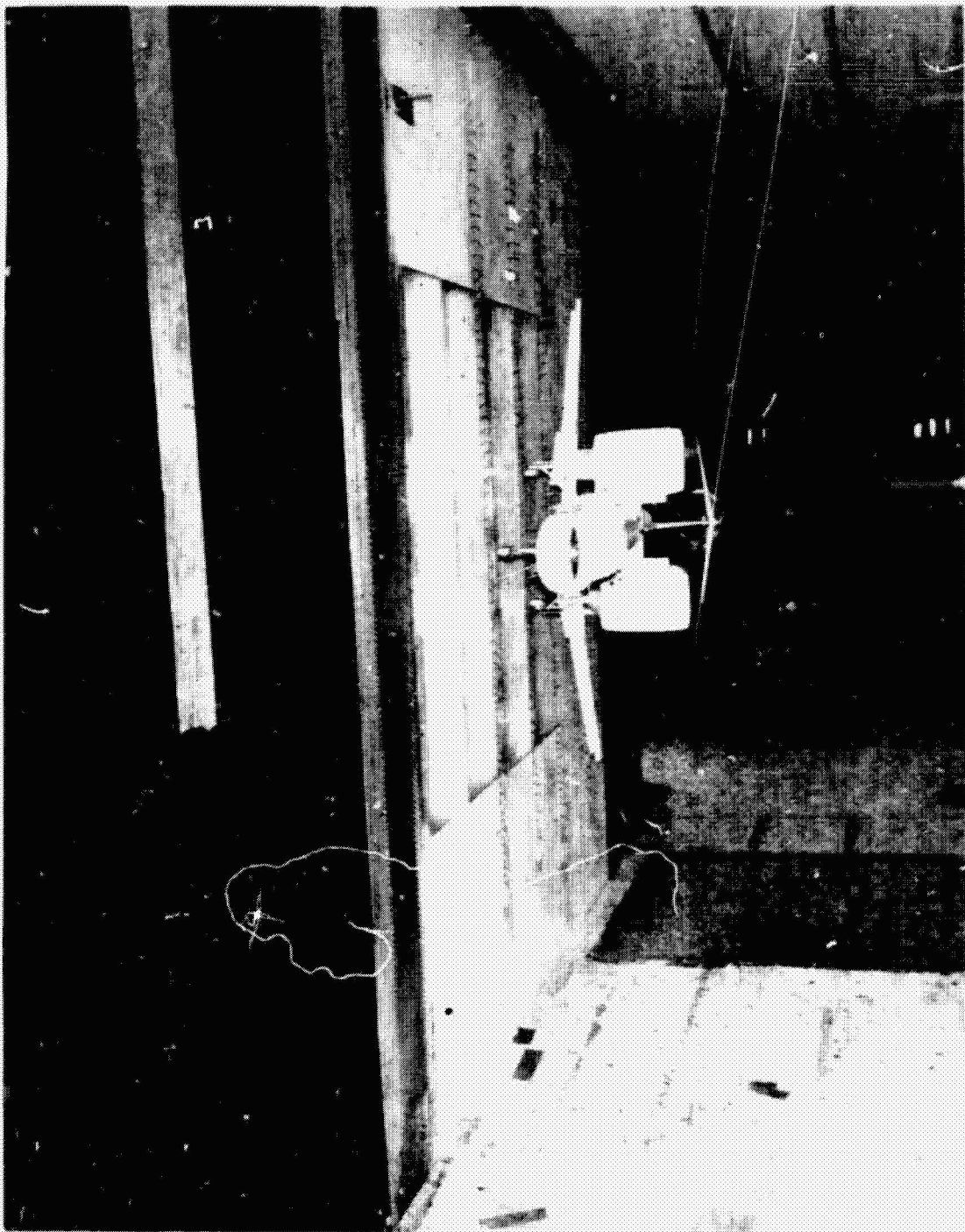


FIGURE 15

GROUND PLANE INSTALLATION

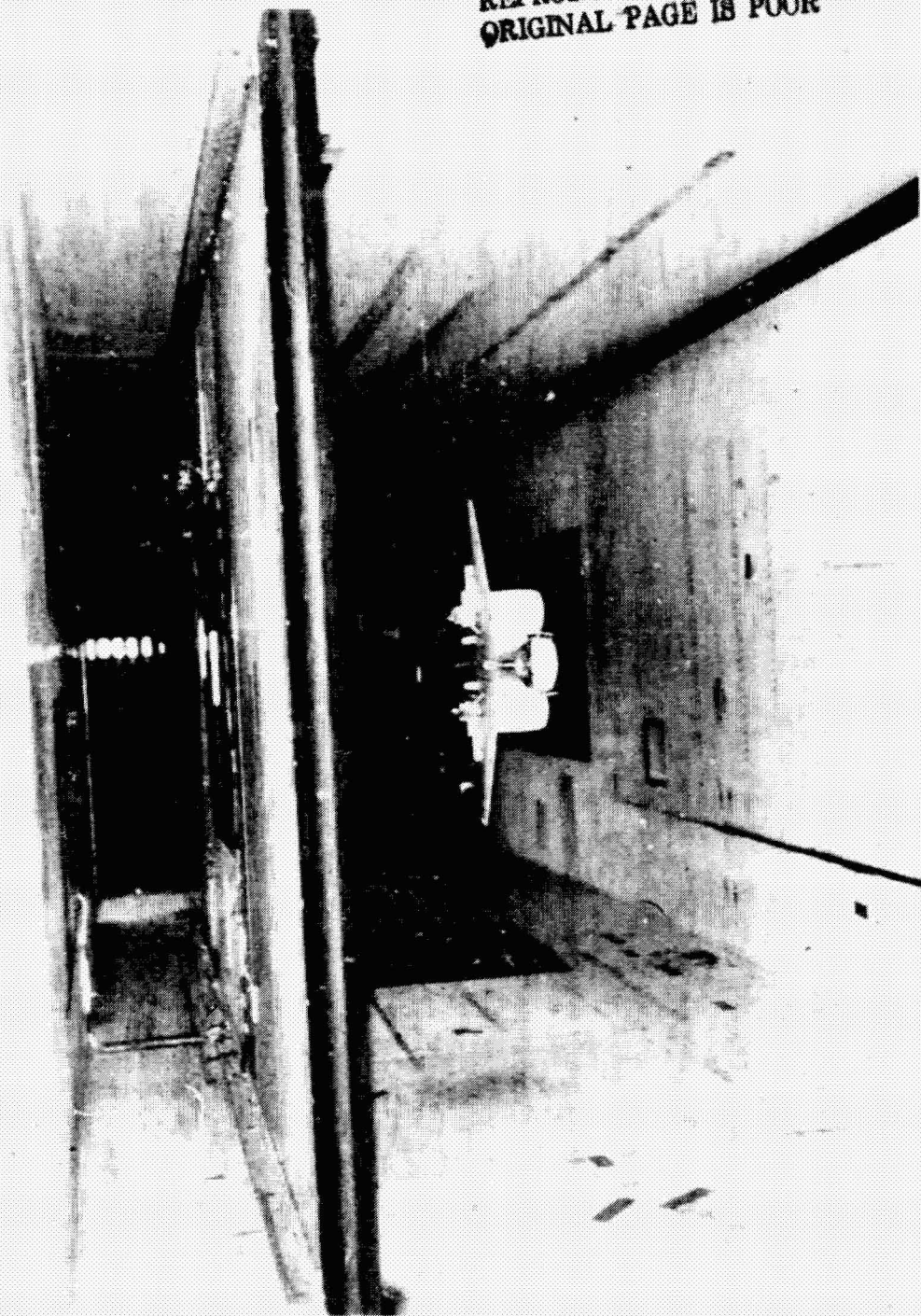
REPRODUCIBILITY OF THE
ORIGINAL PAGE IS POOR



GROUND PLANE INSTALLATION



REPRODUCIBILITY OF THE
ORIGINAL PAGE IS POOR



GROUND PLANE INSTALLATION



CONFIG.	IN G.E.	OUT OF G.E.	VARIABLES EXPLORED						
			L/C FAN TILT ANGLE λ	PITCH ANGLE α	SIDESLIP ANGLE β	TUNNEL SPEEDS M/SEC (KTS)	THRUST COEFF. (NOMINAL)	H. TAIL	COMPONENT EFFECT
VTOL	<input checked="" type="checkbox"/>		90°	$0^{\circ}; 5^{\circ}$	0°	15.44 (30) 30.88 (60)	6.0; 22.0	0° ; OFF	HORIZONTAL TAIL
				0°	$0^{\circ}; 10^{\circ}$	15.44 (30) 30.88 (60)	6.0; 22.0	0° ; OFF	DIFF. THRUST YAW VANES SIDESLIP
			$80^{\circ}; 90^{\circ}; 95^{\circ}$	0°	0°	15.44 (30) 30.88 (60)	6.0; 22.0	OFF	ENGINE TILT ANGLE
STOL	<input checked="" type="checkbox"/>	<input checked="" type="checkbox"/>	50°	$0^{\circ}; 8^{\circ}; 14^{\circ}$	0°	46.33 (90) 41.18 (80) 33.46 (65)	1.8 3.7 5.5	OFF	RUDDER EFFECT. AILERON " VERT. TAIL "
LOITER		<input checked="" type="checkbox"/>	0°	VAR.	$0^{\circ}; 10^{\circ}$	61.77 (120)	NACELLES OFF	$0^{\circ}; 10^{\circ}$	H. TAIL EFFECT SIDESLIP

FIGURE 17 WIND TUNNEL TEST CONDITIONS

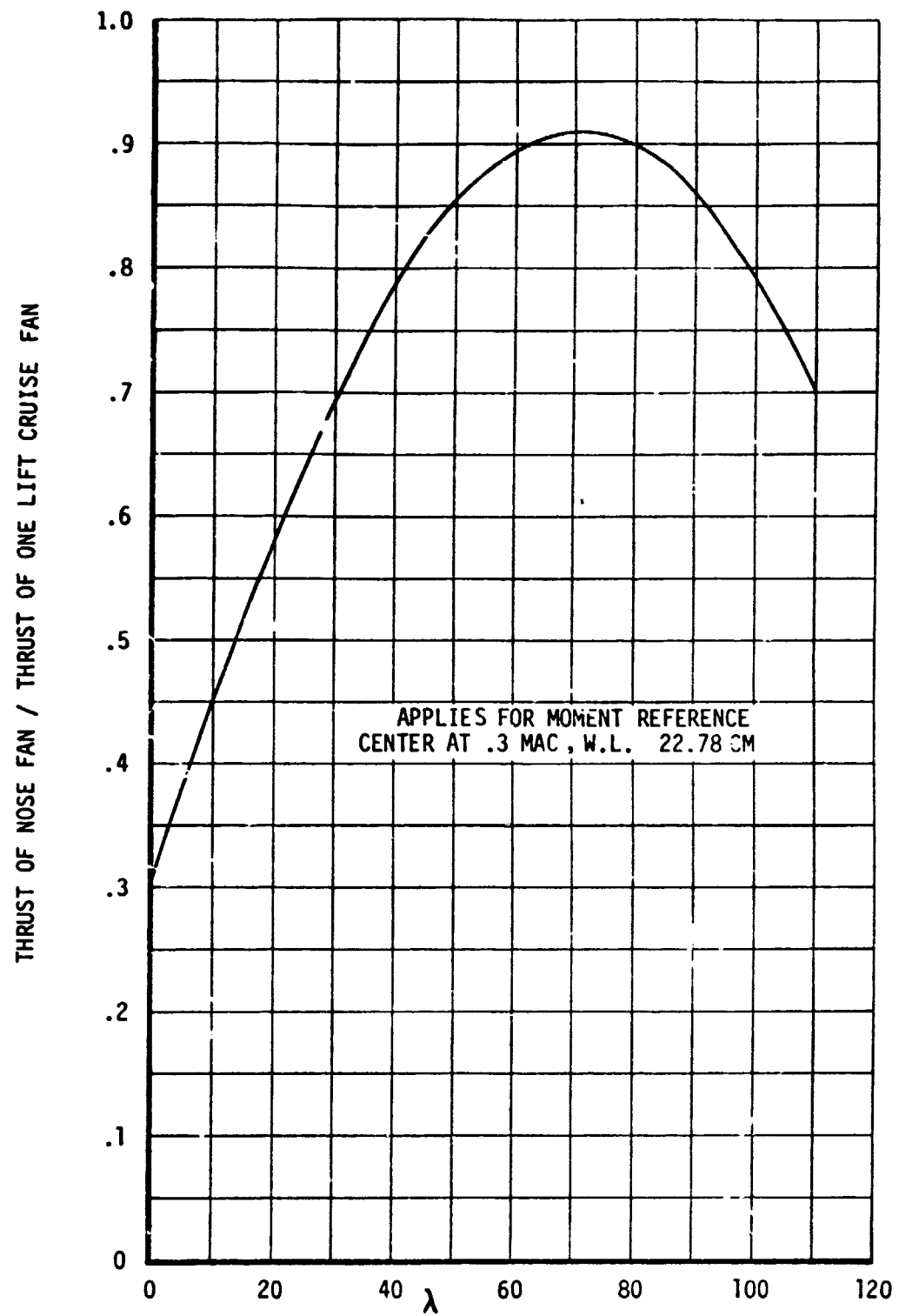
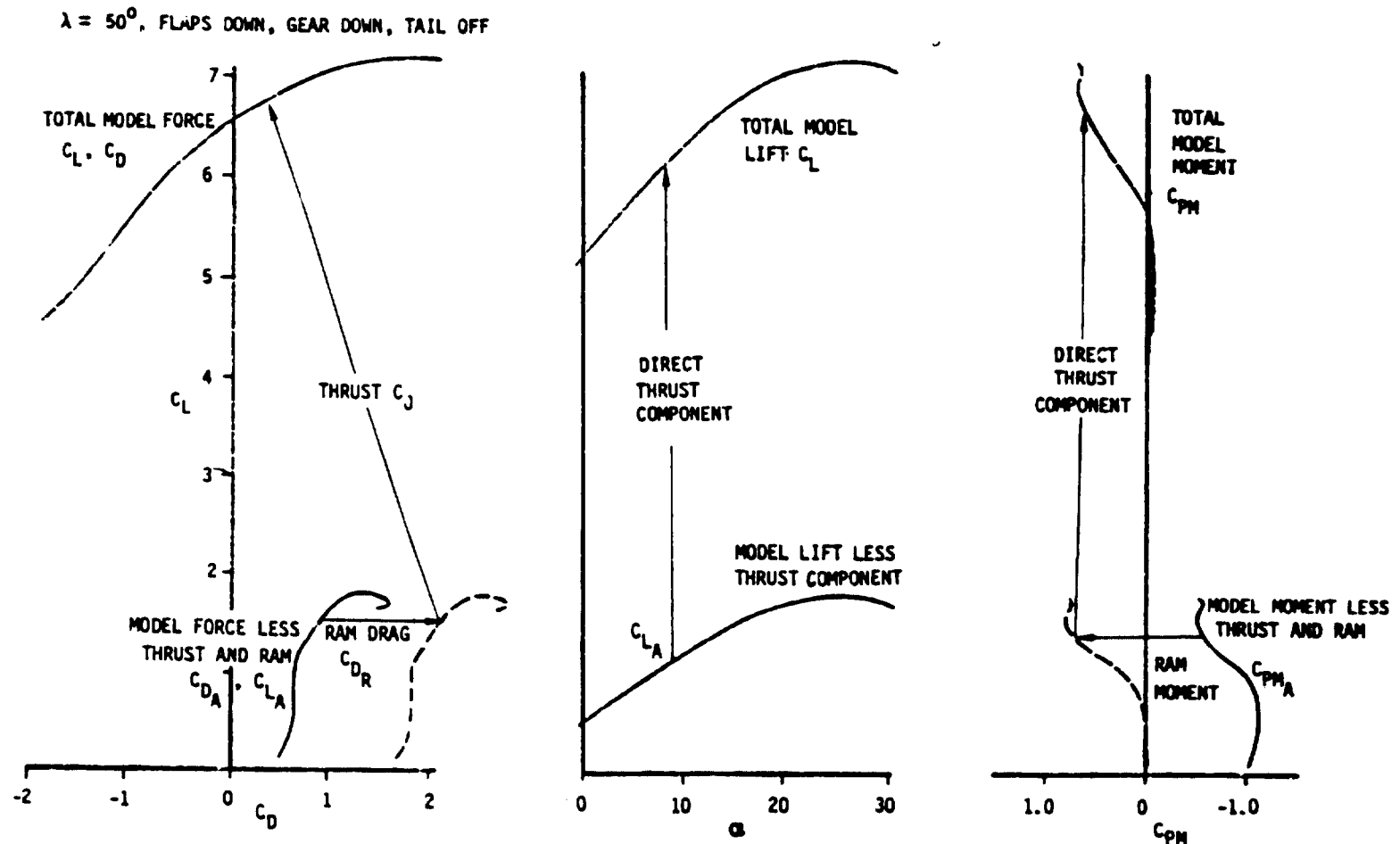


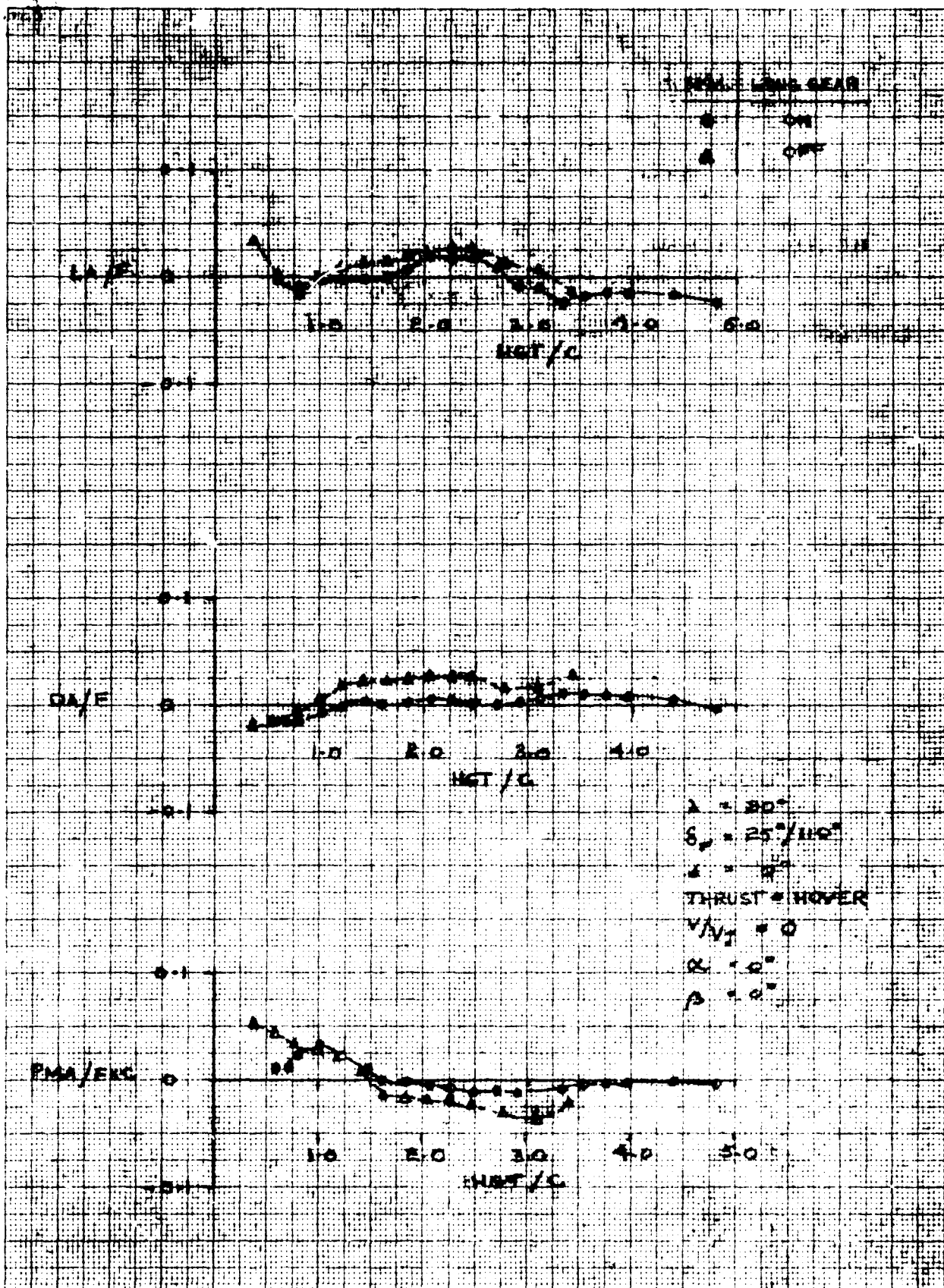
FIGURE 18 NOSE FAN THRUST REQUIRED FOR PITCHING MOMENT TRIM
IN STATIC FREE AIR HOVER

74

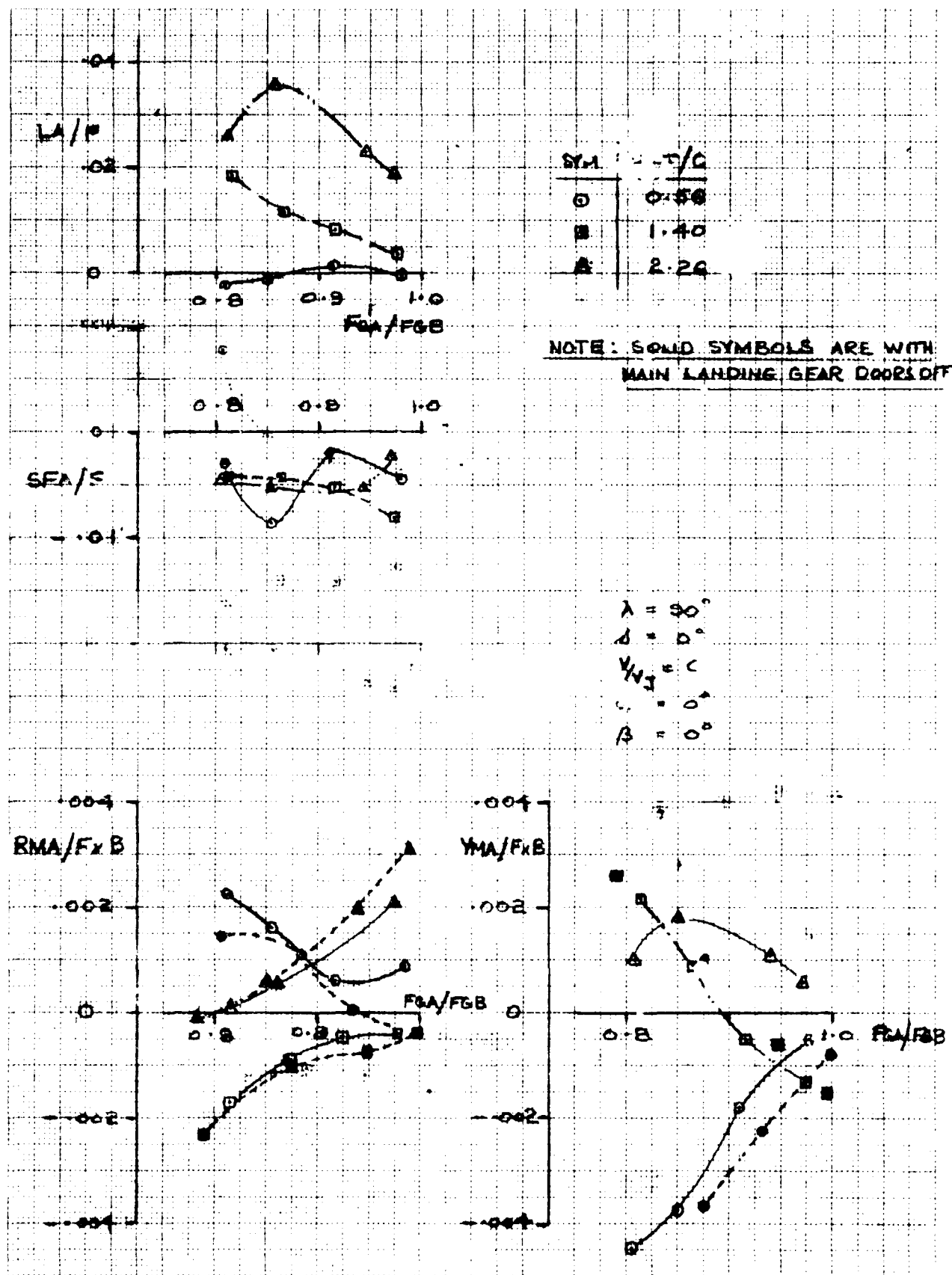


THE BOEING COMPANY

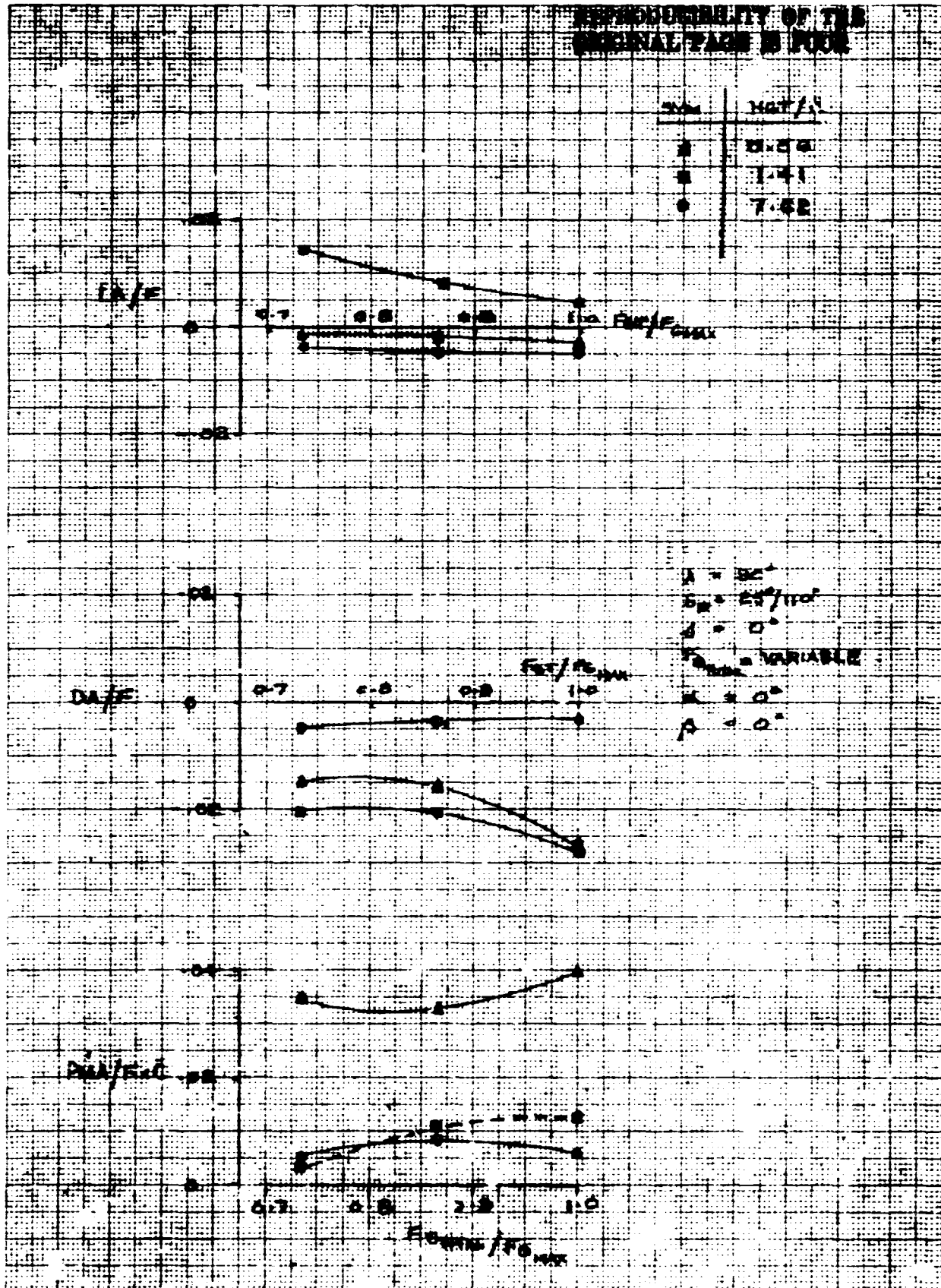
FIGURE 19 RELATIONSHIP OF AERODYNAMIC FORCES TO TOTAL FORCES



CALC			REVISED	DATE	VTOL - IN GROUND EFFECT EFFECT OF LANDING GEAR THE BOEING COMPANY	FIG. 20 PAGE 75
CHECK						
APR						
APR						



CALC			REVISED	DATE	VTOL - IN GROUND EFFECT	
CHECK					EFFECT OF DIFF'ENTIAL THRUST	
APR						
APR						
					THE BOEING COMPANY	
					FIG. 21	
					PAGE 76	



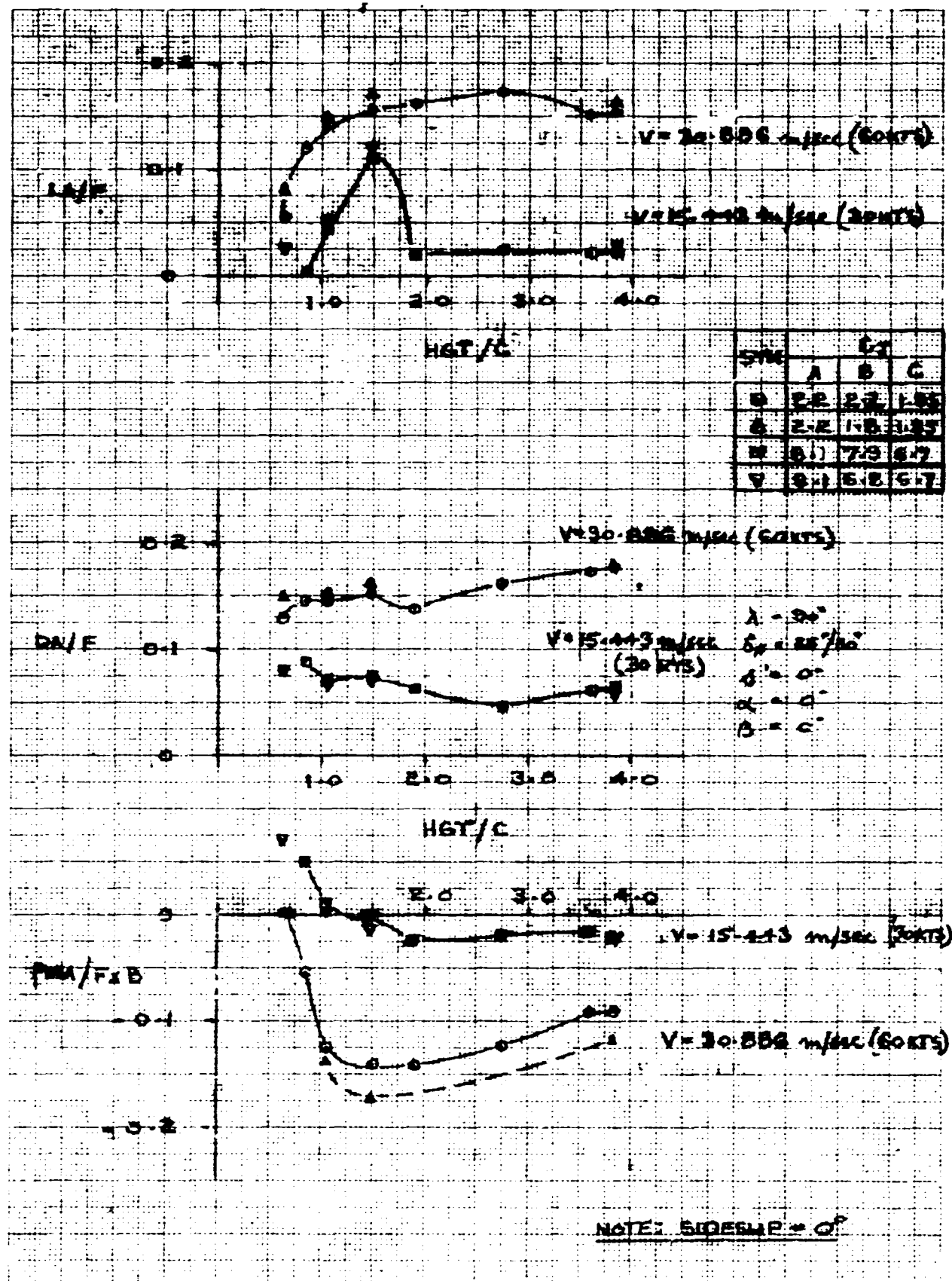
CALC		REVISED	DAT.	
CHECK				
TP				
PPR				

VTOL - IN GROUND EFFECT
EFFECT OF TOTAL THRUST

THE BOEING COMPANY

FIG.22

PAGE 77

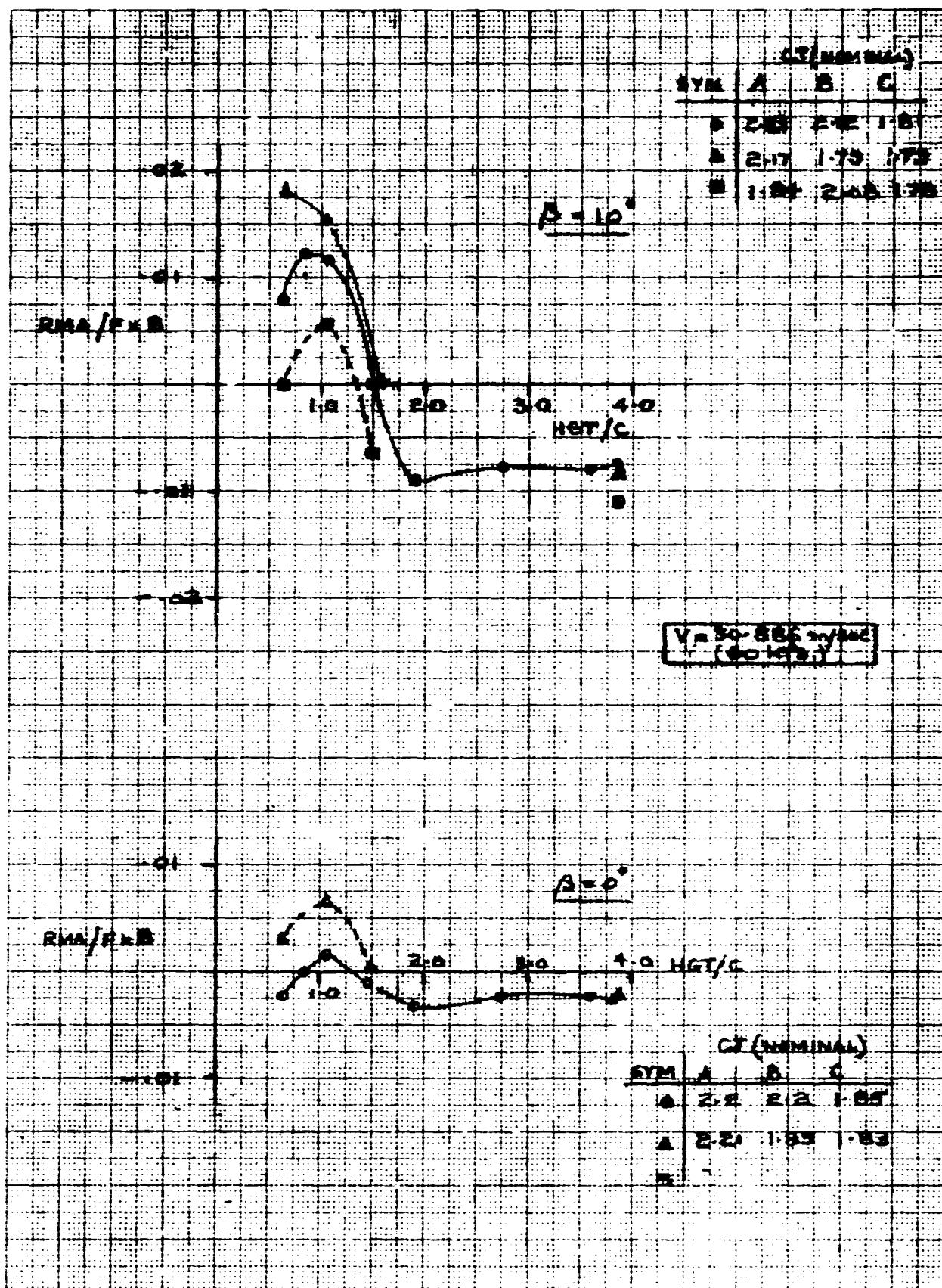


CALC		REVN	TR
CHECK			
APR			
APG			

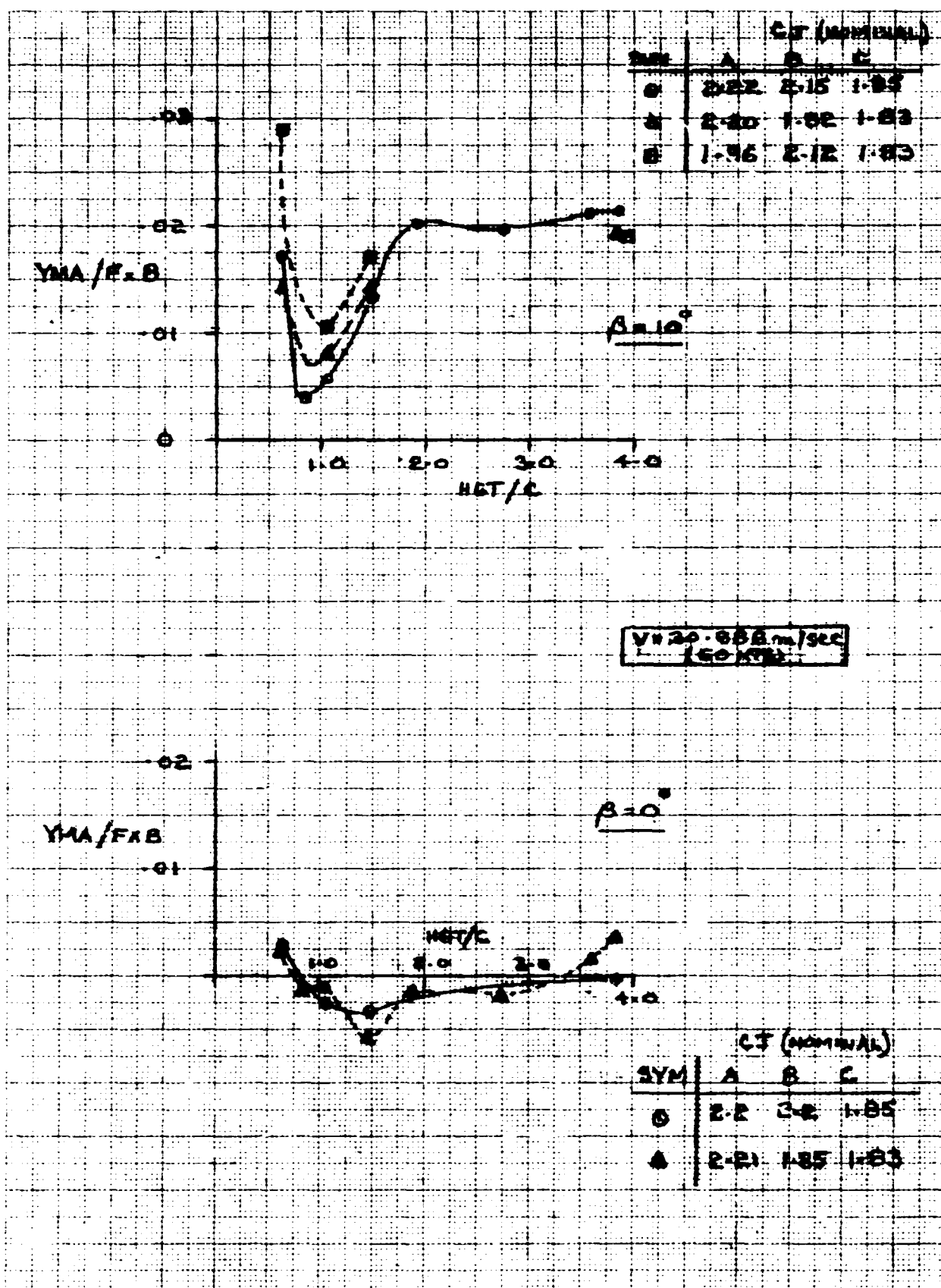
VTOL - IN GROUND EFFECT
EFFECT OF DIFF. THRUST

THE BOEING COMPANY

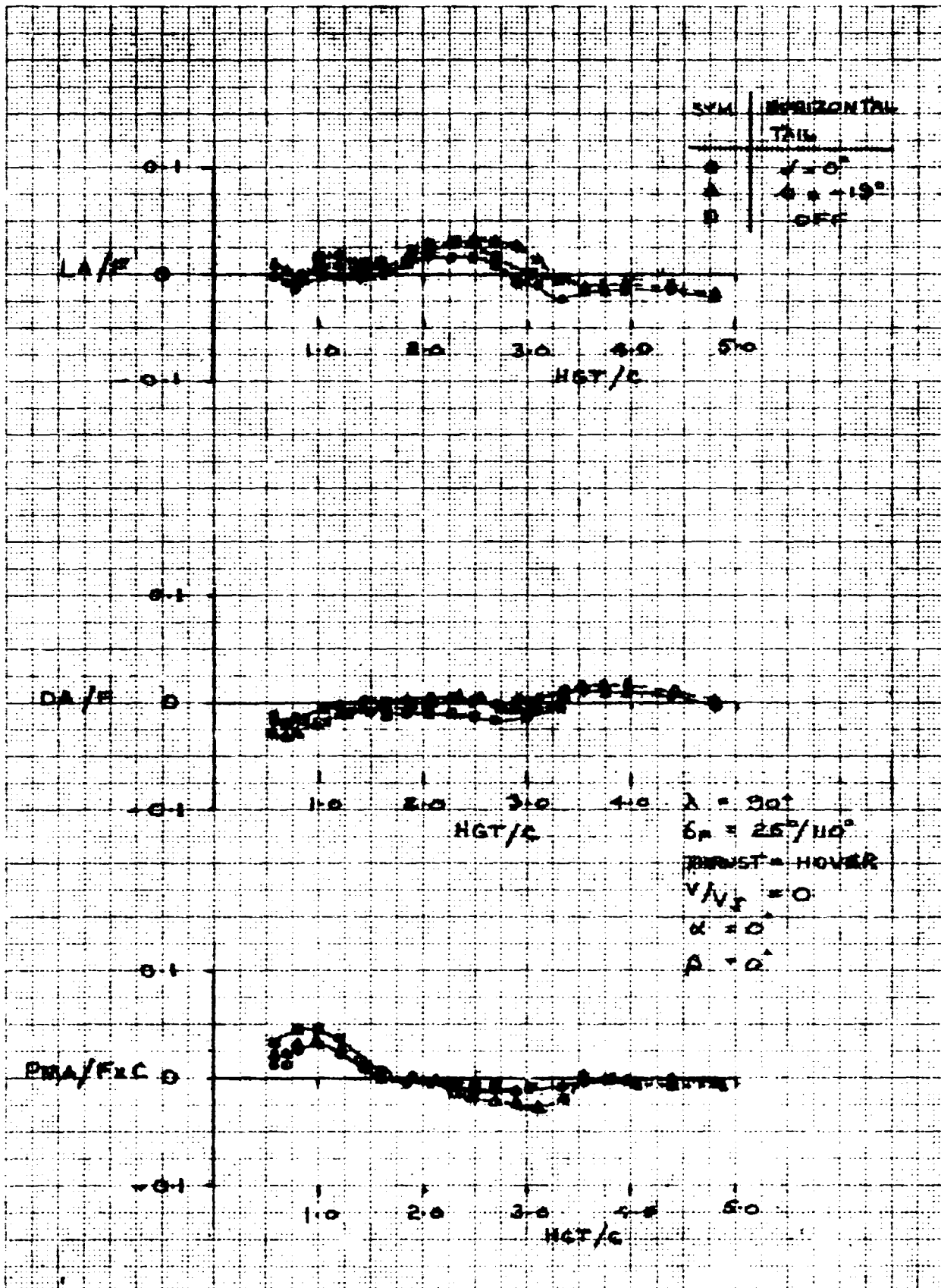
FIG. 23
PAGE 78



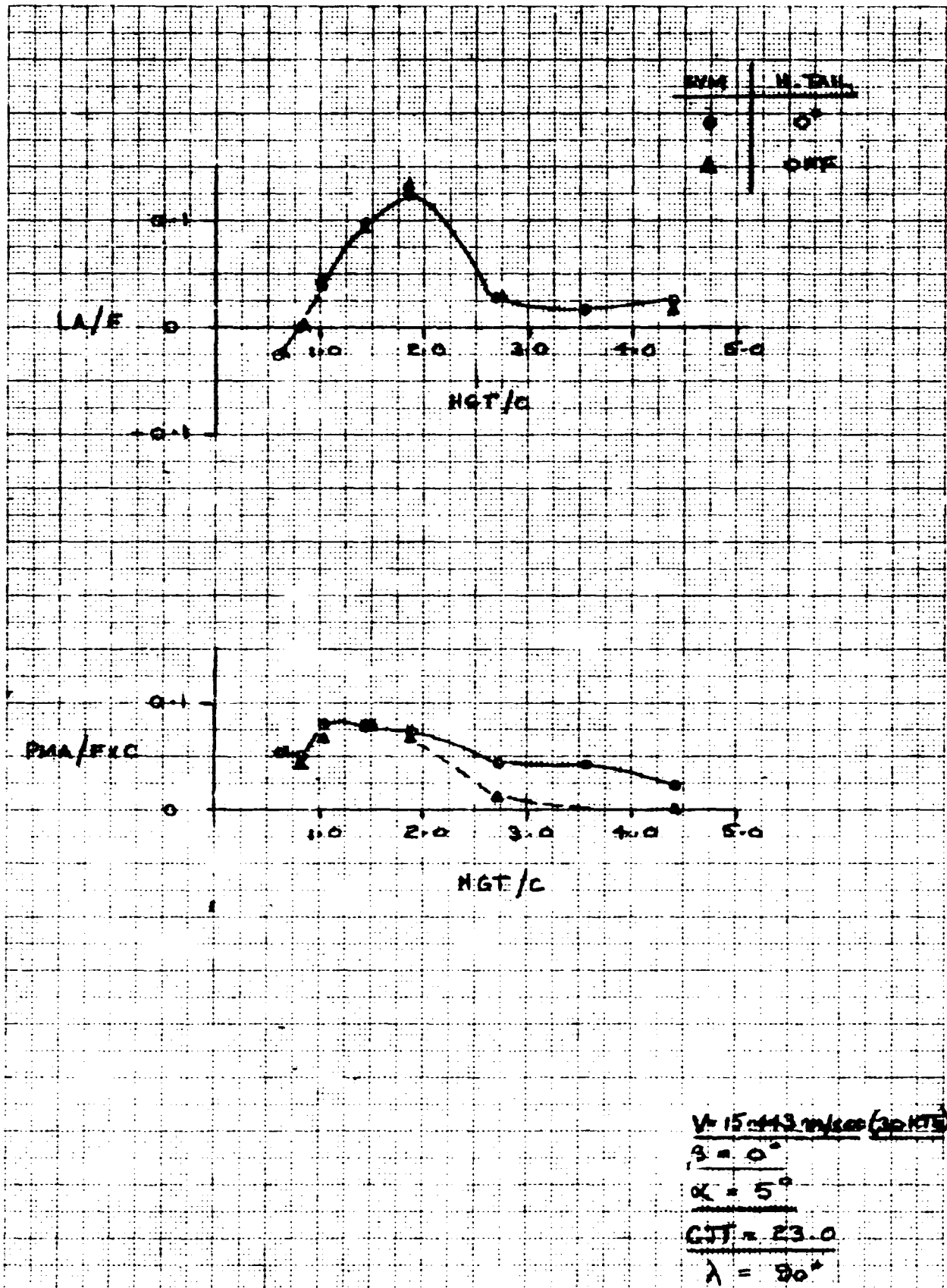
CA: C		REVISED	DATE	VTOL - IN GROUND EFFECT		
CHECK				EFFECT OF DIFF. THRUST ON RMA	FIG. 24(4)	
DR						
APR						
				THE BOEING COMPANY	PAGE 79	



CALC		REVISED	DATE	VTOL - IN GROUND EFFECT EFFECT OF DIFF. THRUST ON YMA	
CHECK					FIG 24(b)
APR					PAGE
APP					80
				THE BOEING COMPANY	



CALC		REVISED	DATE	VTOL - IN GROUND EFFECT EFFECT OF HORIZONTAL TAIL	
CHECK					FIG. 25
APR					
APR					PAGE 91
				THE BOEING COMPANY	



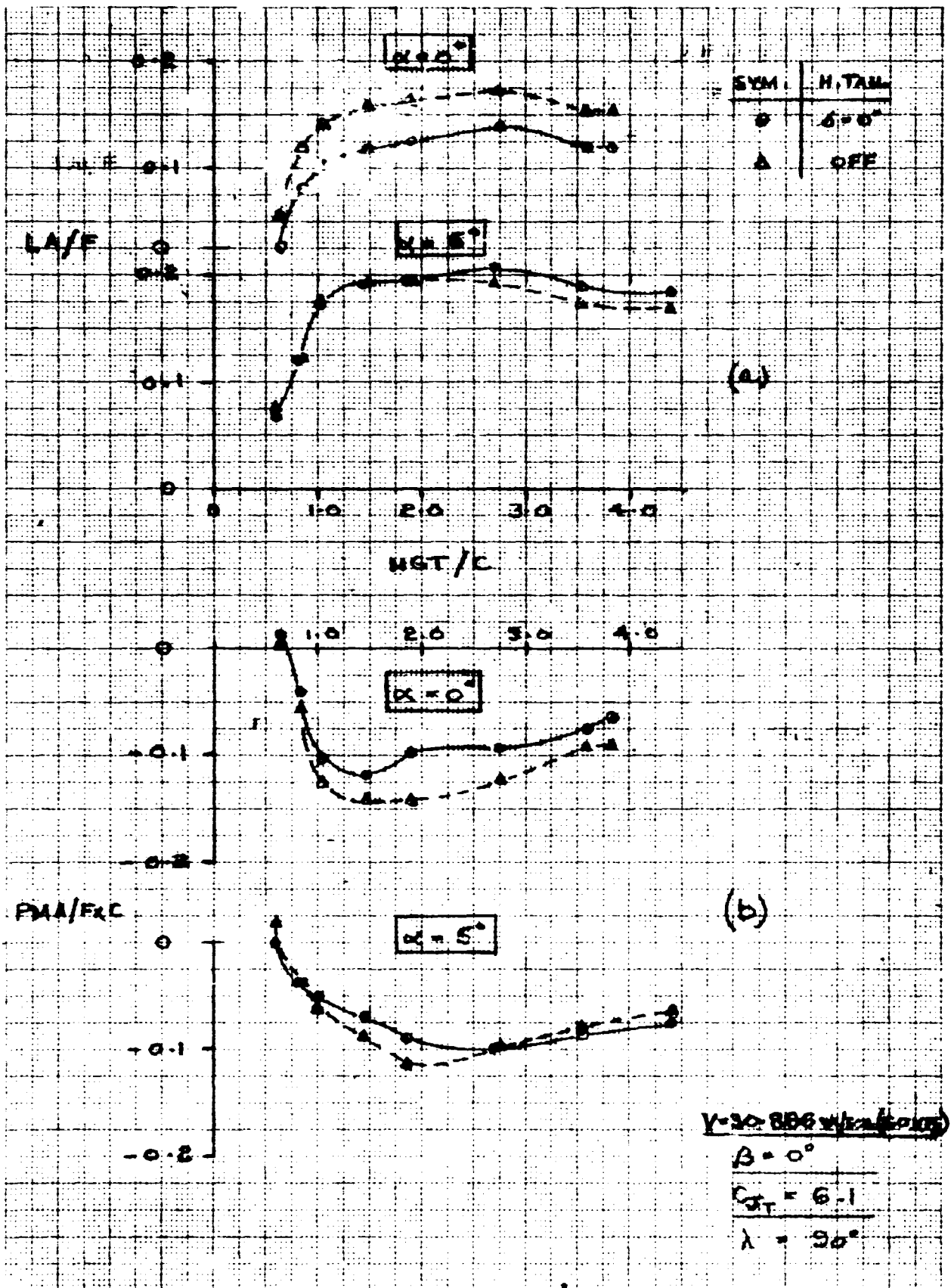
CALC			REVISED	DATE
CHECK				
APR				
APR				

VTOL - IN GROUND EFFECT
EFFECT OF H.TAIL

THE BOEING COMPANY

FIG. 26

PAGE 82



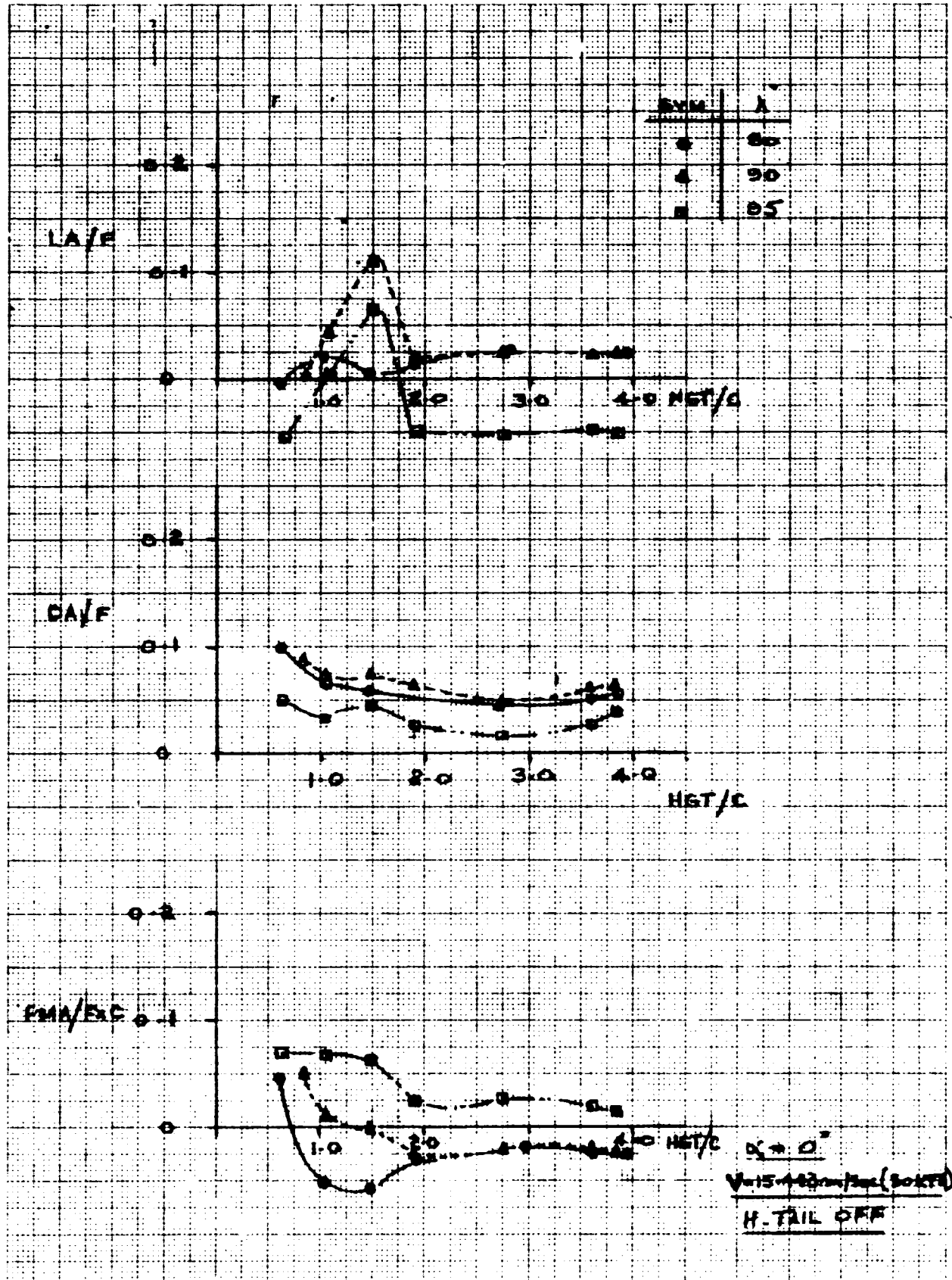
CALC		REVISED	DATE
CHECK			
APR			
APR			

VTOL - IN GROUND EFFECT

EFFECT OF H. TAIL

THE BOEING COMPANY

FIG. 27
PAGE 83



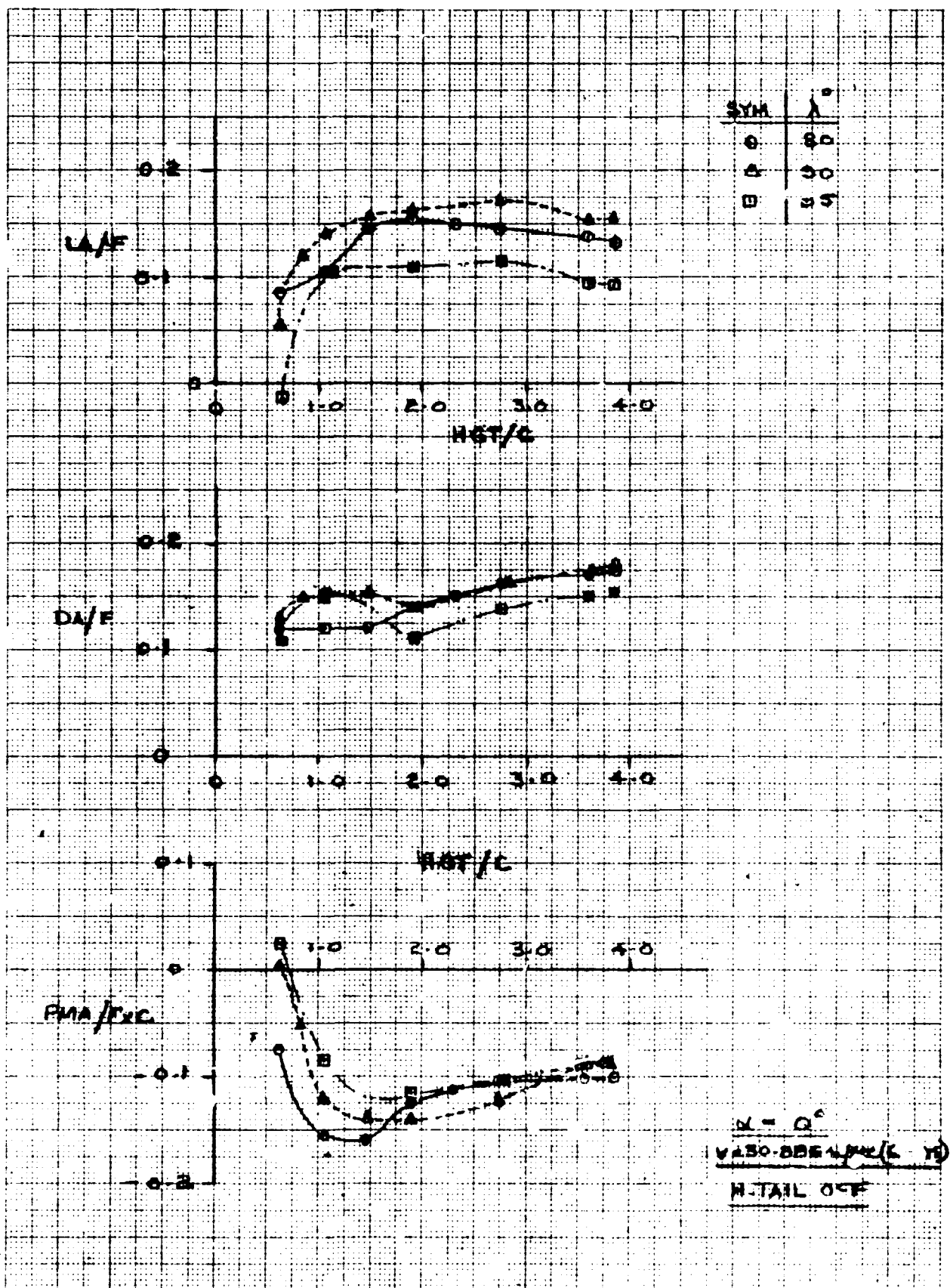
CALC			REVISED	DATE	
CHECK					
APR					
APR					

VTOL - IN GROUND EFFECT
EFFECT OF ENGINE TILT ANGLE

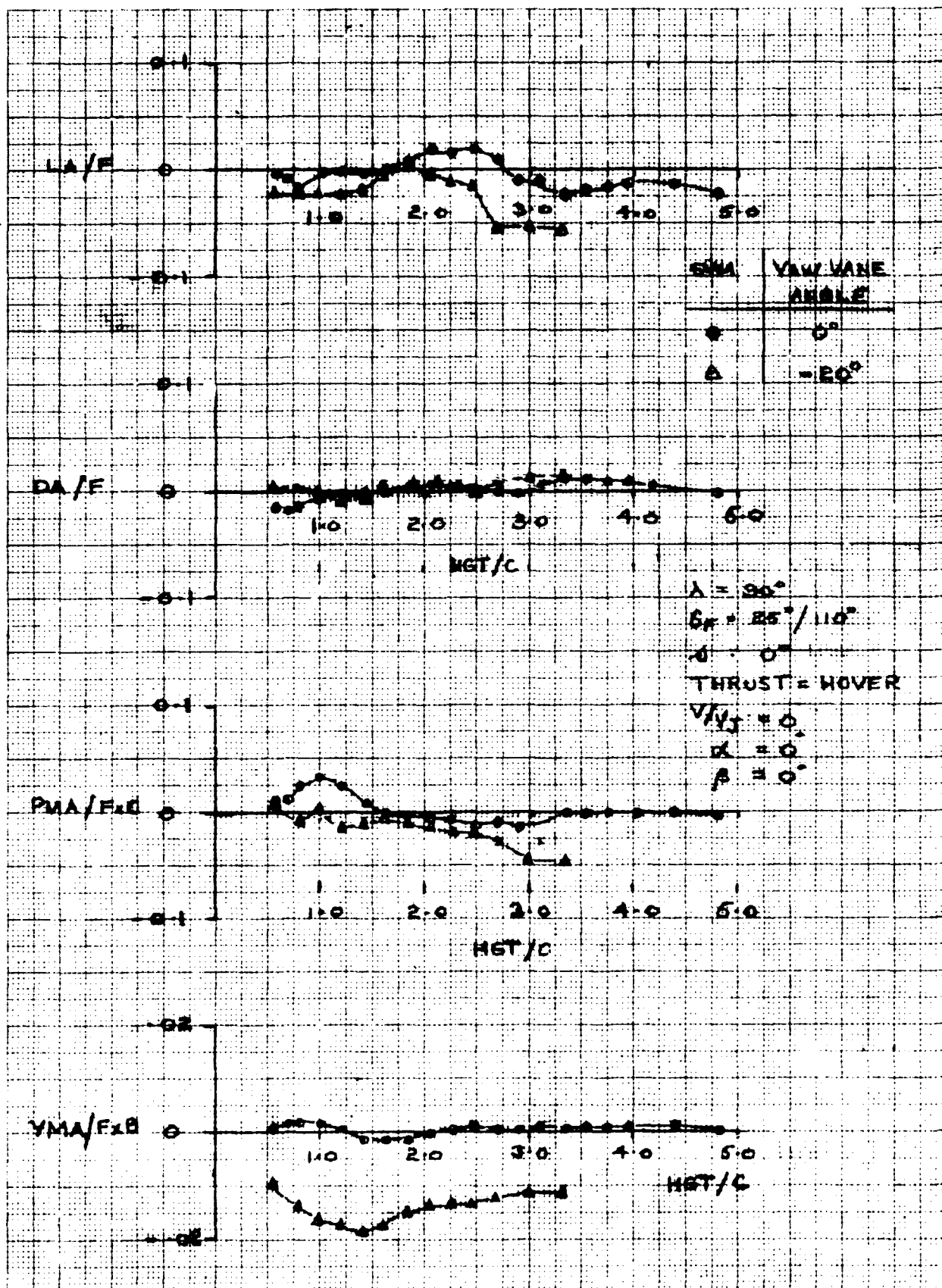
FIG.28

THE BOEING COMPANY

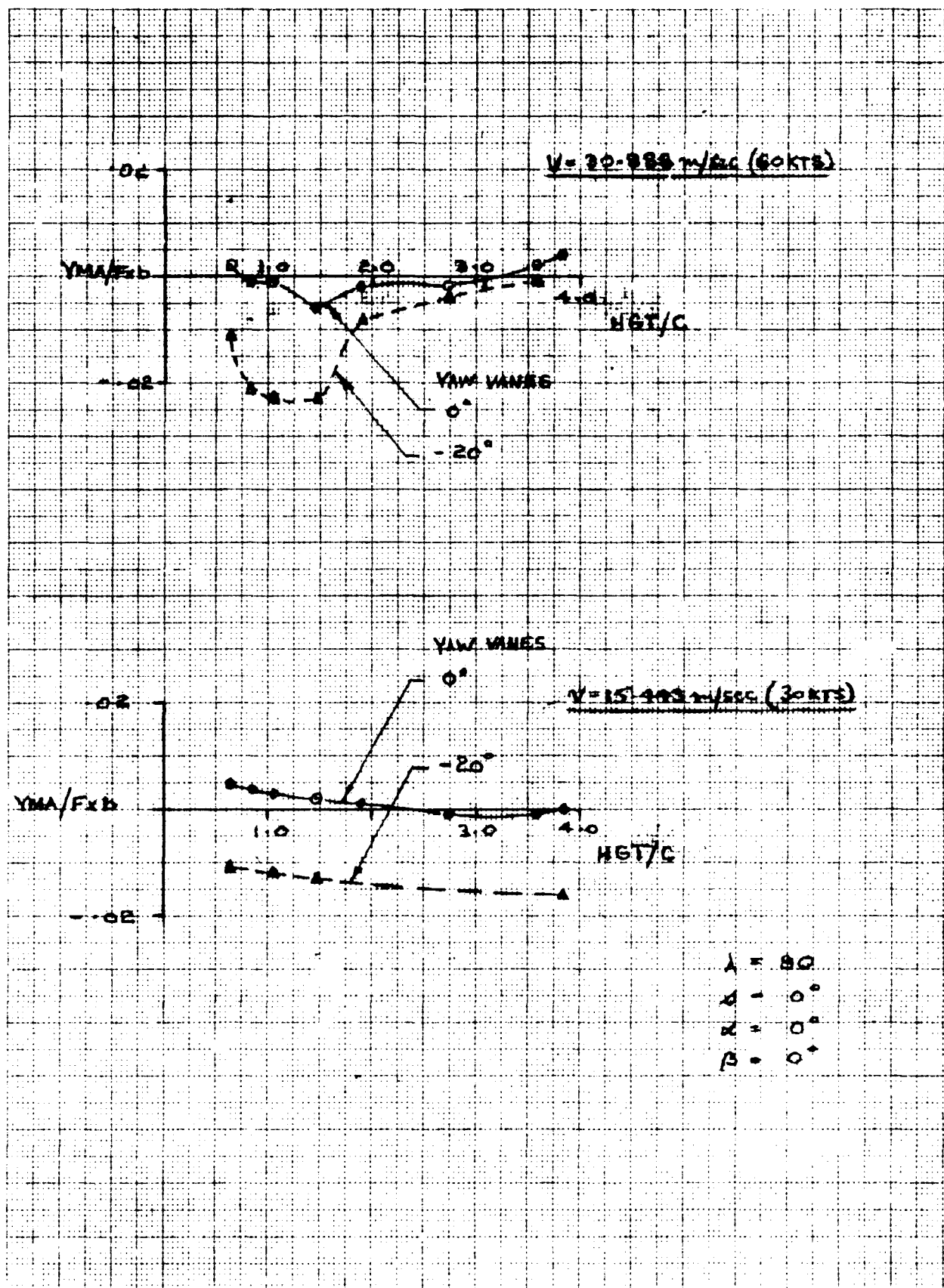
PAGE 84



CALC		REVISED	DATE	V-TOL - IN GROUND E' ECT	FIG. 29
CHECK				EFFECT OF ENGINE TILT ANGLE	
APR				THE BOEING COMPANY	PAGE 85
APR					

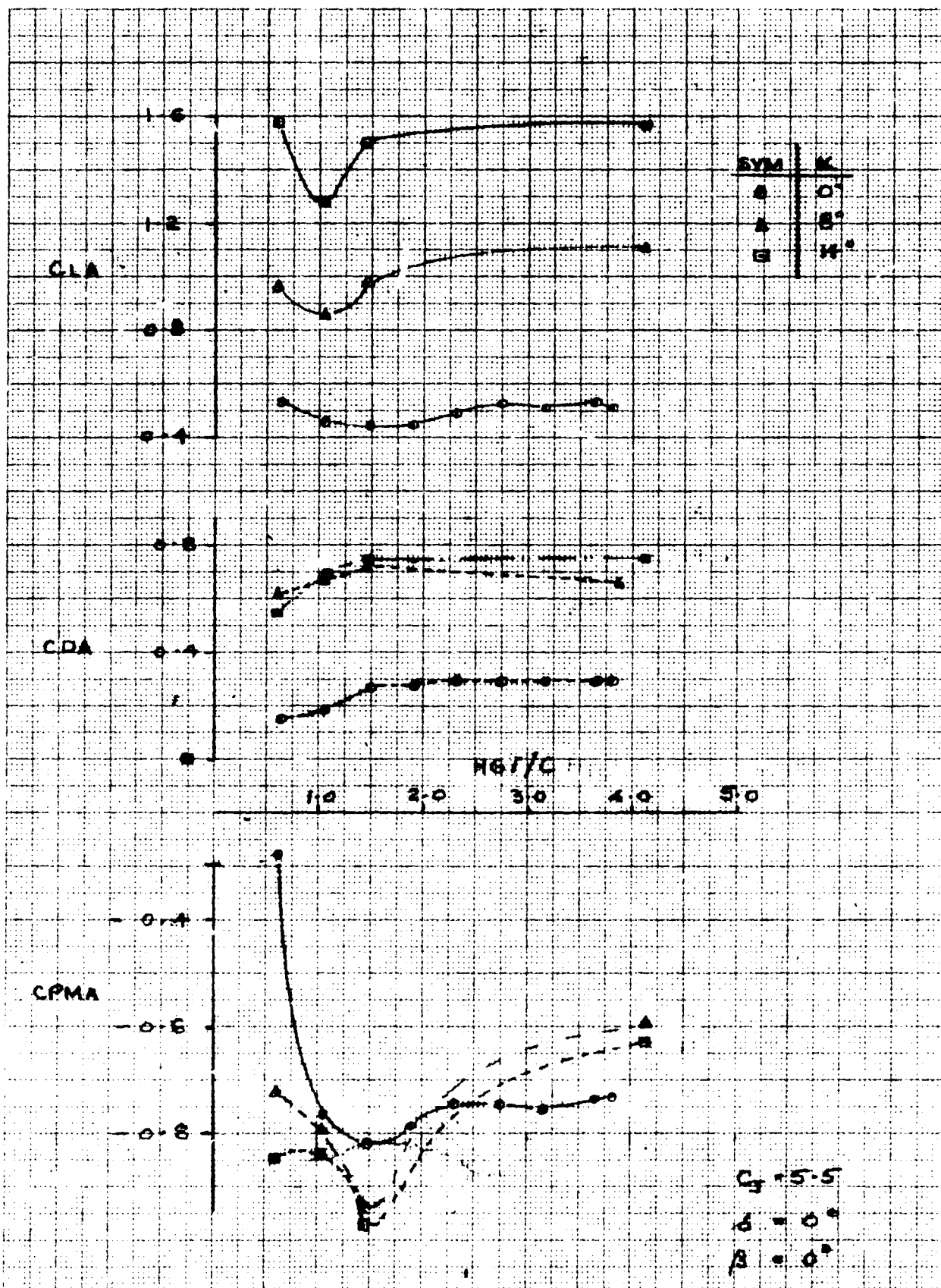


CALC			REVISED	DATE	HOVER - IN GROUND EFFECT YAW VANE EFFECTIVENESS	FIG. 30
CHECK						
APR						
APR						
					THE BOEING COMPANY	PAGE 86



CALC			REVISED	DATE	VTOL - IN GROUND EFFECT YAW VANE EFFECTIVENESS	FIG. 31
CHECK						
APR						
APR						

THE BOEING COMPANY



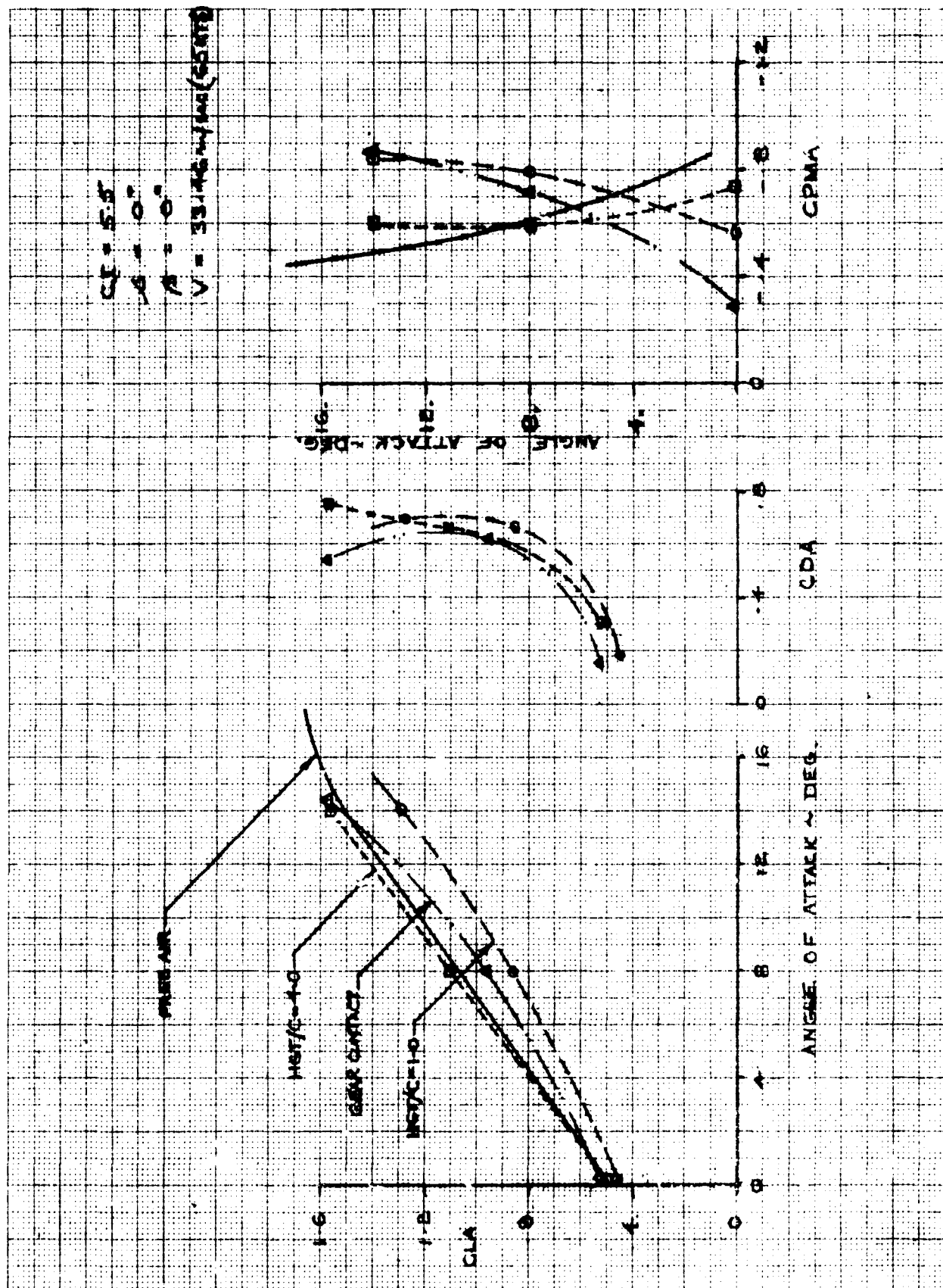
STOL - IN GROUND EFFECT
EFFECT OF ANGLE OF ATTACK

THE BOEING COMPANY

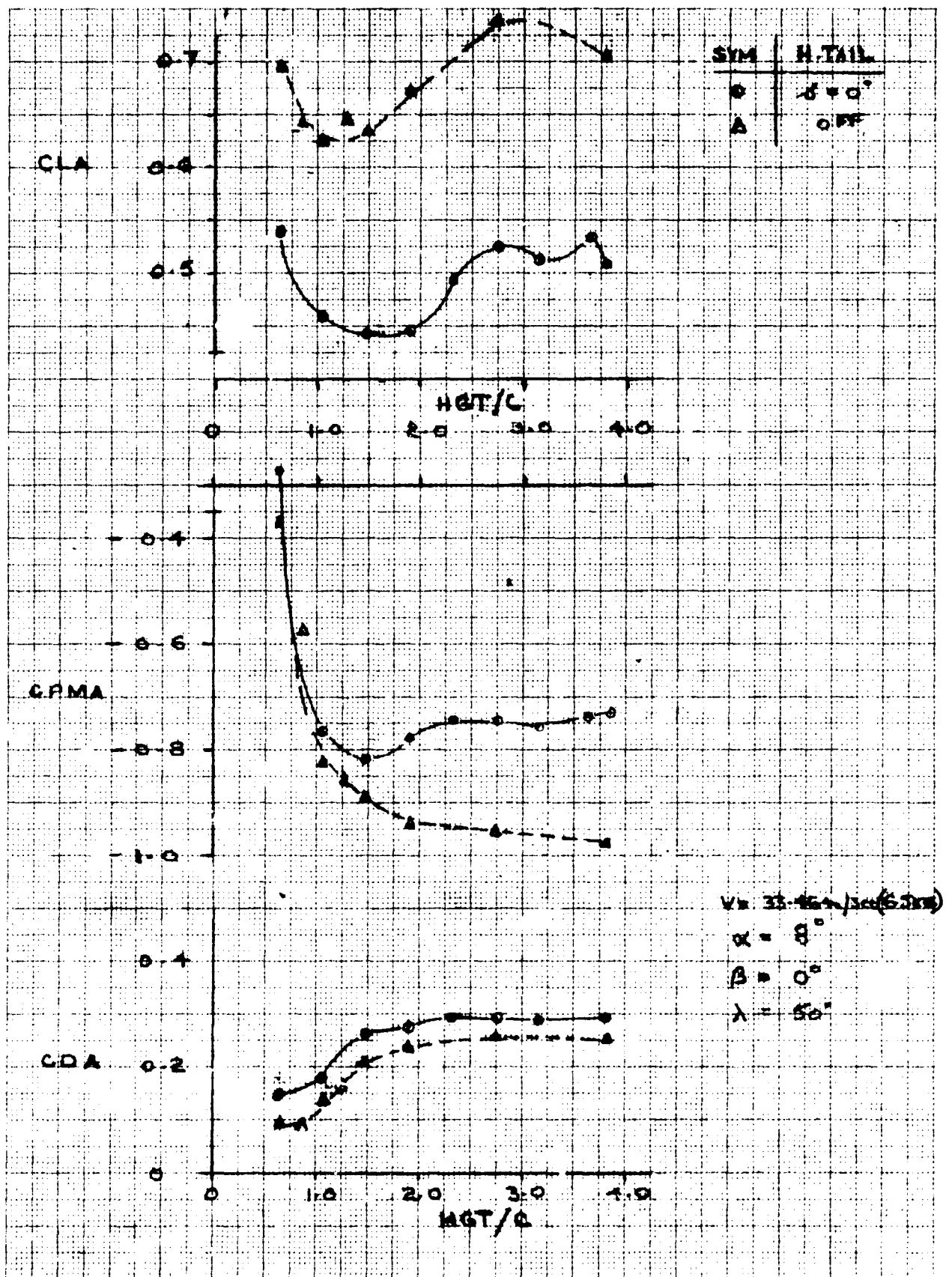
FIG. 32

PAGE 88

CALC	REVISED	DATE
CHECK		
APR		
APR		



CALC		REVISED	DATE	STOL CHARACTERISTICS GROUND EFFECT VS FREE AIR	
CHECK					FIG. 33
APR					PAGE
APR					89
				THE BOEING COMPANY	

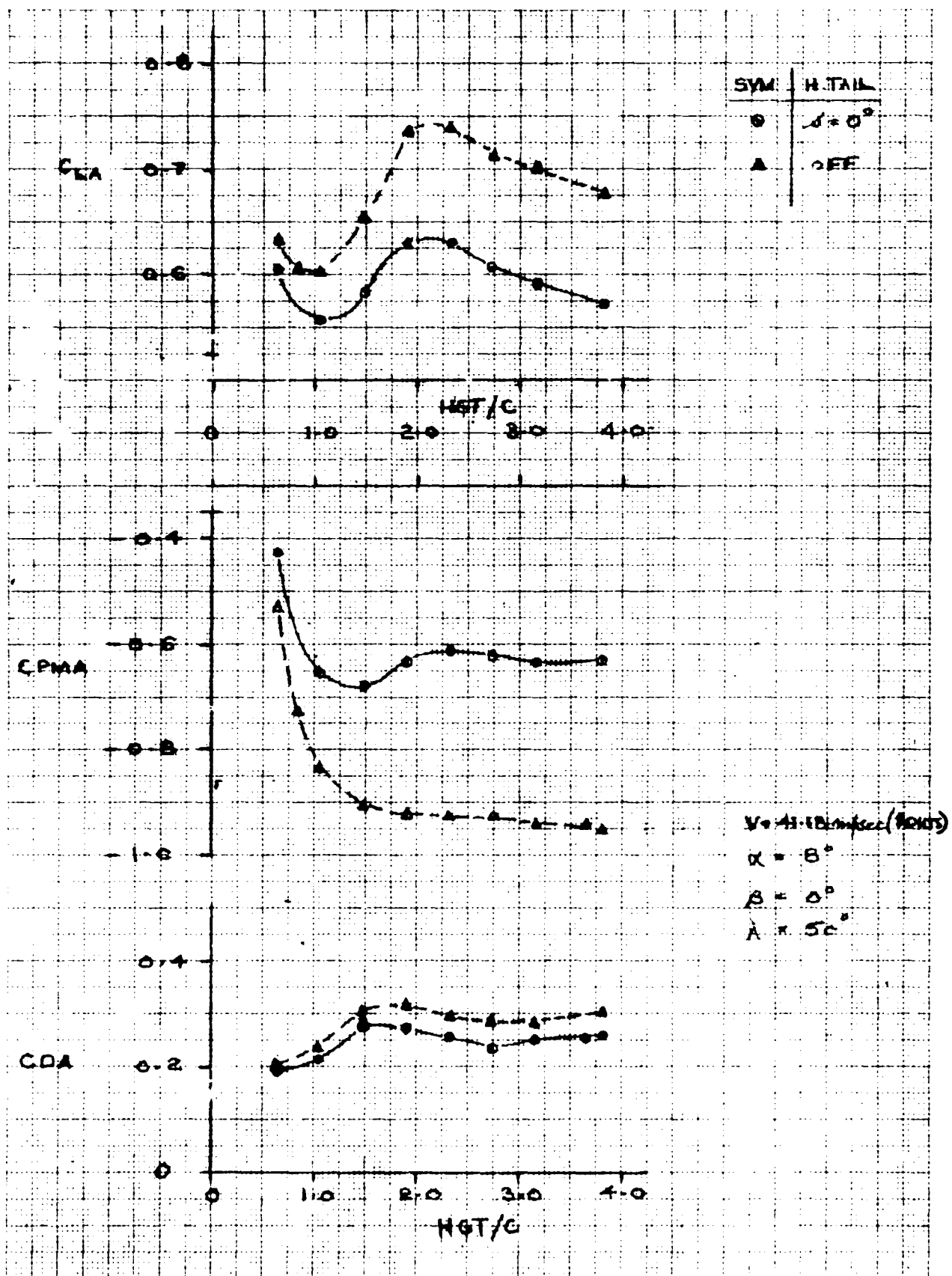


STOL - IN GROUND EFFECT
EFFECT OF H.TAIL $C_J = 5.5$

FIG. 34

THE BOEING COMPANY

PAGE 90

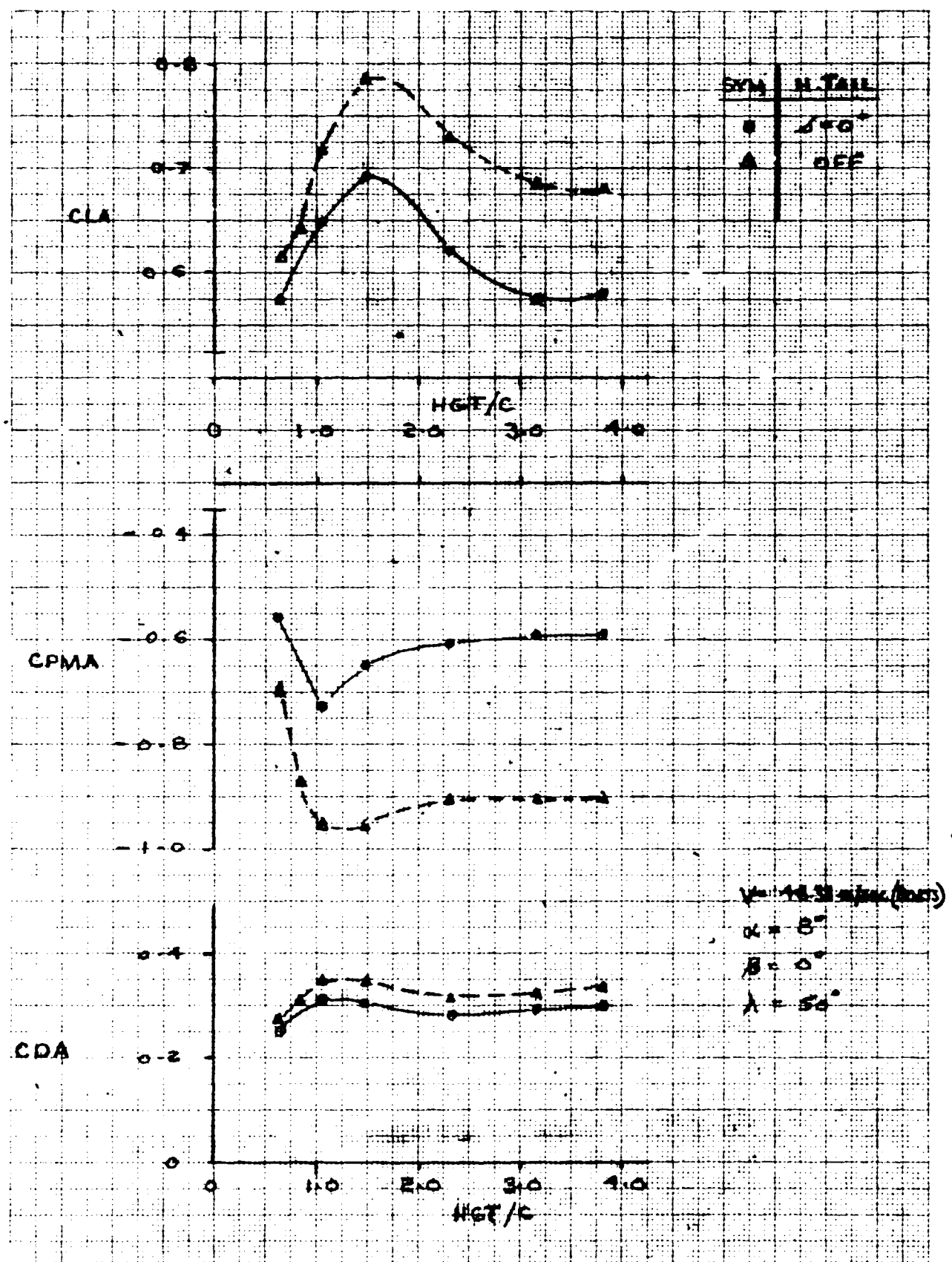


CALC		REVISED	DATE
CHECK			
APR			
APR			

STOL - IN GROUND EFFECT
EFFECT OF H.TAIL $C_J = 3.7$

THE BOEING COMPANY

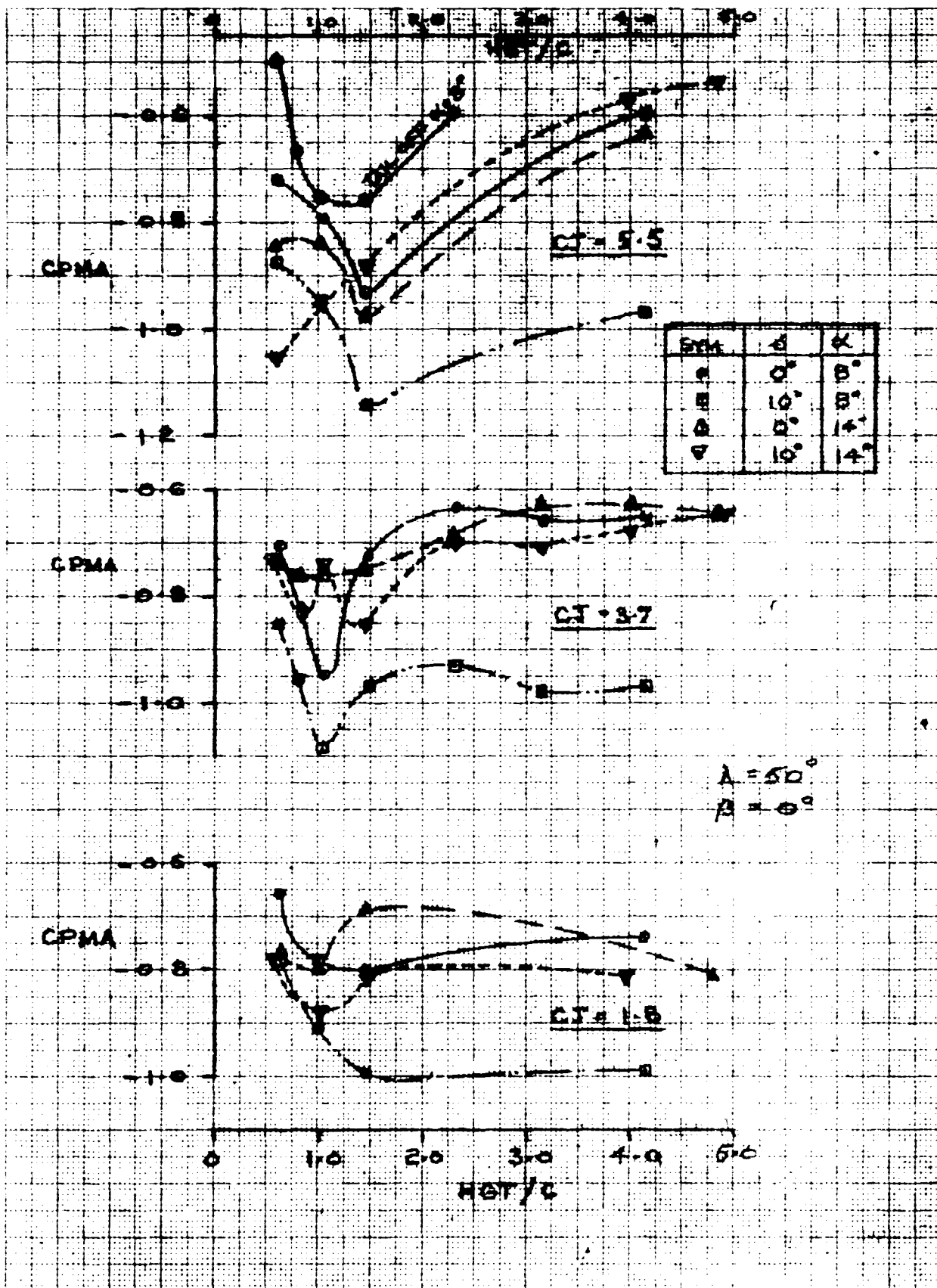
FIG. 35
PAGE 91



CALC			REVISED	DATE	STOL - IN GROUND EFFECT EFFECT OF H.TAIL $C_J = 1.8$	FIG.36
CHECK						
APR						
APR						

THE BOEING COMPANY

PAGE 92



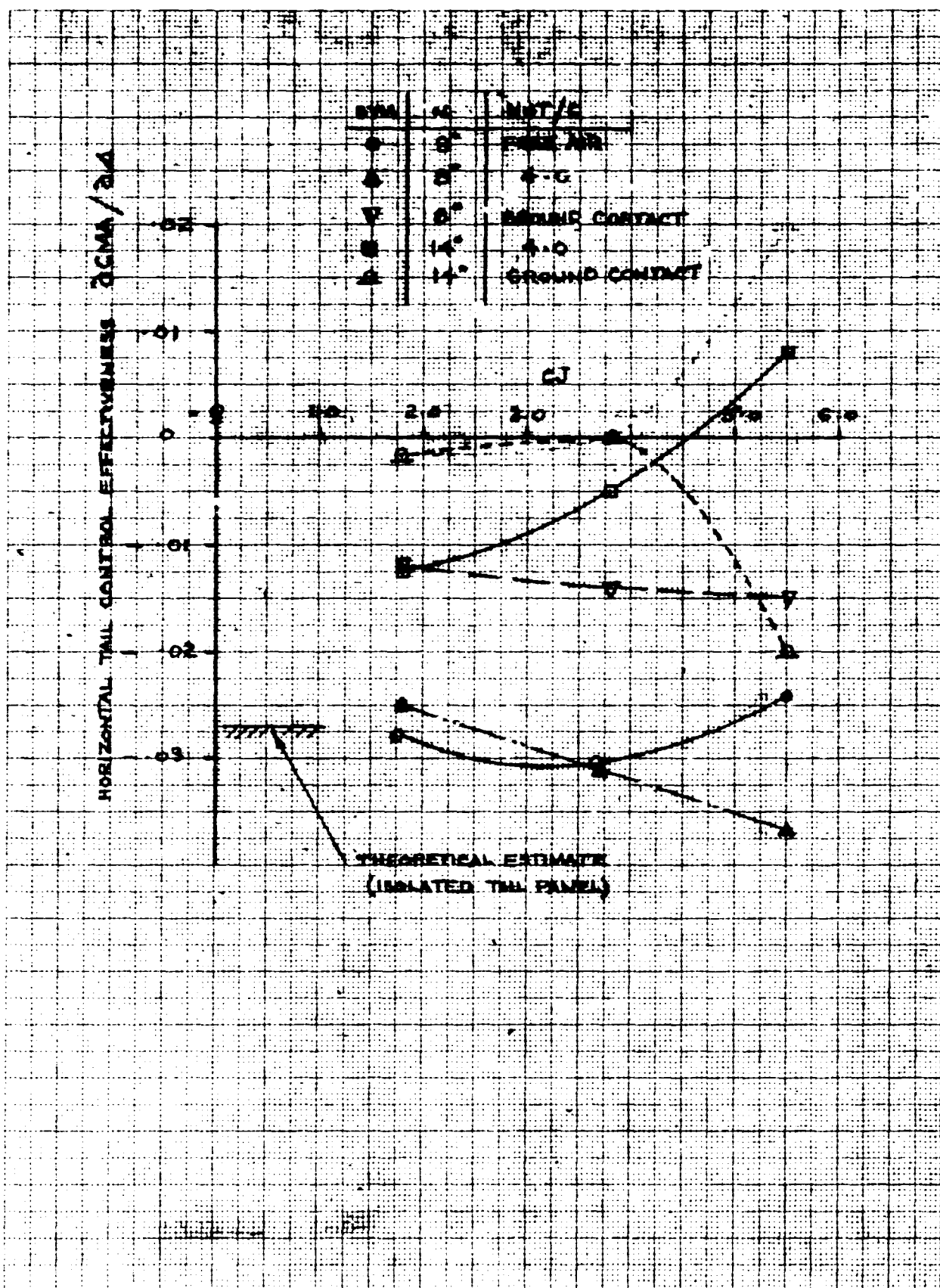
CALC		REVISED	DATE
CHECK			
APR			
APR			

STOL - IN GROUND EFFECT
H-TAIL EFFECTIVENESS

THE BOEING COMPANY

FIG. 37

PAGE 93



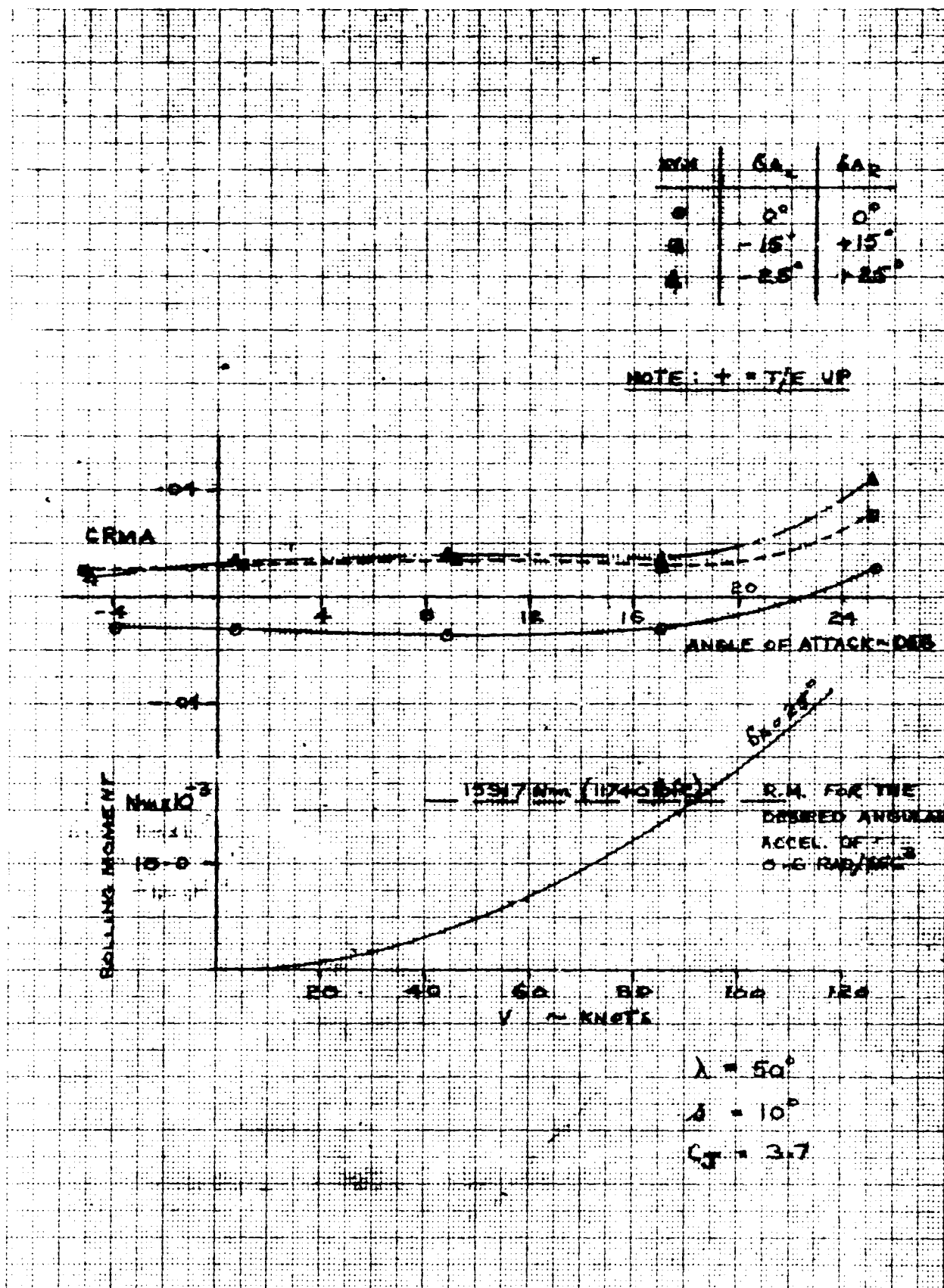
CALC			REVISED	DATE
CHECK				
APR				
APR				

EFFECT OF THRUST ON
H.TAIL EFFECTIVENESS

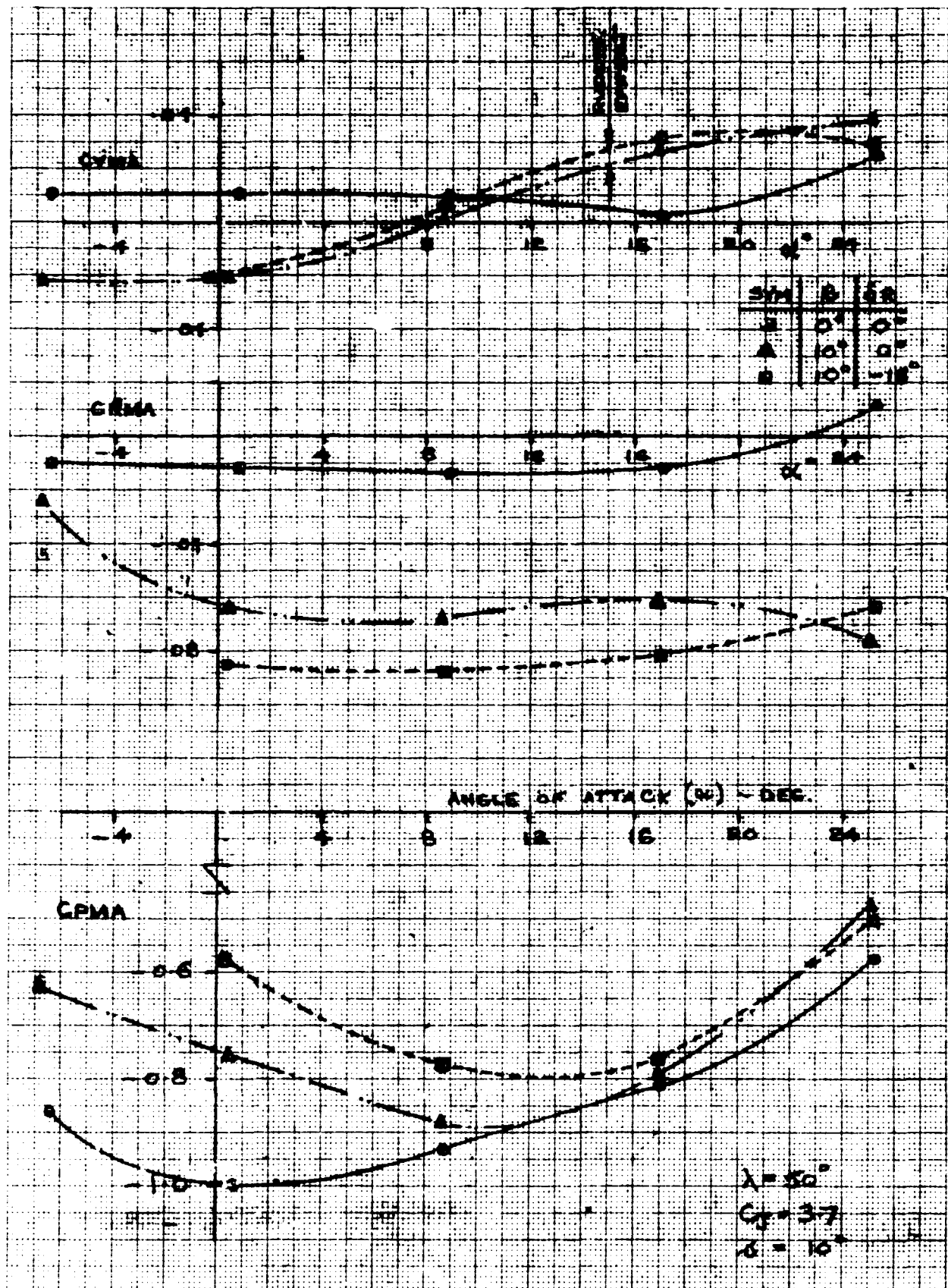
THE BOEING COMPANY

FIG. 38

PAGE 94



CALC		REVISED	DATE	STOL - OUT OF GROUND EFFECT AILERON EFFECTIVENESS	FIG. 39
CHECK					
APR					
APR					
THE BOEING COMPANY				PAGE	95



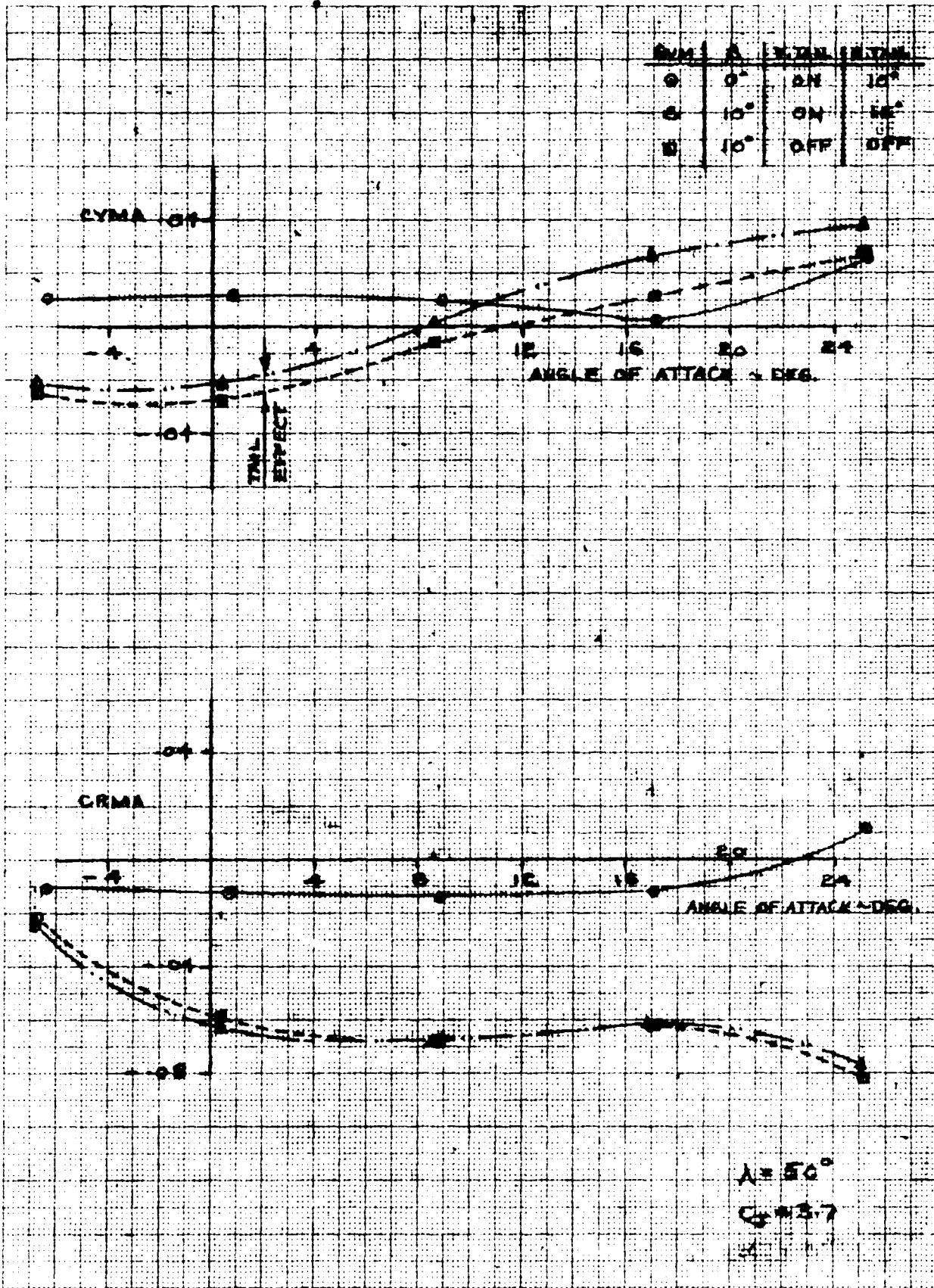
CALC		REVISED	DATE
CHECK			
APR			
APR			

STOL - OUT OF GROUND EFFECT
RUDDER EFFECTIVENESS

FIG. 40

THE BOEING COMPANY

PAGE 96



CALC			REVISED	DATE
CHECK				
APR				
APR				

STOL - OUT OF GROUND EFFECT
VERTICAL TAIL EFFECTIVENESS

FIG. 41

THE BOEING COMPANY

PAGE 97

15412

**REPRODUCIBILITY OF THE
ORIGINAL PAGE IS POOR**

◎ 俗文化研究



REV SYM

OIL FLOW VISUALIZATION OF EMPENNAGE

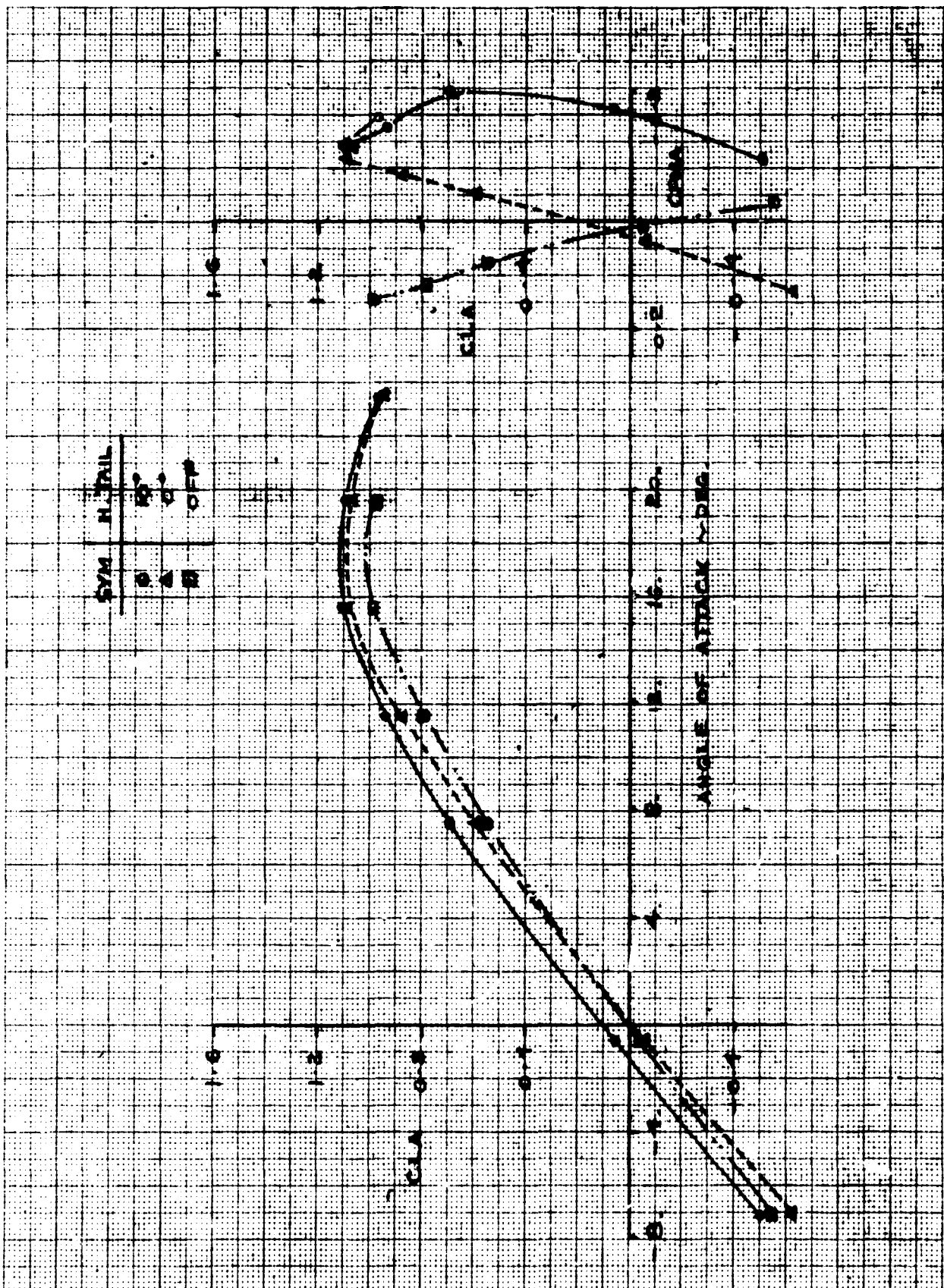
BOEING

NO. FIGURE 42

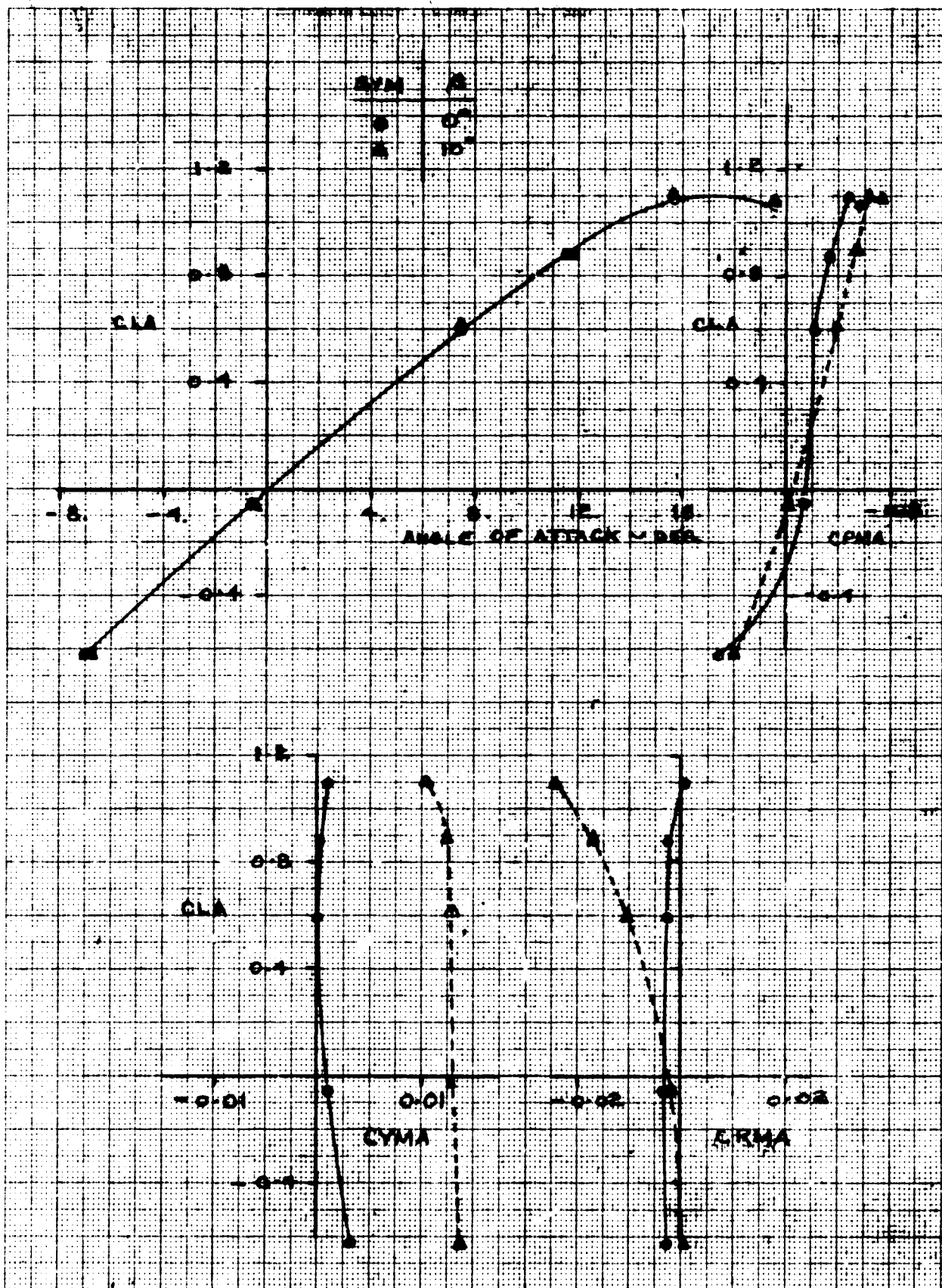
PAGE 98



6x300



CALC		REVISED	DATE	LOITER MODE - NACELLES OFF	
CHECK					FIG.43
APR				EFFECT OF H.TAIL	
APR					
				THE BOEING COMPANY	PAGE 99



CALC		REVISED	DATE	LOITER MODE - NACELLES OFF EFFECT OF SIDESLIP	FIG. 44
CHECK					
APR					
APR					
THE BOEING COMPANY		PAGE	100		

APPENDIX

Computer-Plotted Test Data

This appendix contains plots of all valid data runs obtained during wind tunnel testing under IR&D. The plots consist of the following:

In Ground Effect

LA/F vs HGT/C

DA/F vs HGT/C

PMA/F vs HGT/C

YMA/F vs HGT/C

RMA/F vs HGT/C

SFA/F vs HGT/C

} Asymmetric runs only

Out of Ground Effect

CLA vs ALPHA

CDA vs CLA

CDA vs ALPHA

CPMA vs ALPHA

CYMA vs ALPHA

CRMA vs ALPHA

CSFA vs ALPHA

} Asymmetric runs only

The aerodynamic data presented in this section contains propulsion induced effects; the direct thrust, ram and tunnel interference effects have been removed. A discussion of the method used in making these adjustments is provided in Reference 1.

Model Nomenclature

The plots in this appendix contain a shorthand notation to designate the specific model configuration. This notation is defined as follows:

- C1 Trailing edge flaps deflected
 Trailing edge flap door down
 Leading edge slat extended
 Nose fan doors in open position (both upper & lower)
 Basic nacelles and nacelle - fuselage fairings installed
- C2 Same as C1 except trailing edge flap door is up
(i.e., it is aligned with the basic trailing
edge flap)
- C3 Trailing edge flaps deflected
 Trailing edge flap door up
 Leading edge slat extended
 Nose fan doors in closed position (both upper & lower)
 Basic nacelles and nacelle - fuselage fairings installed
- C4 Trailing edge flaps & flap door nested
 Leading edge slat nested
 Nose fan doors in closed position (both upper & lower)
 Basic nacelles and nacelle - fuselage fairings installed
- C5 The lift/cruise nacelles and the portion of the nacelle -
 fuselage fairing attached to the nacelles are removed from
 the model. The resulting cavities on the body sides are
 taped over for a smooth fairing.
 Nose fan doors in closed position
 Leading edge slat nested
 Trailing edge flap position as noted by "F" designation
- G Main and nose landing gear and landing gear doors installed

THE **BOEING** COMPANY

V Vertical tail installed

H Horizontal tail installed

F25/25 Trailing edge flap deflected
 Trailing edge flap door aligned with flap

F25/110 Trailing edge flap deflected
 Trailing edge flap door down

Note: C1 thru C5 do not have tail surfaces and gear installed
unless followed by the appropriate symbols,

Example: C1GVH is C1 with gear, vertical tail and horizontal tail
installed.

INDEX OF FIGURES IN THE APPENDIX

<u>FIGURE NUMBER</u>	<u>TITLE</u>	<u>PAGE</u>
<u>VTOL - IN GROUND EFFECT</u>		
Effect of Horizontal Tail		
1	V = 60KTS ALPHA = 0°	107-109
2	V = 60KTS ALPHA = 5°	110-112
3	V = 30KTS ALPHA = 5°	113-115
4	Effect of Beta V = 60KTS	116-119
Effect of Differential Thrust		
5	V = 60KTS BETA = 0°	120-123
6	V = 30KTS BETA = 0°	124-127
7	V = 60KTS BETA = 10°	128-131
8	V = 30KTS BETA = 10°	132-135
9	Effect of Yaw Vanes + Diff. Thrust	136-139
10	Effect of Yaw Vanes	140-143
11	Effect of Engine Tilt Angle V = 60KTS	144-147
12	Effect of Engine Tilt Angle V = 30KTS	148-151

STOL - IN GROUND EFFECT

PAGE

Effect of Horizontal Tail

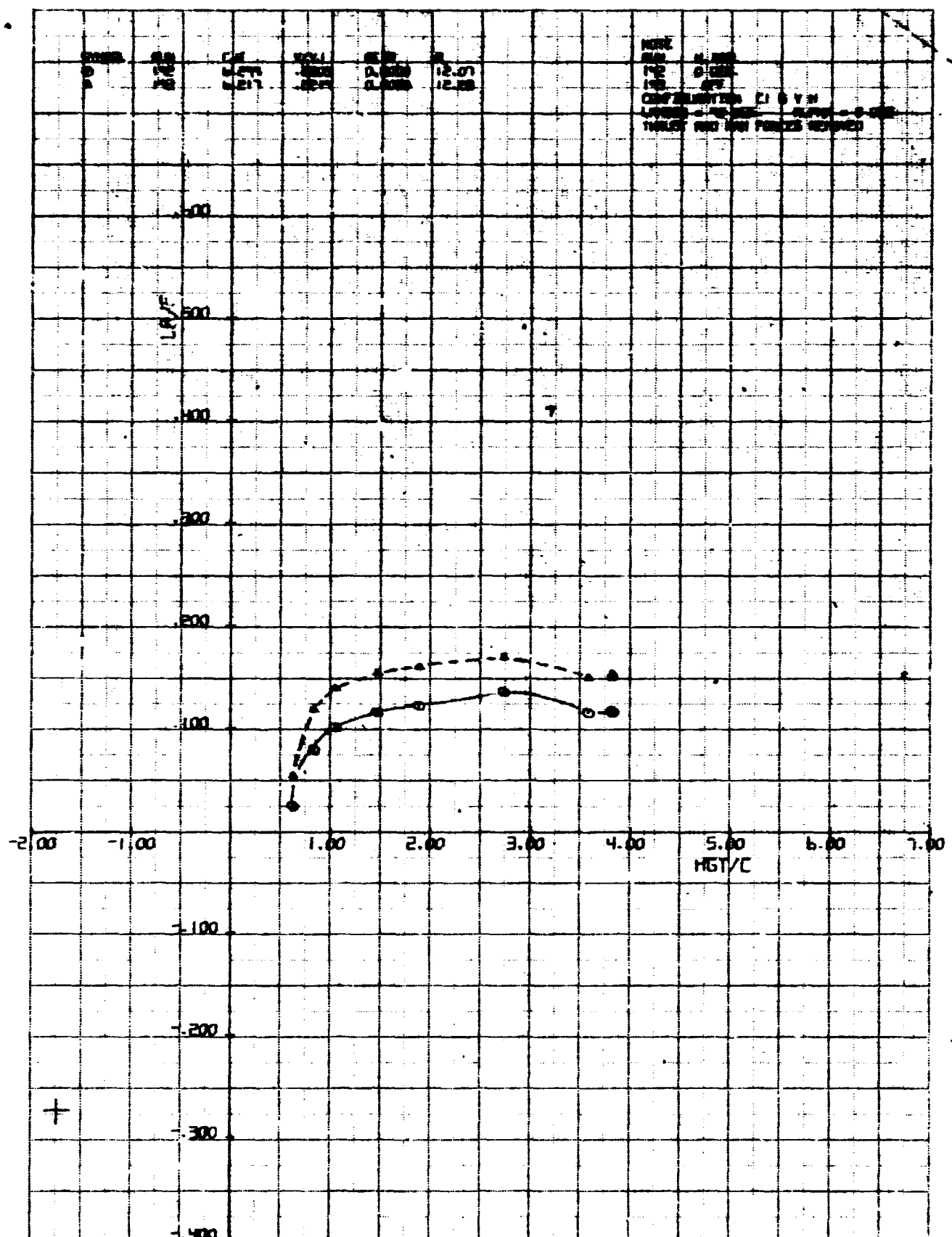
13	CJ = 1.8 ALPHA = 0°	152-154
14	CJ = 3.7 ALPHA = 0°	155-157
15	CJ = 5.5 ALPHA = 0°	158-160
16	CJ = 1.8 ALPHA = 8°	161-163
17	CJ = 3.7 ALPHA = 8°	164-166
18	CJ = 5.5 ALPHA = 8°	167-169
19	CJ = 1.8 ALPHA = 14°	170-172
20	CJ = 3.7 ALPHA = 14°	173-175
21	CJ = 5.5 ALPHA = 14°	176-178
22	Effect of Angle of Attack Tail-off	179-181
23	Effect of Angle of Attack Tail-on	182-184

STOL - OUT OF GROUND EFFECT

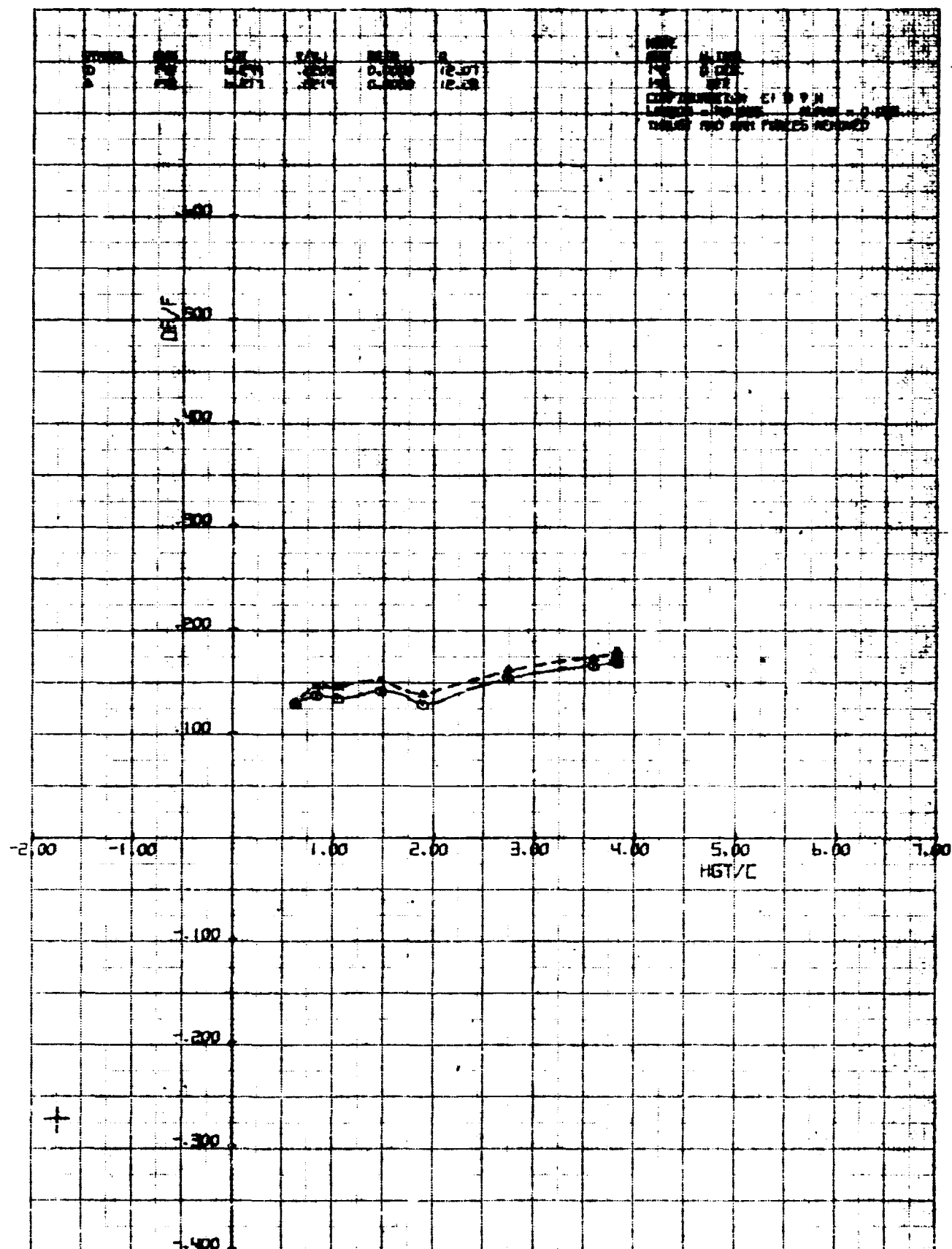
24	Rudder Effectiveness	185-191
25	Aileron Effectiveness	192-198
26	Vertical Tail Effectiveness	199-205

CRUISE CONFIGURATION, NACELLES OFF - OUT OF GROUND EFFECT

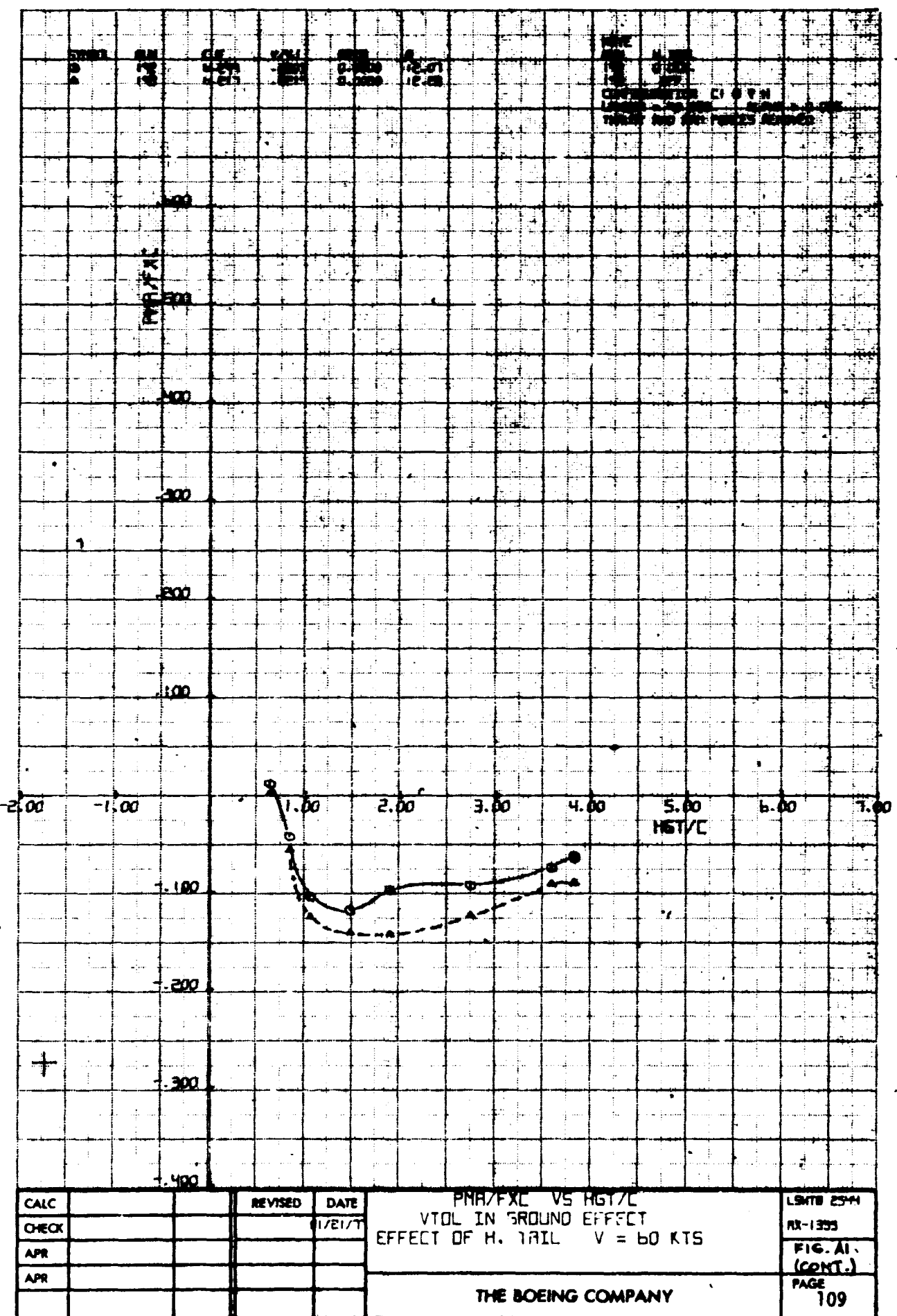
27	Effect of Horizontal Tail	206-208
28	Effect of Sideslip	209-215



TD 4610	THE BOEING COMPANY	PAGE 107
---------	--------------------	-------------



CALC	REVISED	DATE	DR/P VS HGT/C VTOL IN GROUND EFFECT EFFECT OF H. TAIL V = 60 KTS	LMTB 254 MR-1333 FIG 1A (CONT'D)
CHECK		1/21/71		
APR				
APR				
			THE BOEING COMPANY	PAGE 108



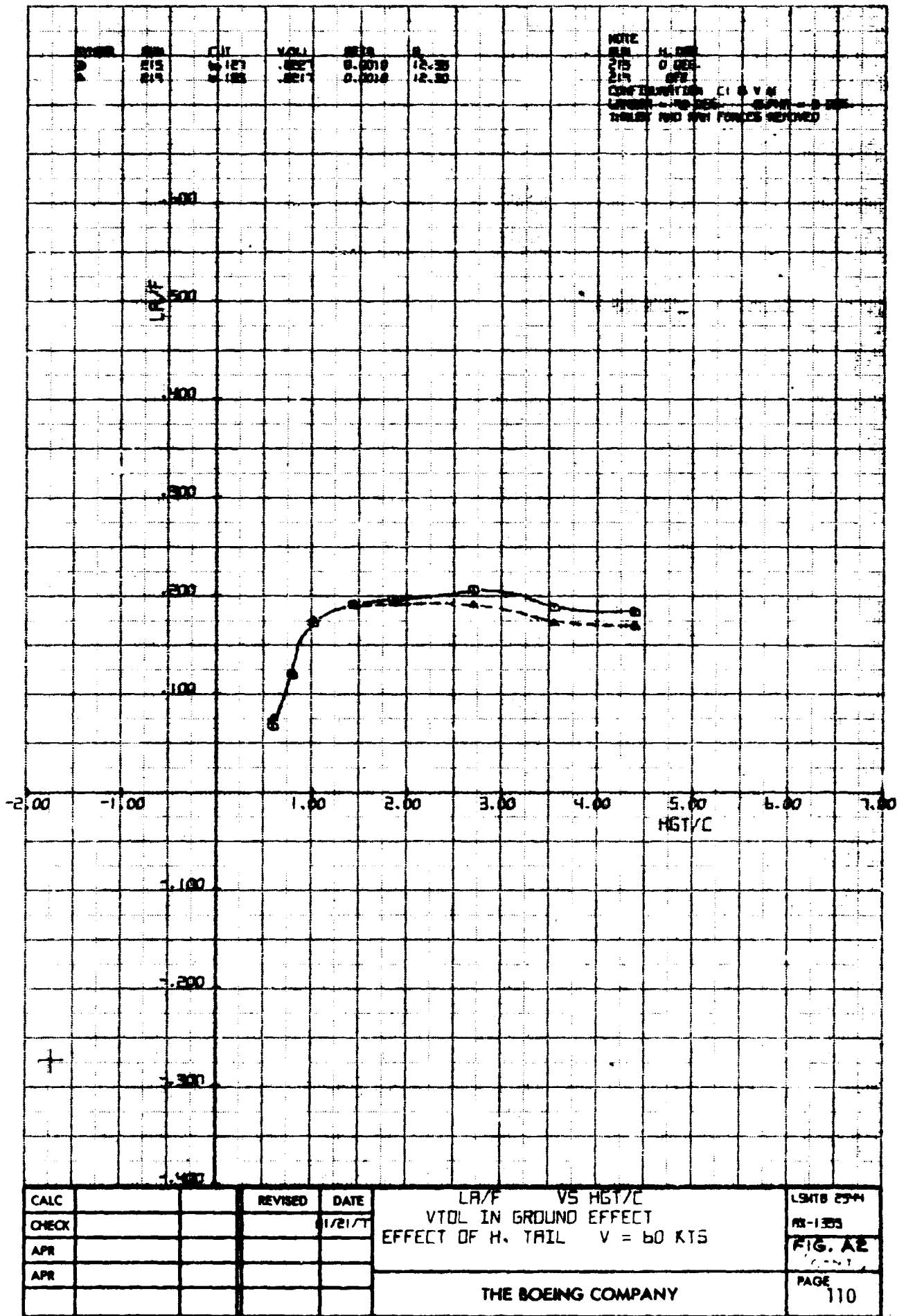


FIG 19
b.

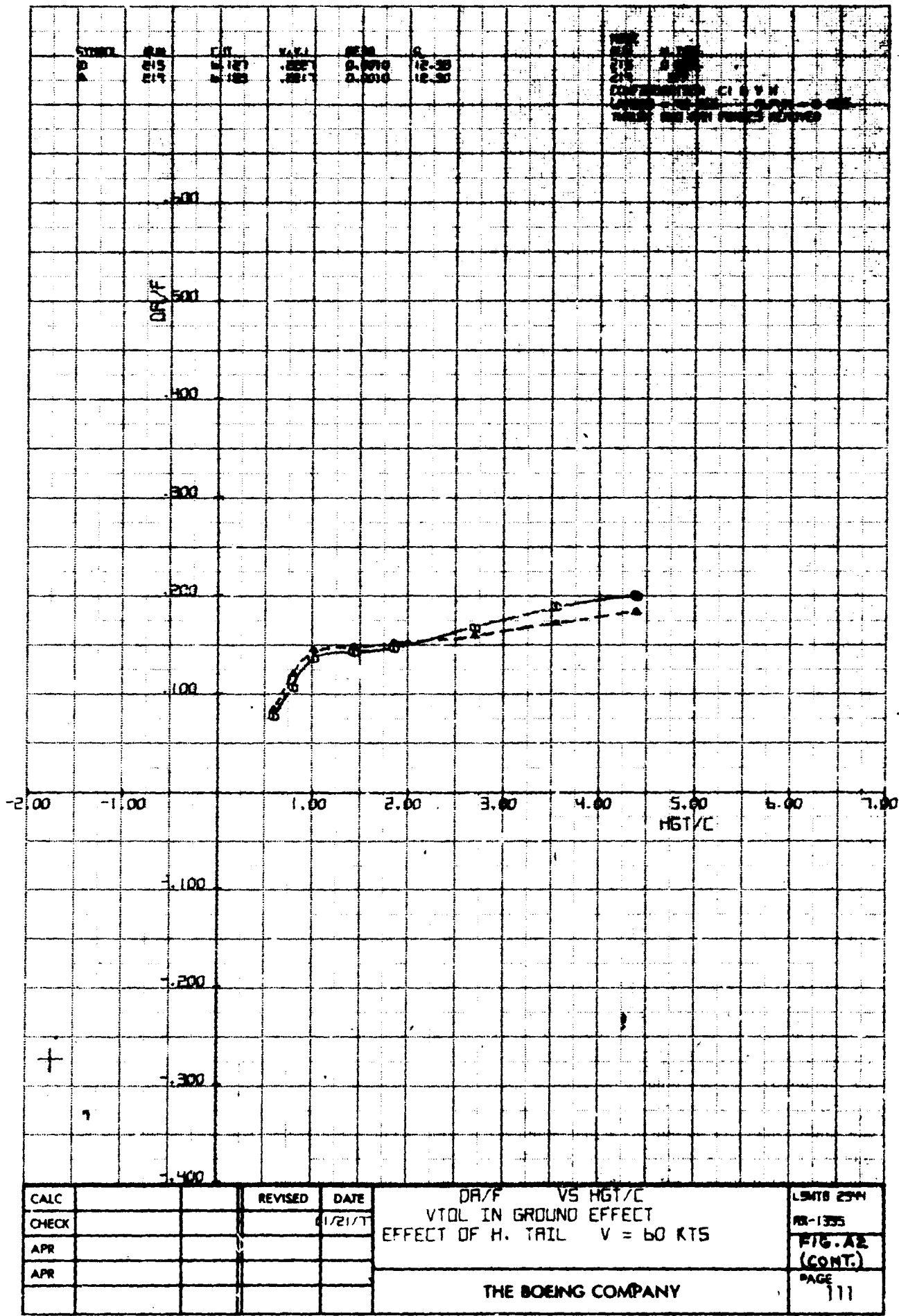
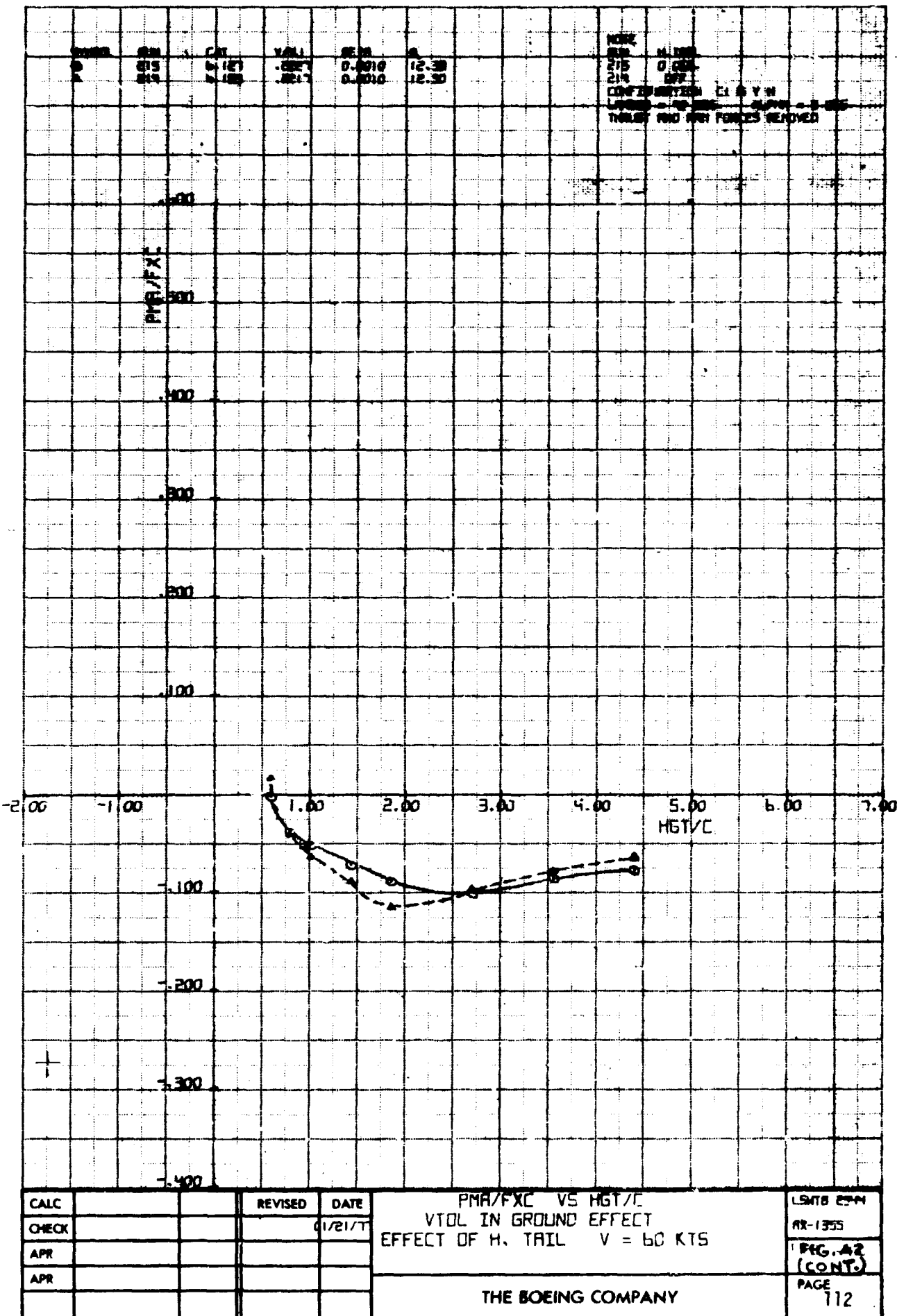
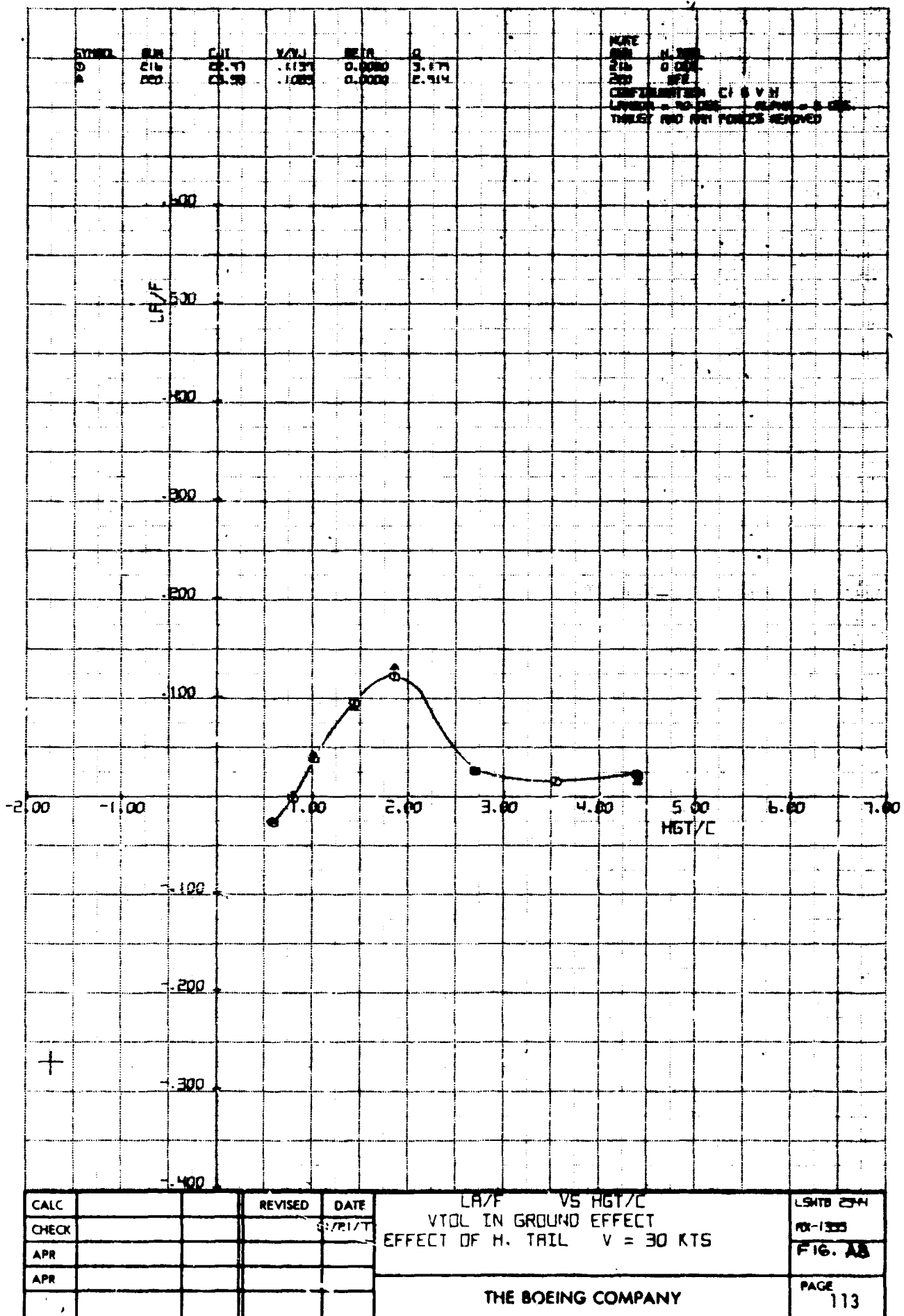
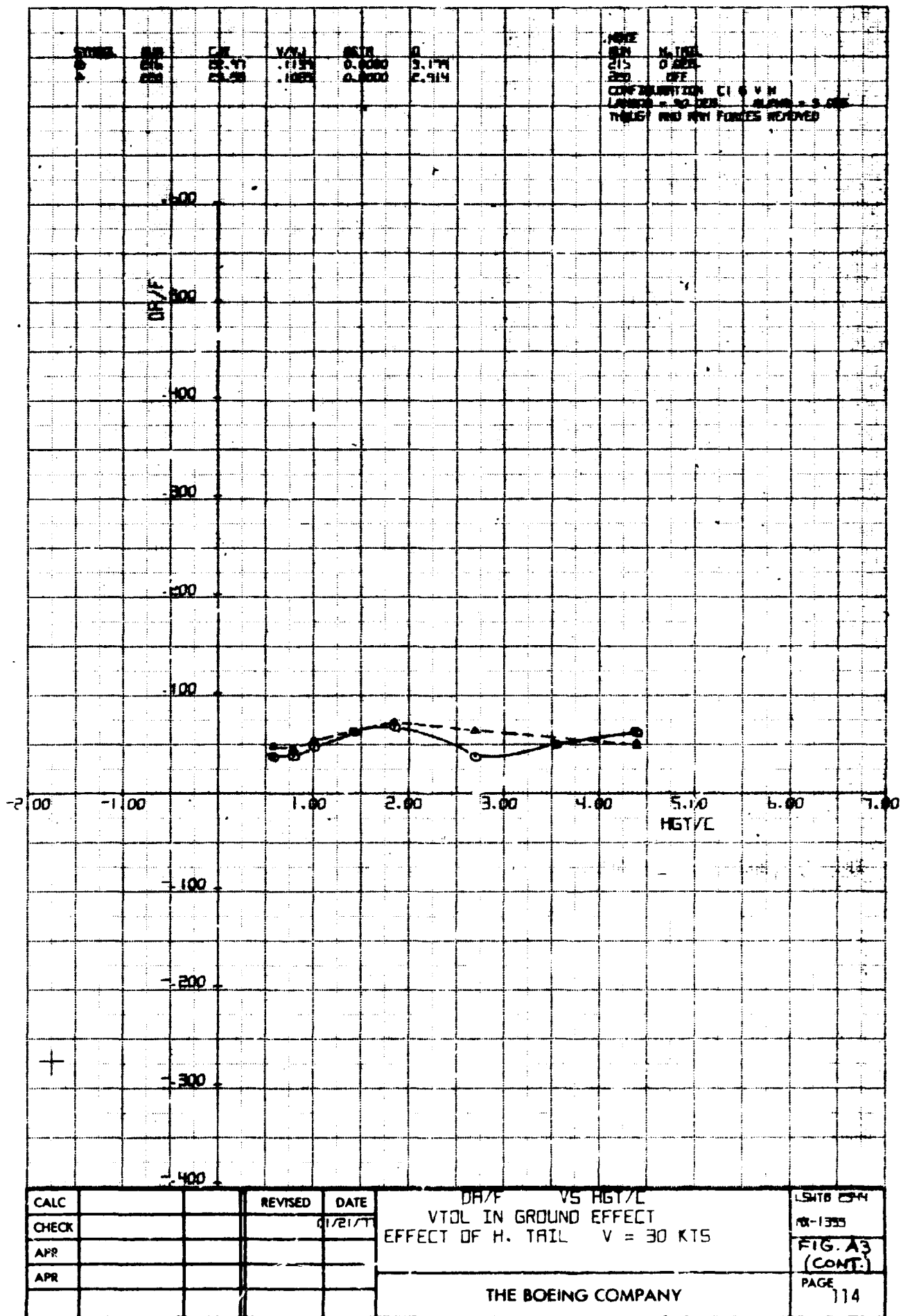
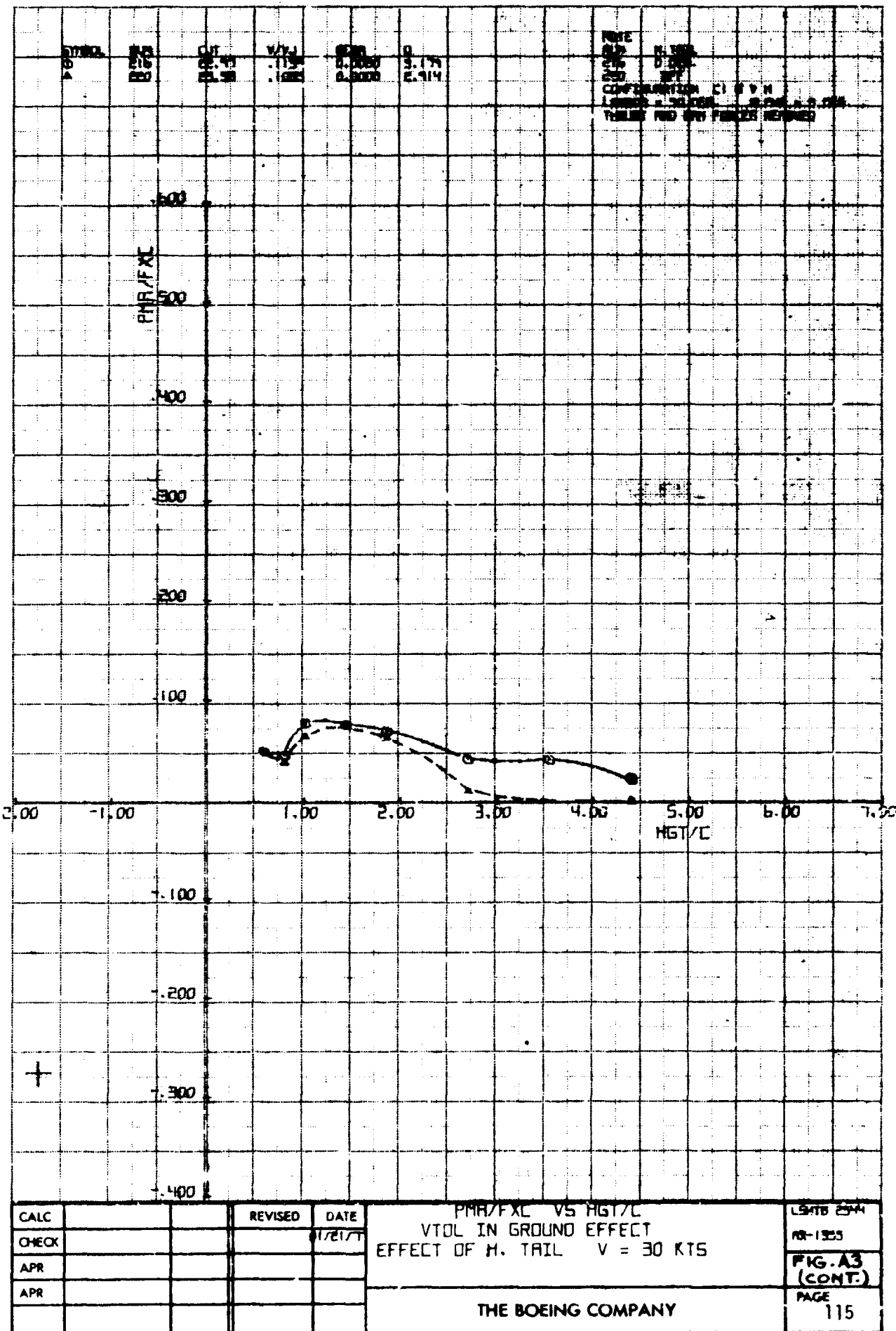


FIG 19
4.









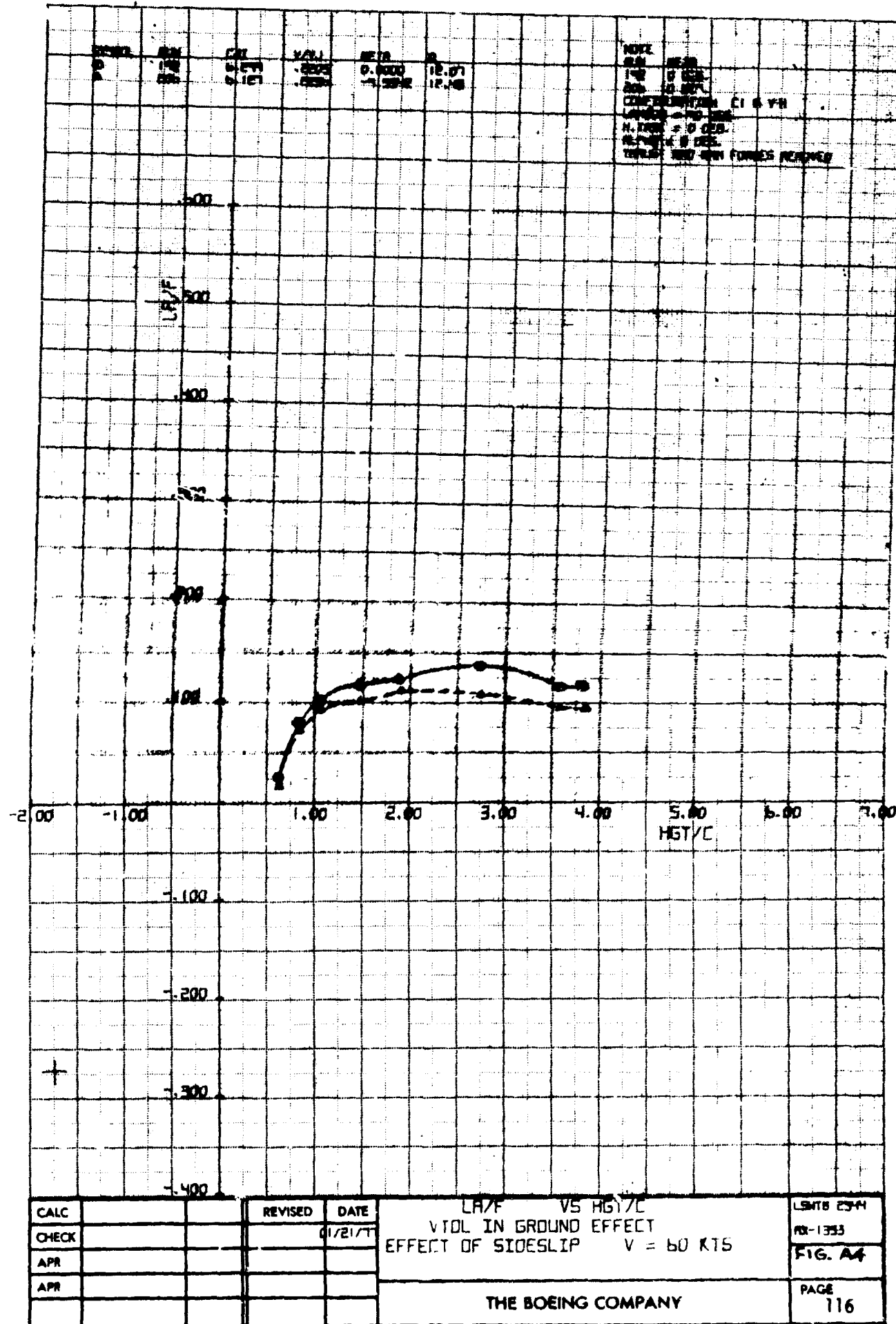


FIG 25
15.

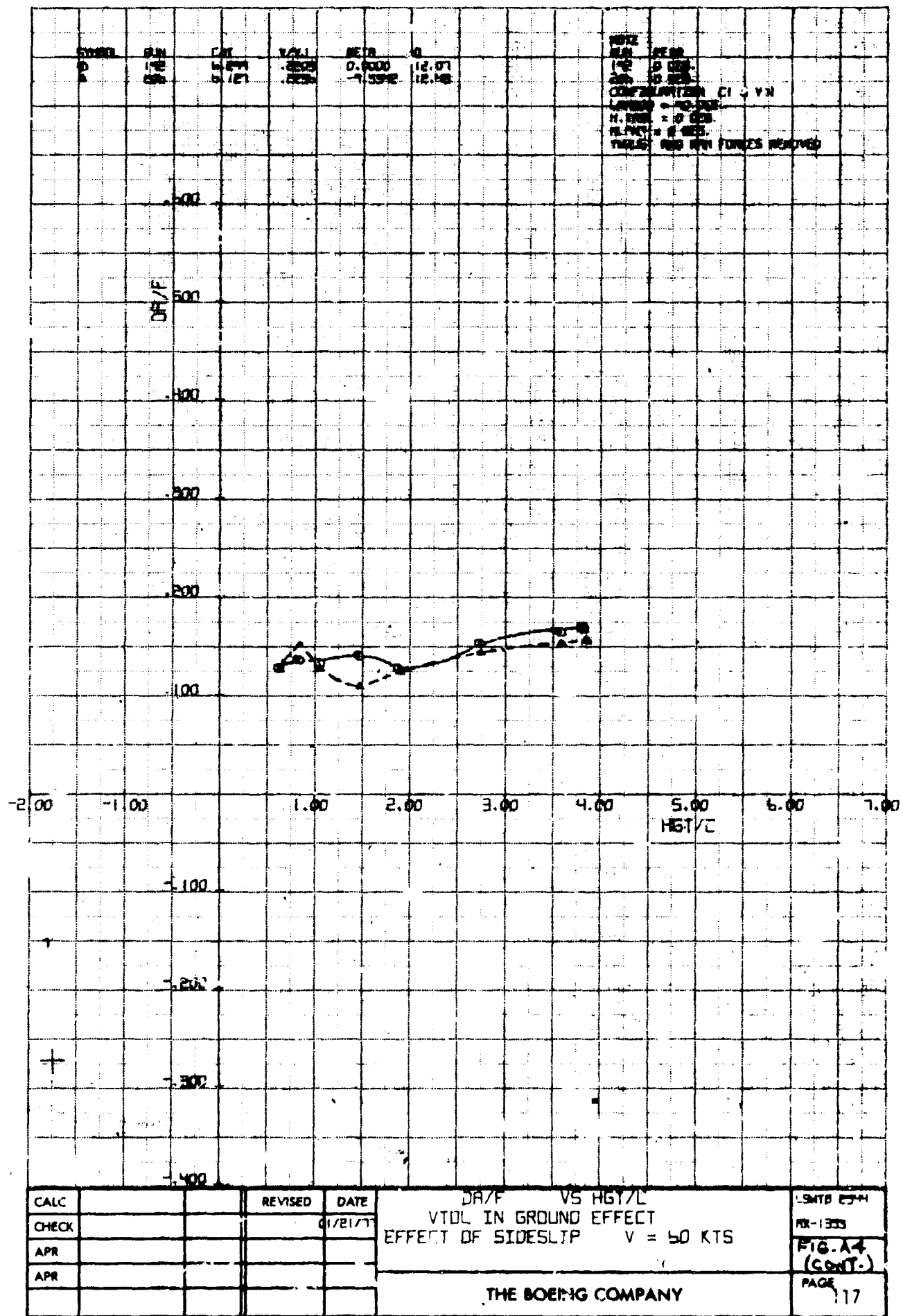
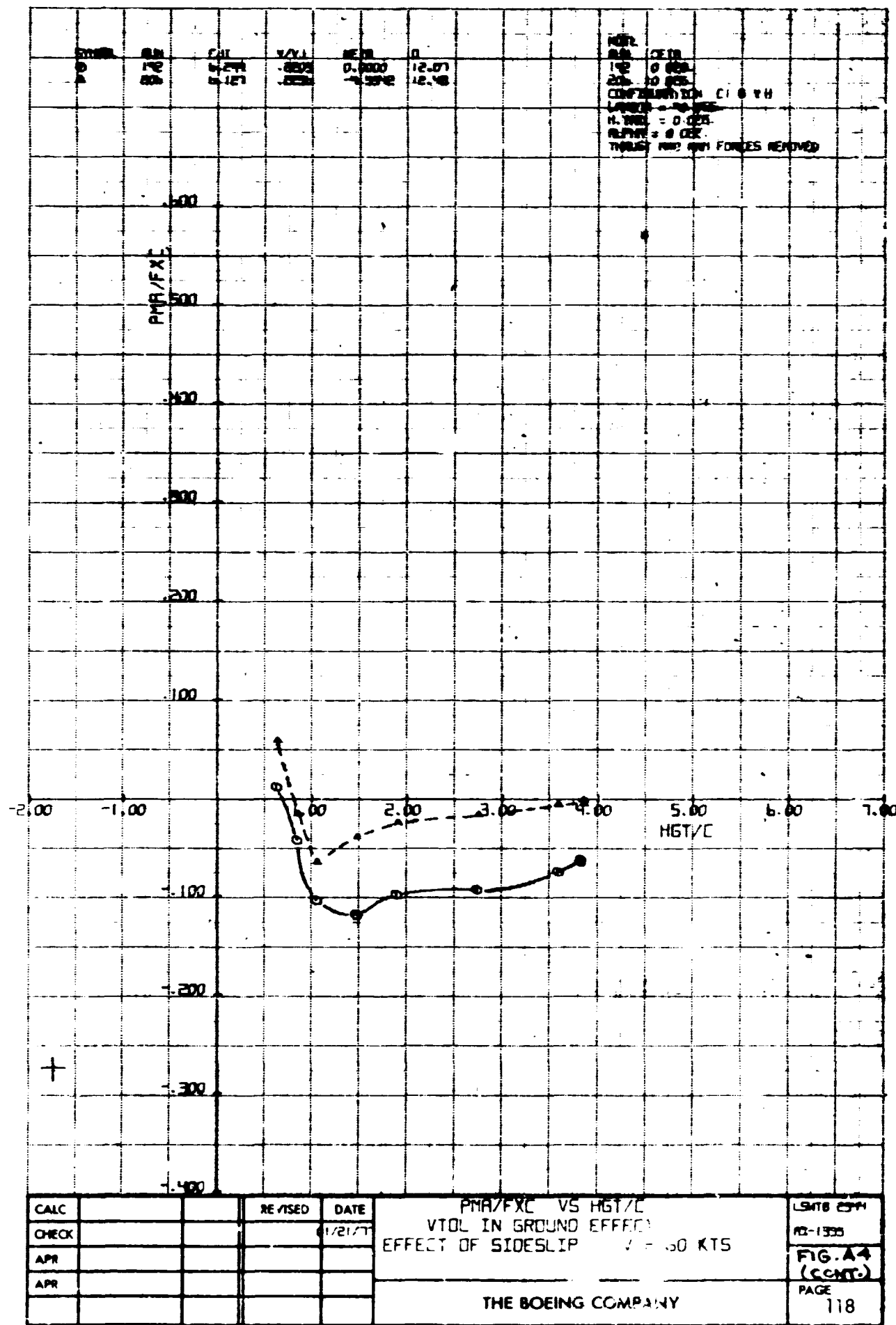
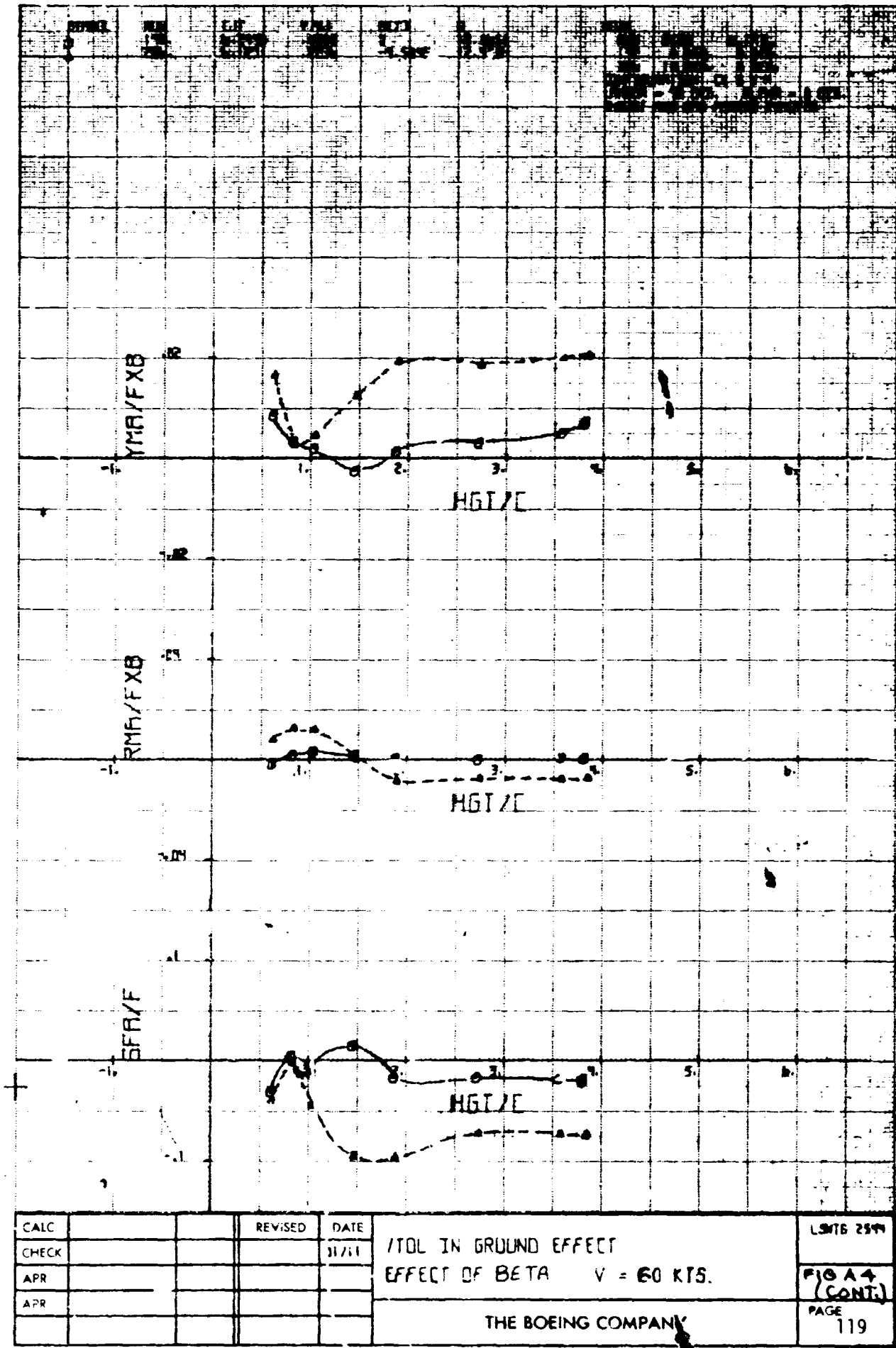
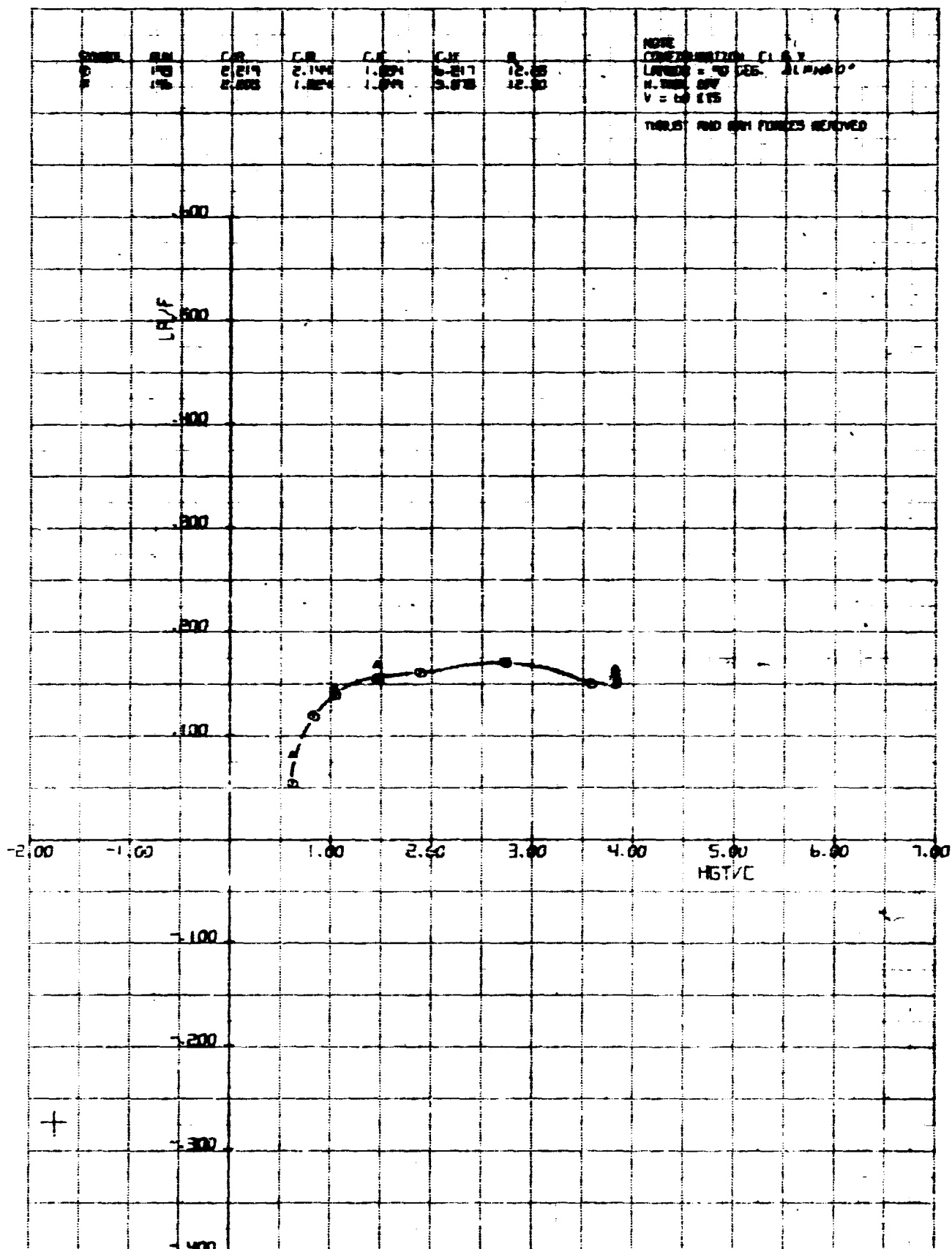


FIG 29
13.







LA/F VS HGT/C
VTOL IN GROUND EFFECT V = 60 KTS
EFFECT OF DIFF. THRUST BETA = 0 DEG.

THE BOEING COMPANY

1900

八一三

FIG. A5

PAGE
120

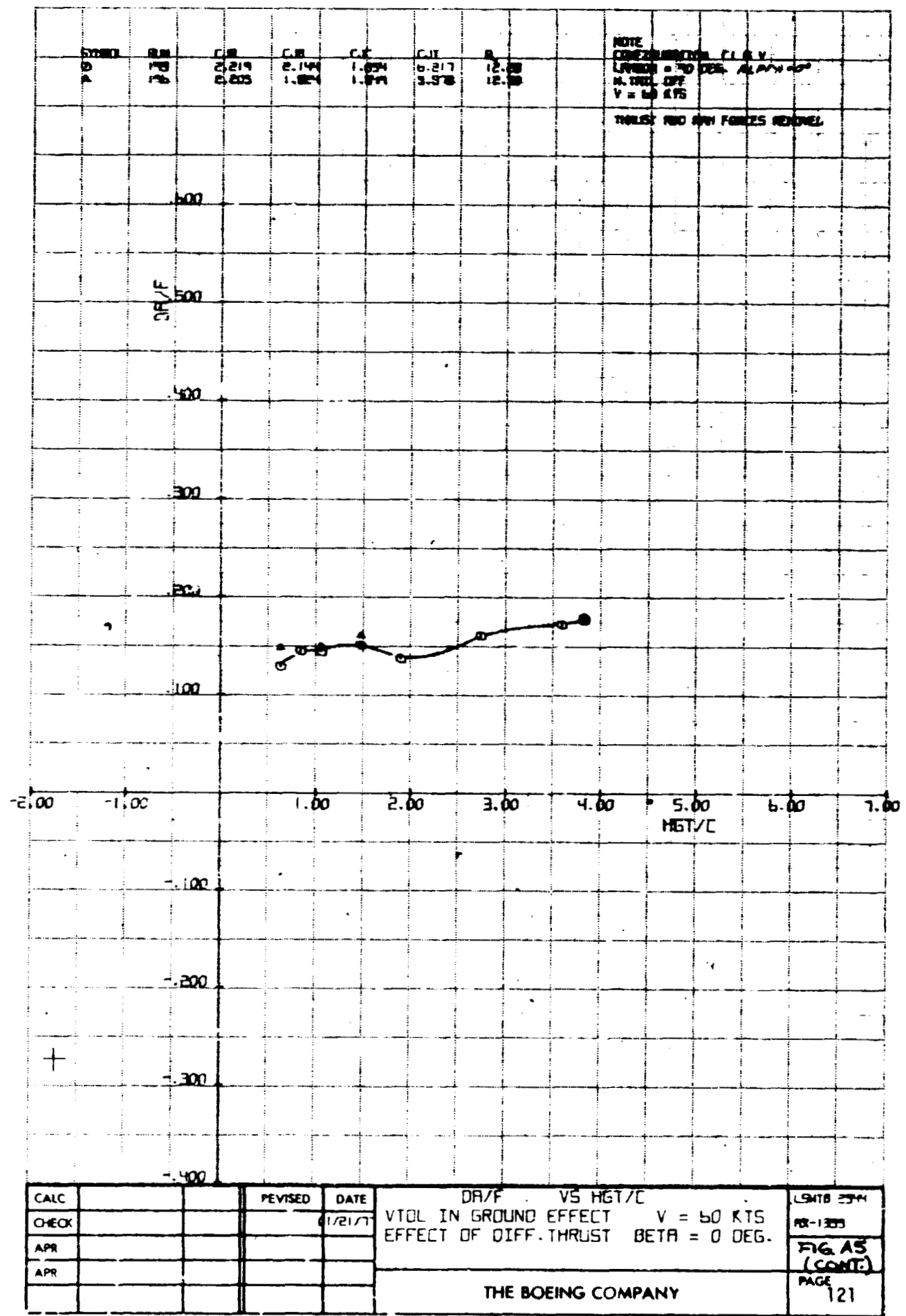
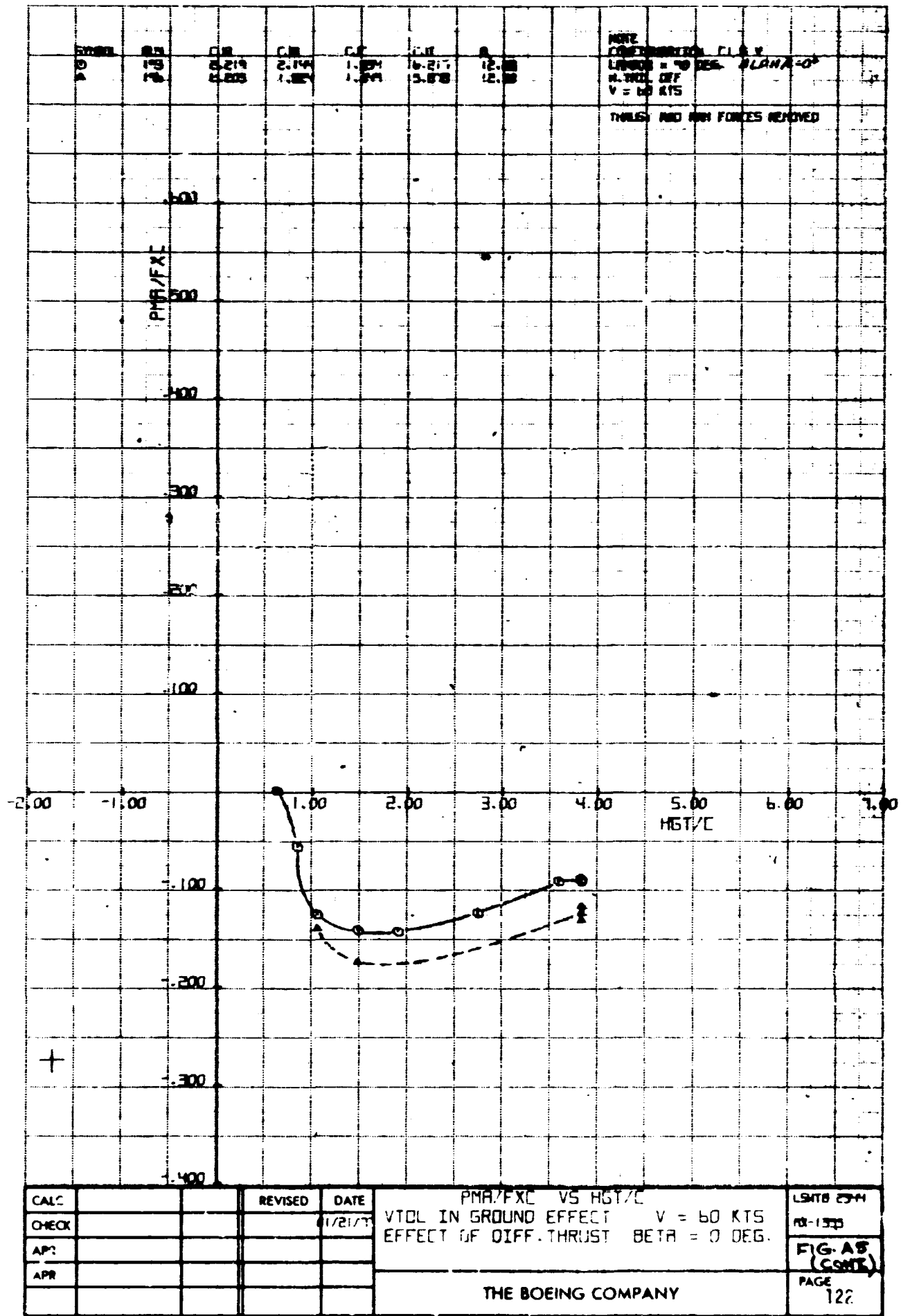


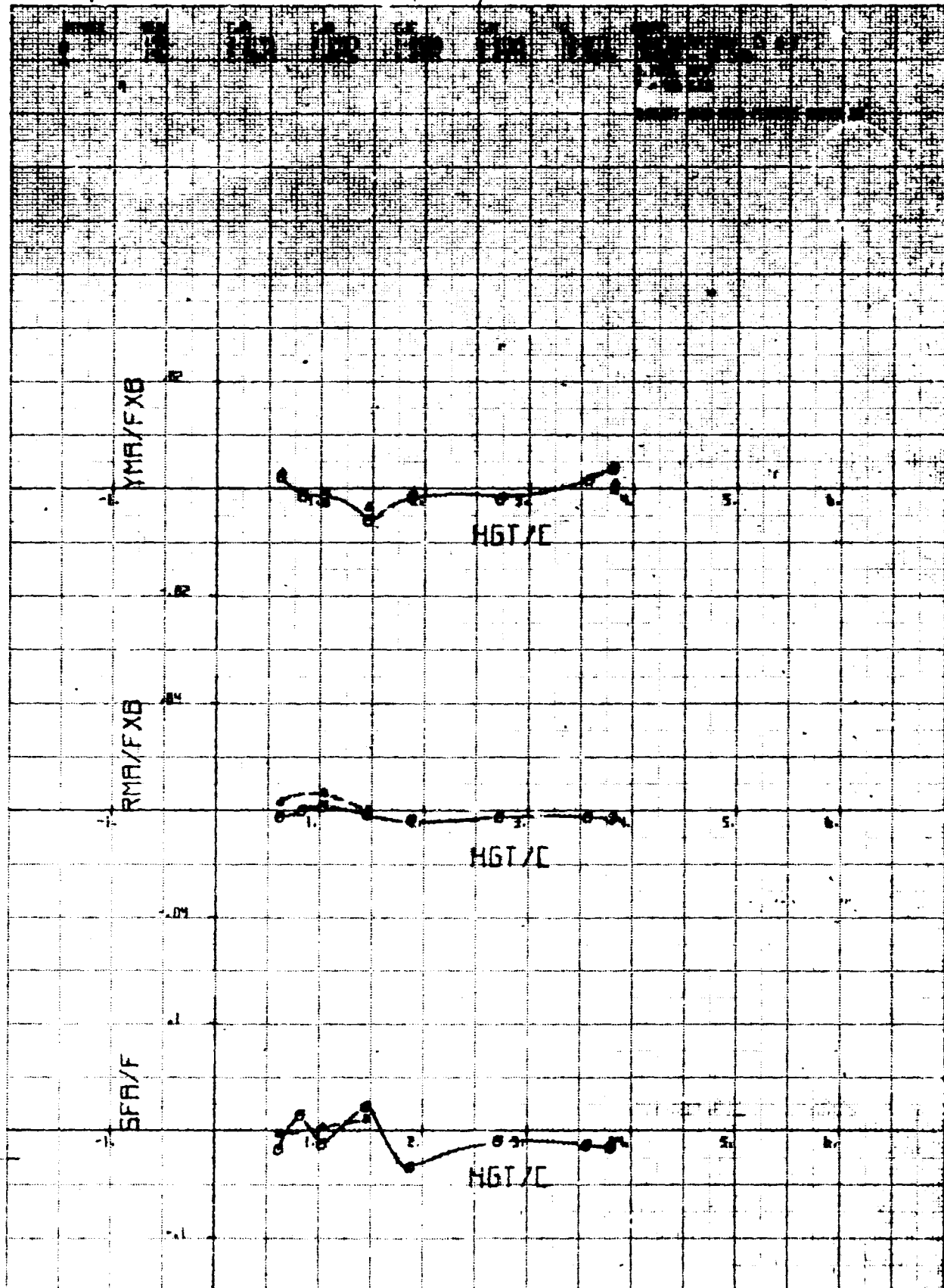
FIG 2:
1.

CALC	REVISED	DATE
CHECK		6/21/71
APR		
APR		

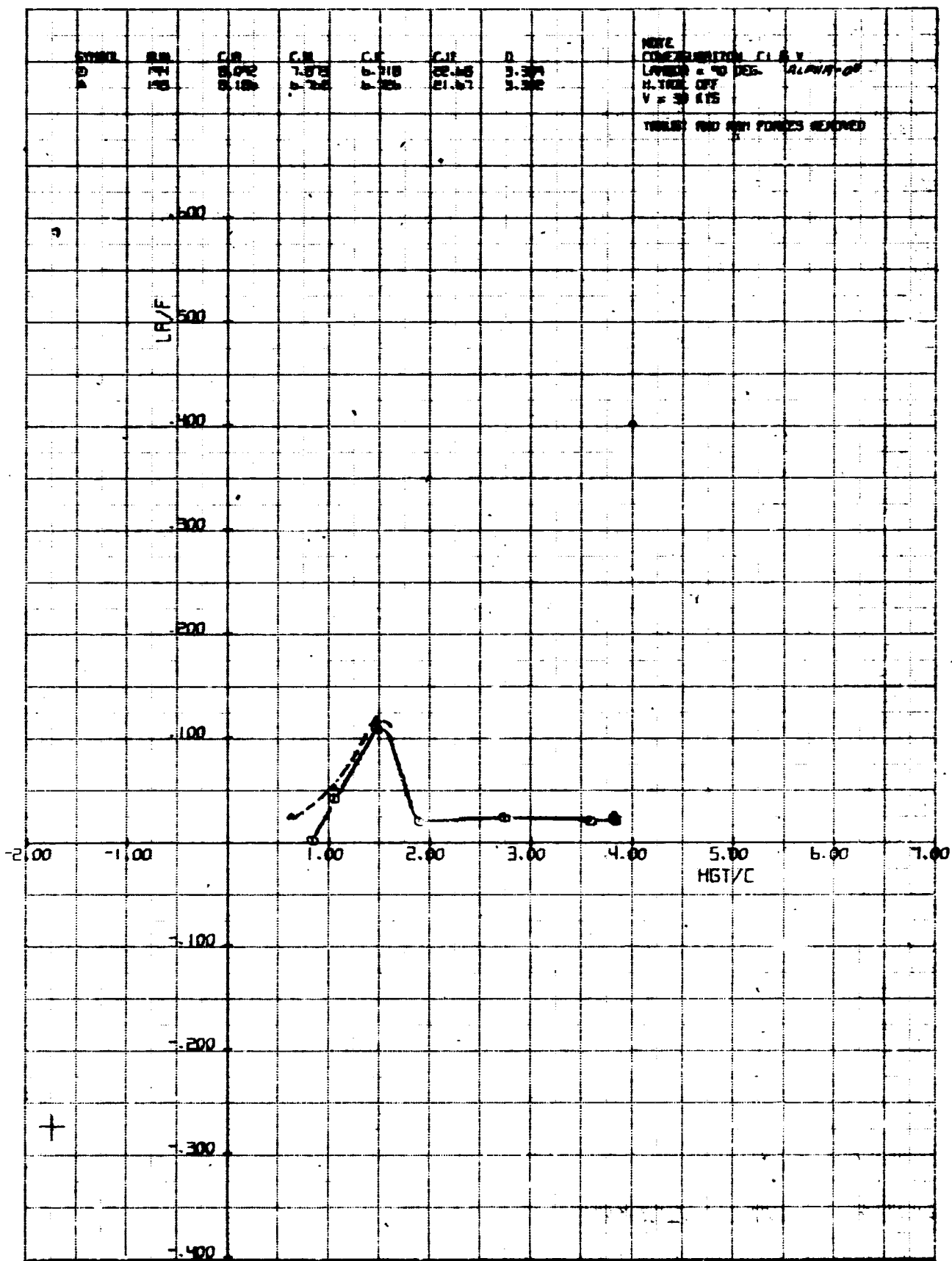
DR/F VS HGT/C
VTOL IN GROUND EFFECT V = 50 KTS
EFFECT OF DIFF. THRUST BETA = 0 DEG.

LMTB 234
RX-1233
FIG. A5
(CONT.)
PAGE 121





CALC		REVISED	DATE	V = 60 KTS	LMTB 2944
CHECK			01/11	EFFECT OF DIFF. THRUST	BETA = 0 DEG.
APR					
APR					
THE BOEING COMPANY					FIG. A5 (CONT.)
					PAGE 123



LA/F VS HGT/L
VTOL IN GROUND EFFECT V = 30 KTS
EFFECT OF DIFF. THRUST BETA_i = 0 DEG.

L9M18 2011

四-135

FIG. A6

THE BOEING COMPANY

PAGE

124

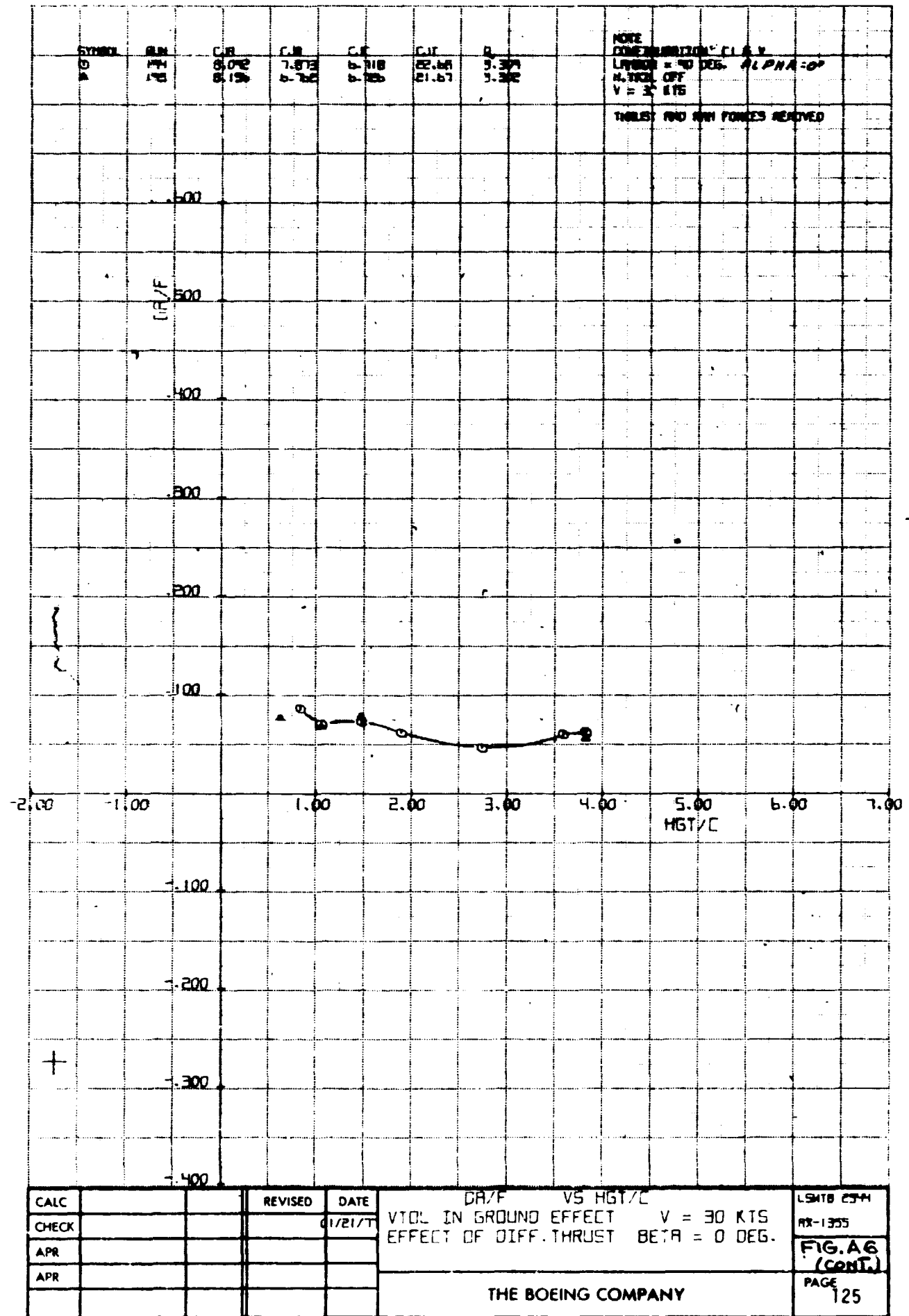
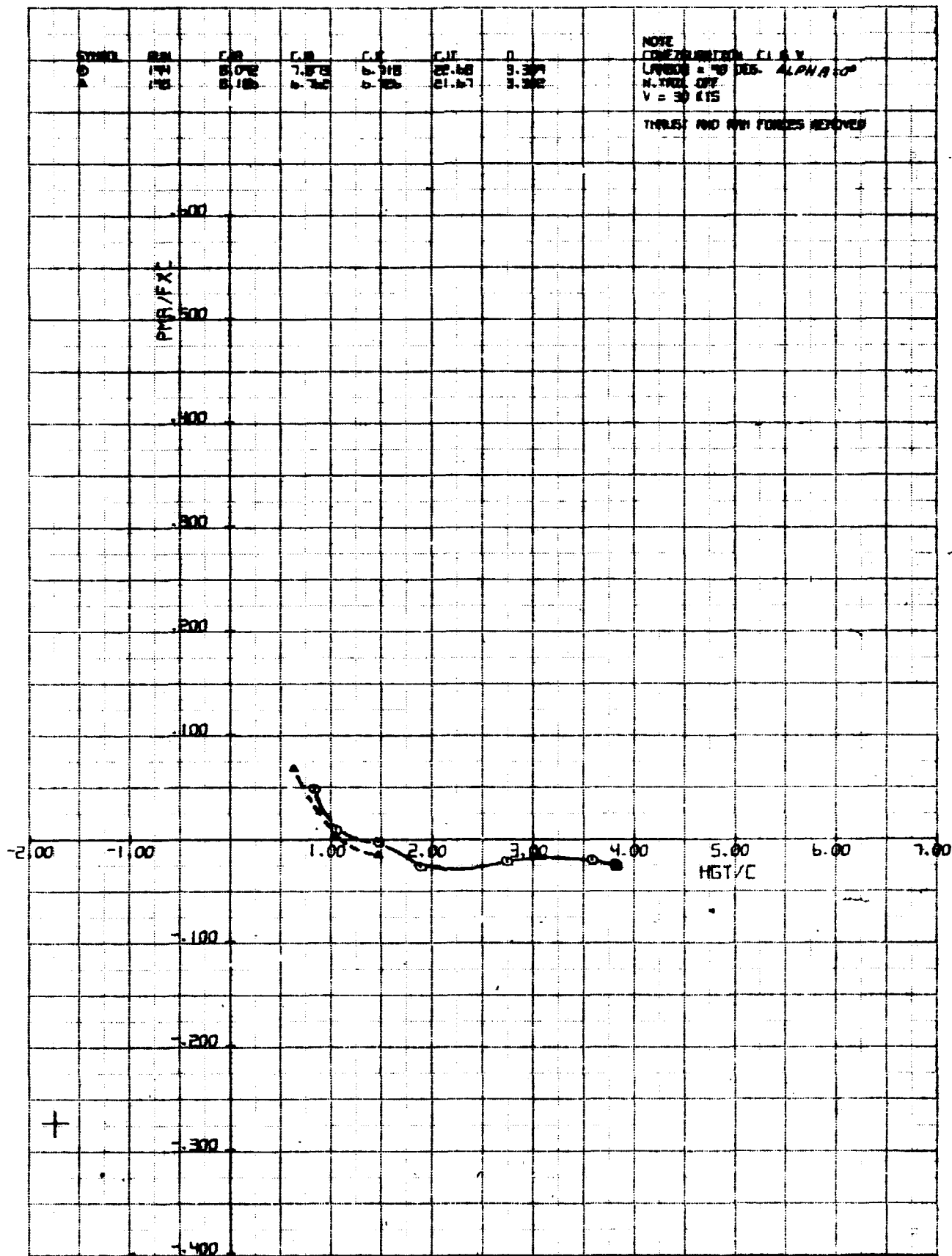


FIG 22



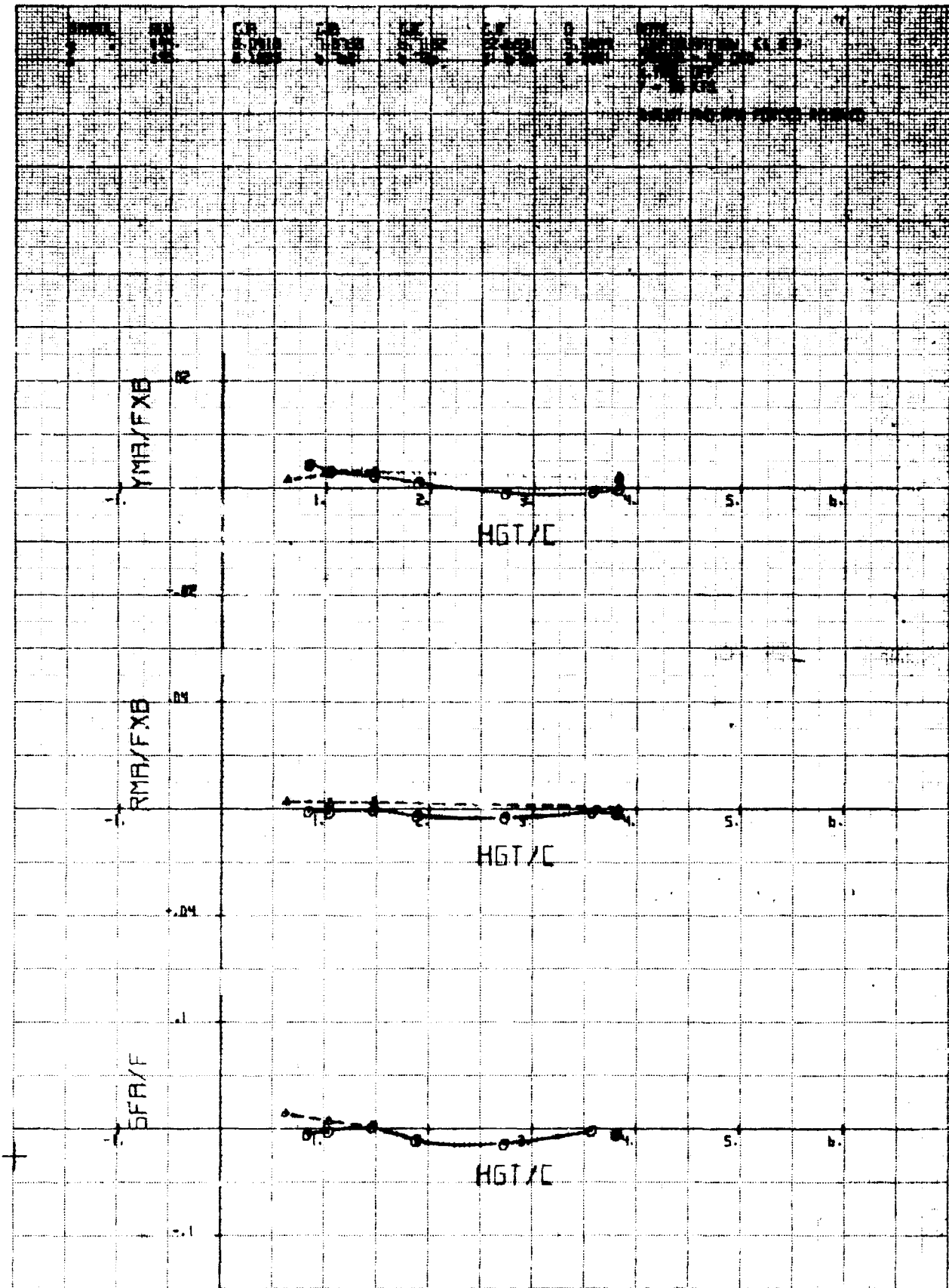
PMA/FXC VS HGT/C
VTOL IN GROUND EFFECT V = 30 KTS
EFFECT OF DIFF. THRUST BETA = 0 DEG.

LSMTB 2344
M-133

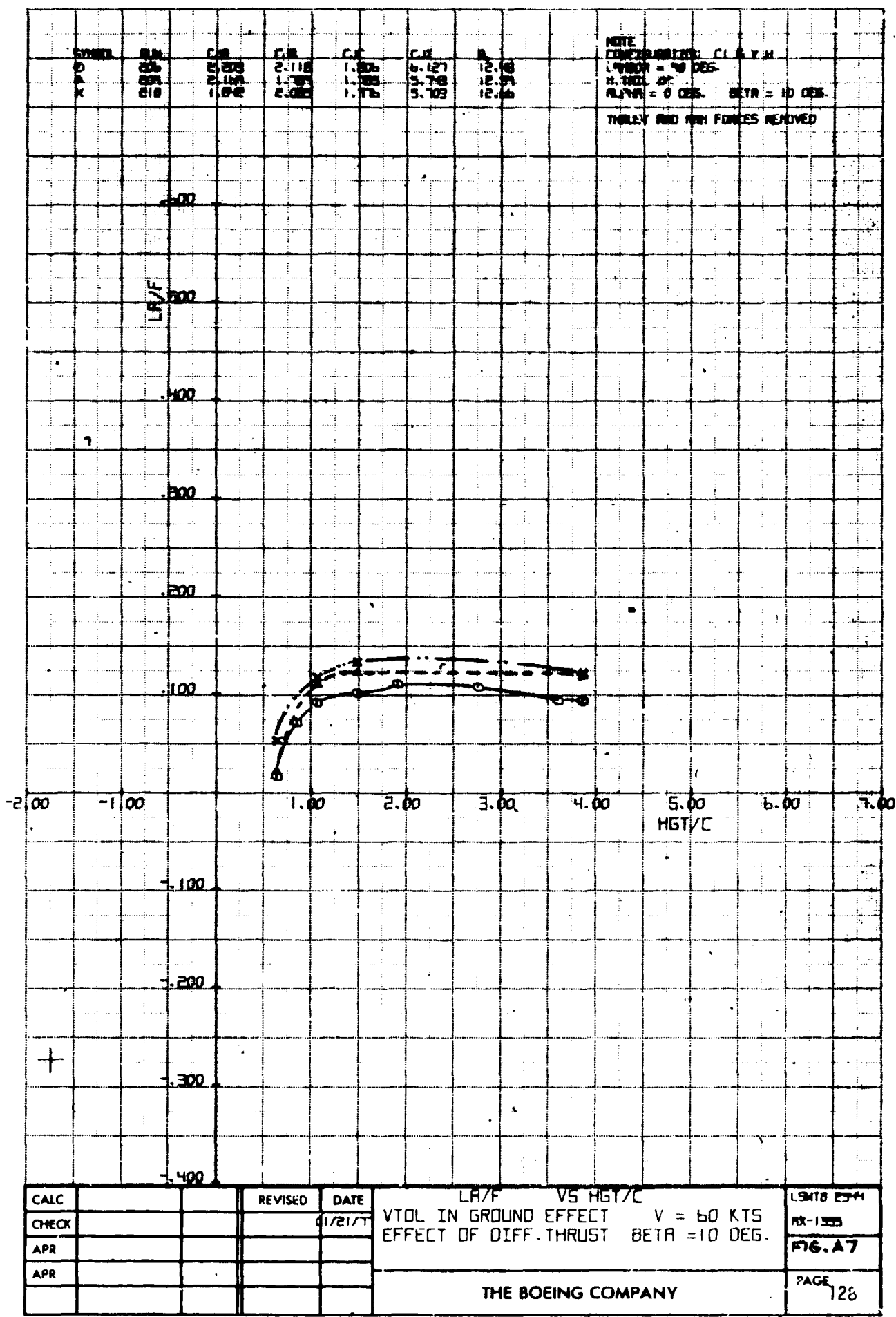
FIG.-A6
(CONT.)
PAGE

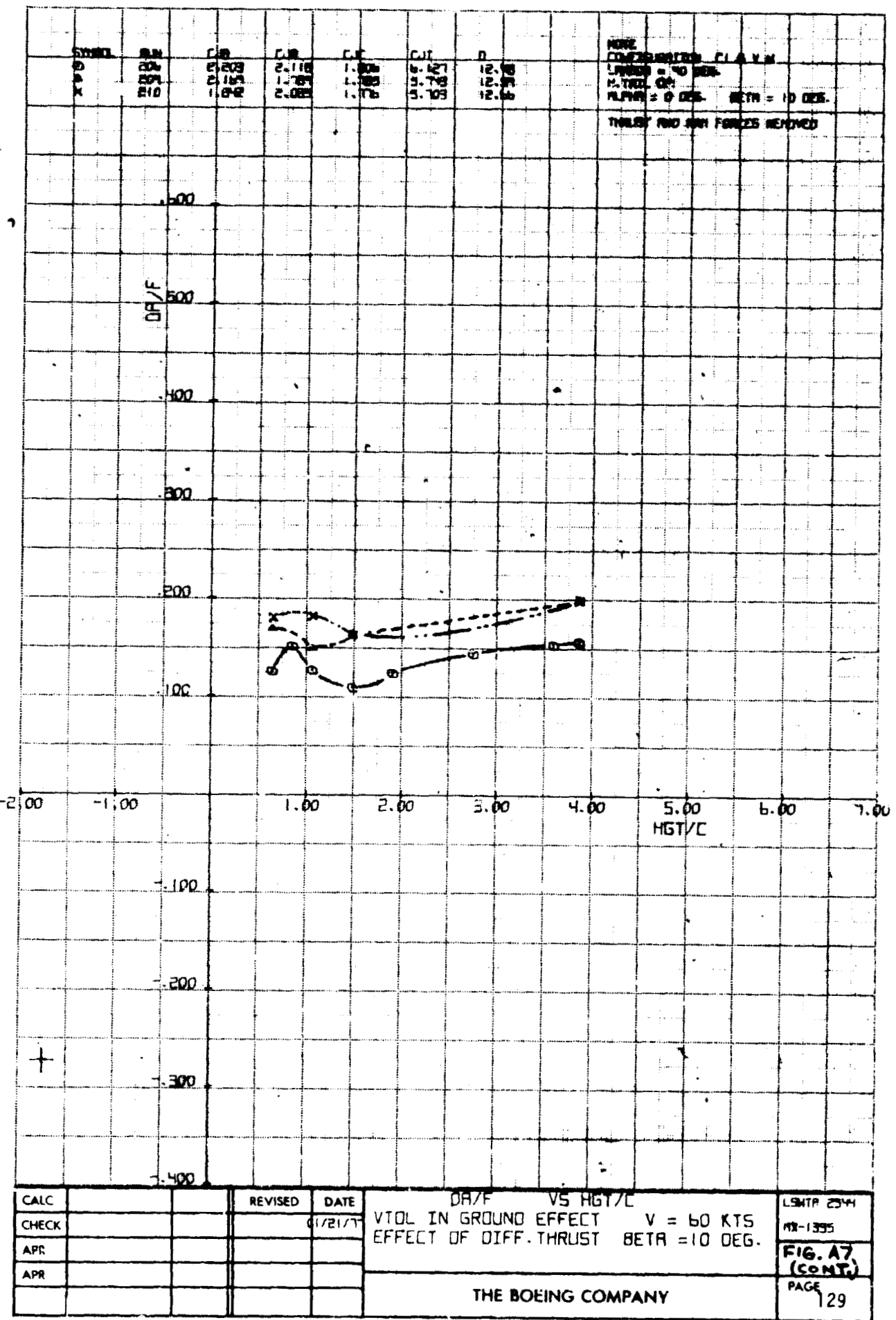
THE BOEING COMPANY

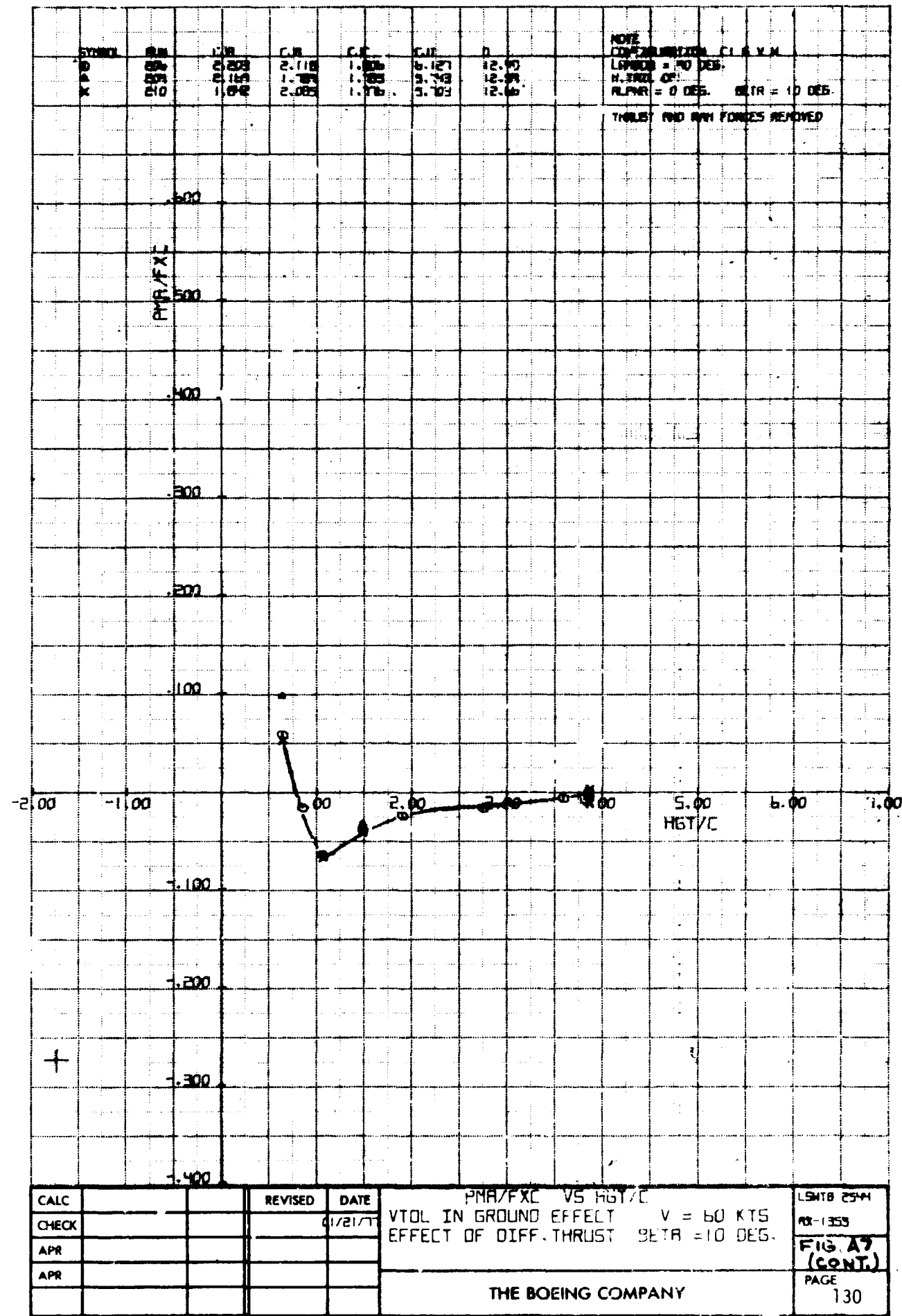
PAGE
126

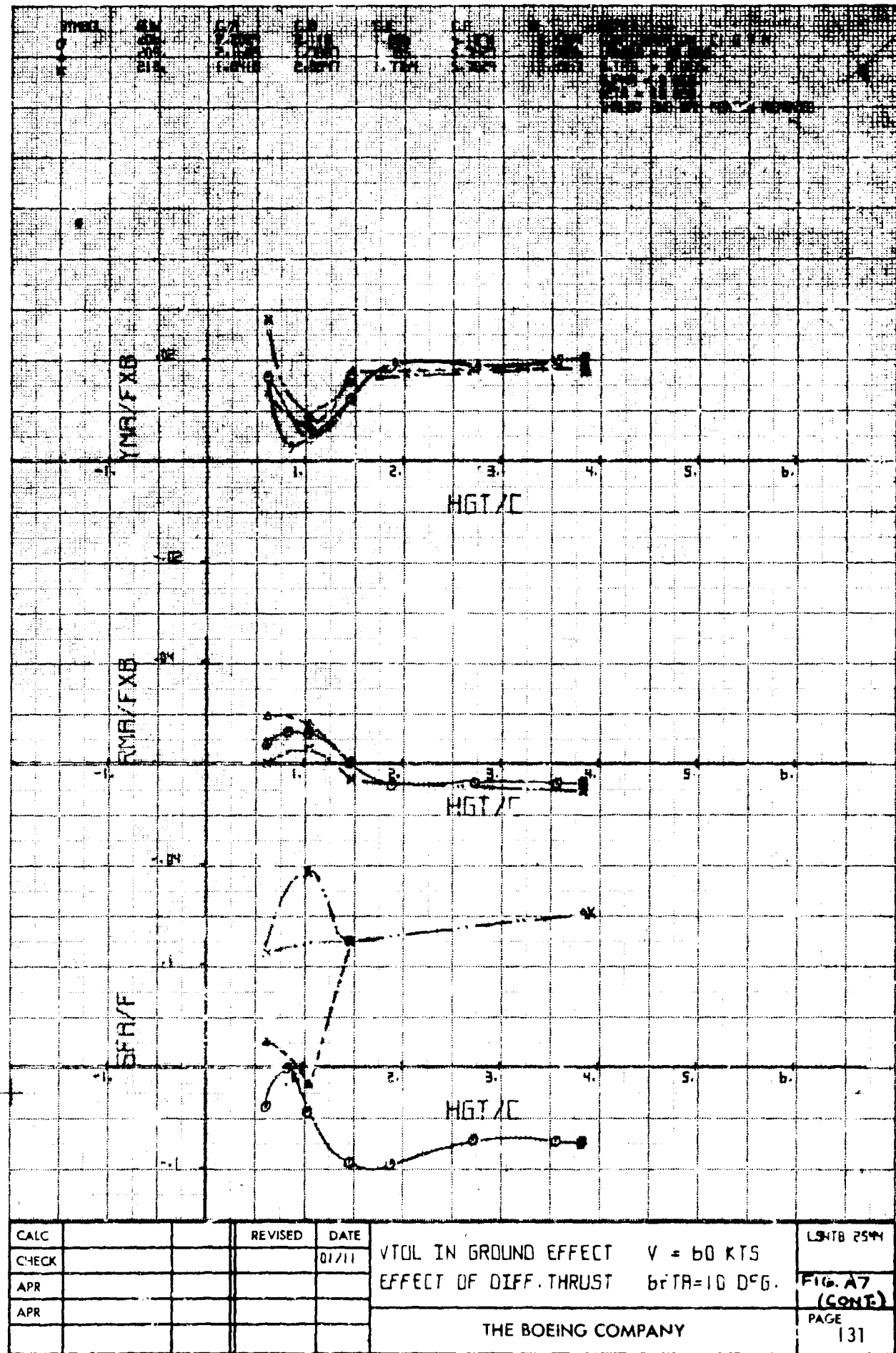


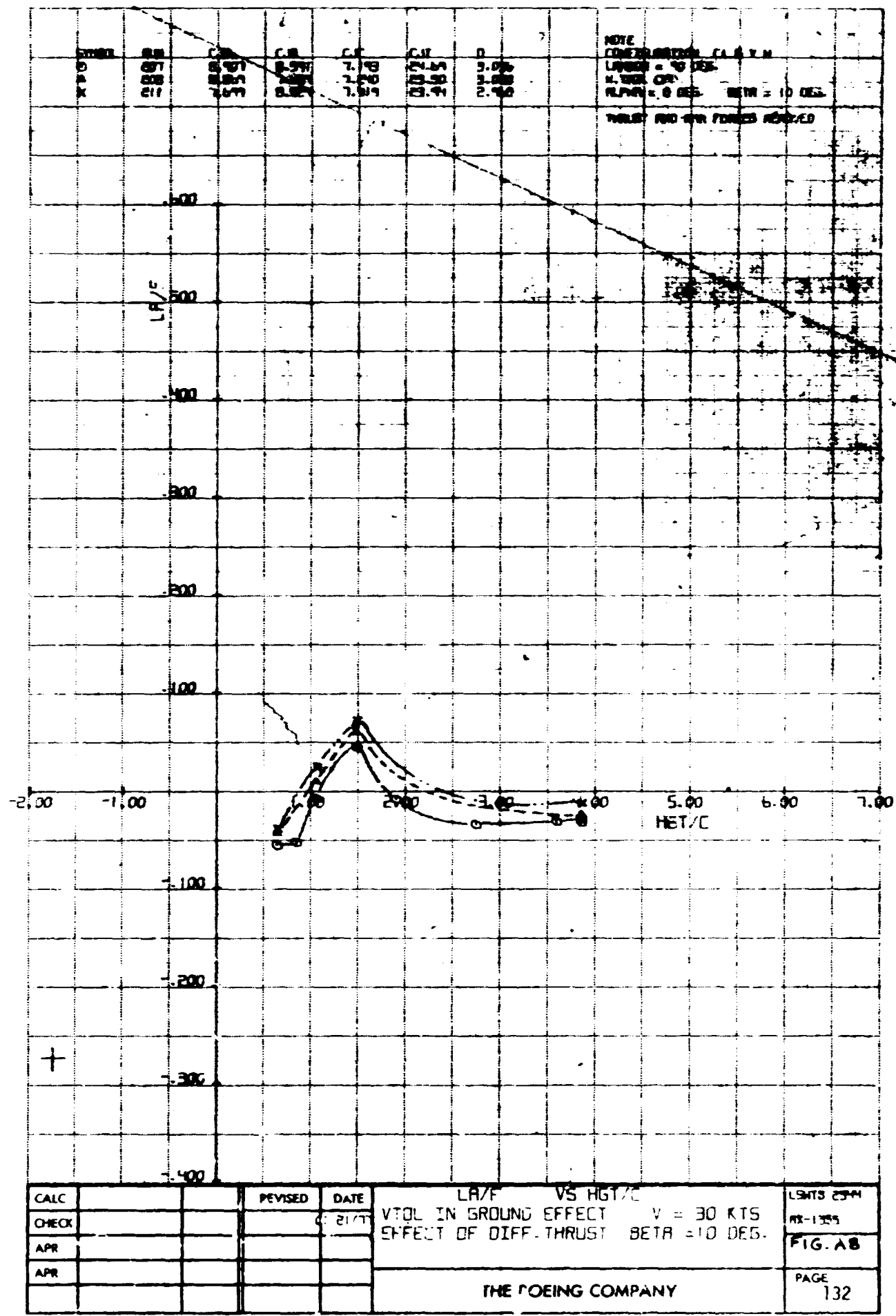
CALC		REVISED	DATE	LMTB 2544
CHEK			01/11	
APR				FIG. AG (CONT.)
APR				PAGE 127
VTOL IN GROUND EFFECT V = 30 KTS EFFECT OF DIFF. THRUST BETA = 0 DEG.				
THE BOEING COMPANY				



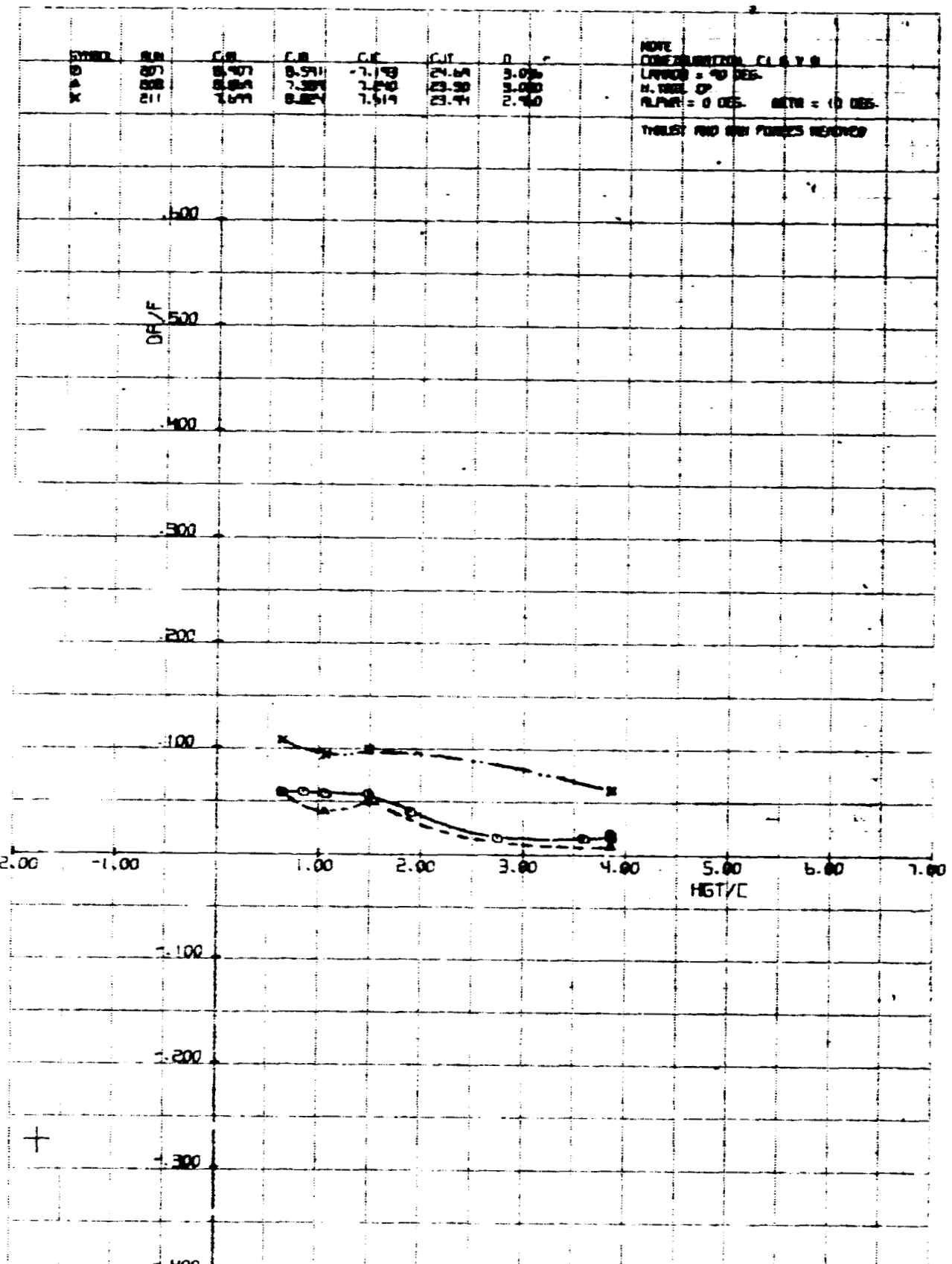




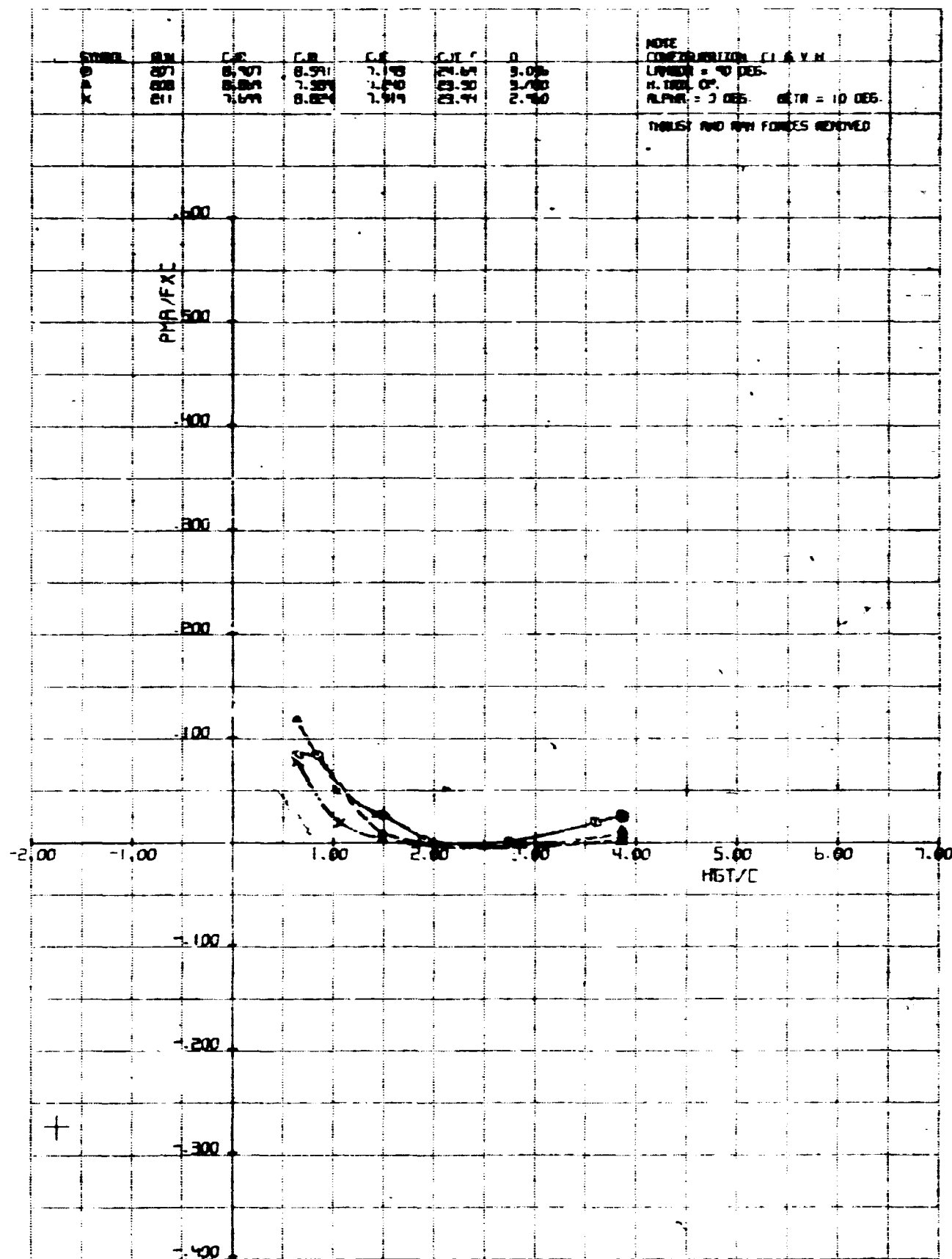


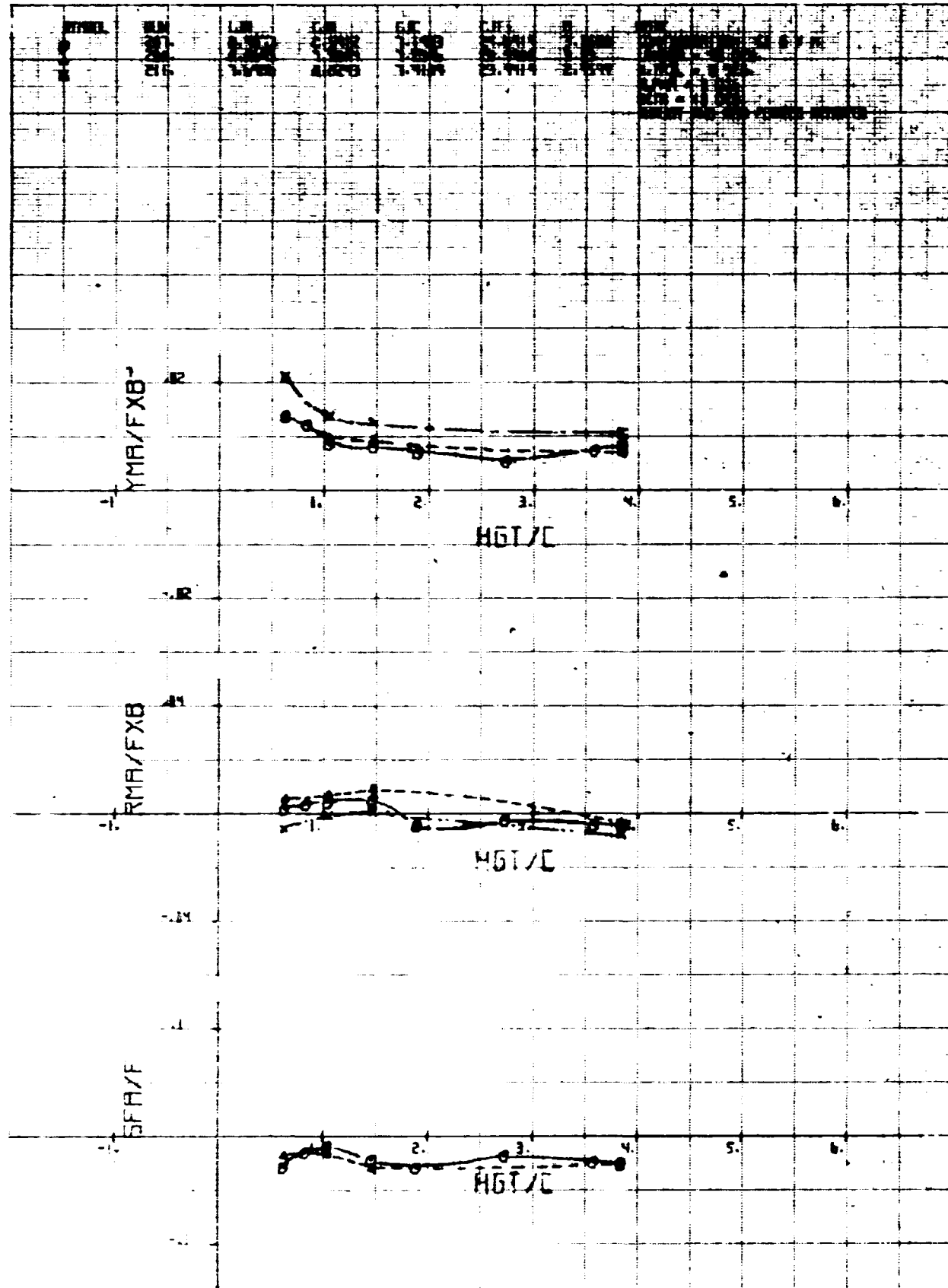


۱۵.



CALC		REVISED	DATE	DR/F VS HGT/C	LSMTB 2544
CHECK			4/21/71	VTOL IN GROUND EFFECT V = 30 KTS	PR-1335
APR				EFFECT OF DIFF. THRUST BETA = 10 DEG.	FIG. A 8 (CONT.)
APR				THE BOEING COMPANY	PAGE 133





CALC		REVISED	DATE	VTOI IN GROUND EFFECT EFFECT OF DIFF. THRUST	V = 30 KTS BETA=10 DEG.	LOM 2544
CHECK			01/11			
APR						FIG A8 (CONT)
APR						PAGE 135

THE BOEING COMPANY

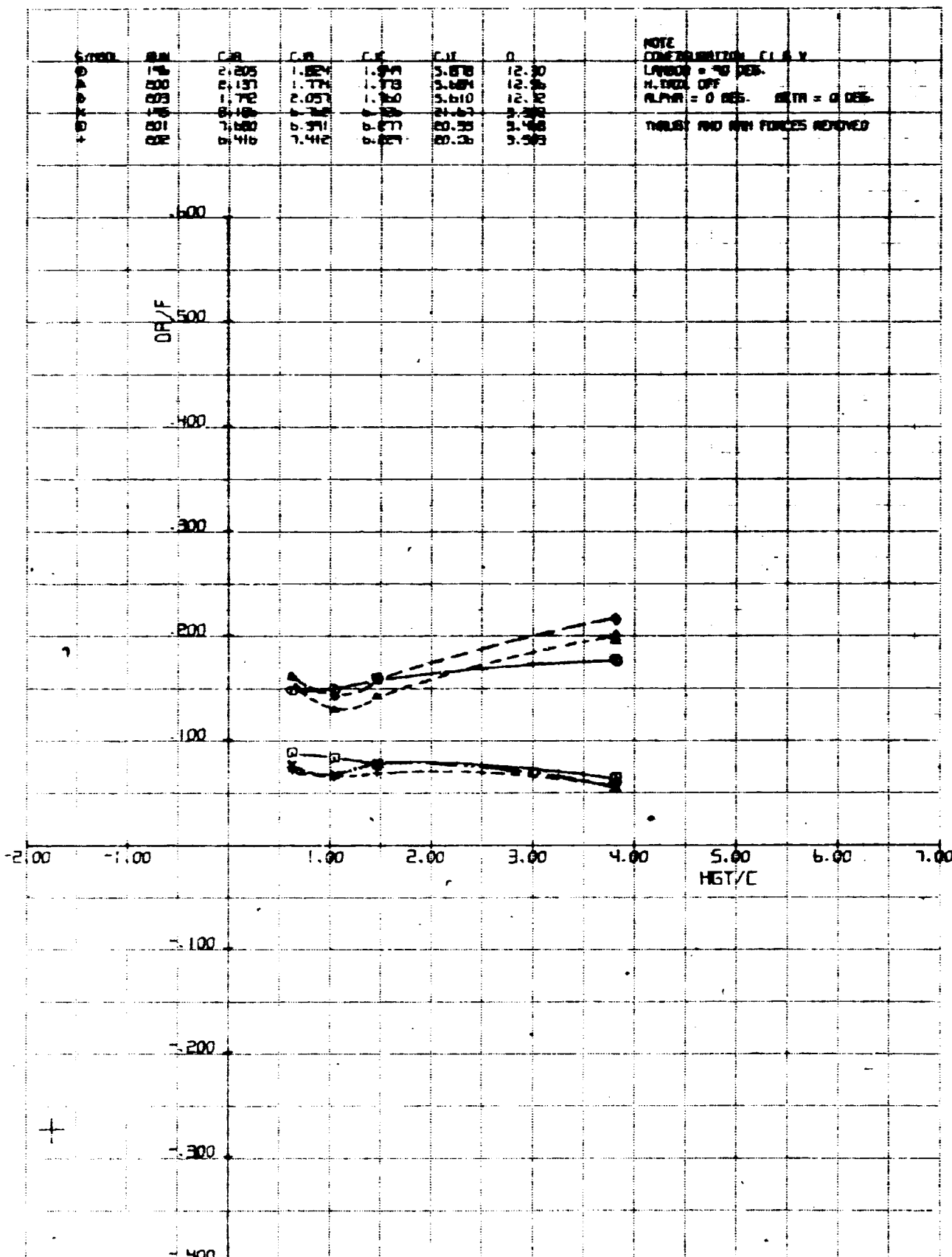
NOTE
COMBINATION C 1 & 2
LATERAL = 70 DEG.
H. TAIL OFF
FLYBY = 0 DEG. BETA = 0 DEG.

CALC	REvised	DATE	LR/F VS HGT/C		LSATB 2744
			VTOL IN GROUND EFFECT	DIFF. THRUST	
CHECK		01/01/77	EFFECT OF YAW VANES	H. TAIL OFF	MA 1355
APR					FIG A9
APR					PAGE
					136

THE BOEING COMPANY

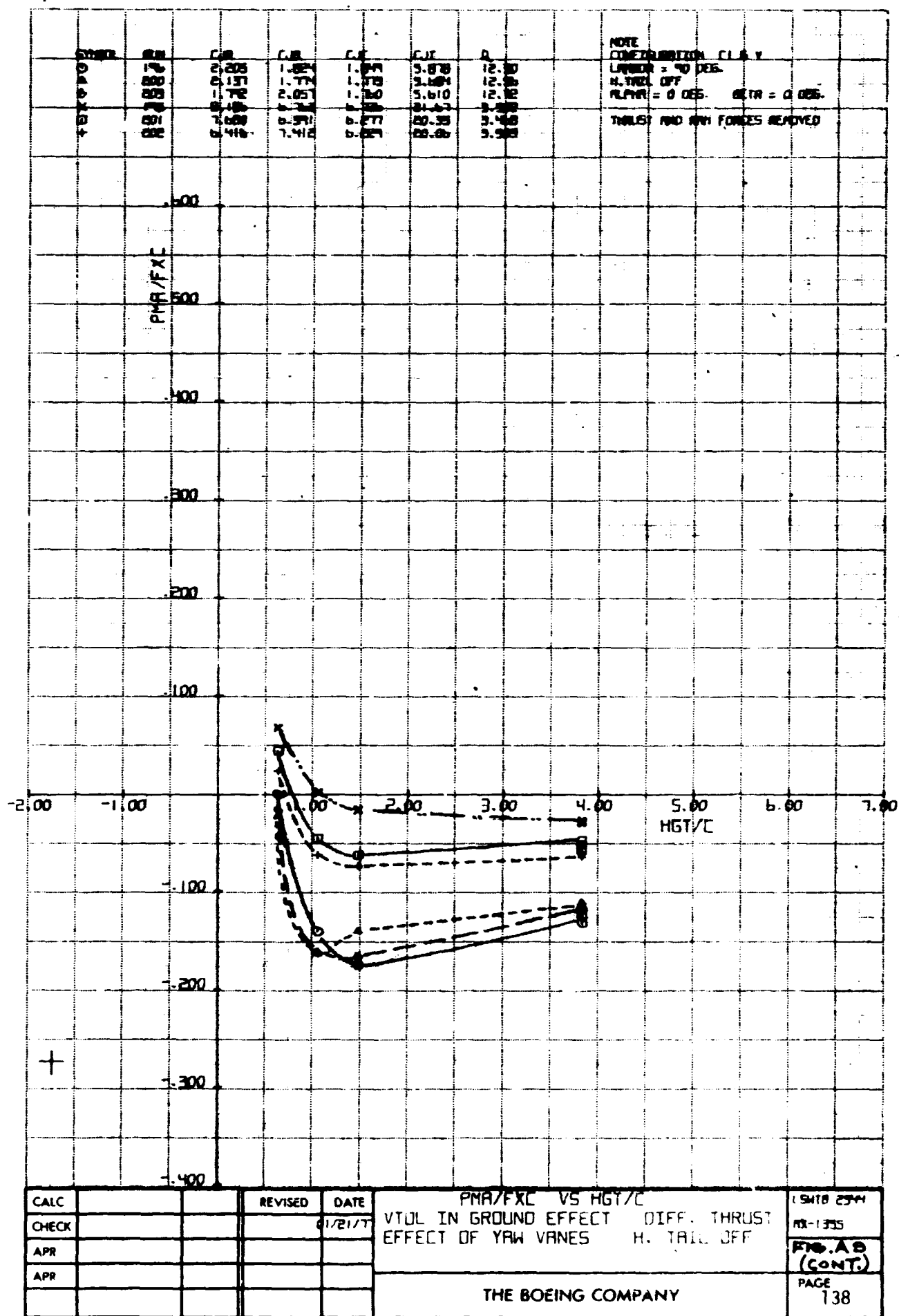
SYN. I YAW VANE(S)	LR/F
0	60° OFF
▲	60°
◆	20°
X	OFF
■	20°
+	20°

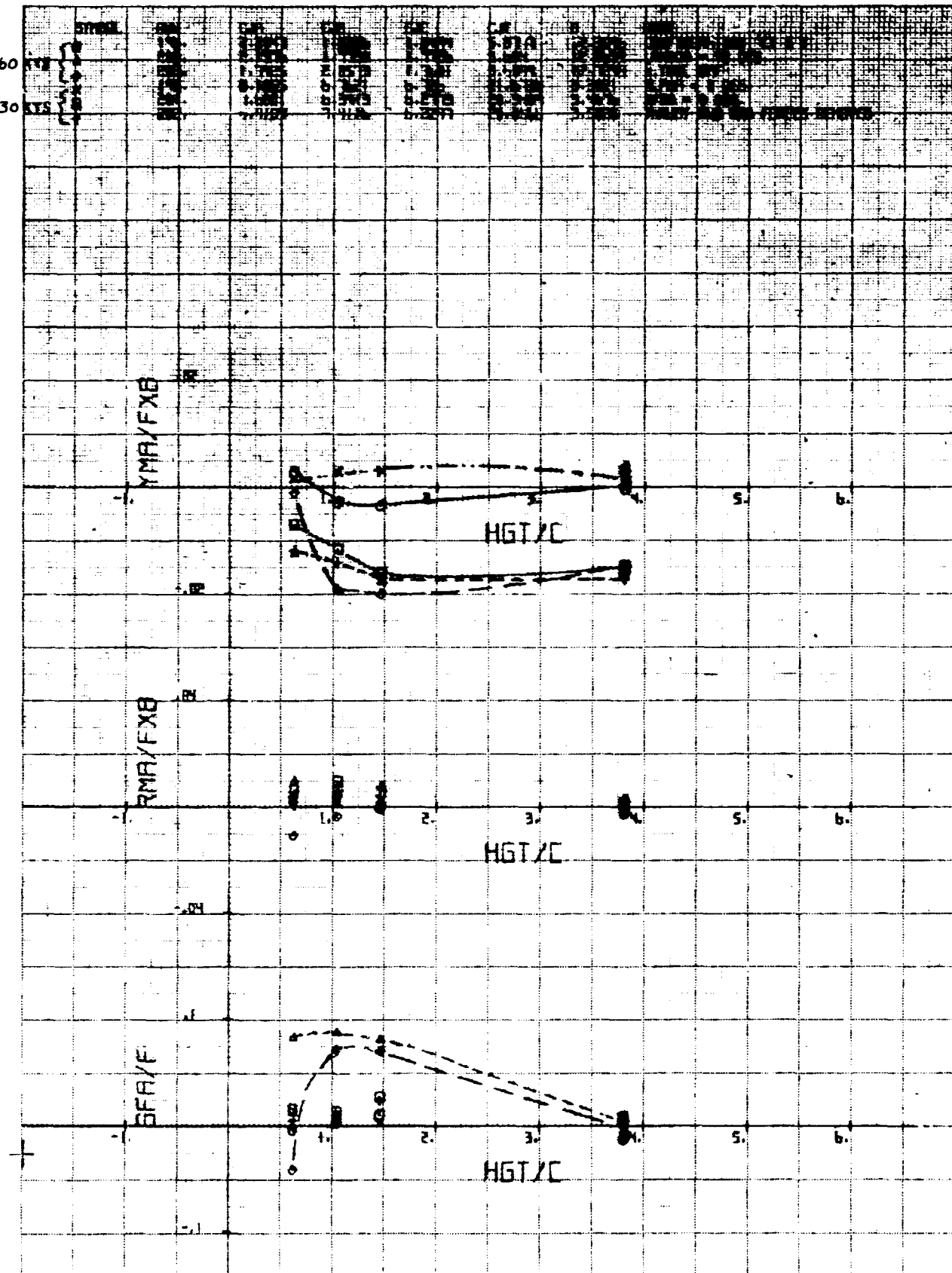
FIB 24



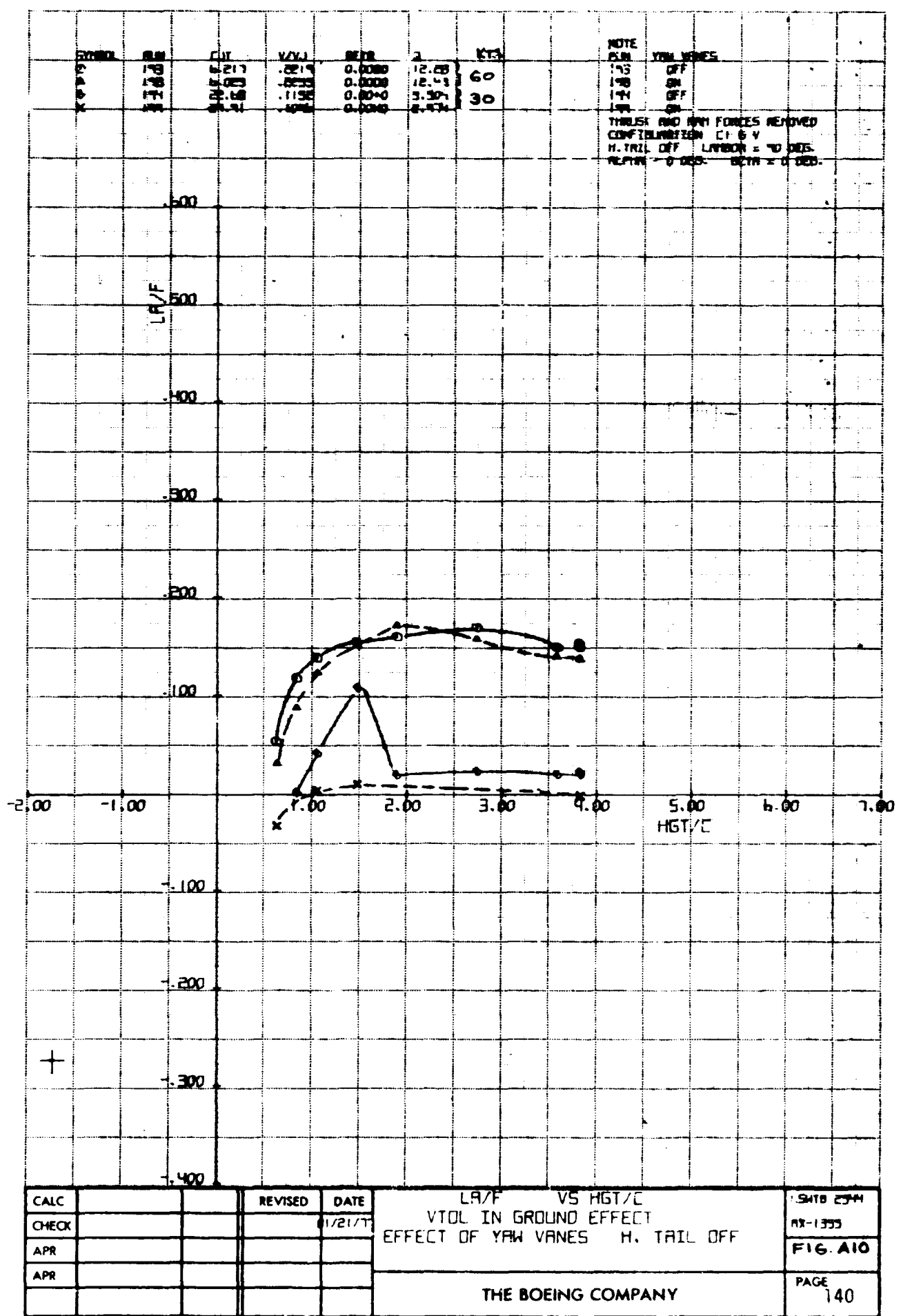
NOTE
CONSIDERATION FIG. 8 V
LAWSON = 70 DEG.
H. TRAIL OFF
ALPHA = 0 DEG. BETA = 0 DEG.

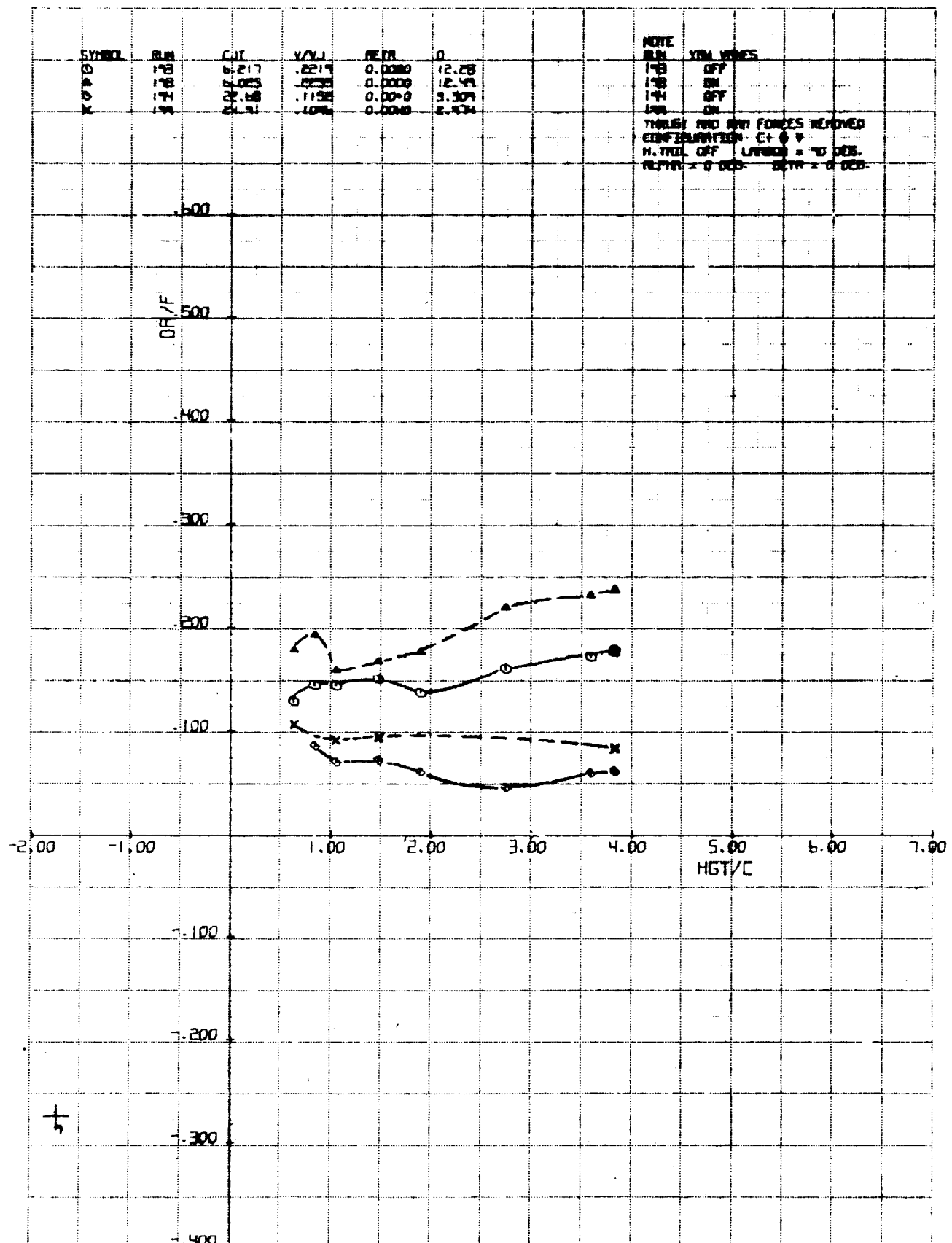
THRUST AND WIND FORCES REMOVED



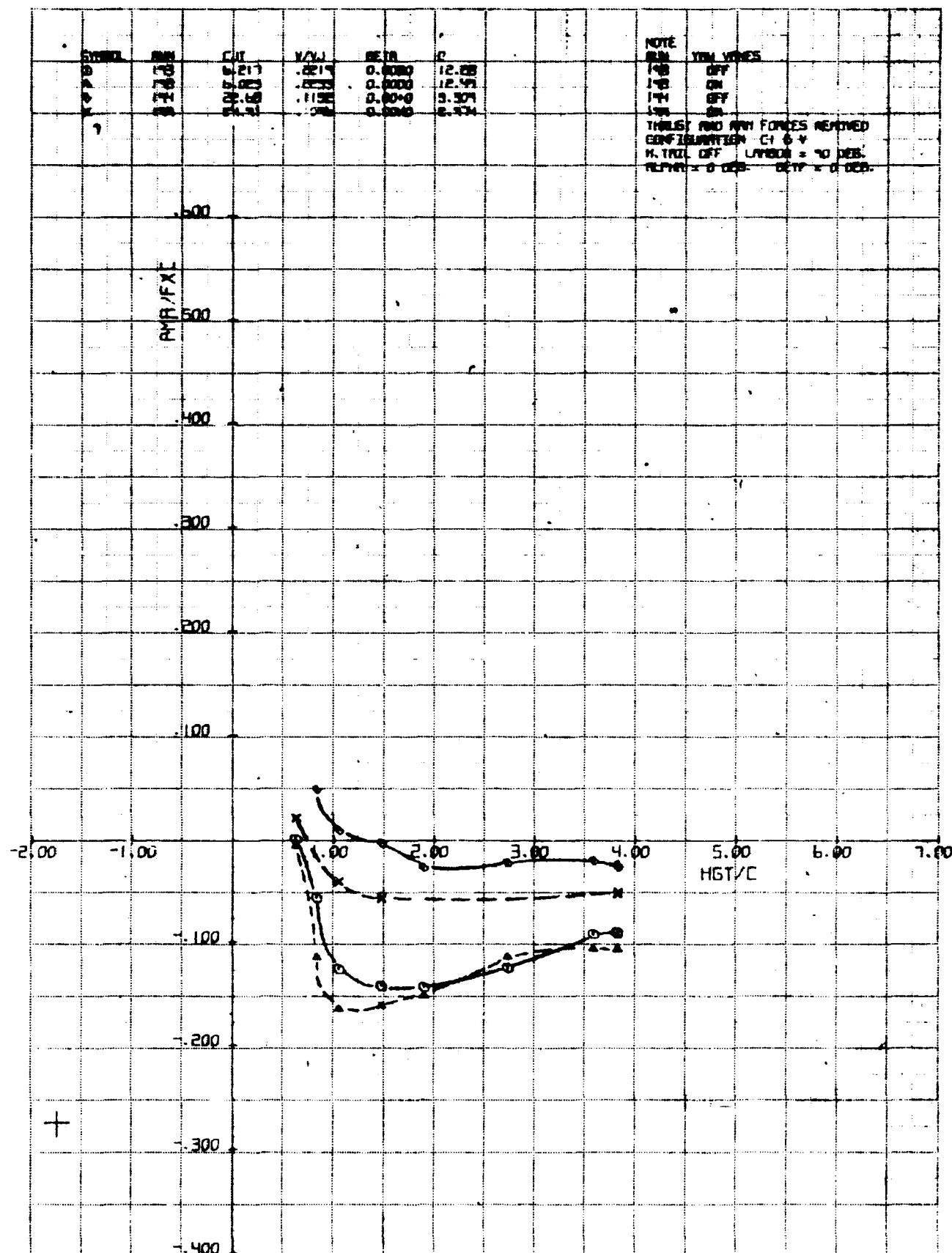


CALC		REVISED	DATE	V = 60 KTS	LWTB 25W
CHECK			01/11	V = 30 KTS	
APR				EFFECT OF DIFF. THRUST	BETA = 0 DEG.
APR					FIG. A5 (CONT.)
				THE BOEING COMPANY	PAGE 139



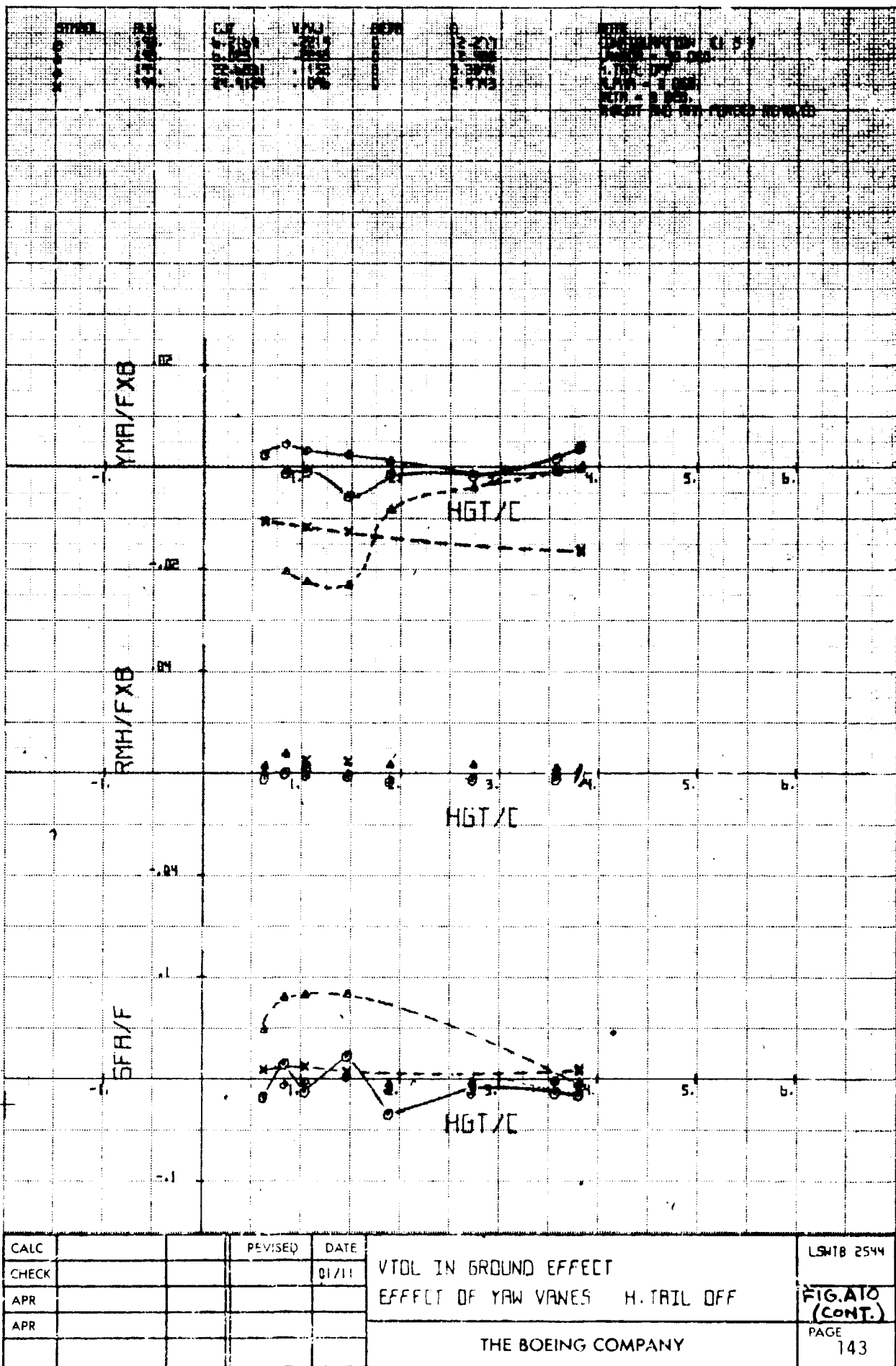


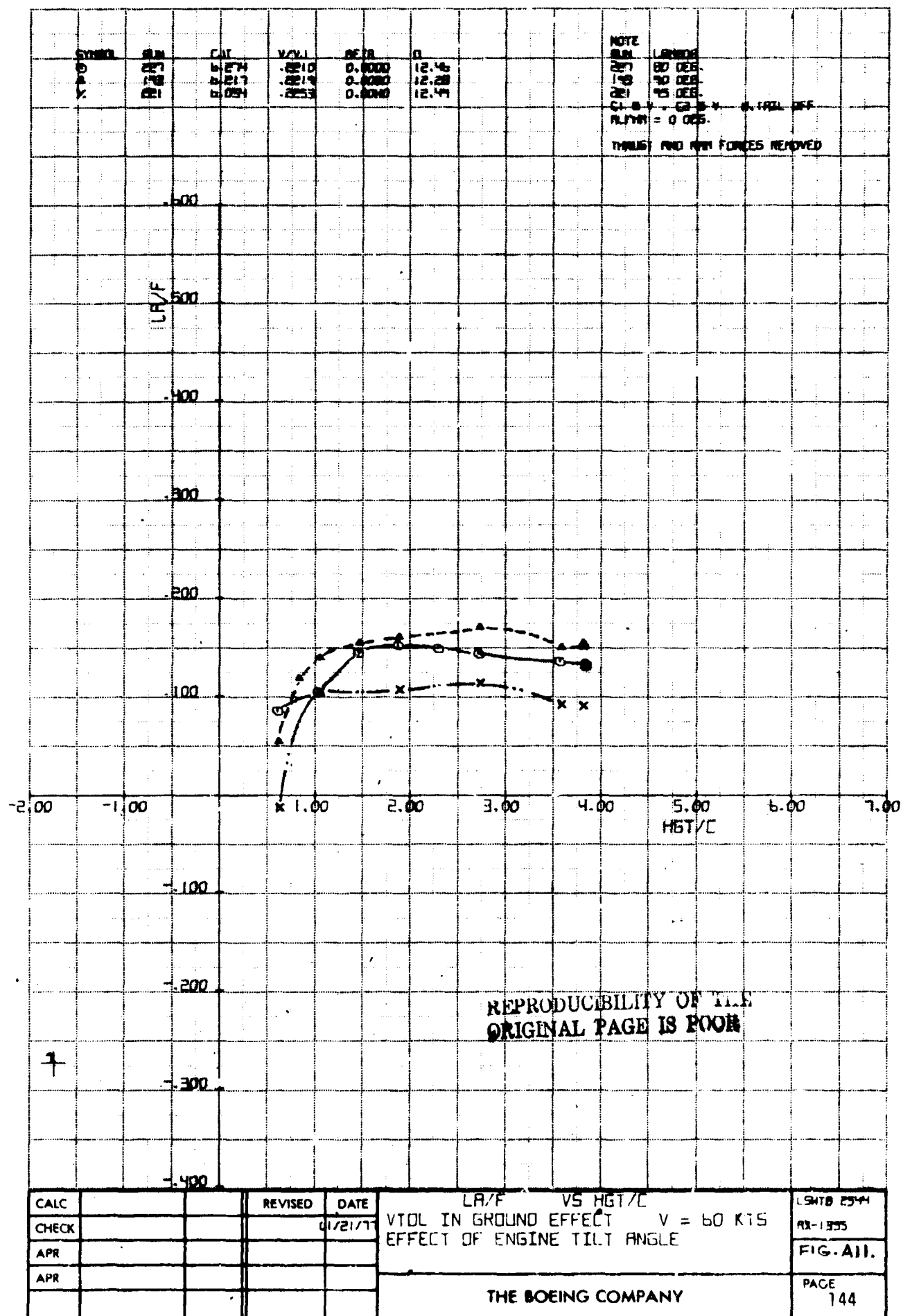
CALC		REVISED	DATE	DR/F VS HGT/C	LSATB 2544
CHECK				VTOL IN GROUND EFFECT	MX-1333
APR				EFFECT OF YAW VANES H. TRAIL OFF	FIG. A.10 (CONT.)
APR				THE BOEING COMPANY	PAGE 141



PMA/FXC VS HGT/C
VTOL IN GROUND EFFECT
EFFECT OF YAW VANES H. TAIL OFF

CALC		REVISED	DATE	PMA/FXC VS HGT/C VTOL IN GROUND EFFECT EFFECT OF YAW VANES H. TAIL OFF	LMTB 2344
CHECK			01/21/11		RX-1355
APR					FIG. A10 (CONT.)
APR					PAGE 142
				THE BOEING COMPANY	





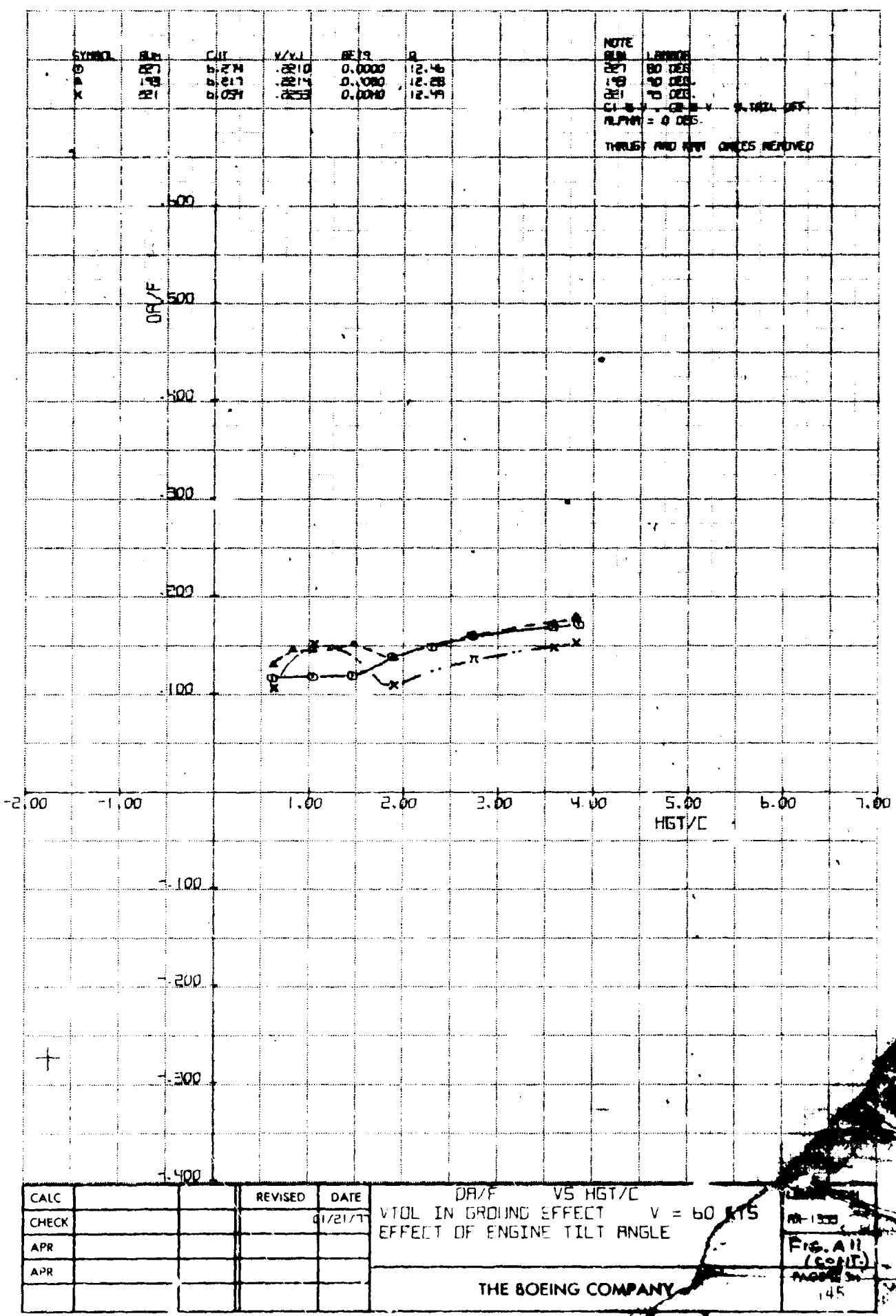
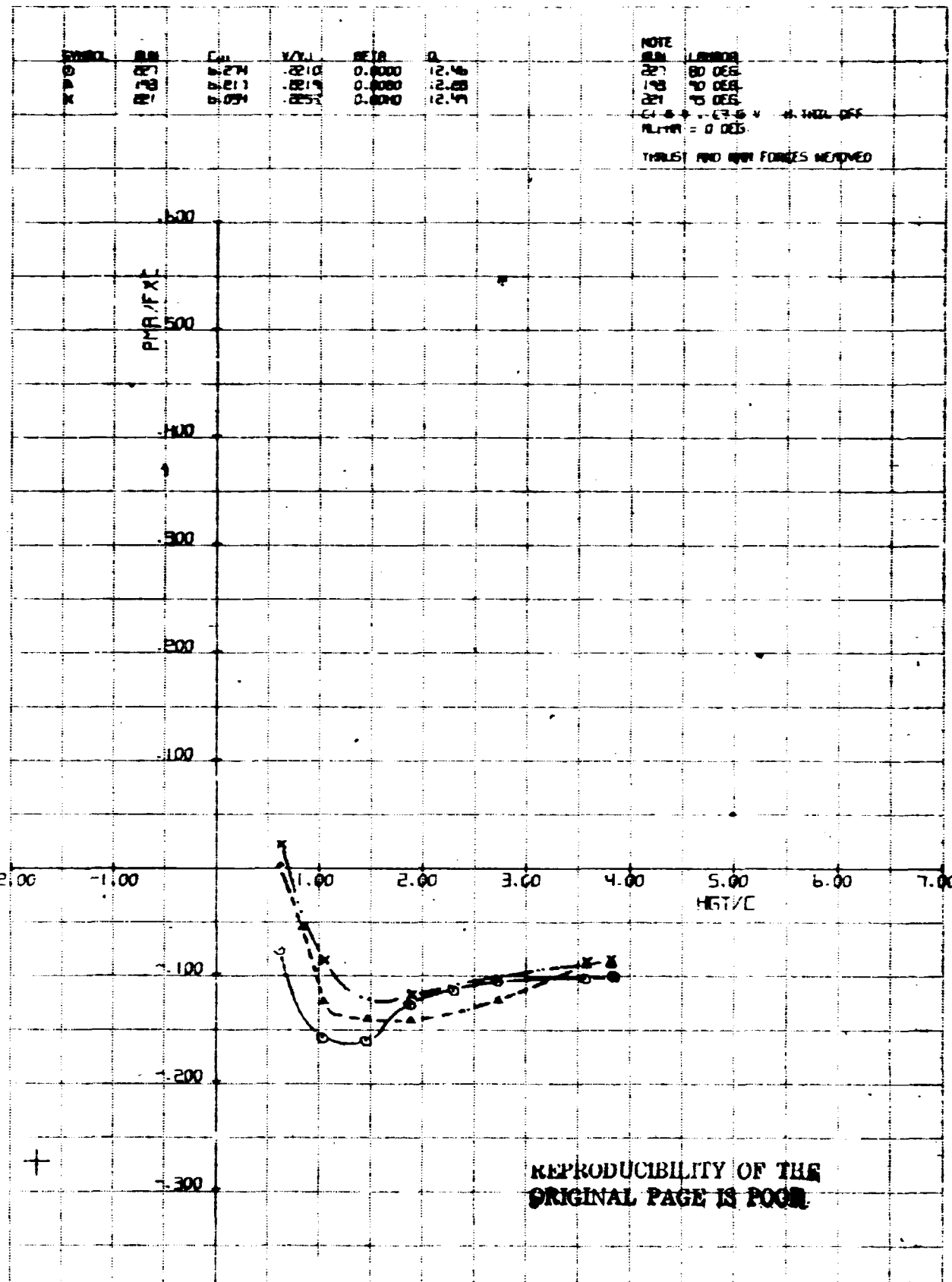
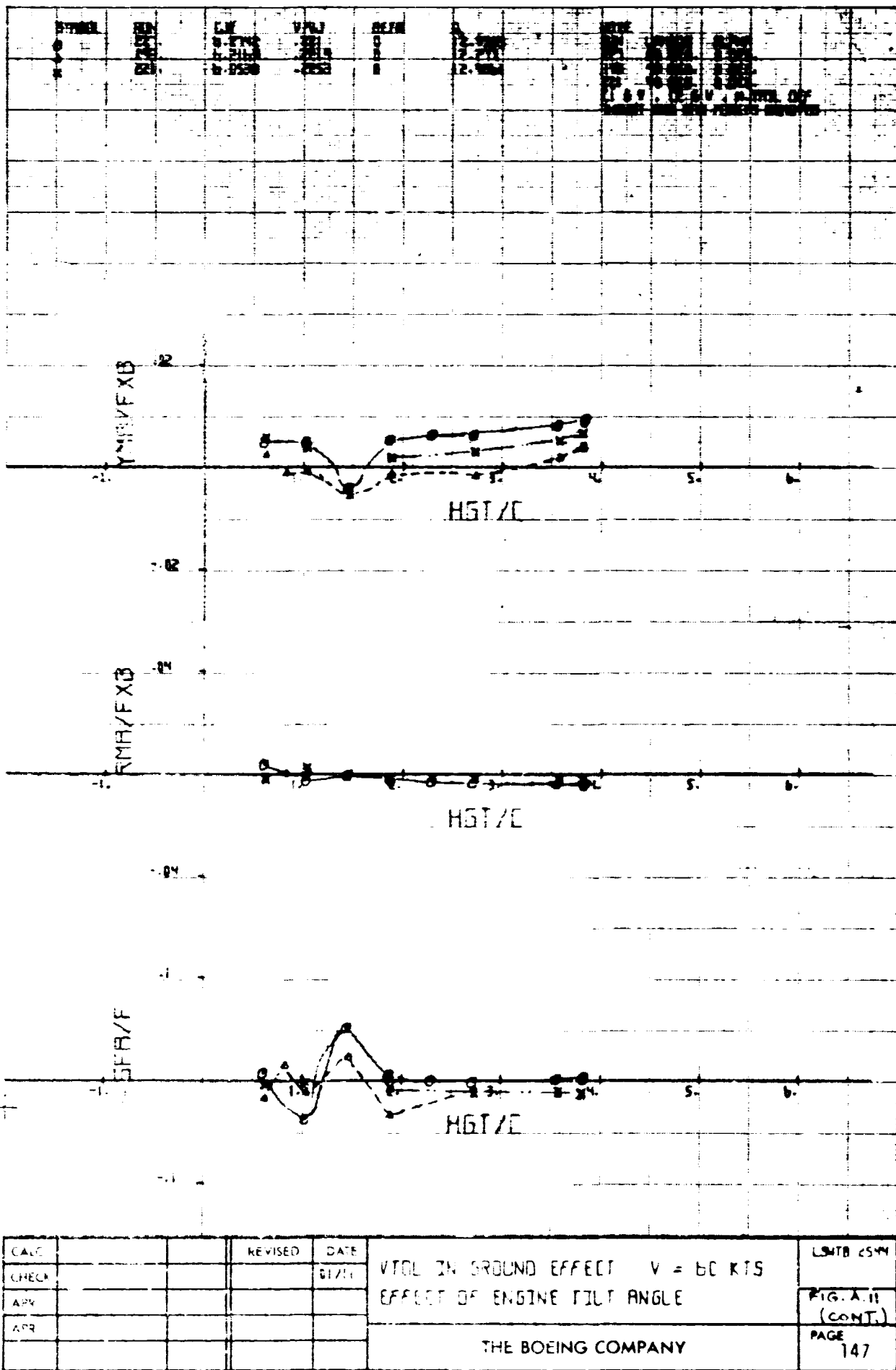
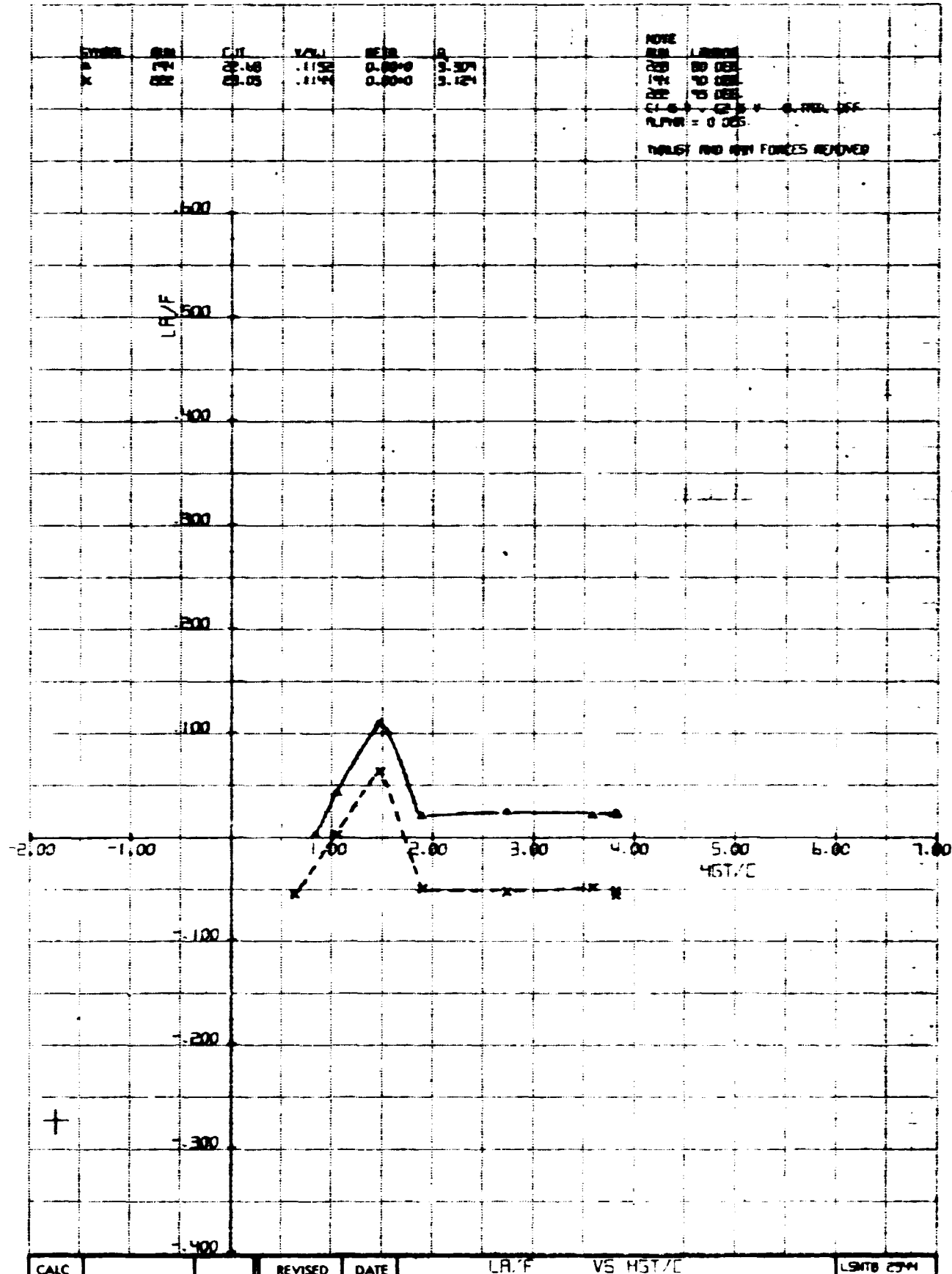


FIG 2B
lb.



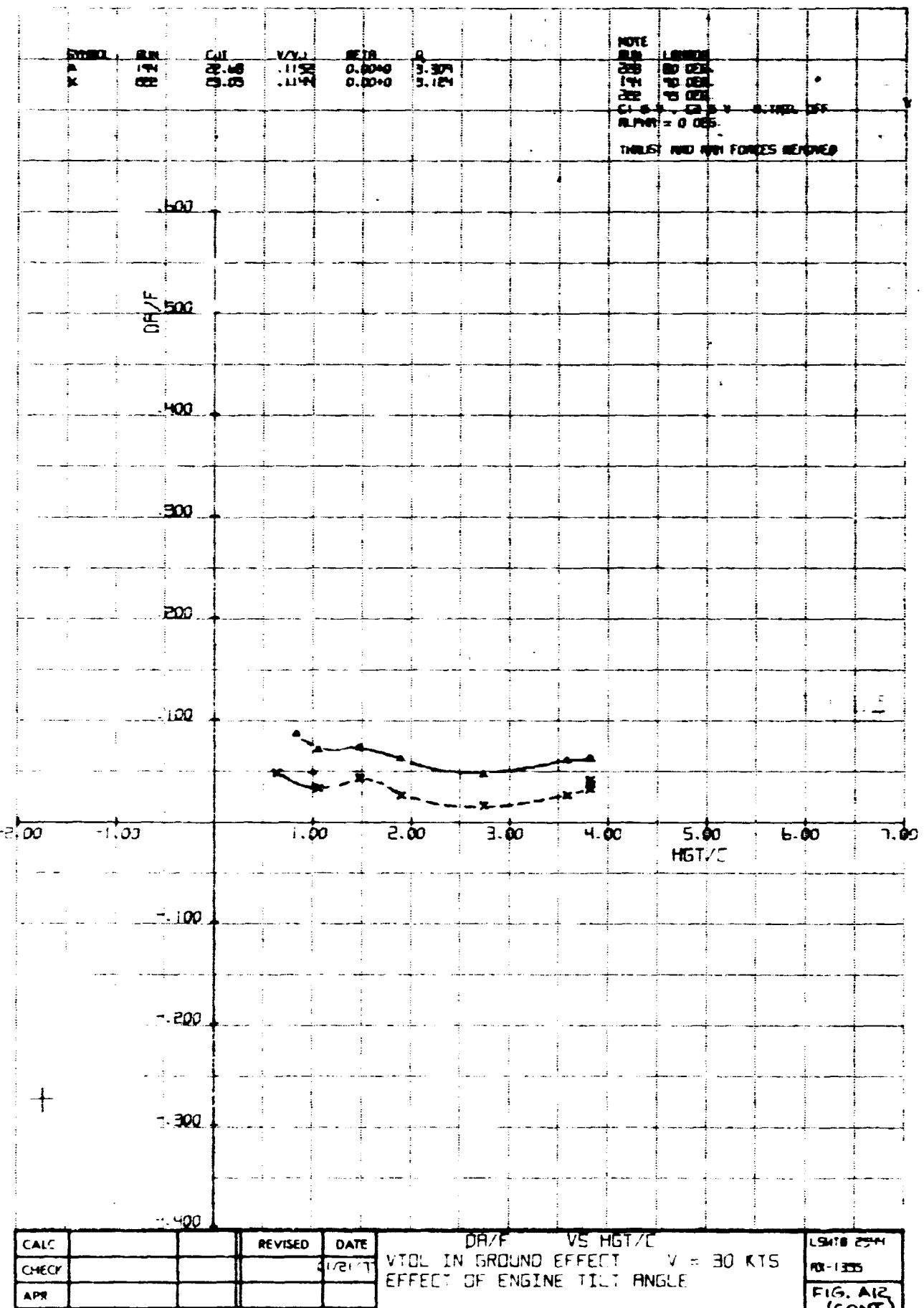
CALC	REVISED	DATE	FMA/FXC VS HGT/C VTOL IN GROUND EFFECT V = 60 KTS EFFECT OF ENGINE TILT ANGLE	LSMTB 2544 AR-1355 FIG. AII (CONT.)
CHECK		01/21/71		
APR				PAGE 14b
APR				
			THE BOEING COMPANY	

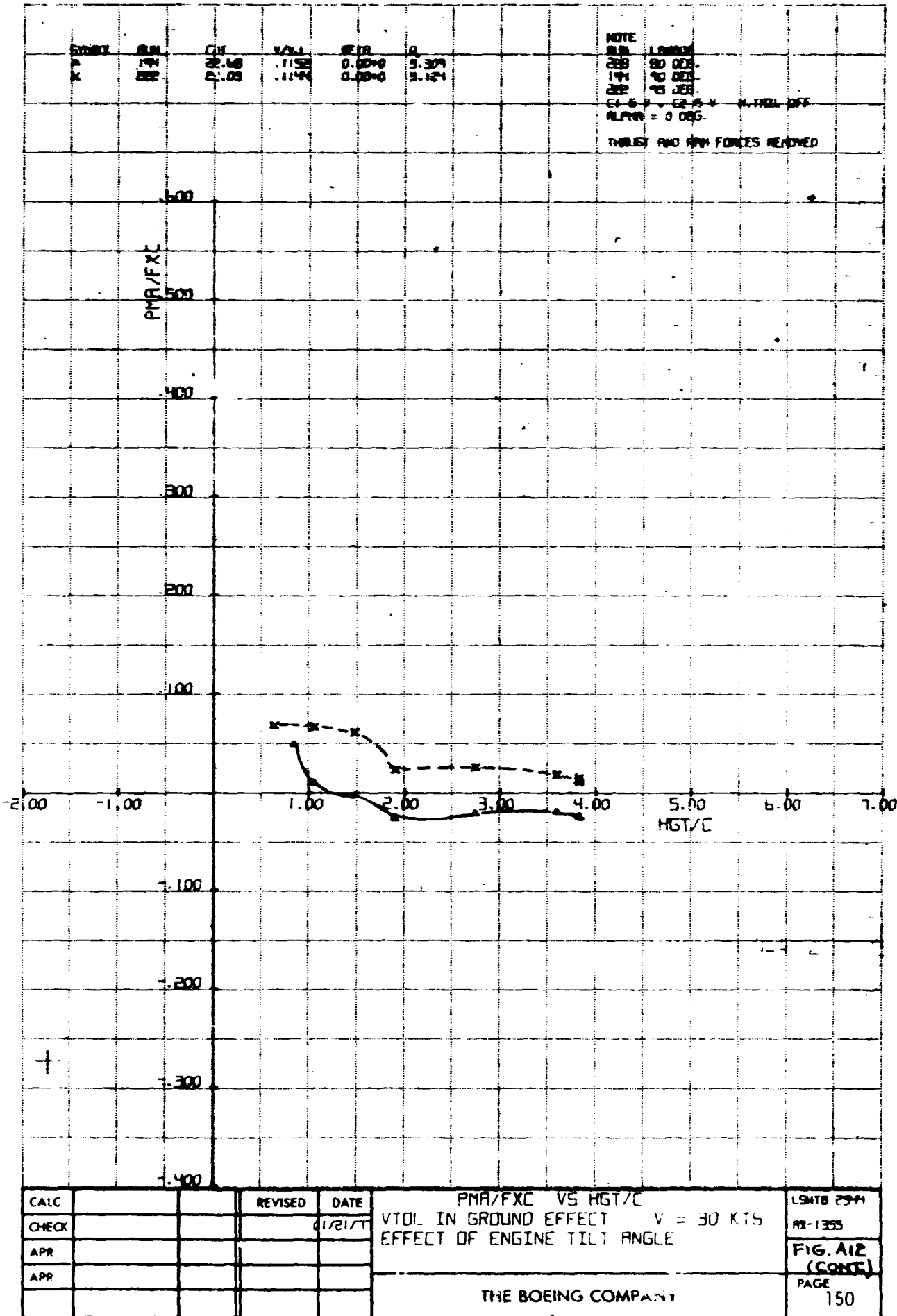


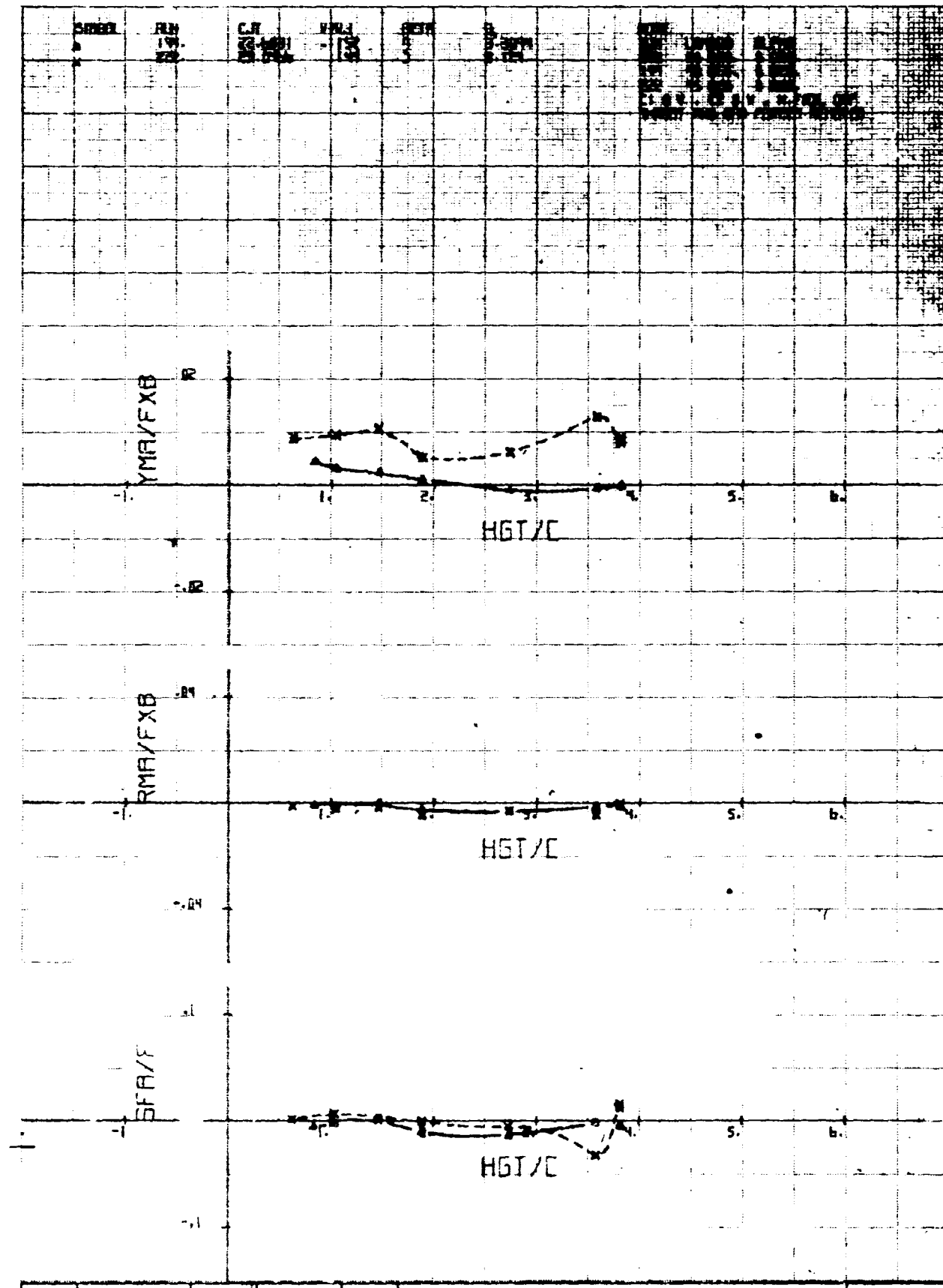


L.A.F. VS HGT/E
VTOLE IN GROUND EFFECT V = 30 KTS
EFFECT OF ENGINE TILT ANGLE

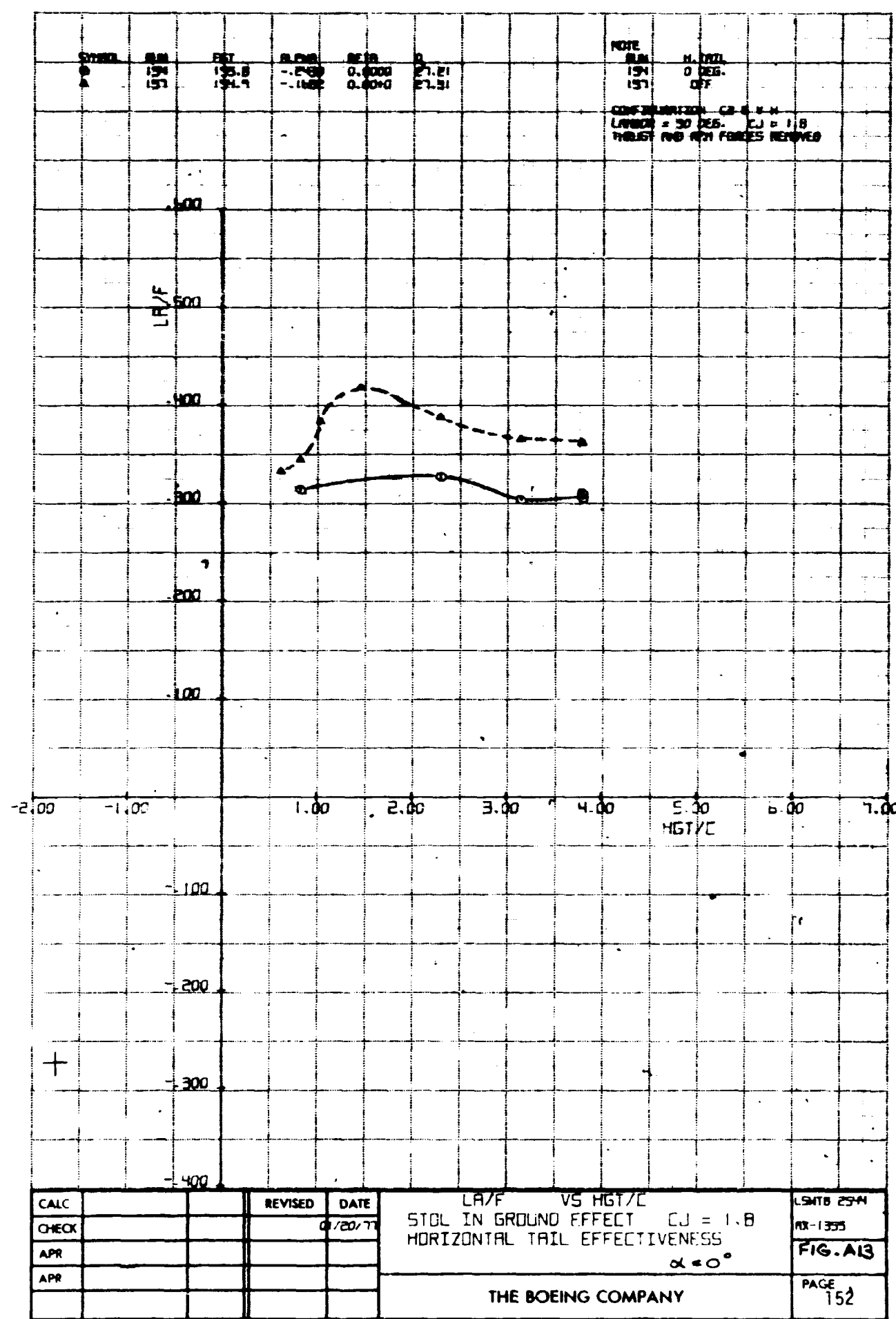
CALC		REVISED	DATE	LR/F VS HST/E VOL IN GROUND EFFECT V = 30 KTS EFFECT OF ENGINE TILT ANGLE	LSMTB 2544 R-1355 FIG.A12
CHECK			01/21/77		
APR					
APR					
				THE BOEING COMPANY	PAGE 148

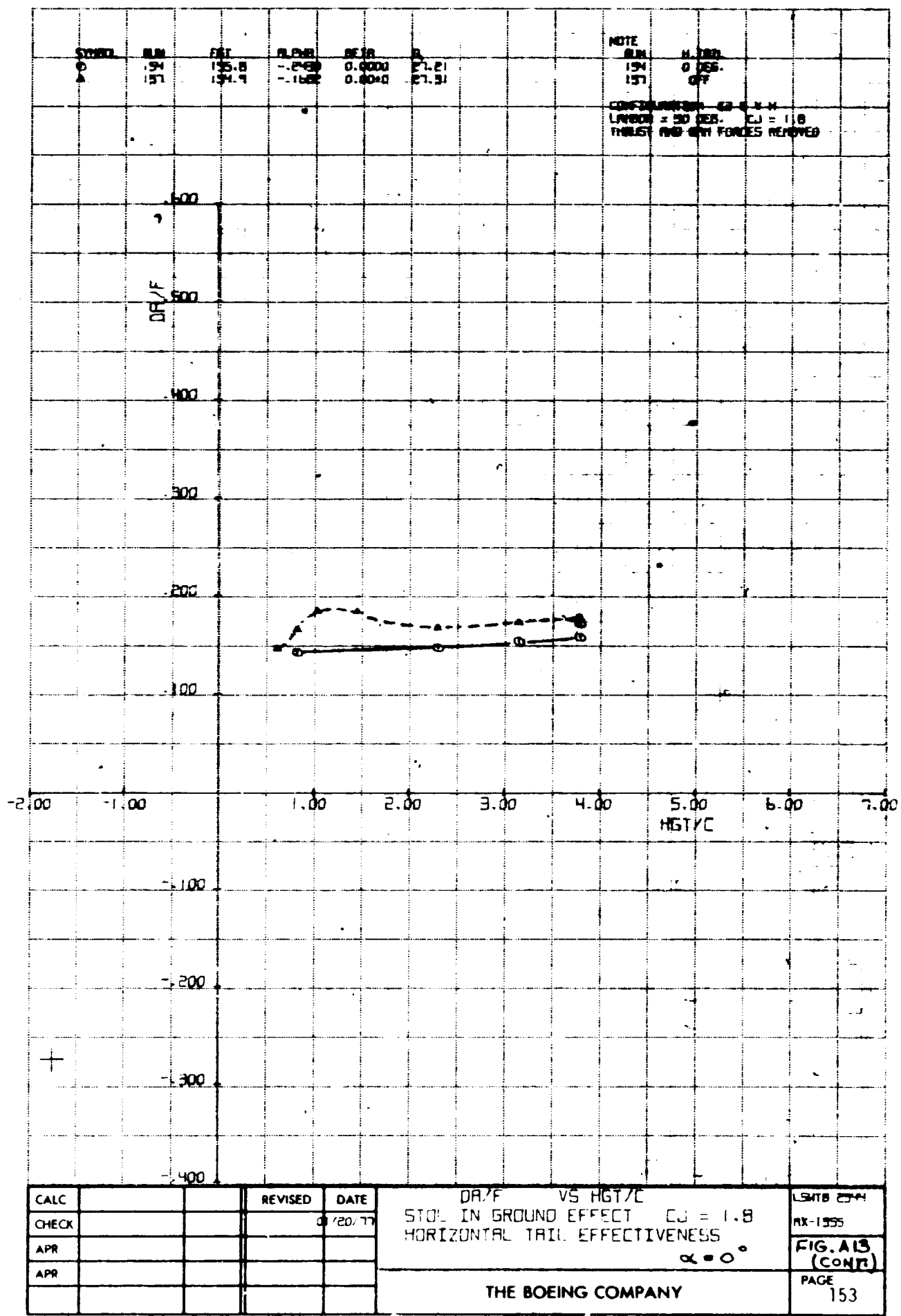






CALC			REVISED	DATE	/TOL IN GROUND EFFECT V = 30 KTS EFFECT OF ENGINE TILT ANGLE	LMTB 2544
CHECK				01/11		FIG. A12 (CONT.)
APP						
APP						
THE BOEING COMPANY					PAGE	151





፩፭

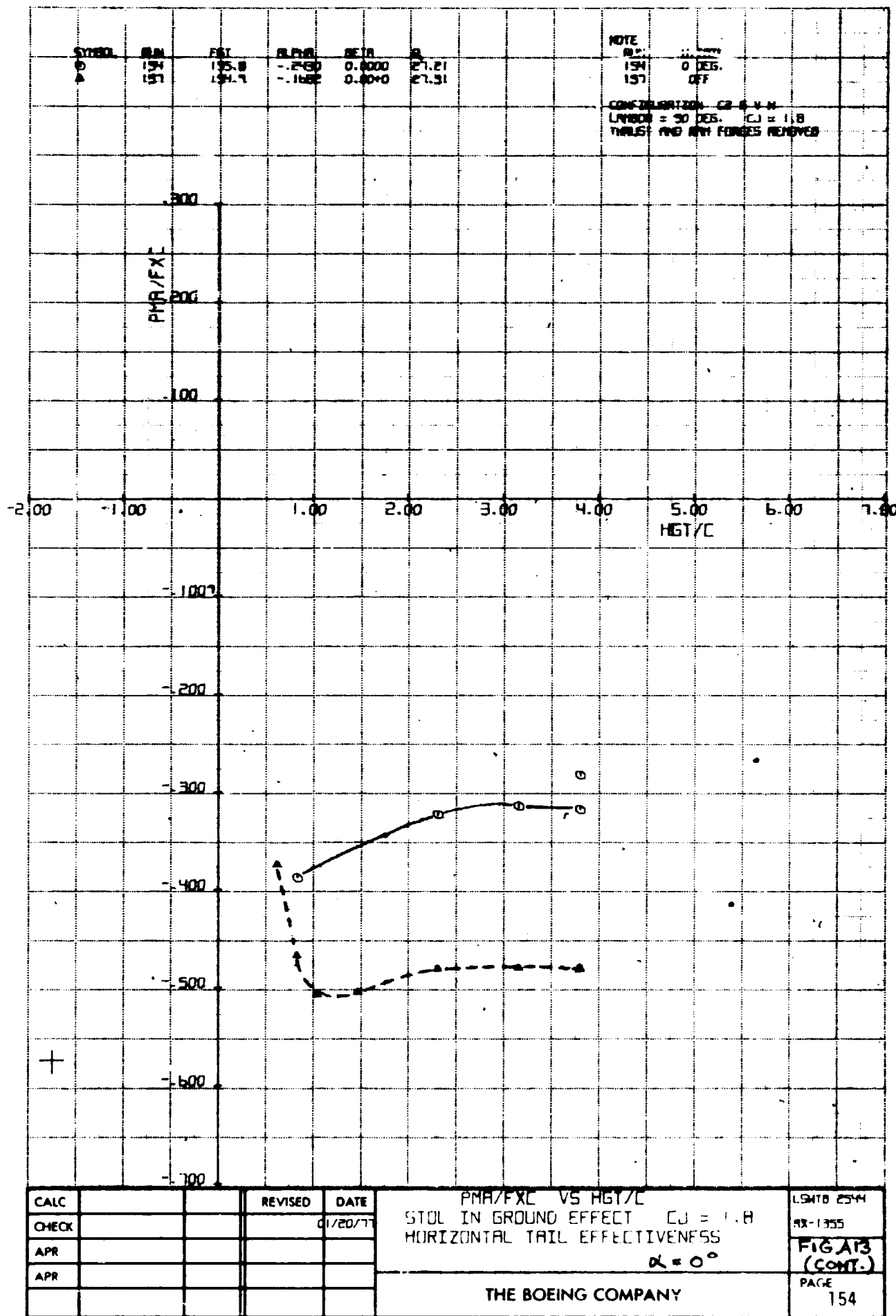
DR/F VS HGT/E
STOL IN GROUND EFFECT $C_J = 1.8$
HORIZONTAL TAIL EFFECTIVENESS

150-244

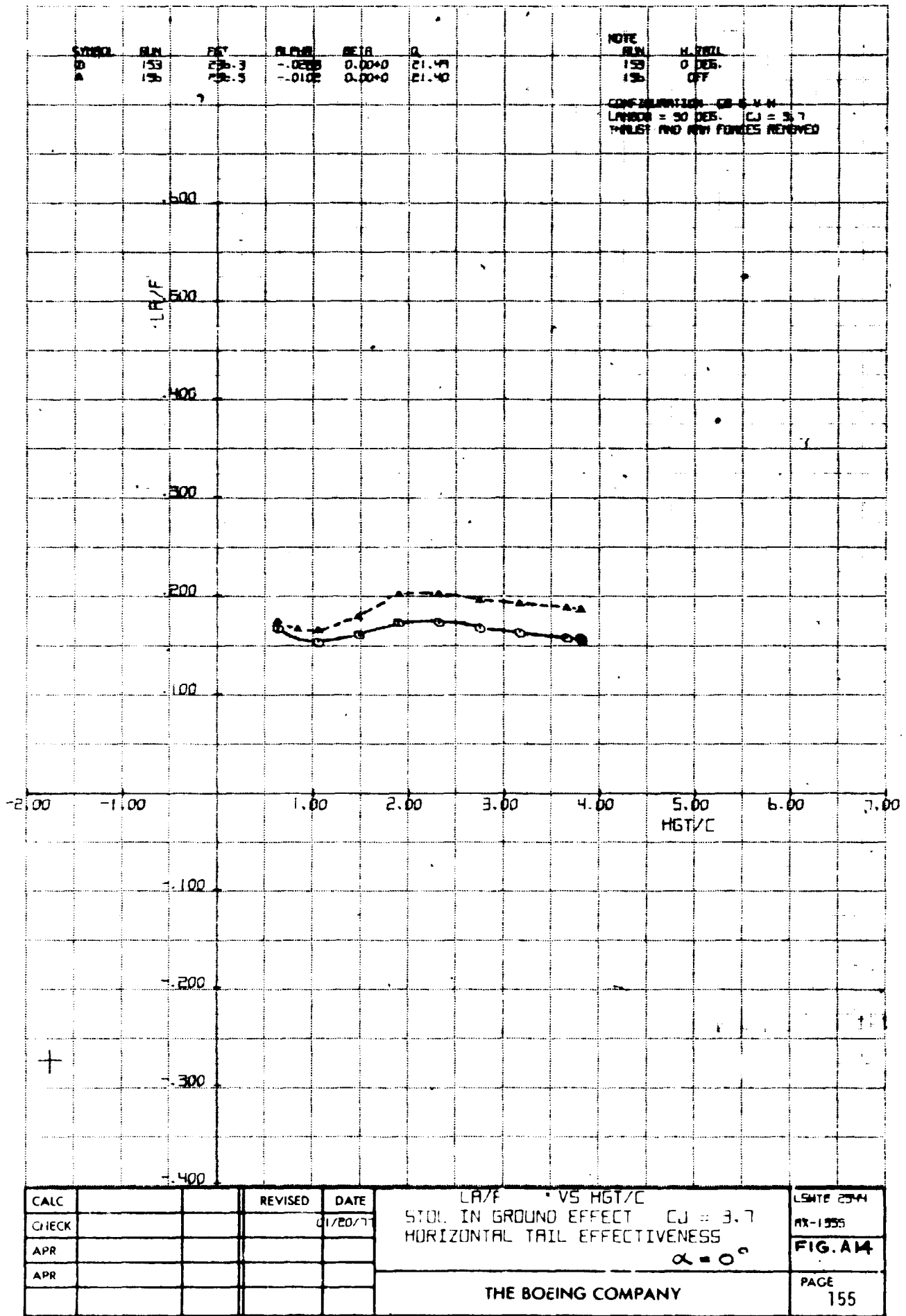
FIG. A13
(CONT)

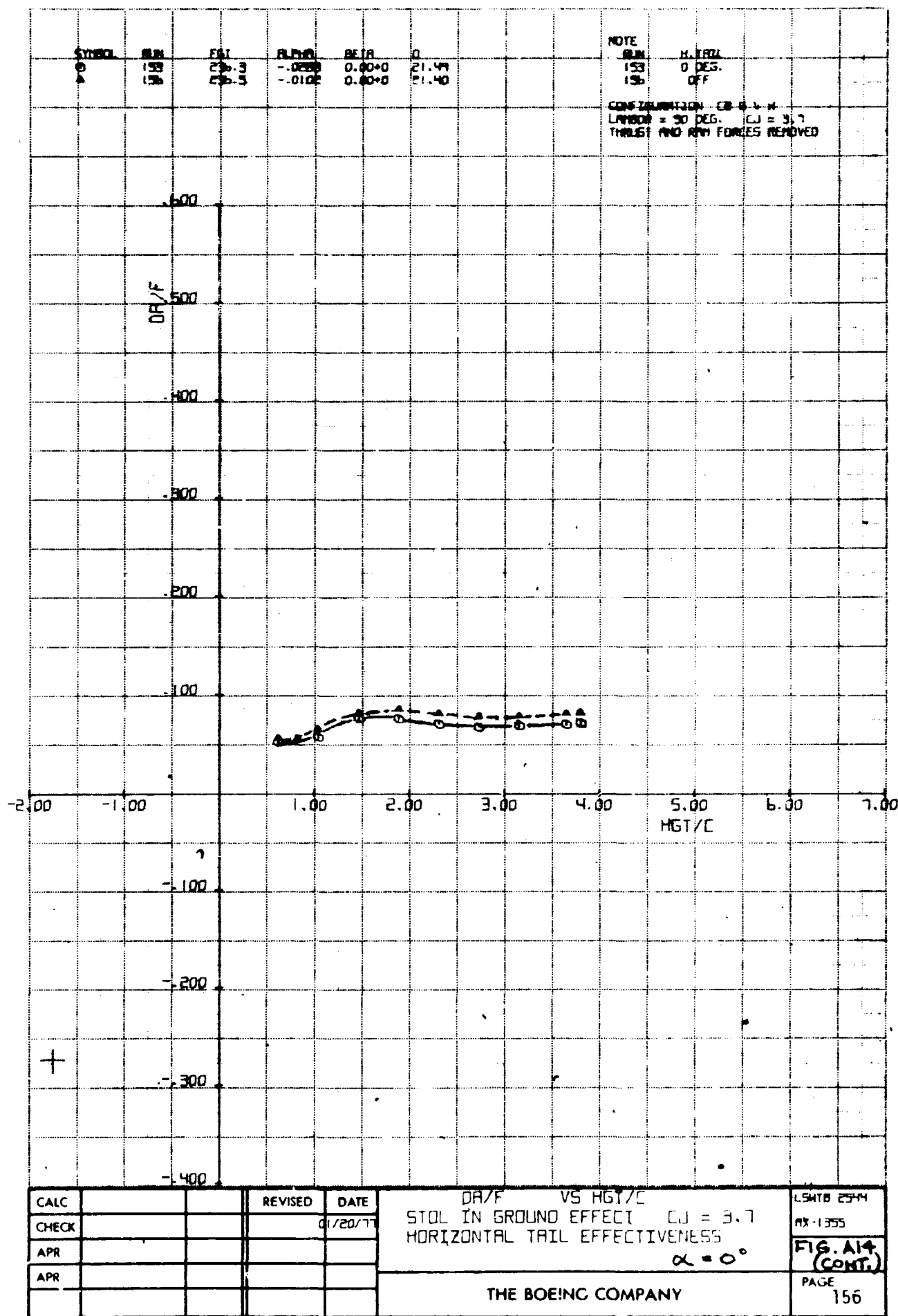
THE BOEING COMPANY

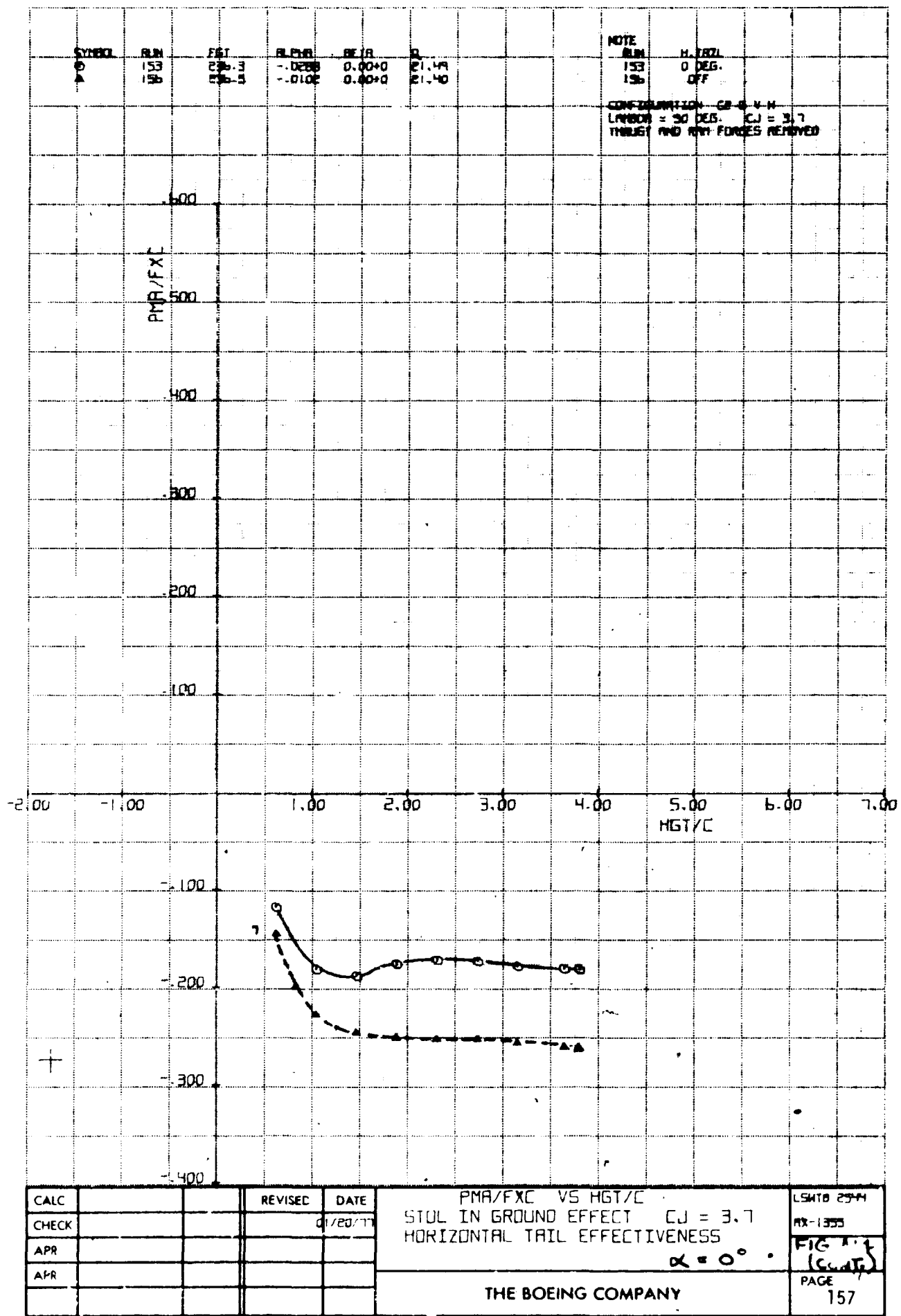
PAGE
153

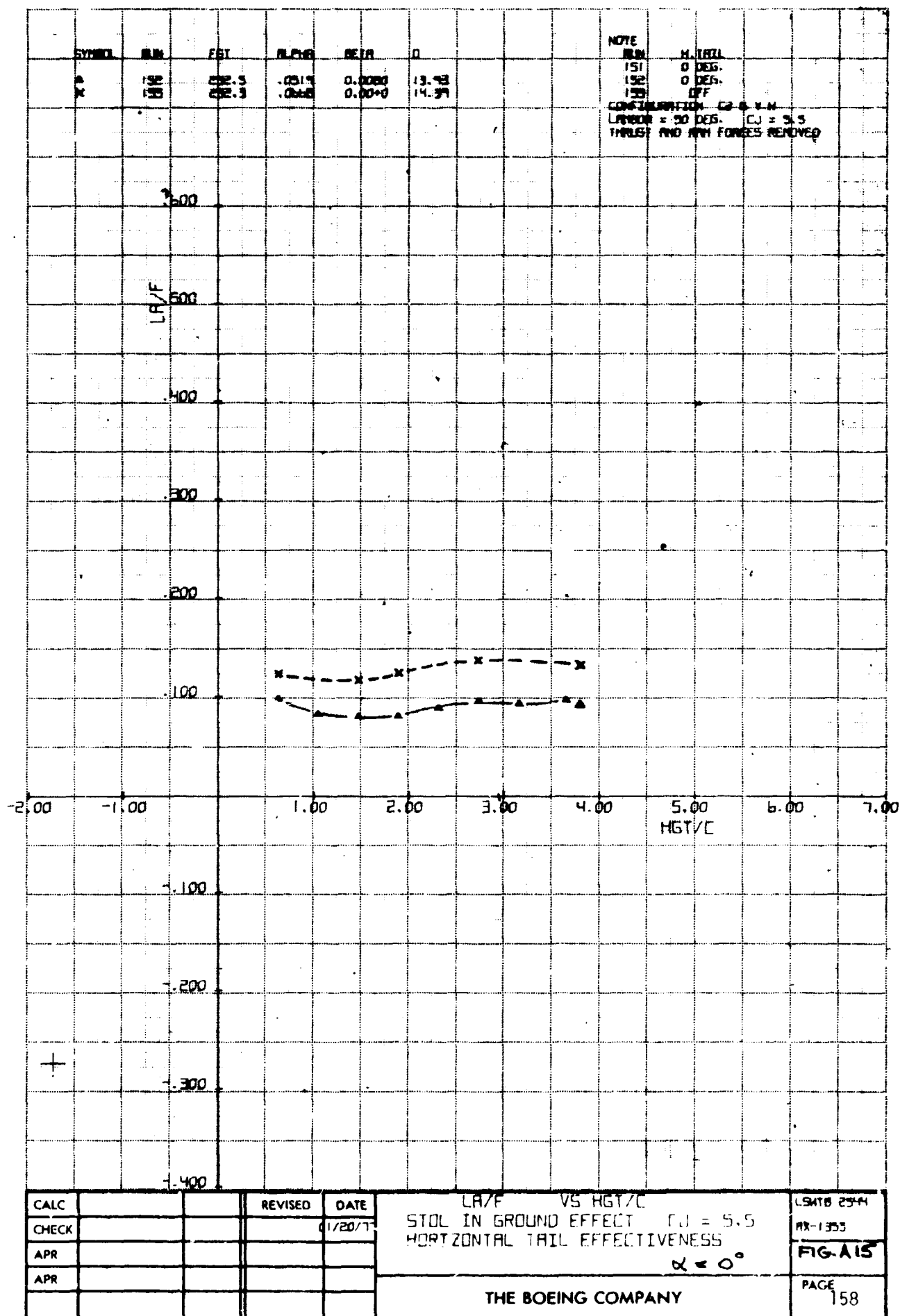


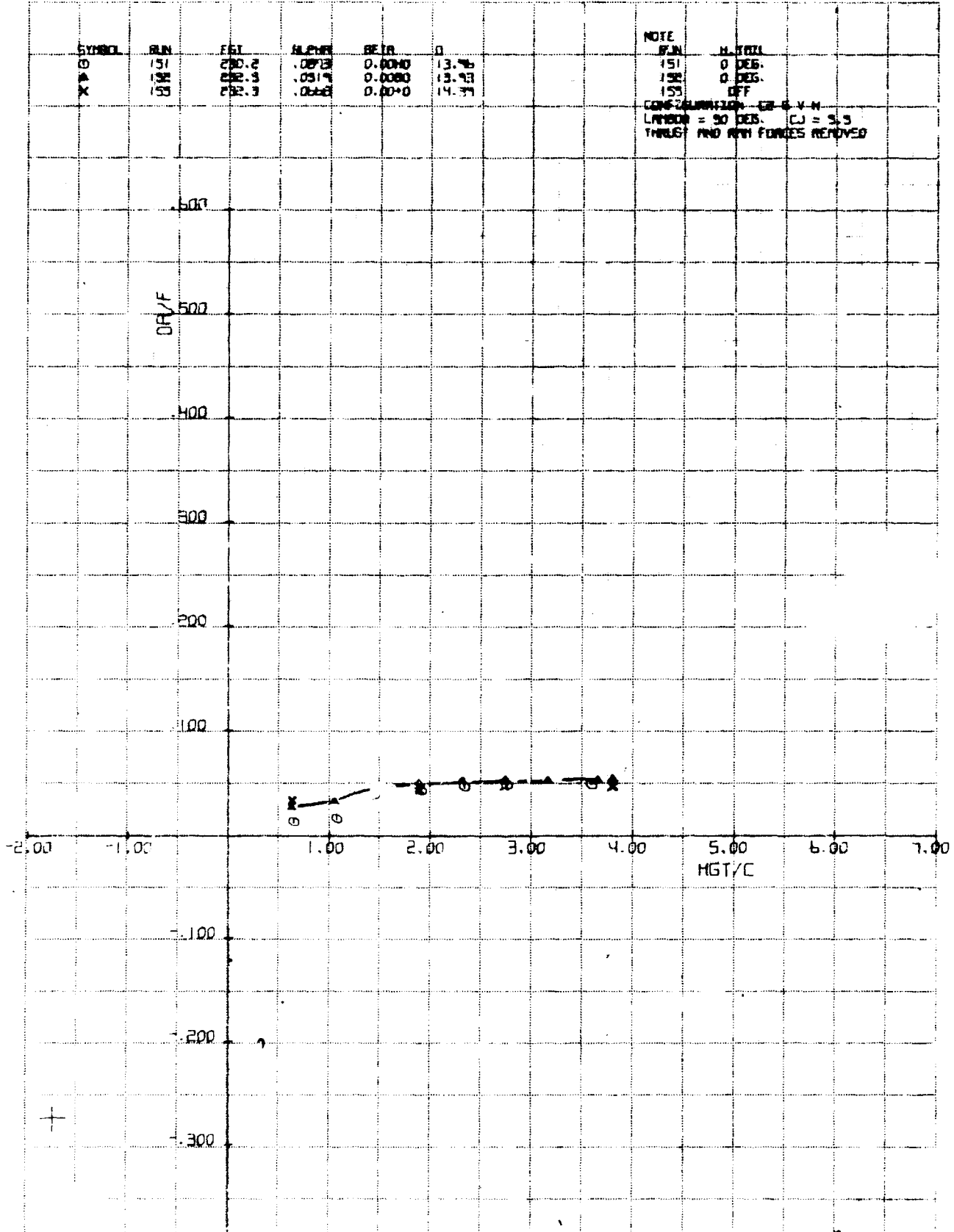
fis
26.







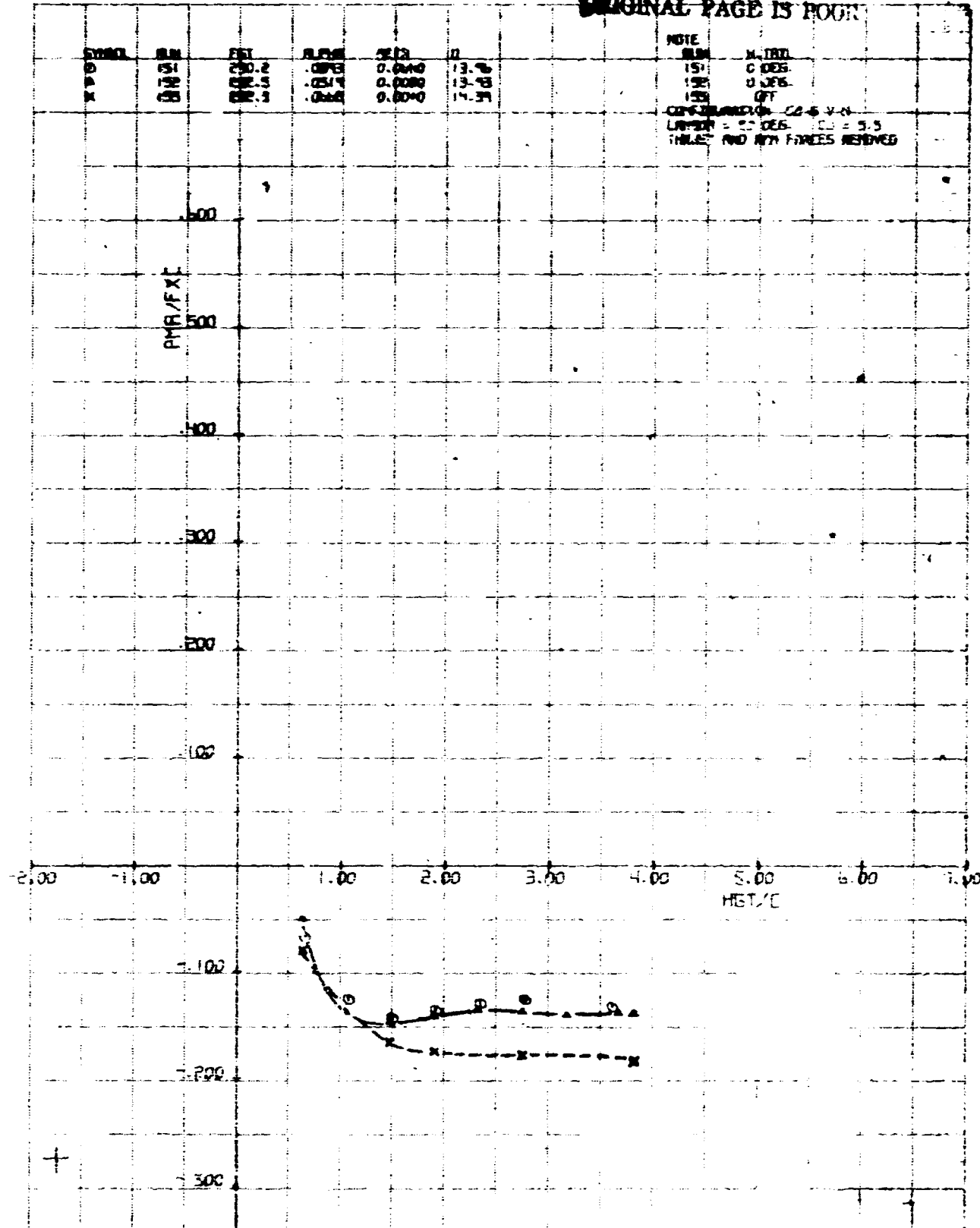




CALC		REVISED	DATE	DR/F VS HGT/C	LSNTO 254
CHECK			01/20/77	SIM IN GROUND EFFECT CJ = 5.5	AR-1355
APP				HORIZONTAL TAIL EFFECTIVENESS	
APP				$\alpha = 0^\circ$	
				THE BOEING COMPANY	PAGE 159

FIG. 9
31

**REPRODUCIBILITY OF THE
ORIGINAL PAGE IS PROVEN**

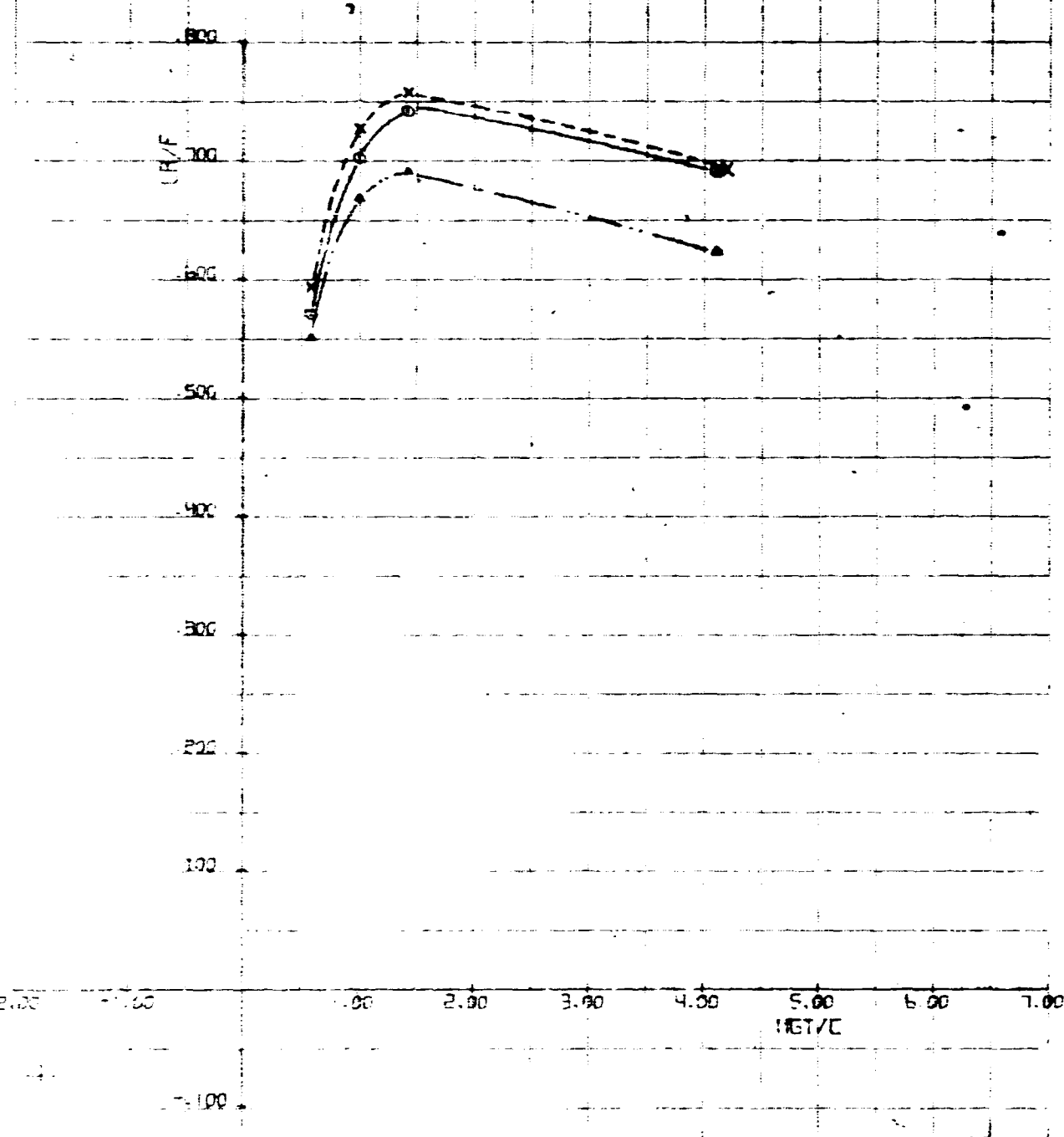


CALC	REVISED	DATE	PMR/FXC VS HGT/E	LMTB 2044
CHECK		1/20/T	STOL IN GROUND EFFECT $C_L = 5.5$	MR-1725
APR			HORIZONTAL TRAIL EFFECTIVENESS	FIG. A15 (CONT.)
APP			$\alpha = 0^\circ$	PAGE 160

THE BOEING COMPANY

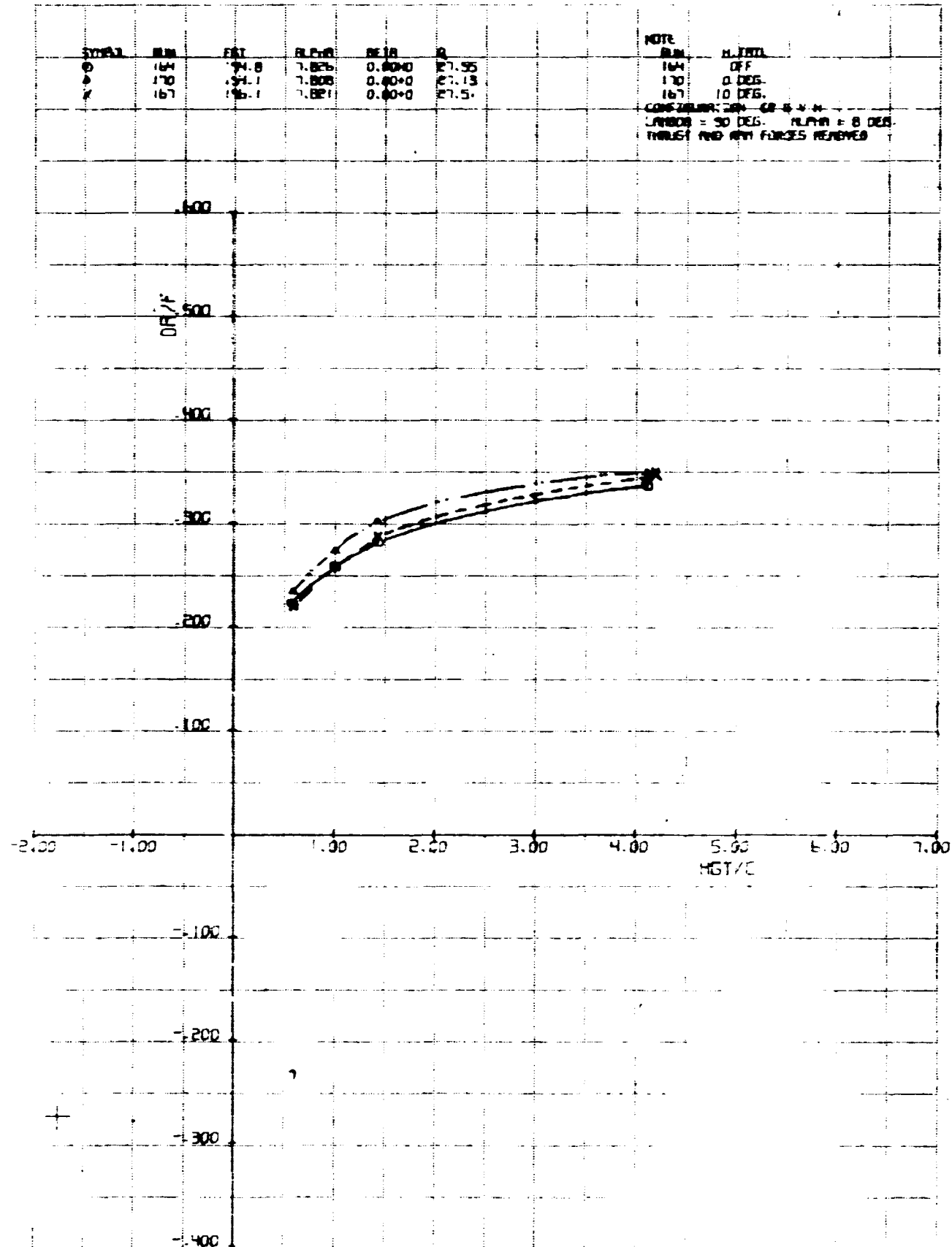
STAB	SLN	FAT	SL.DIA.	SL.DIA.	SL.DIA.	NOTE	SL.DIA.
O	55	134.6	7.888	0.000	21.95	100% OFF	100% OFF
O	70	134.7	7.888	0.000	21.13	100% 0 DEG.	100% 0 DEG.
X	67	136.6	7.887	0.000	21.51	100% 10 DEG.	100% 10 DEG.

DISCREPANCY = 0.4 X 10⁻³
LATERAL = 30 DEG. WILDER F B DEG.
TRAILING AND SWI FORCES REMOVED

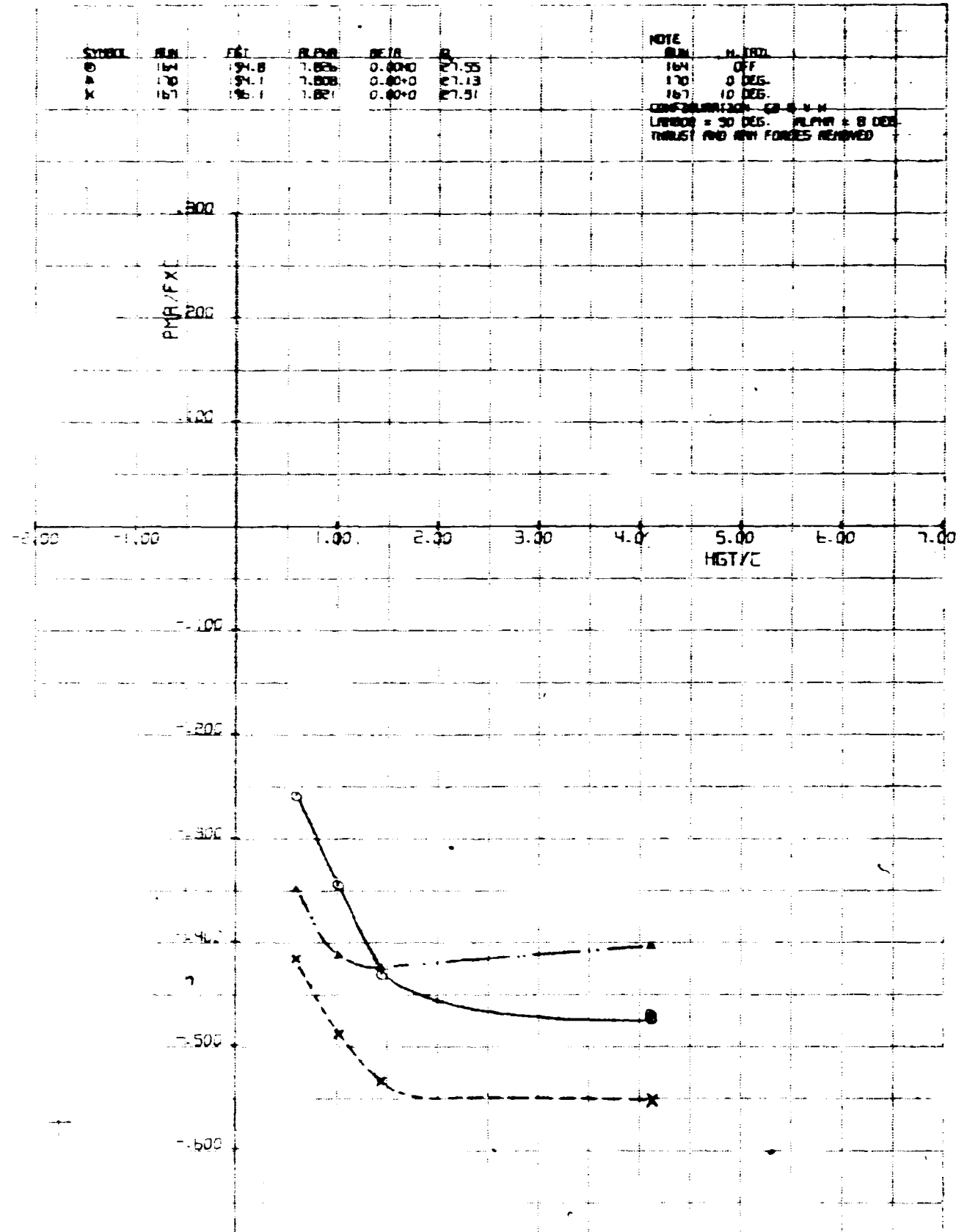


CALC	REVISED	DATE	L/A/F VS MGT/C STOL IN GROUND EFFECT CU = 1.8 EFFECT OF H. TAIL ALPHA = 8 DEG.	LSMTB 204 FD-1355 FIG. AM6
DRCK		12/27/71		
A/R				
APT				PAGE 161

THE BOEING COMPANY

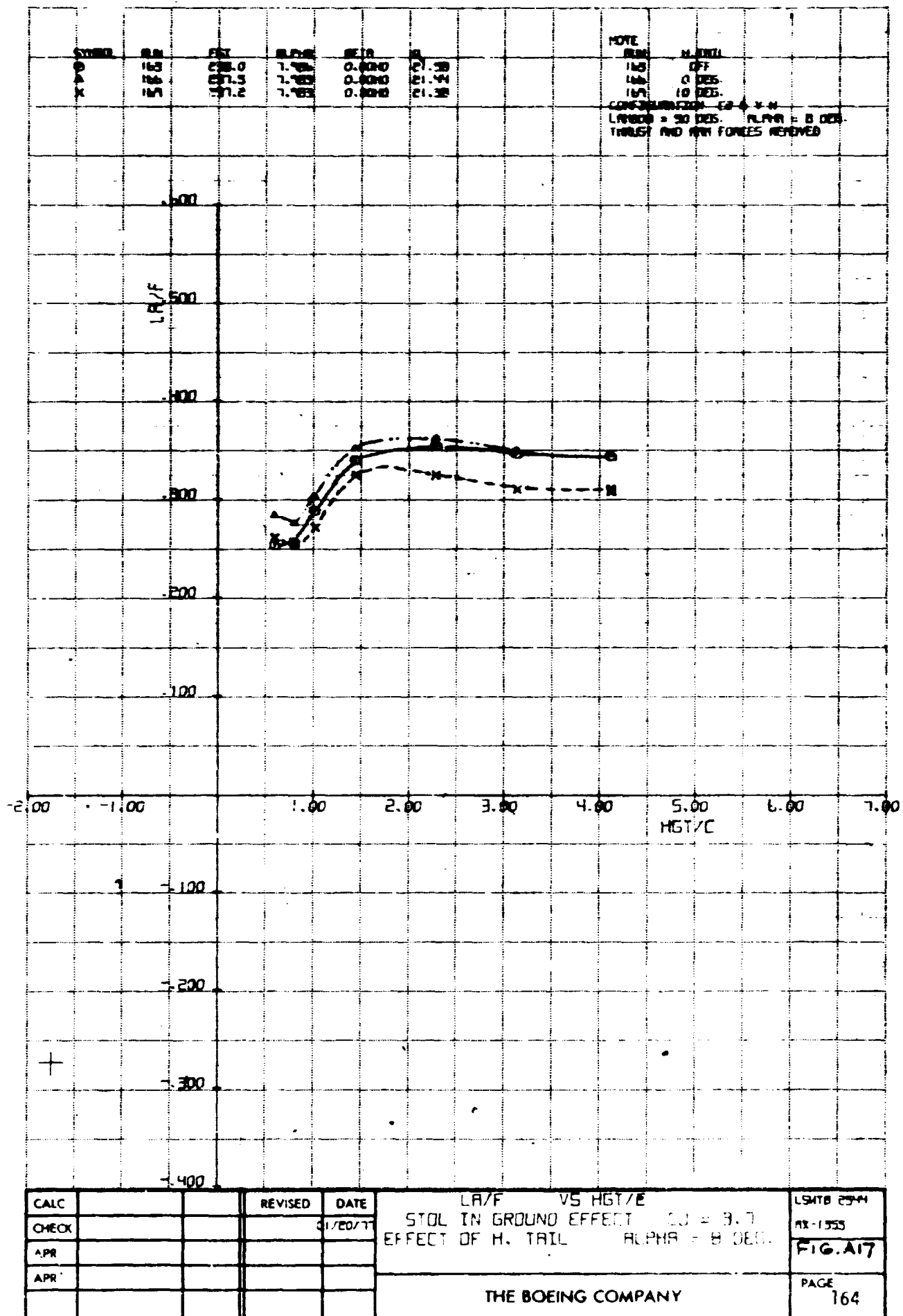


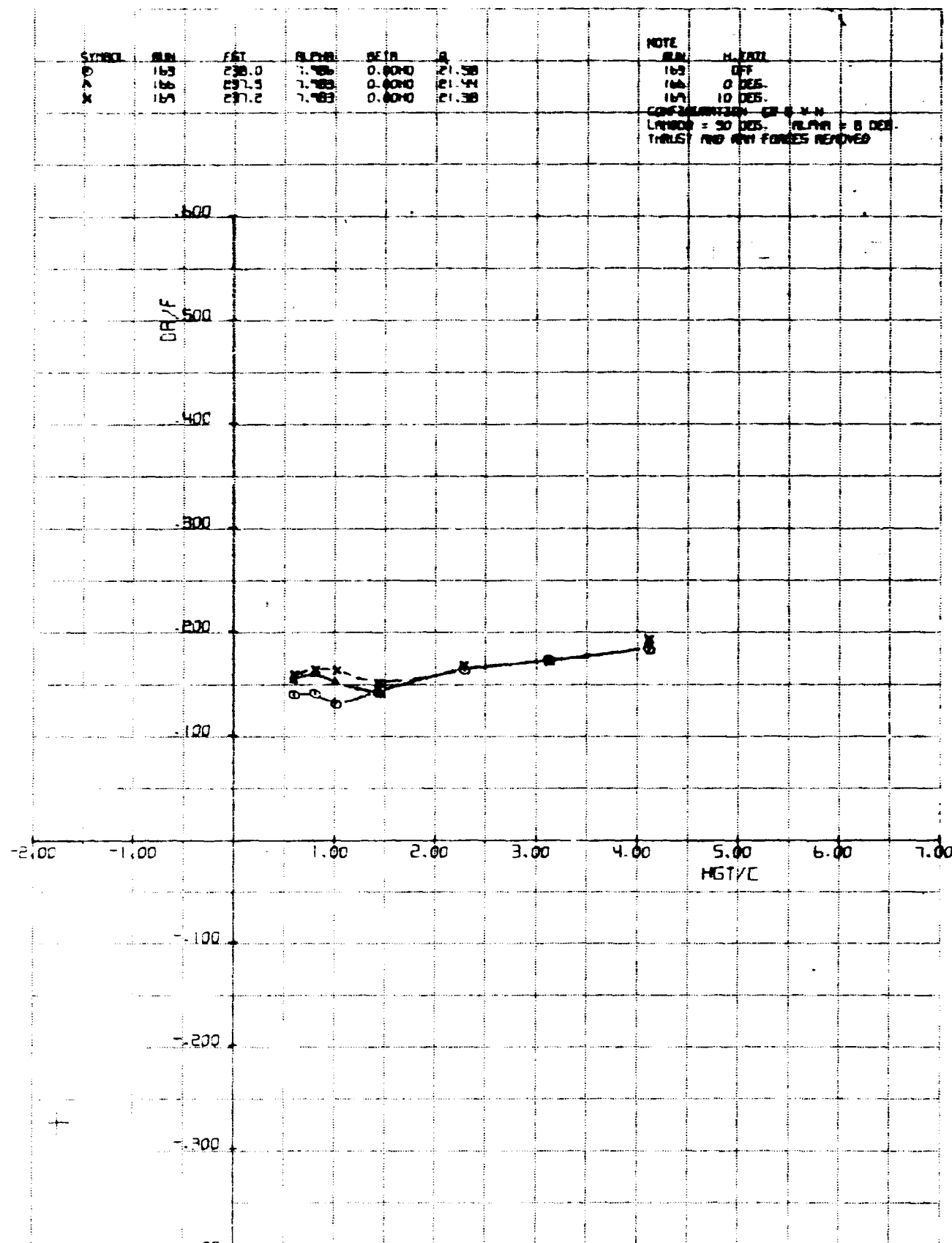
CALC		REVISED	DATE	DR/F VS HGT/C STUDY IN GROUND EFFECT C = 1.8 EFFECT OF H. TAIL ALPHAS = 8 DEG.	SDTB 2544 18-1365 FIG A16 (CONT.) PAGE 162
CHECK			6/20/11		
APR					
APR					
				THE BOEING COMPANY	



CALC		REVISED	DATE	PMR/FXC VS HGT/C SINGLE IN GROUND EFFECT. CD = 1.8 EFFECT OF H. TAIL. ALPHA = 8 DEG	LMTB 2344 RX-1555
CHECK			01-20-71		FIG. A16 (CONT)
APR					PAGE
APR					163

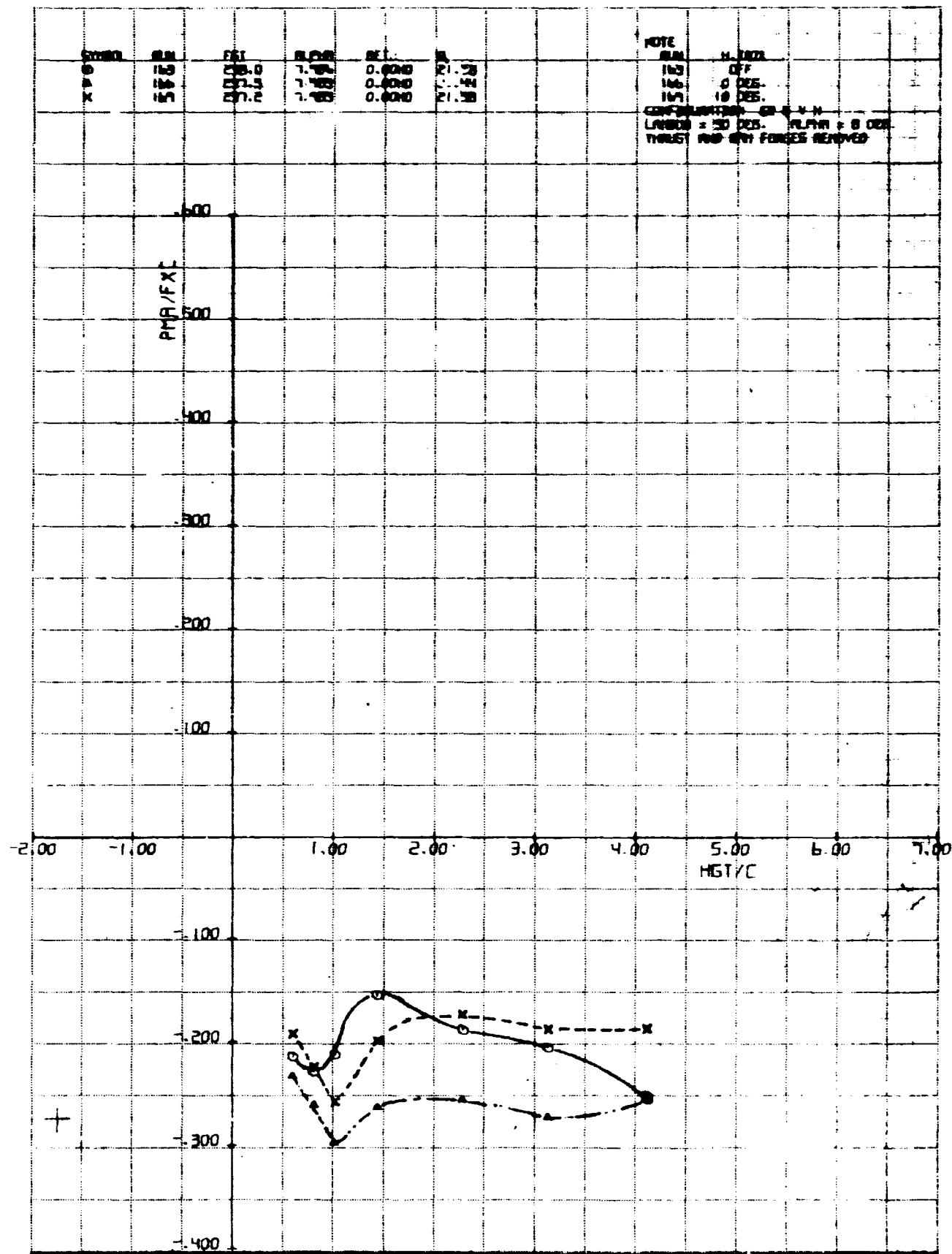
THE BOEING COMPANY



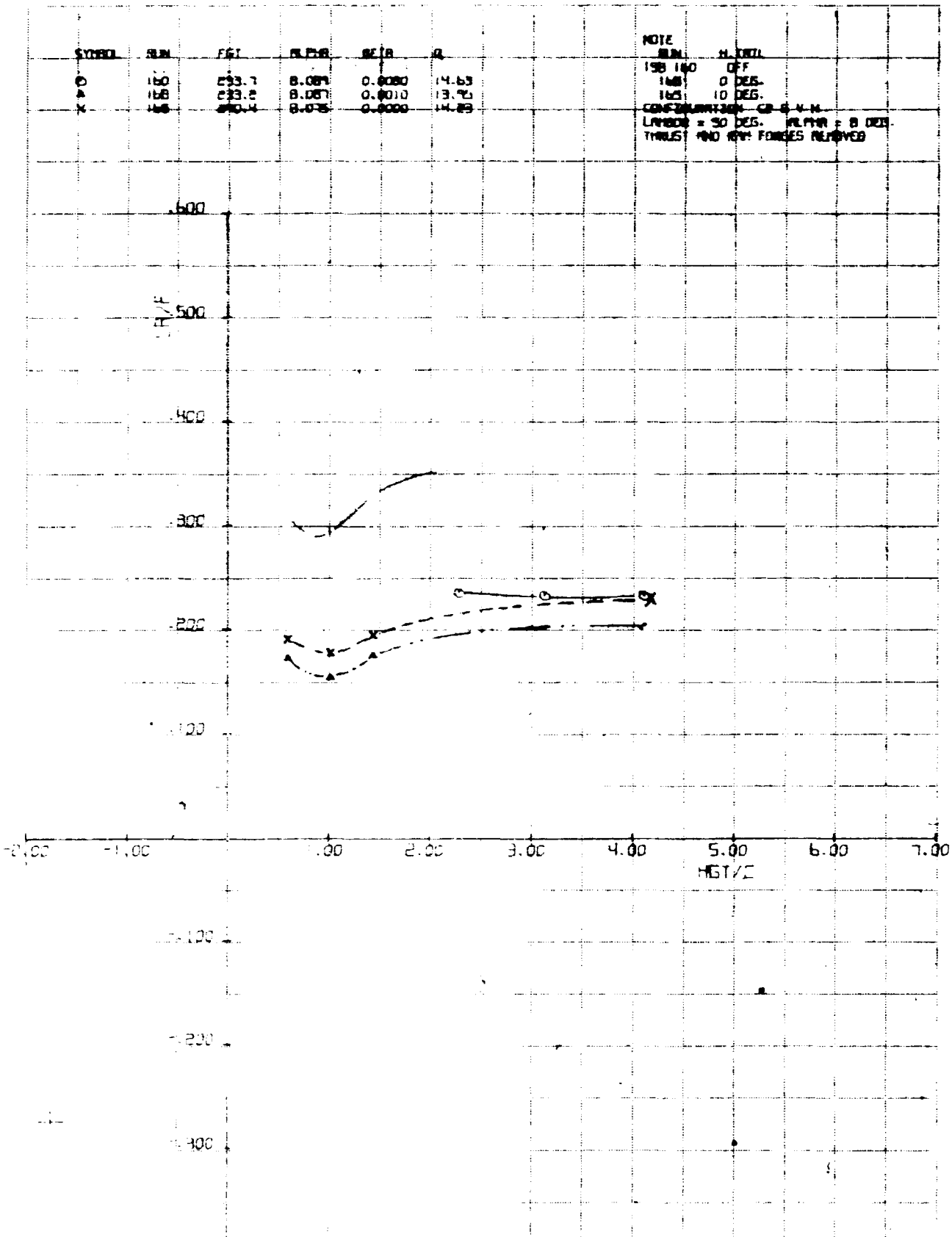


CALC	REVISED	DATE	DR/D _E VS HGT/C	LMTB 2344
CHECK		01/20/11	STAB IN GROUND EFFECT C _J = 3.7	RX-1355
APR			EFFECT OF H. TAIL ALPHA = 8 DEG.	FIG.A17 (CONT.)
APR			THE BOEING COMPANY	PAGE 165

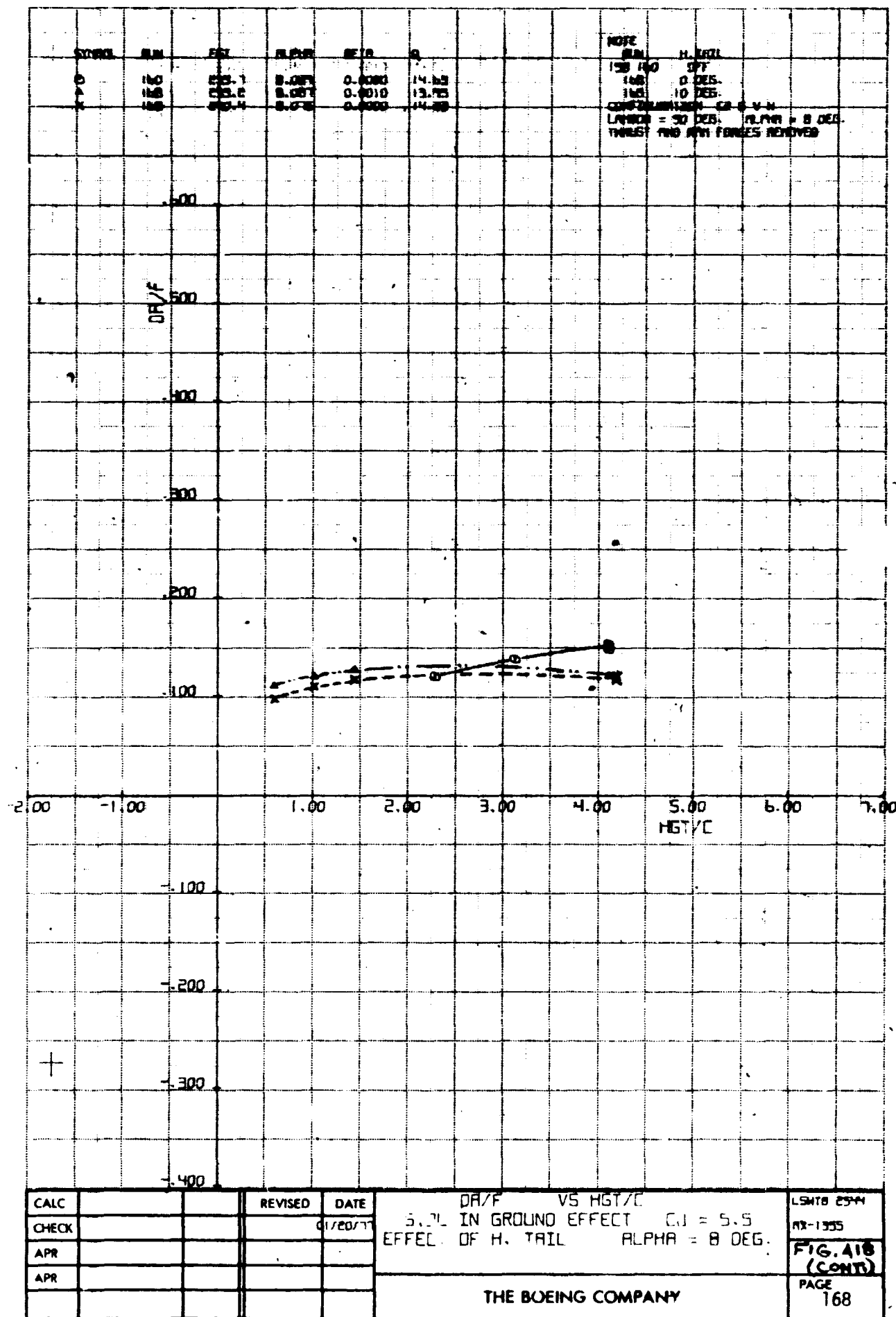
FIG. A17
13.

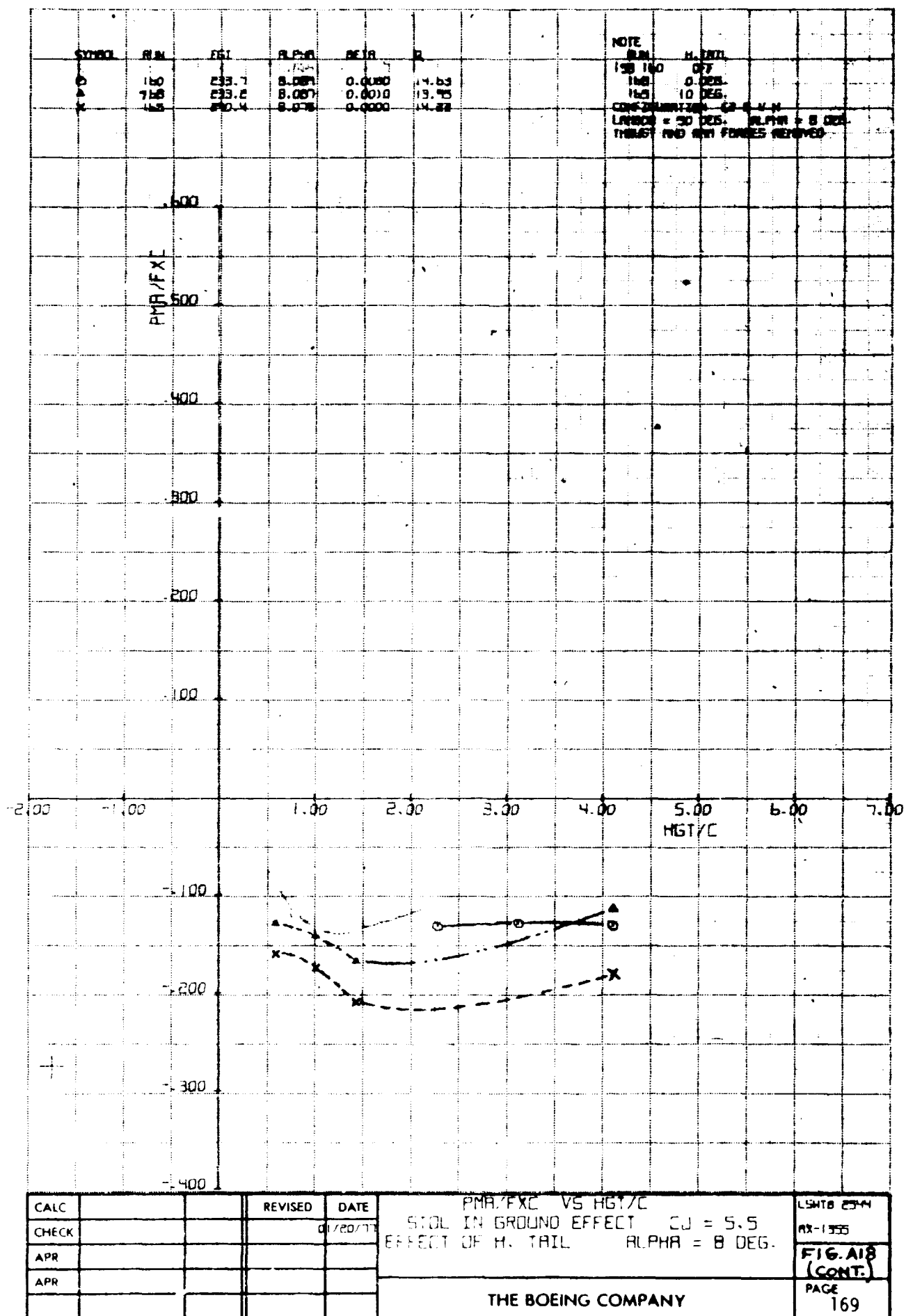


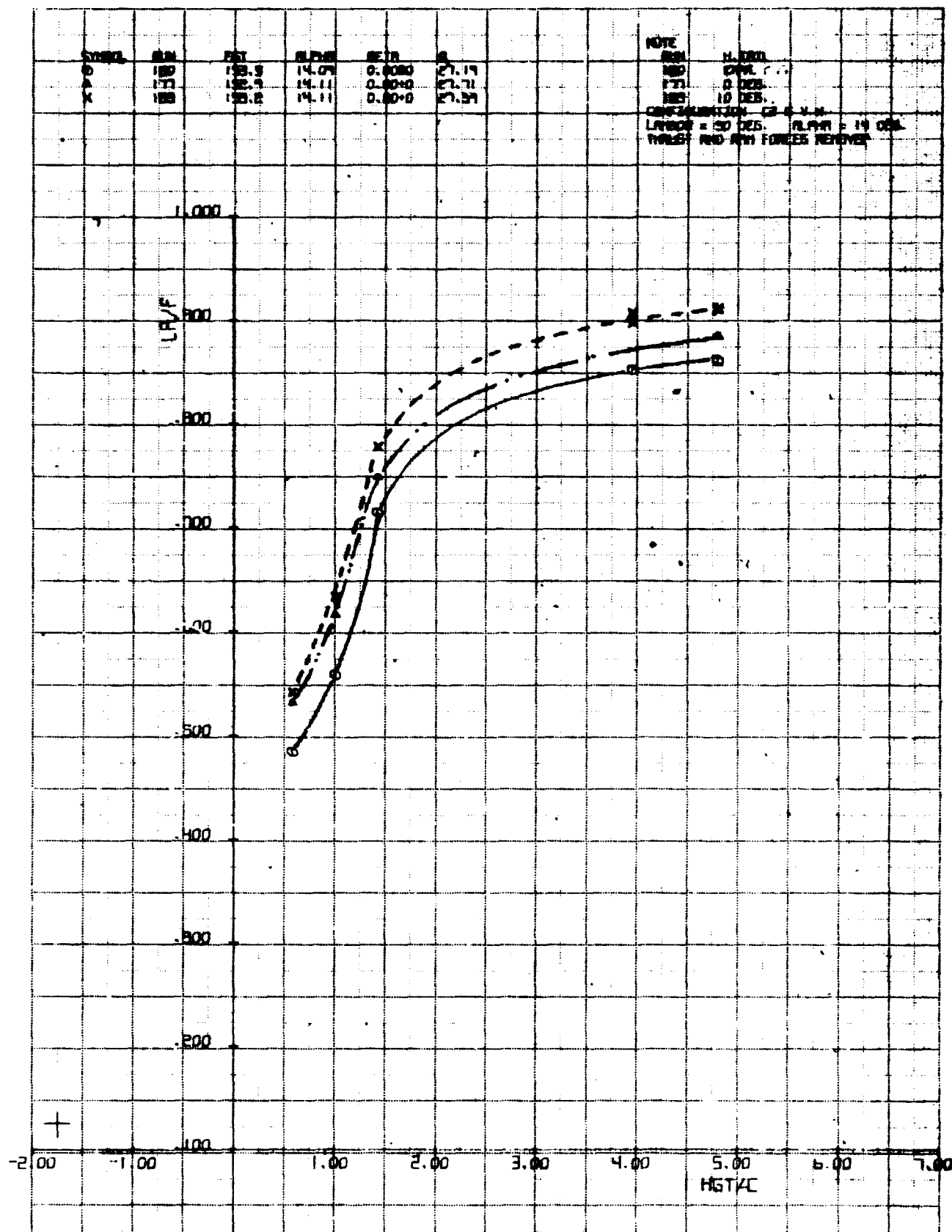
CALC		REVISED	DATE	PMAX/XC VS HGTC STOL IN GROUND EFFECT (J = 3.7) EFFECT OF H. TRAIL ALPHA = 8 DEG.	SITE 2344 PA-1555 FIG. A17 (CONT.)
CHECK			01/20/77		
APR					
APR					PAGE 166



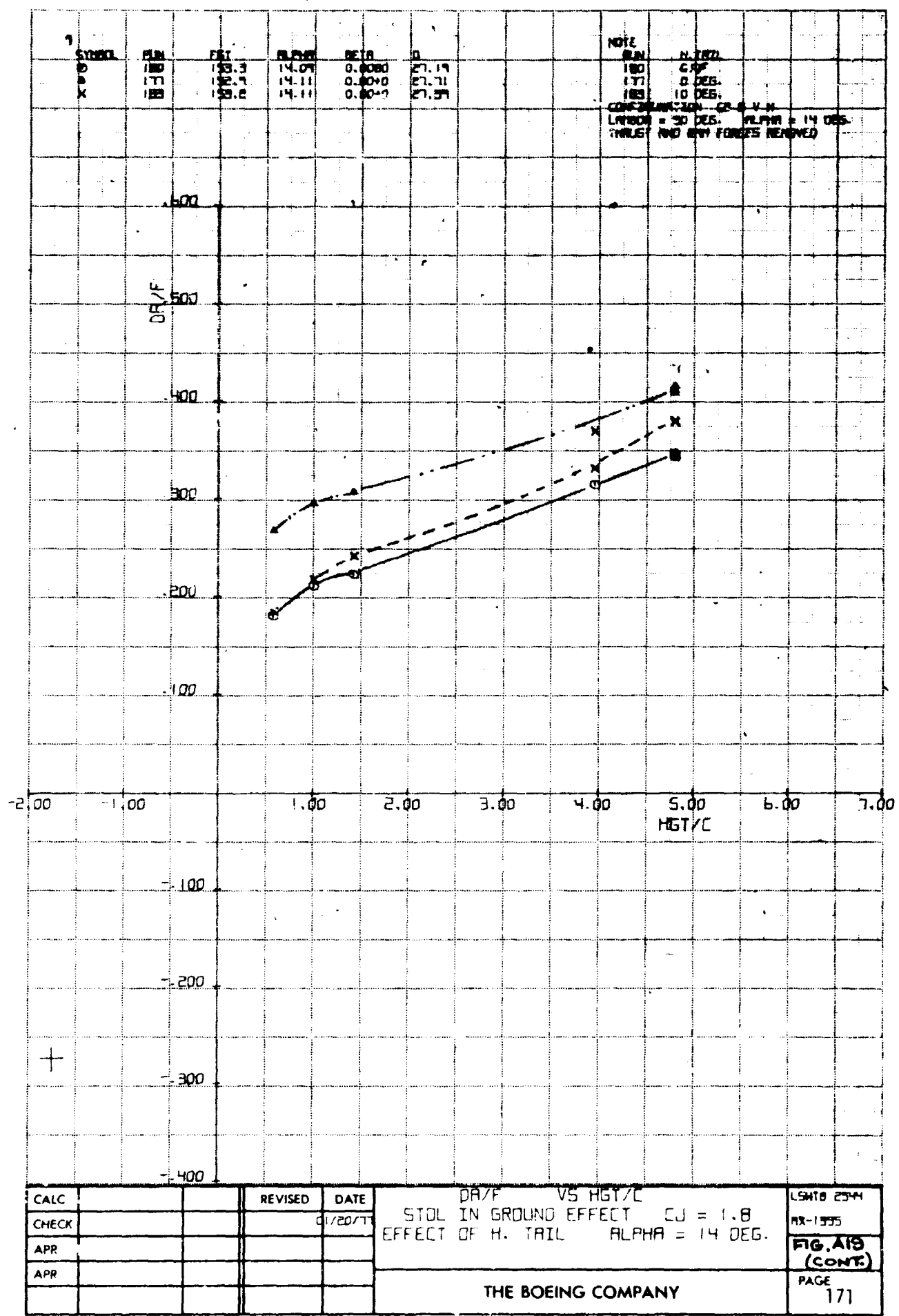
CALC			REVISED	DATE	CL/E VS HGT/Z	LSMTB 2544
CHECK				04-60-01	STAB IN GROUND EFFECT CL = 5.5	MX-1555
APR					EFFECT OF H. THRU. ALPHAS = 8 DEG	FIG. A18
APR					THE BOEING COMPANY	PAGE 167

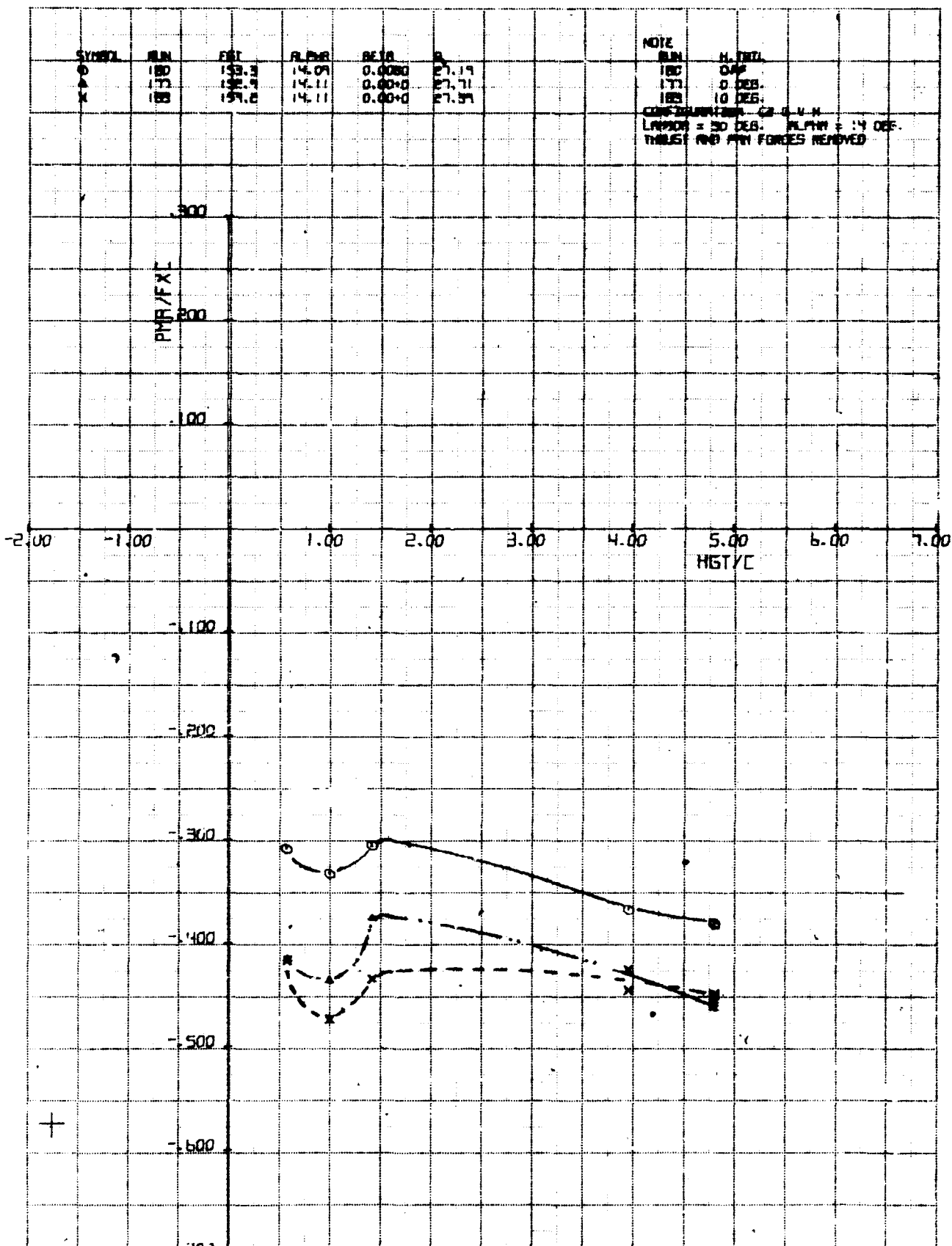






CALC	REVISED	DATE	LA/F VS HGT/C	LMTB 2944 MX-1355 FIG. A39
CHECK		01/20/77	STOL IN GROUND EFFECT C.J. = 1.8 EFFECT OF H. TAIL ALPHA = 14 DEG.	
APR				
APR			THE BOEING COMPANY	PAGE 170



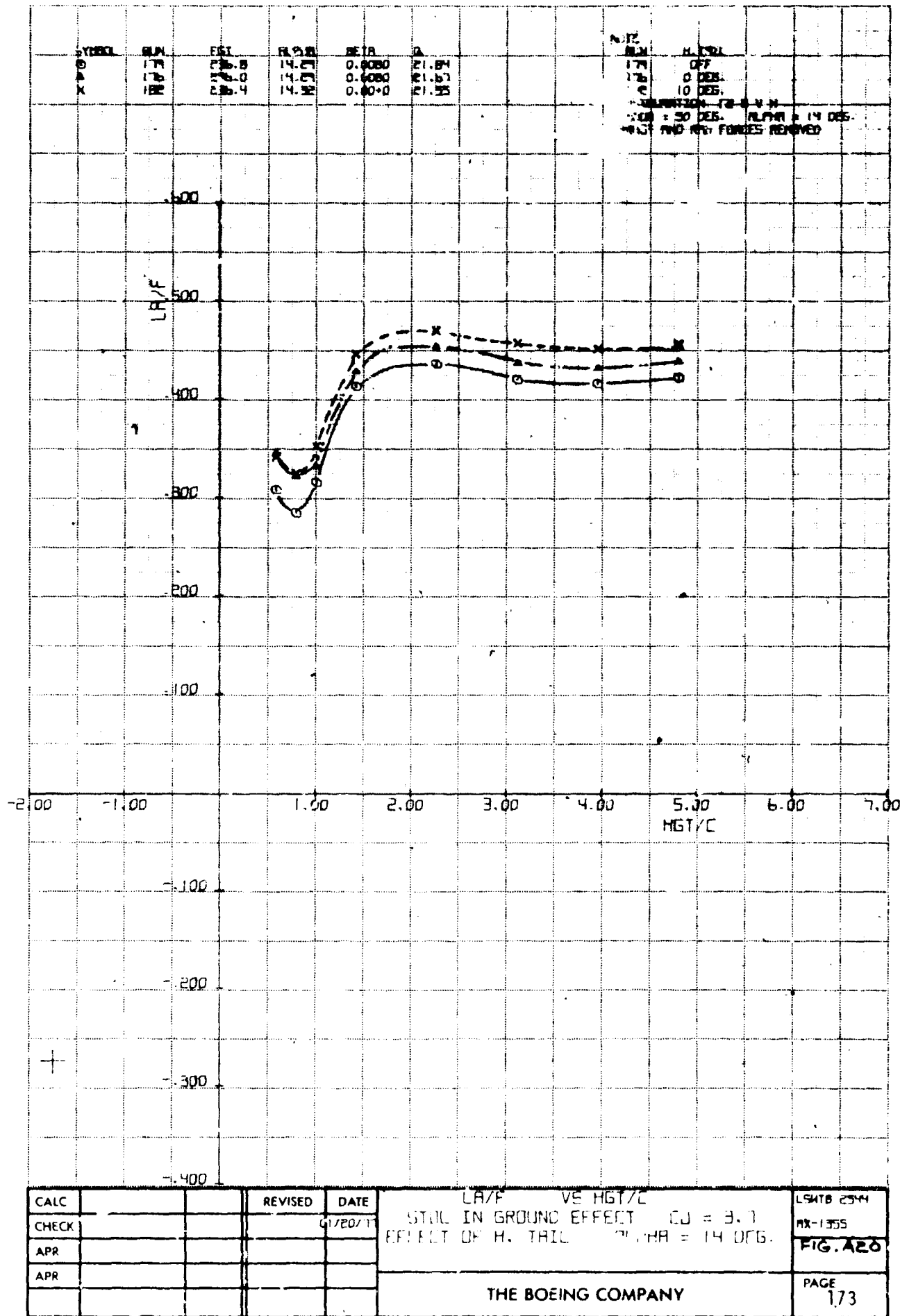


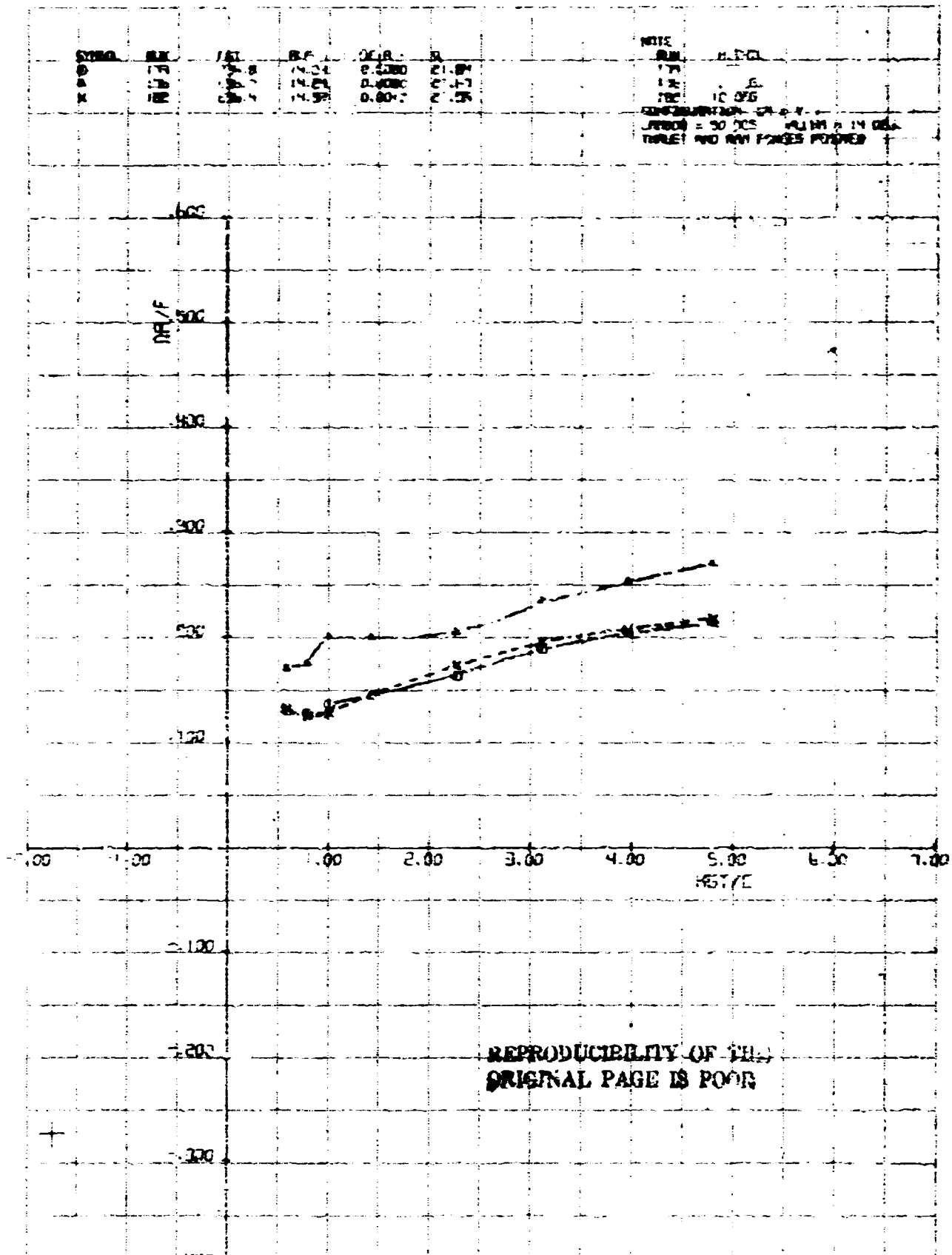
CALC		REVISED	DATE
CHECK		07/07/71	
APR			
APR			

PMA/FXC VS HGT/C
STOL IN GROUND EFFECT $CJ = 1.8$
EFFECT OF H. TAIL $\text{ALPHA} = 14 \text{ DEG.}$

LMTB 2544
RX-1355
**FIG.A19
(CONT.)**
PAGE 172

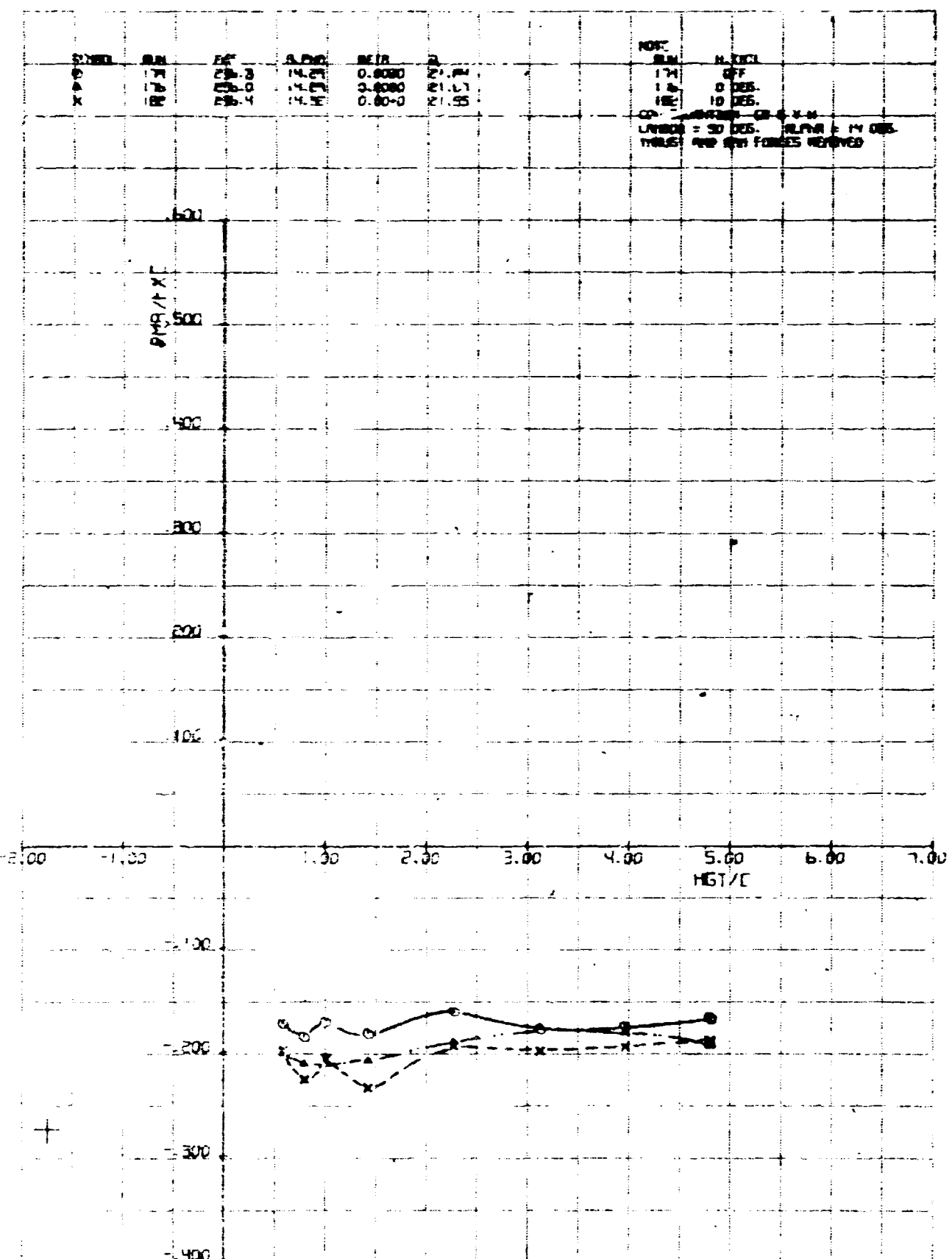
THE BOEING COMPANY



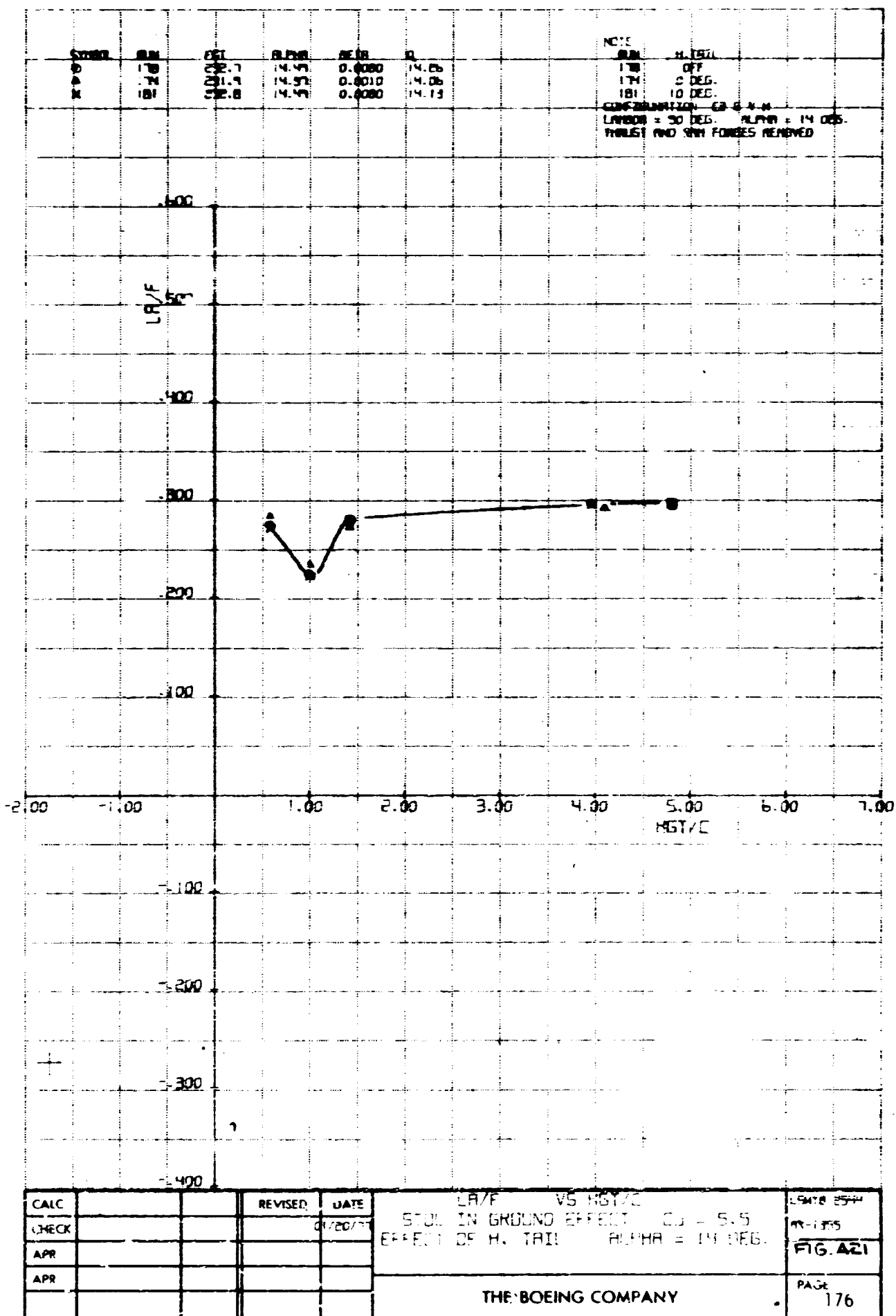


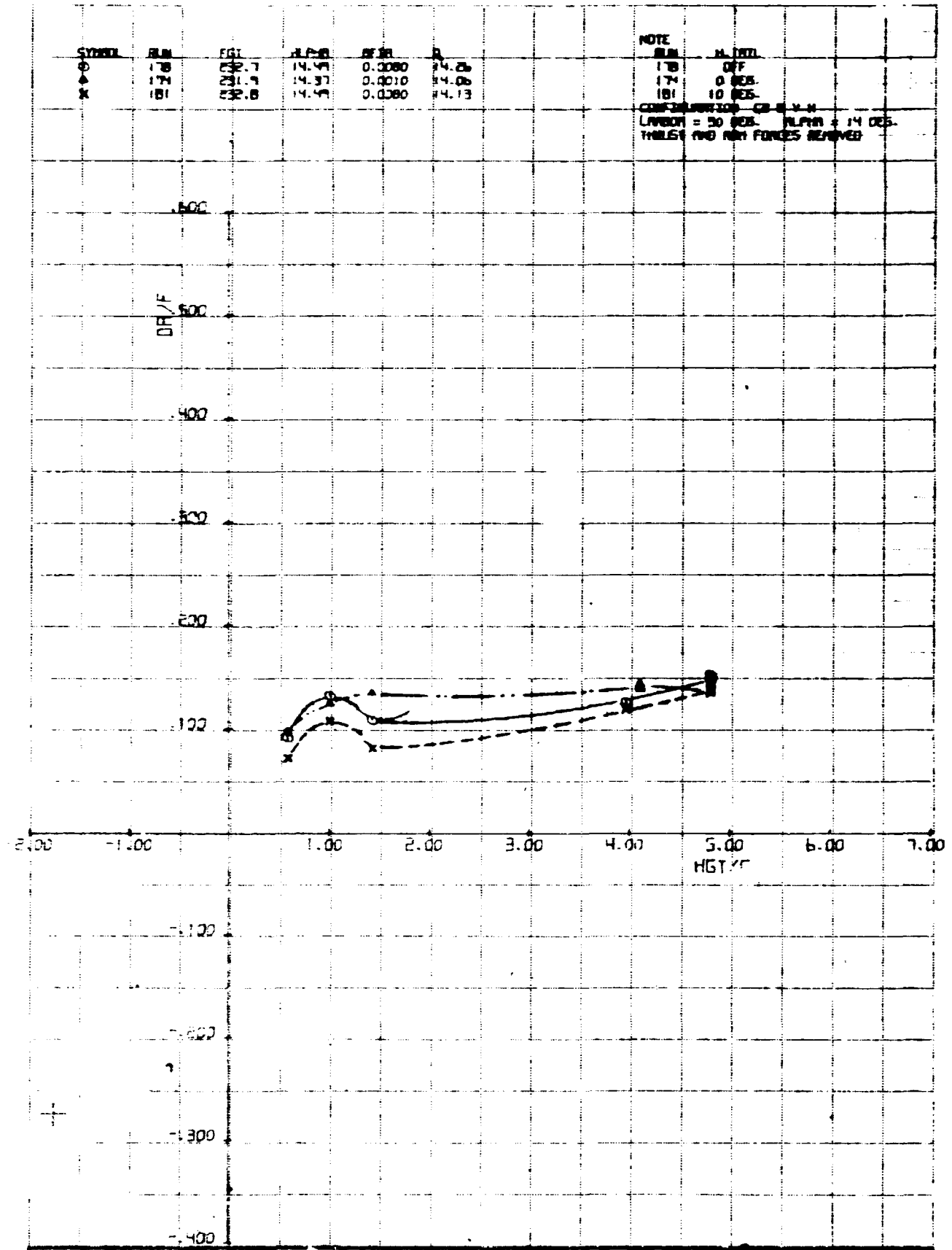
**REPRODUCIBILITY OF THE
ORIGINAL PAGE IS POOR**

CALC	REvised	CAT	DRAF VS. RETA STOL IN GROUND EFFECT EFFECT OF H. TAIL ALPH = 14 DEG.	L-16 25M NO 125 PIS. ABO (CONT)
CHECK		07/07/71		
AIR				
APP				
			THE BOING COMPANY	PAGE 174

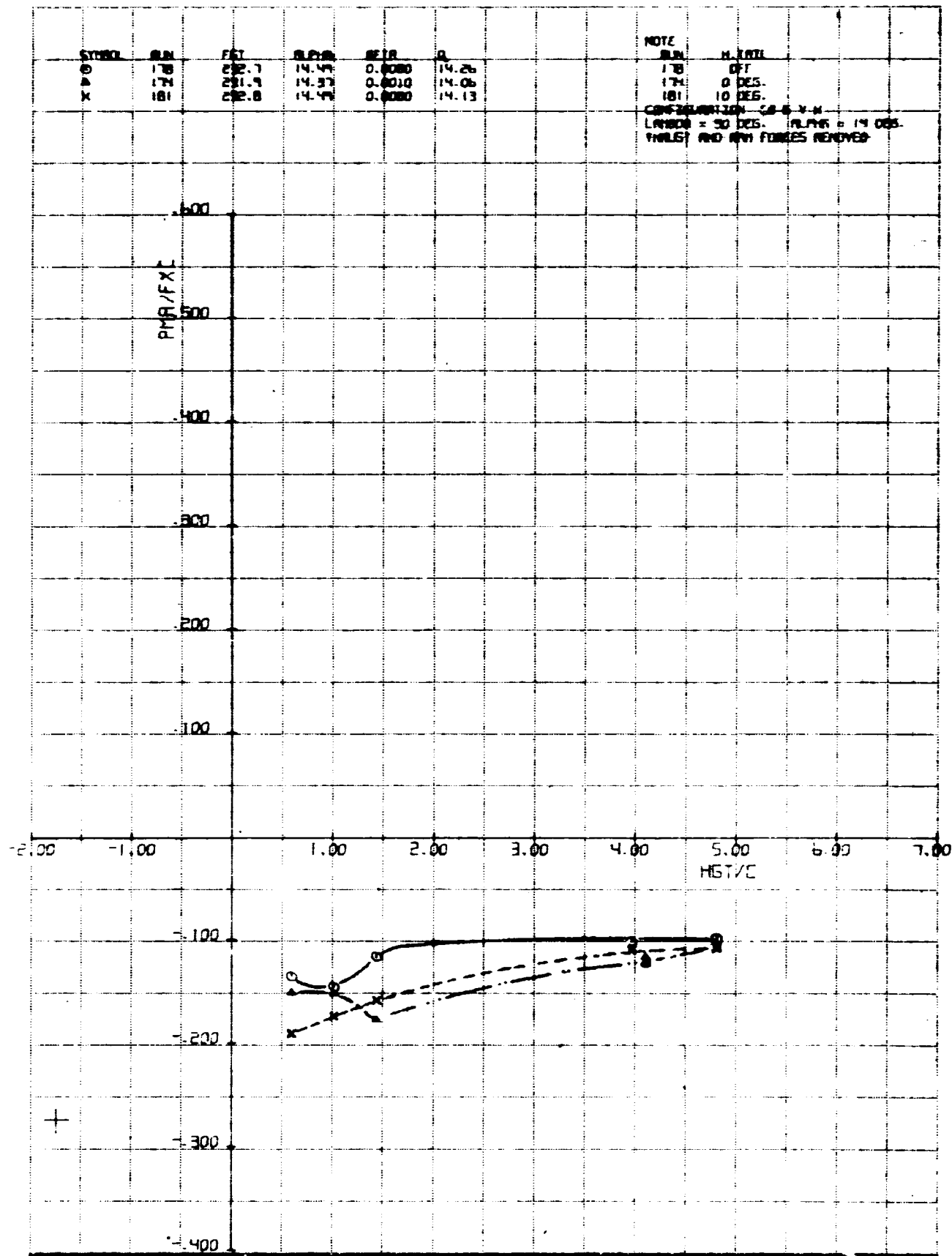


CALC			DATE 3/20/77	PMA/FXC VS HGT/E STOL IN GROUND EFFECT CJ = 3.7 EFFECT OF H. TAIL ALPHA = 14 DEG.	L-949-2544 TR-1555 F-6 A20 CONT'D SAC 175
CHECK					
APR					
JPP					
				THE BOEING COMPANY	





CALC		REVISED	DATE	DP/F VS HGT/C STOL IN GROUND EFFECT EJ = 5.5 EFFECT OF H. TAIL ALPHA = 14 DEG.	LMTB 2344 MX-1355 FIG.A21 (CONT)
CHECK			01-20-77		
APR					
APP					
				THE BOEING COMPANY	PAGE 177

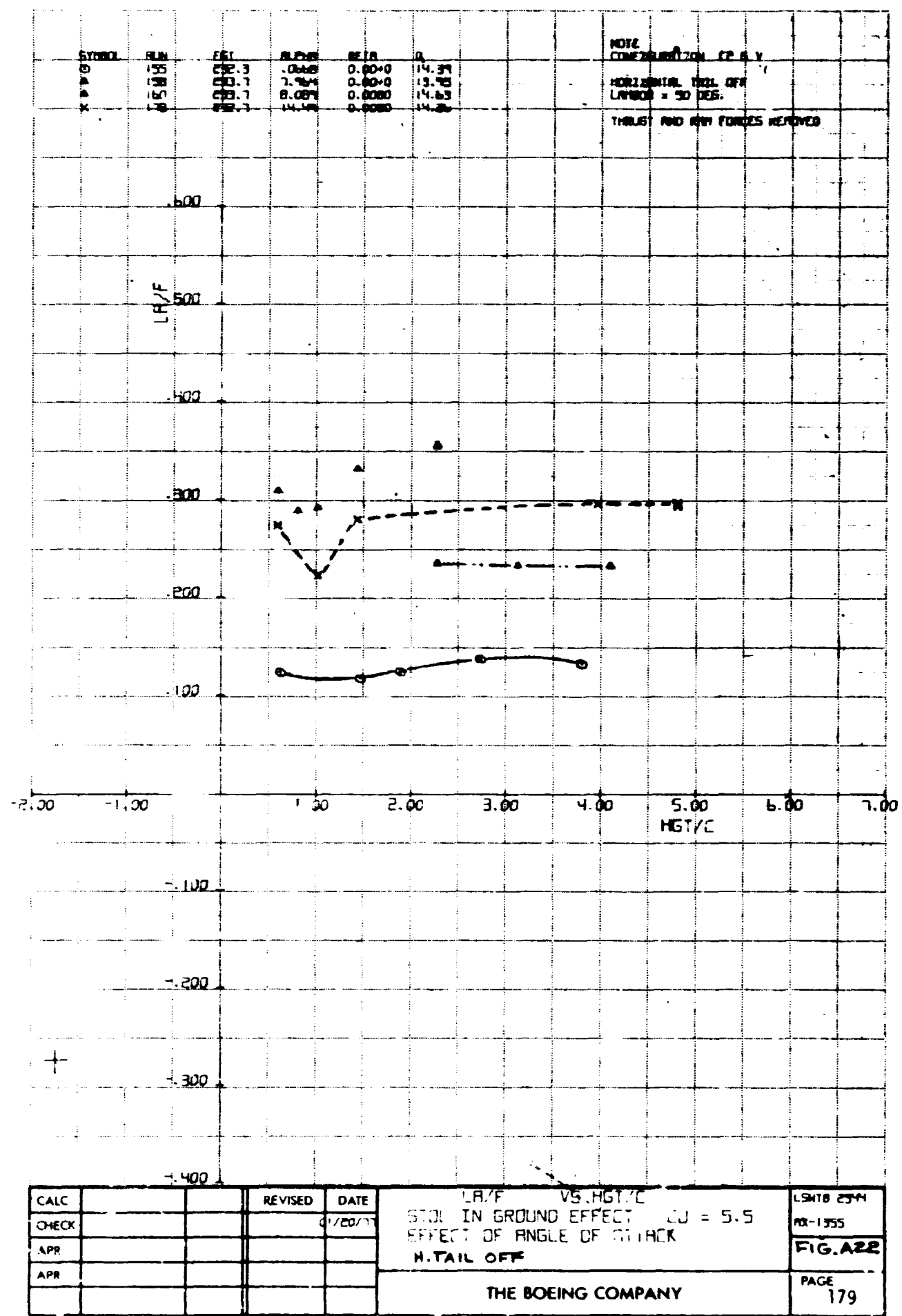


CALC		REVISED	DATE
CHECK			01/20/71
APR	0		
APR			

PMR/FXC VS HGT/V
 STUDY IN GROUND EFFECT: $\beta_0 = 5.5$
 EFFECT OF H. TAIL: ALPHR = 14 DEG.

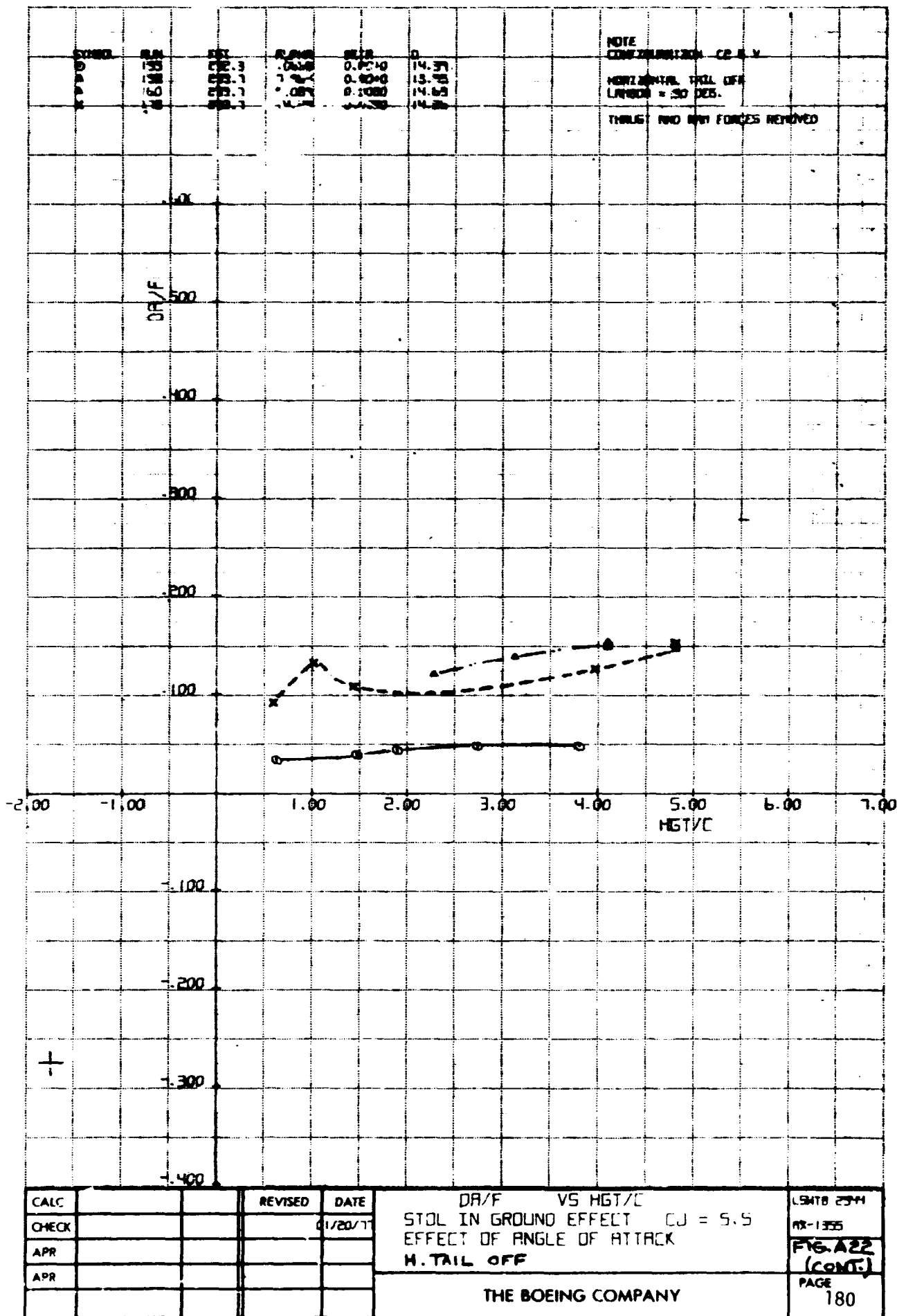
LS-6-254
 RX-1215
 FIG. A-2
 (CONT.)
 PAGE 173

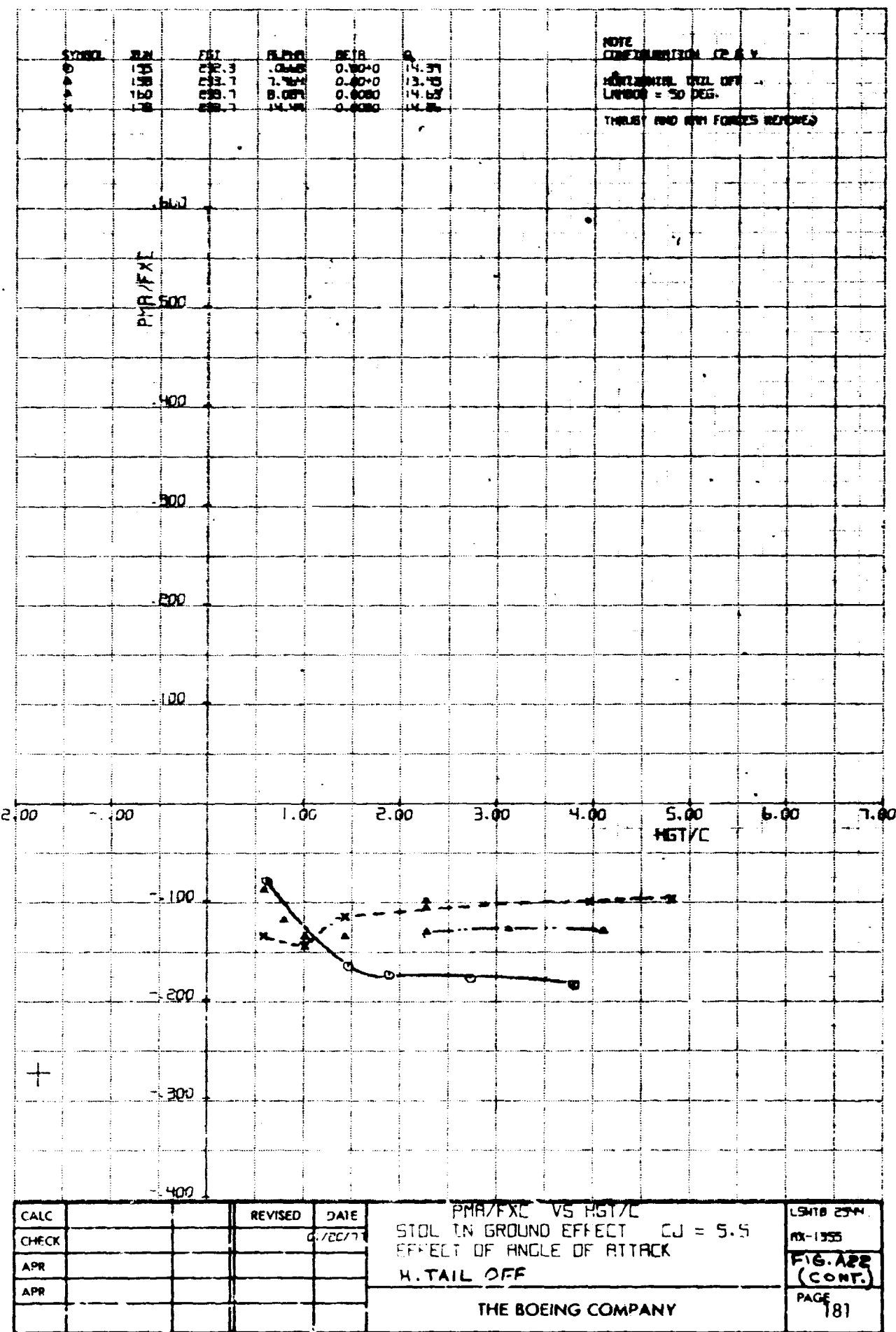
THE BOEING COMPANY

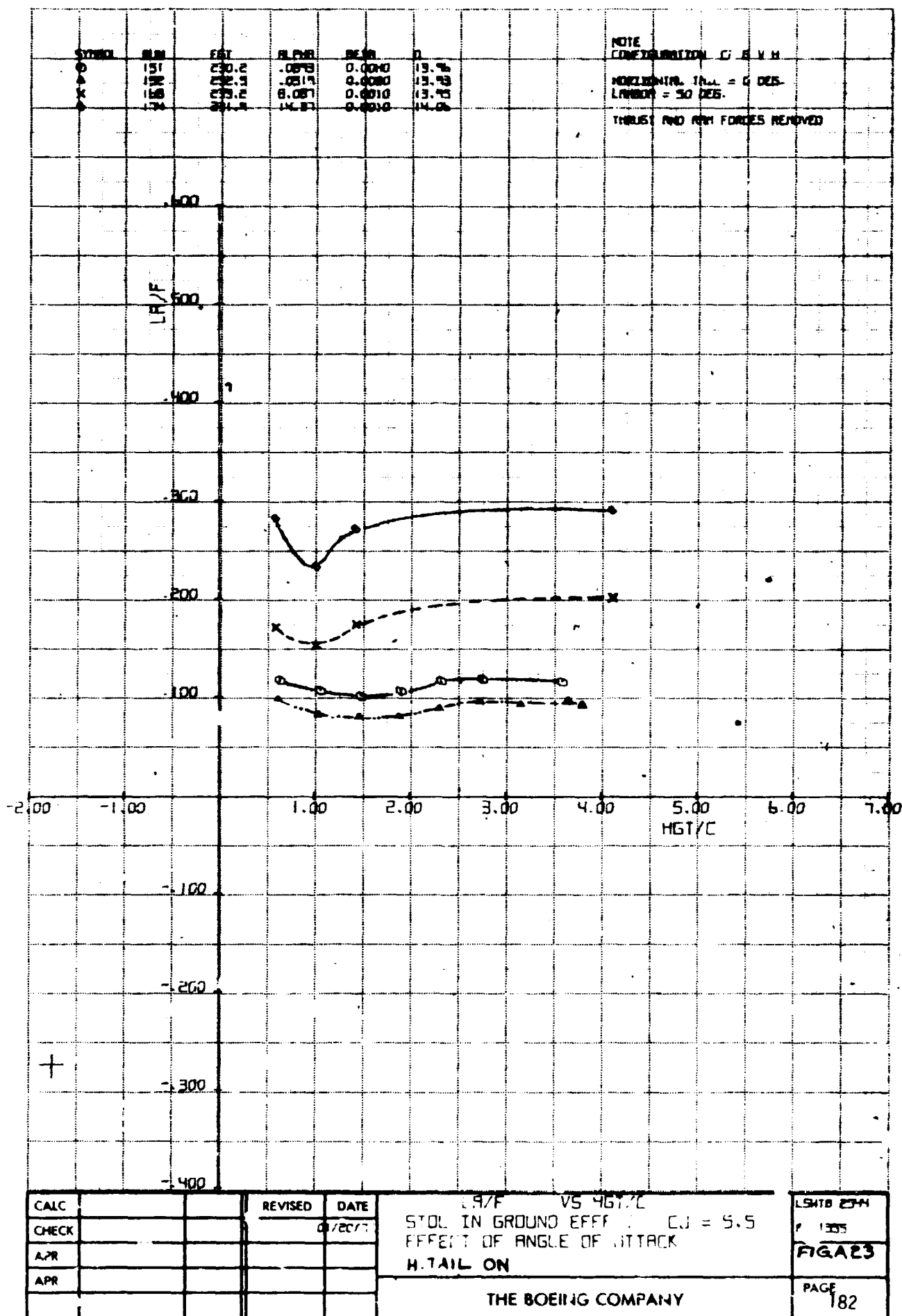


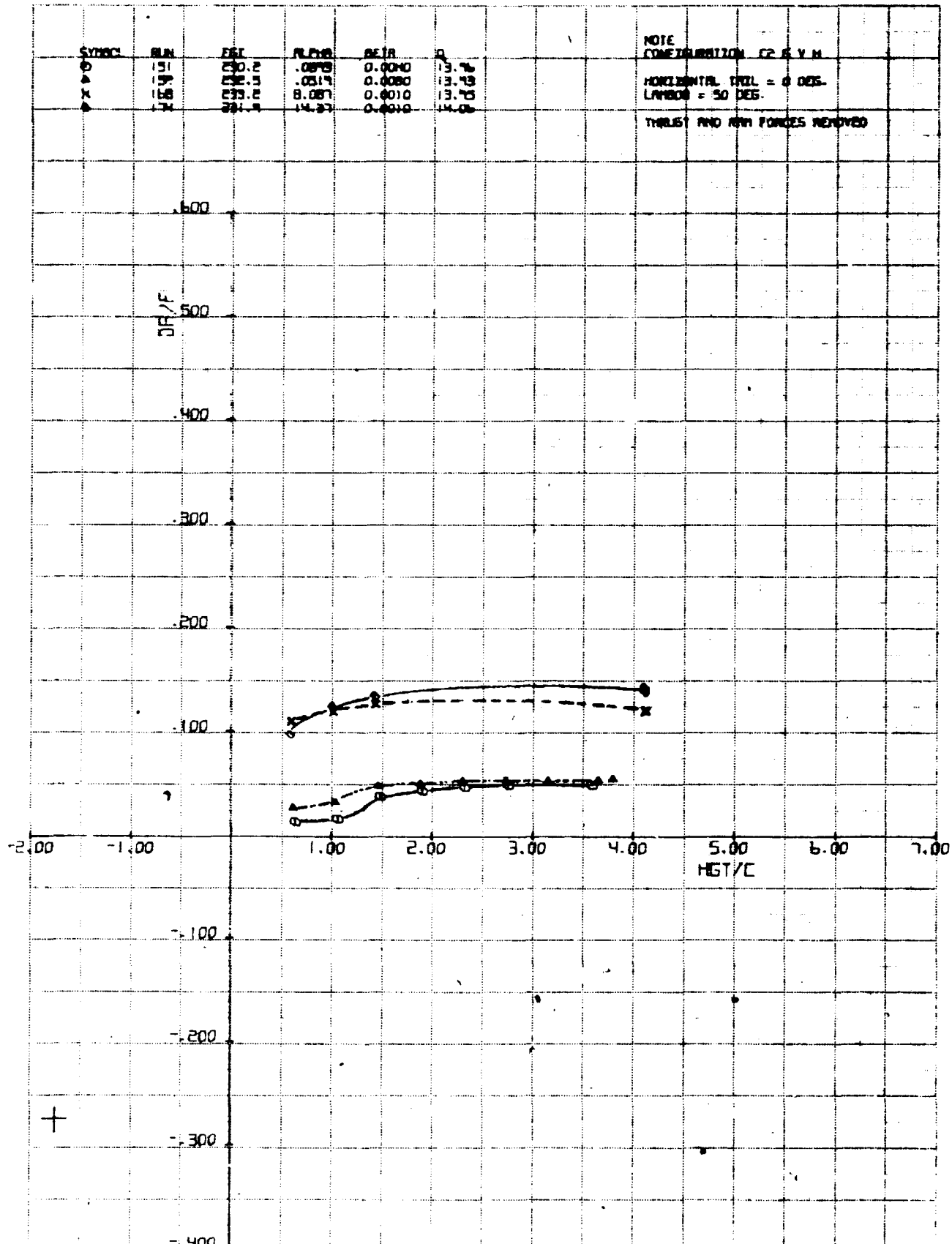
CALC		REVISED	DATE
CHECK			01/20/77
APR			
APR			

LSM18 294
PA-1355
FIG. A22





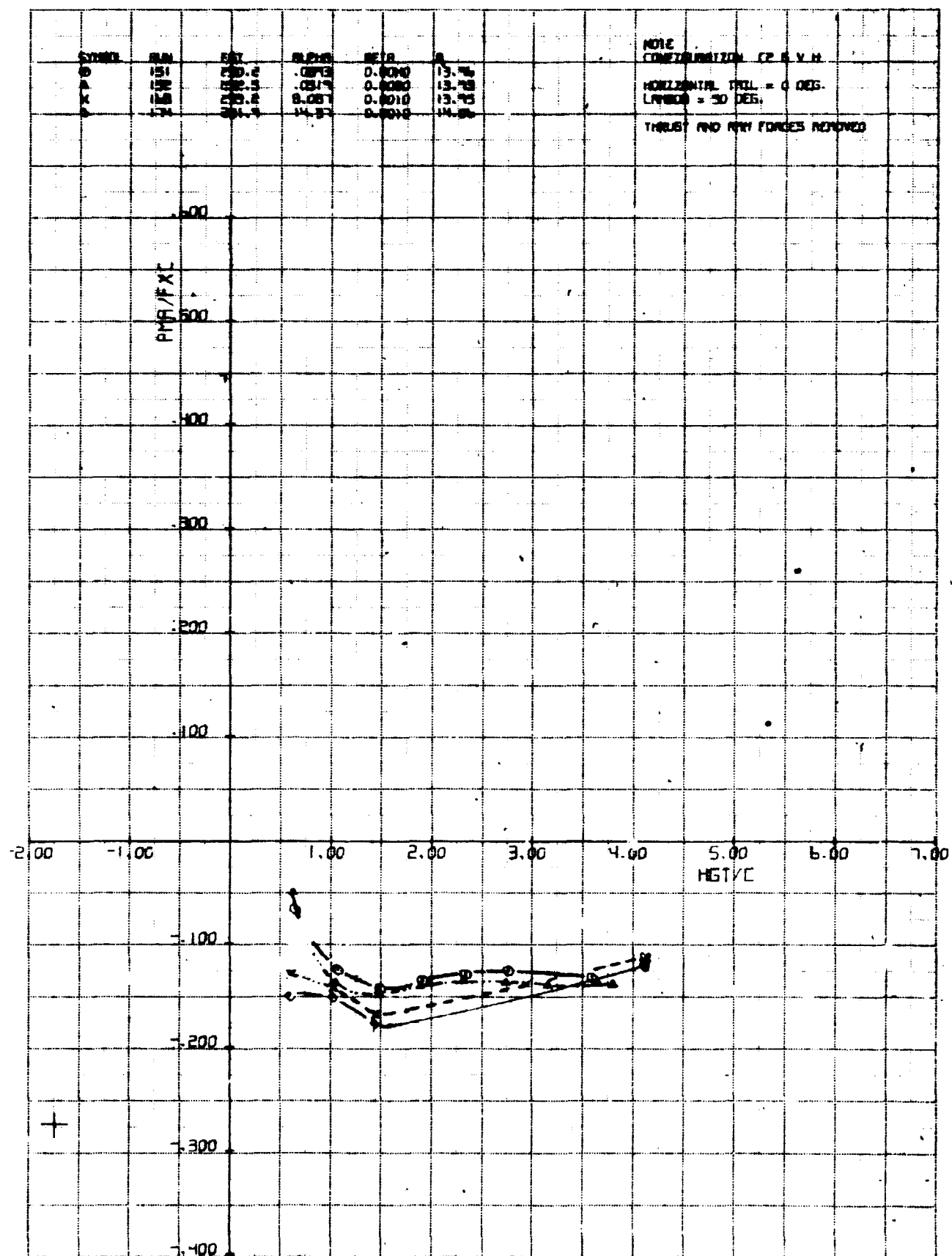




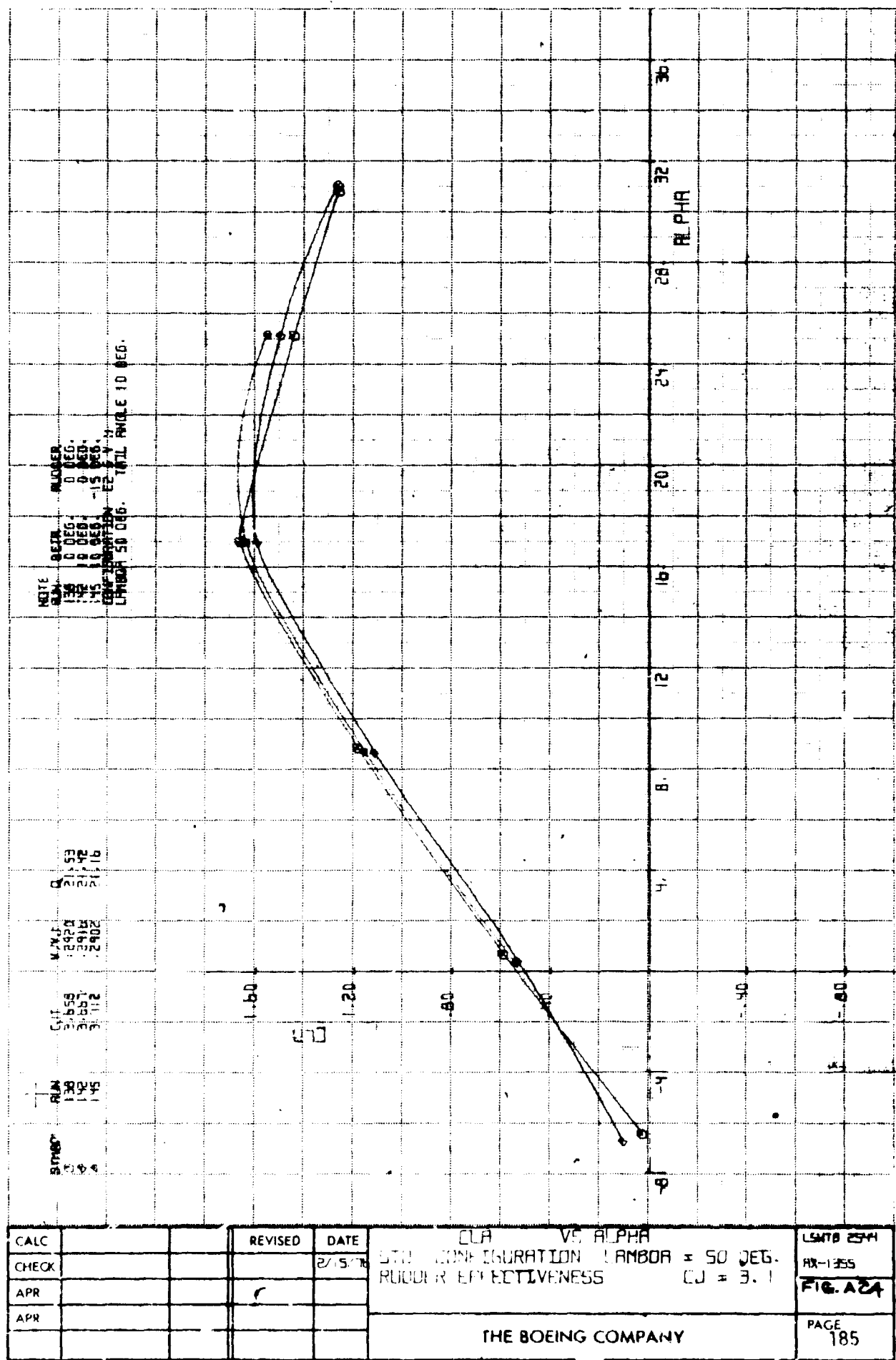
DR/F VS HGT/C
SOL IN GROUND EFFECT CJ = 5.5
EFFECT OF ANGLE OF ATTACK
H.TAIL ON

THE BOEING COMPANY

LMTB 2544
10-1953
FIG. A2
(CONT.)
PAGE
183



CALC		REVISED	DATE	PMH/FXC VS HGT/C STOL IN GROUND EFFECT C.L = 5.5 EFFECT OF ANGLE OF ATTACK	LSHTB 2514
CHECK			01/02/11		NA-1555
APR					FIG. A23 (CONT.)
APR					PAGE 184
				THE BOEING COMPANY	



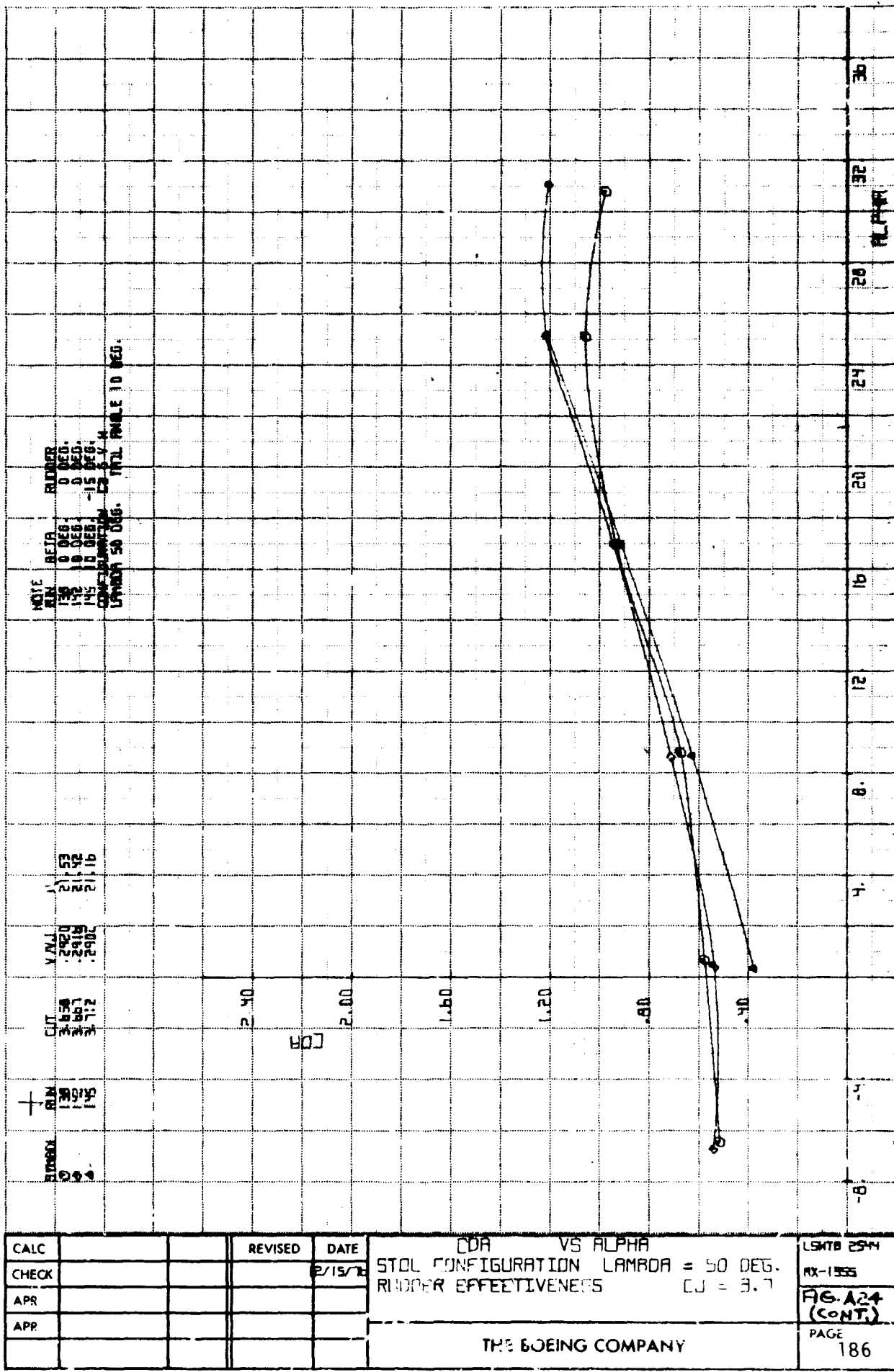
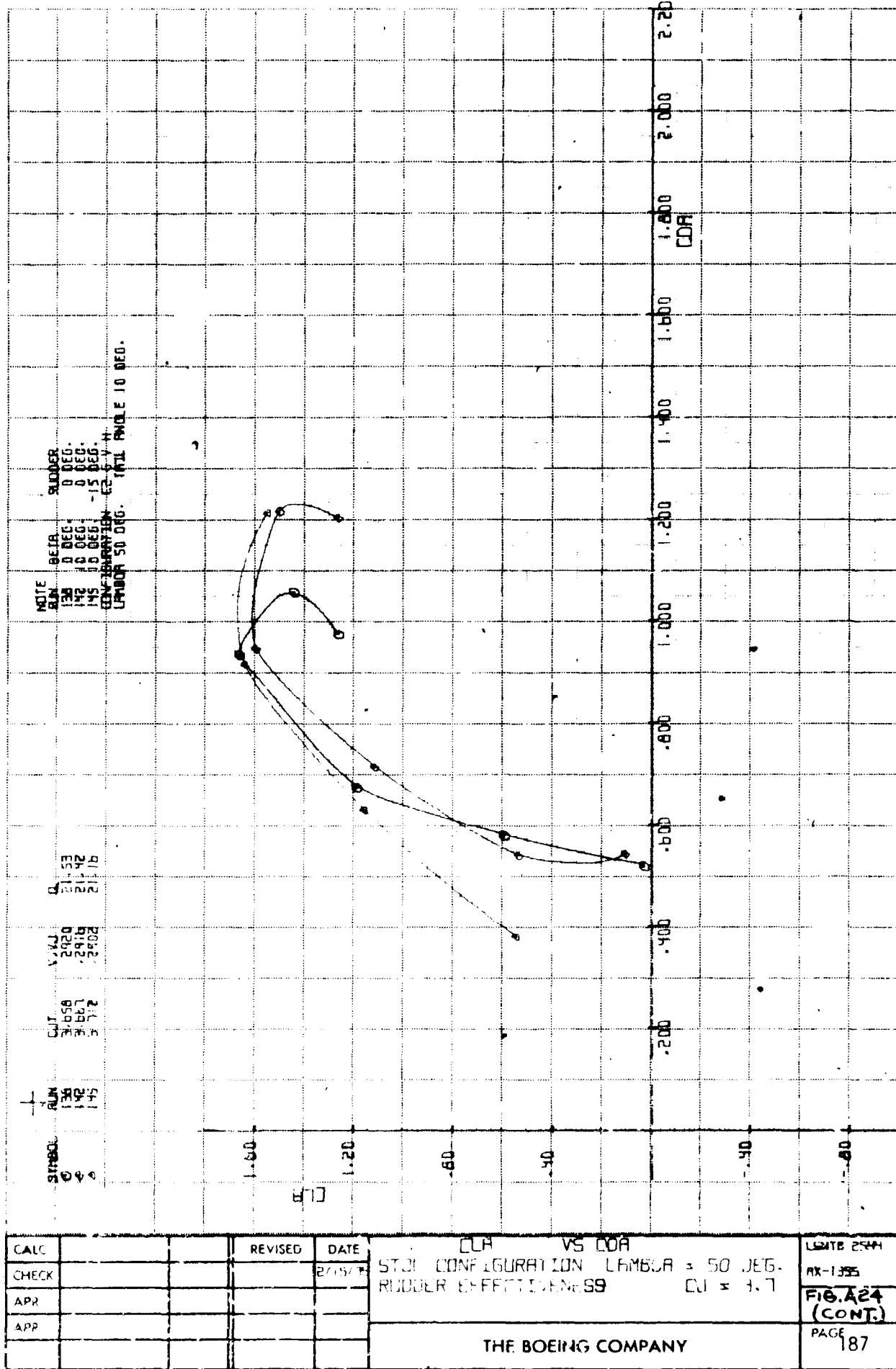
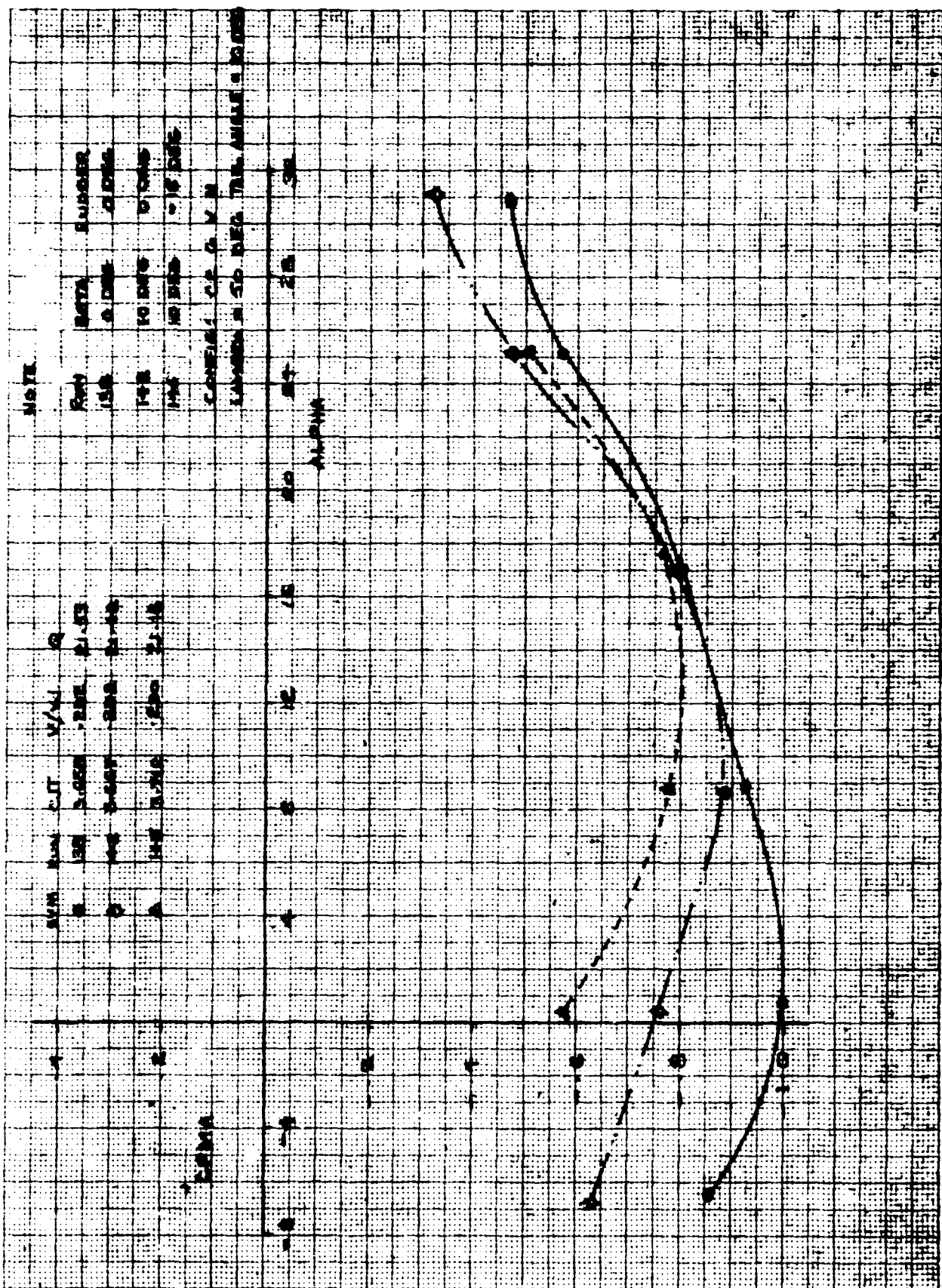


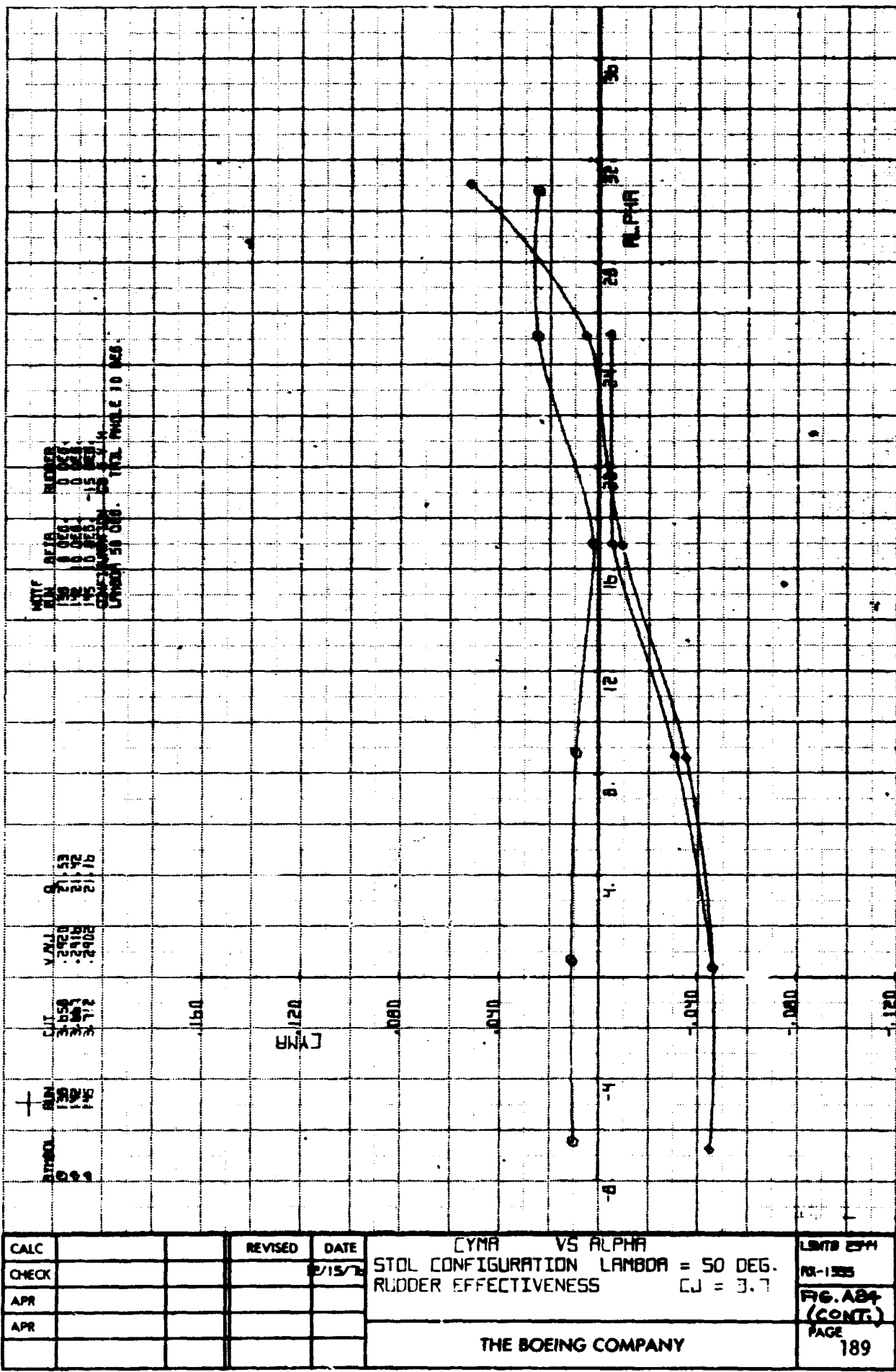
FIG 4
3.

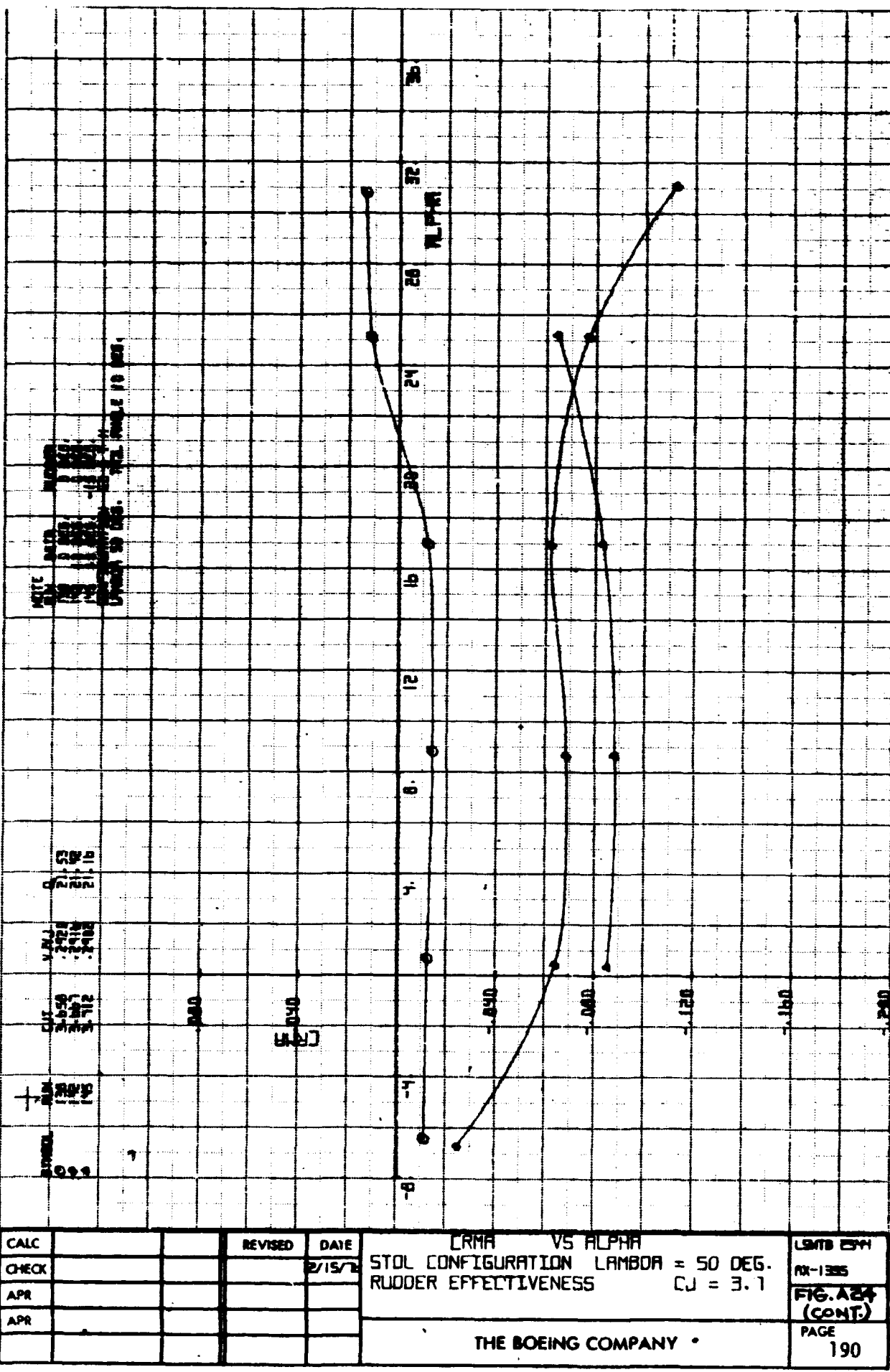


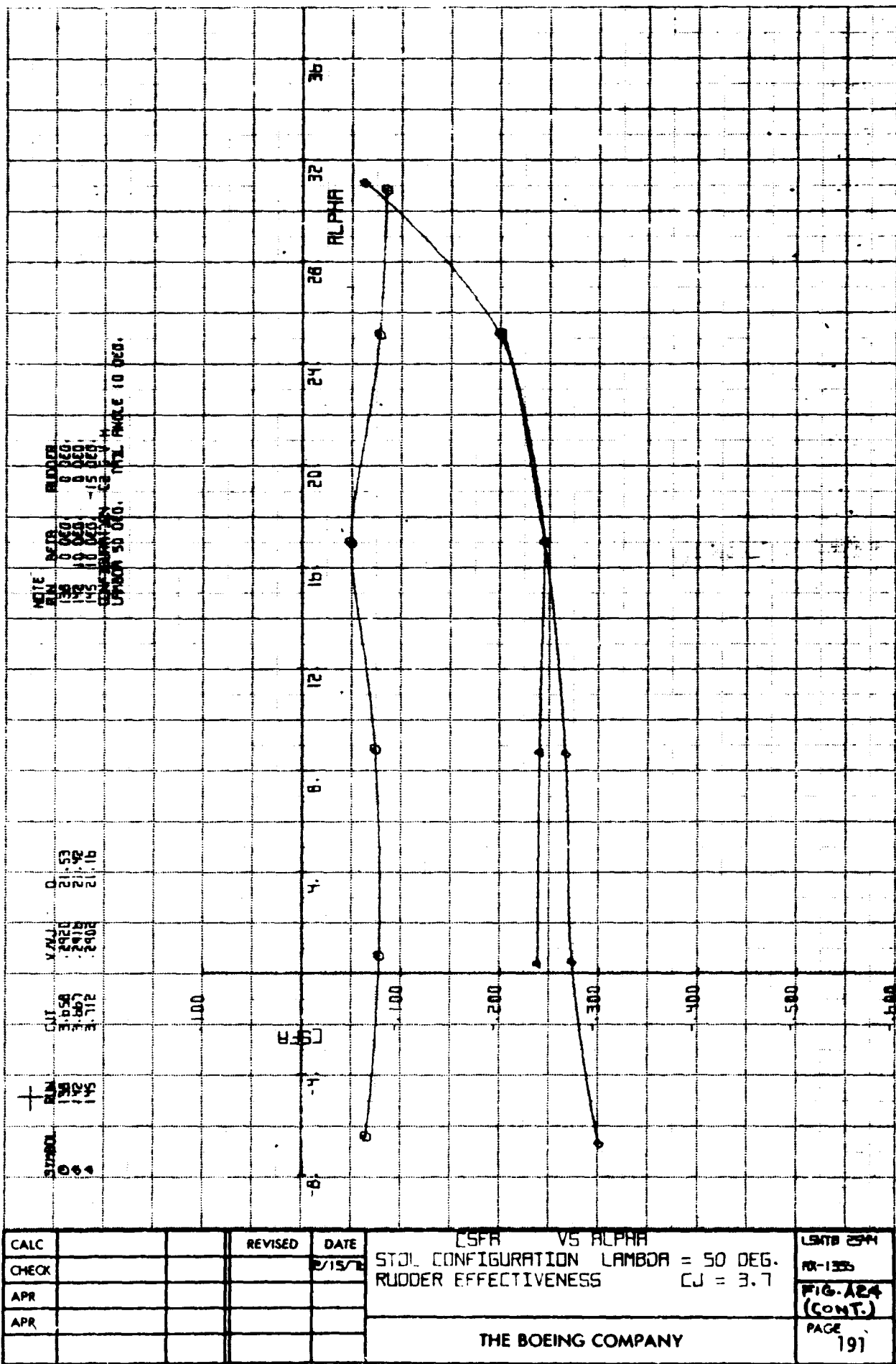
१८

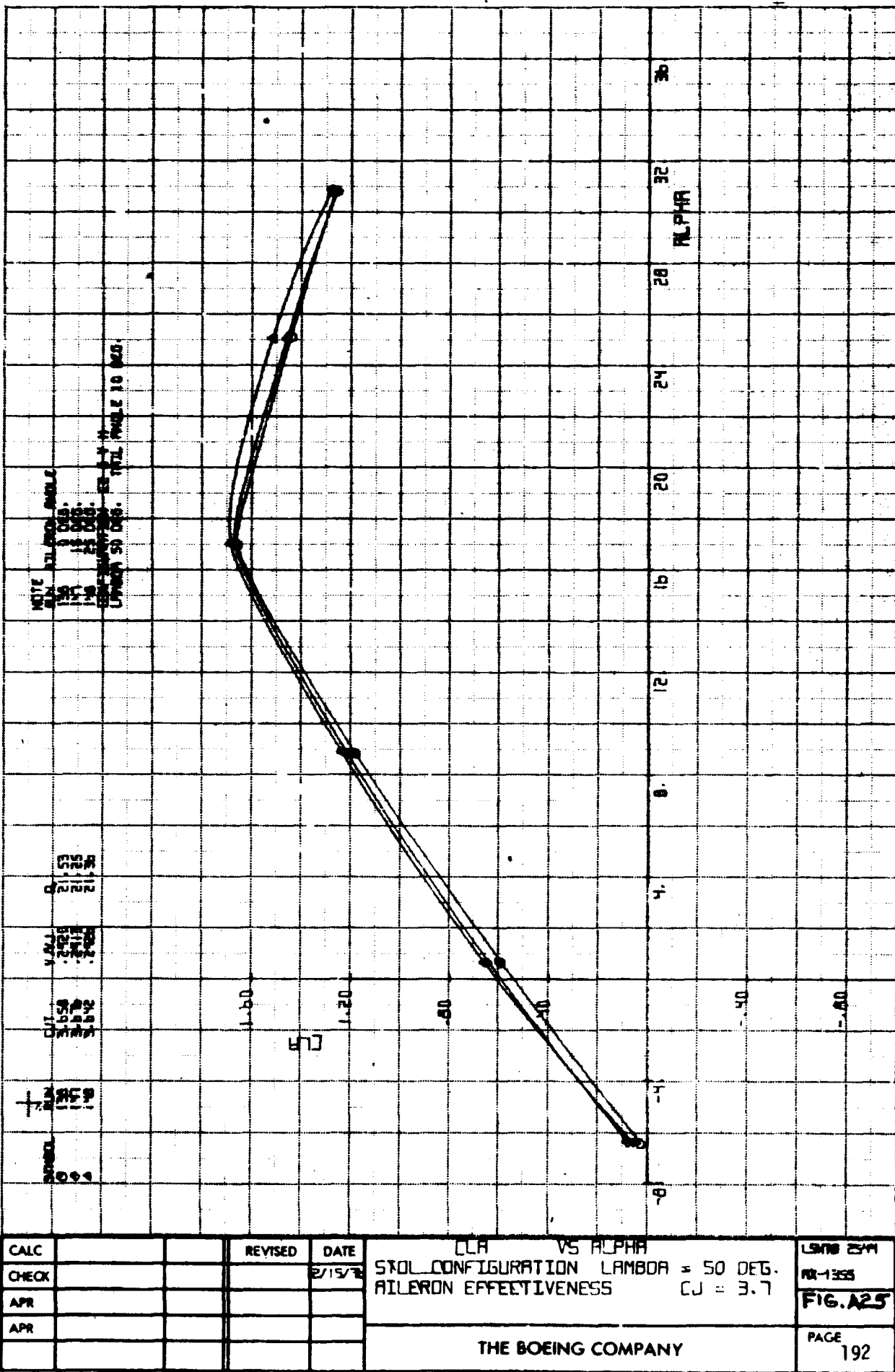


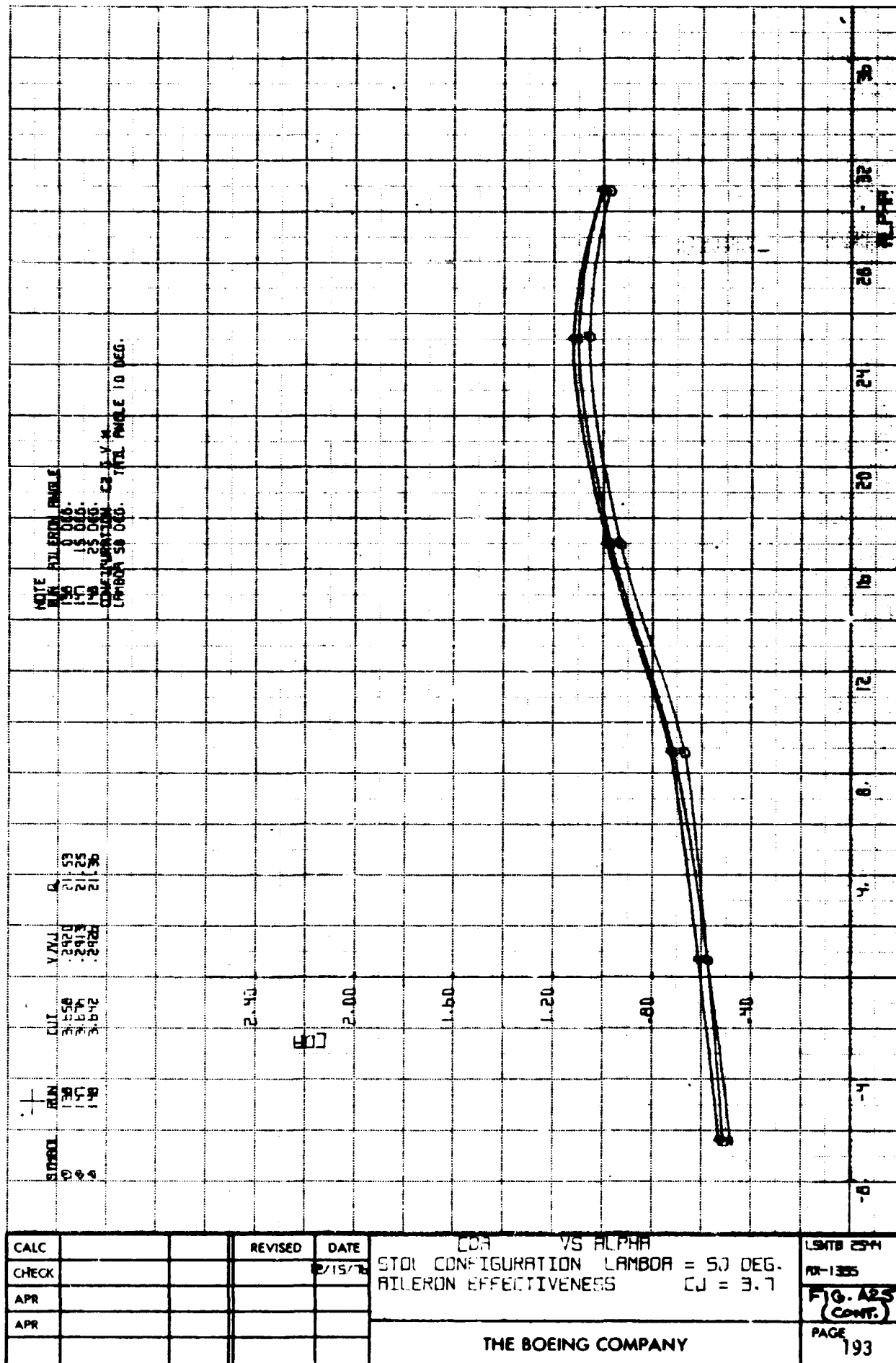
CALC		REVISED	DATE	CPMA VS ALPHA STOL CONFIG. LAMBDA = 50 DEG RUDDER EFFECTIVENESS (J = 3.7)	LWWTB REF 41 AX-124 FIG. A24 (CONT.)
CHECK					
APR					
APR					
				THE BOEING COMPANY	PAGE 188

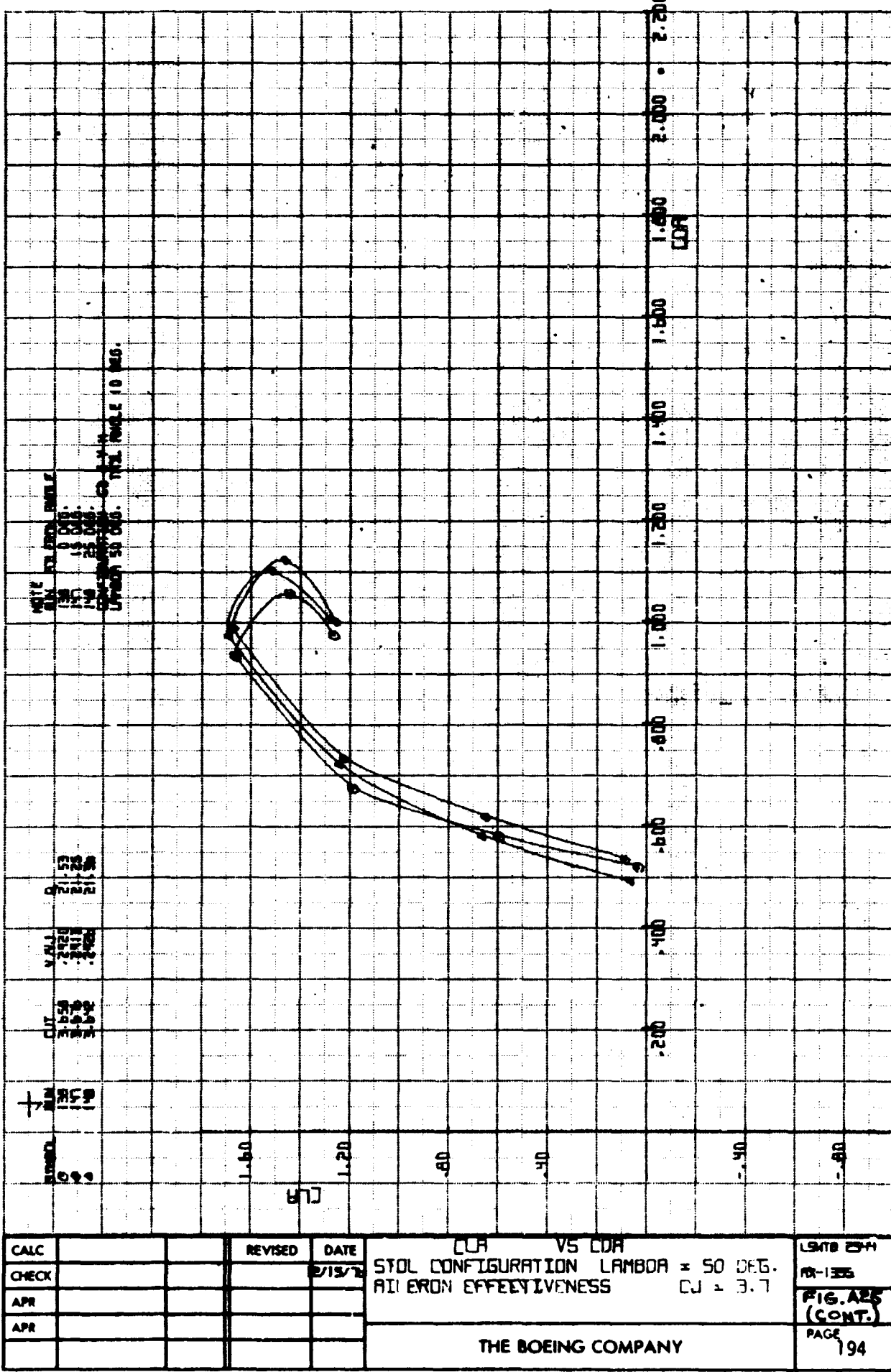


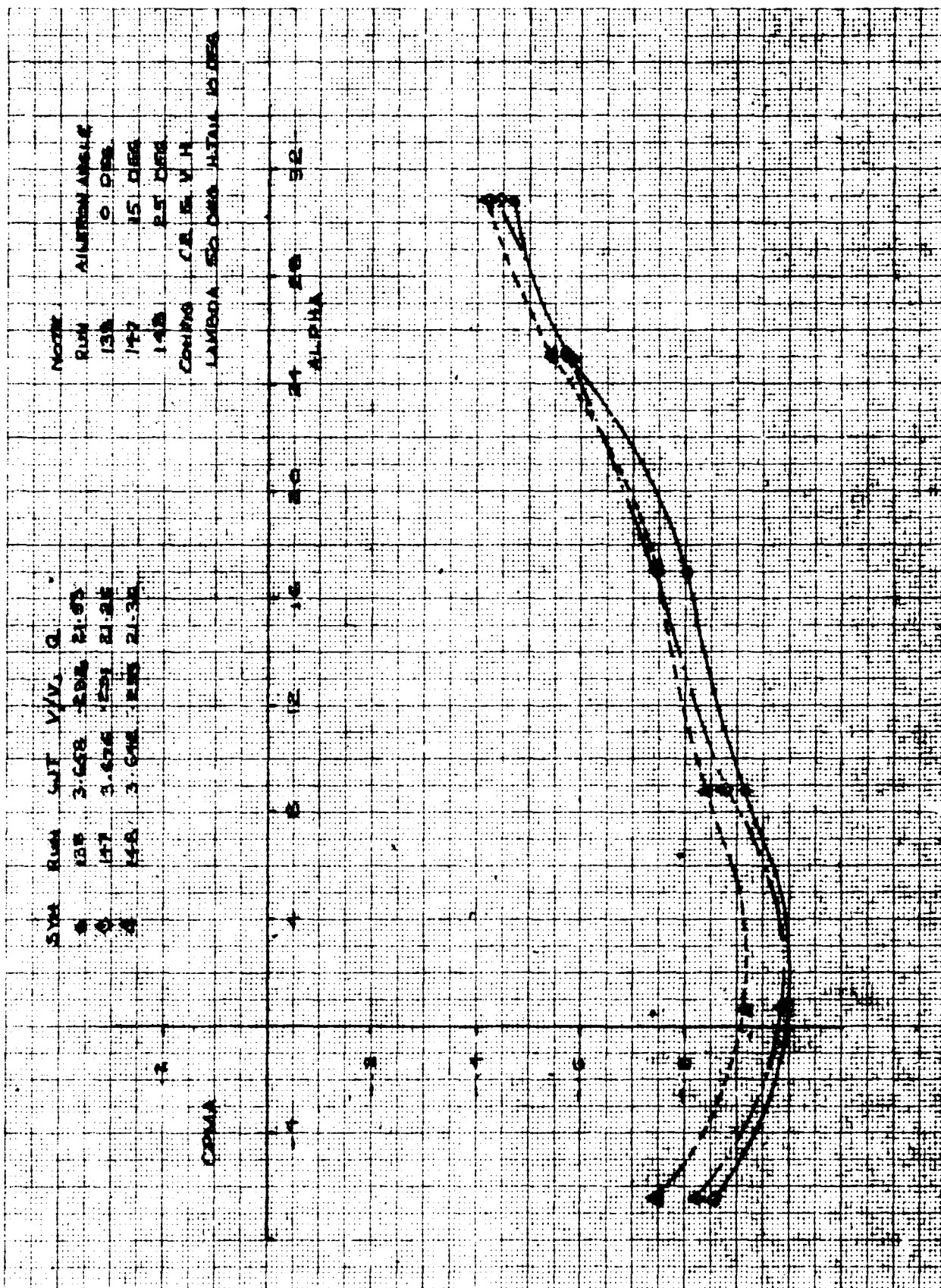










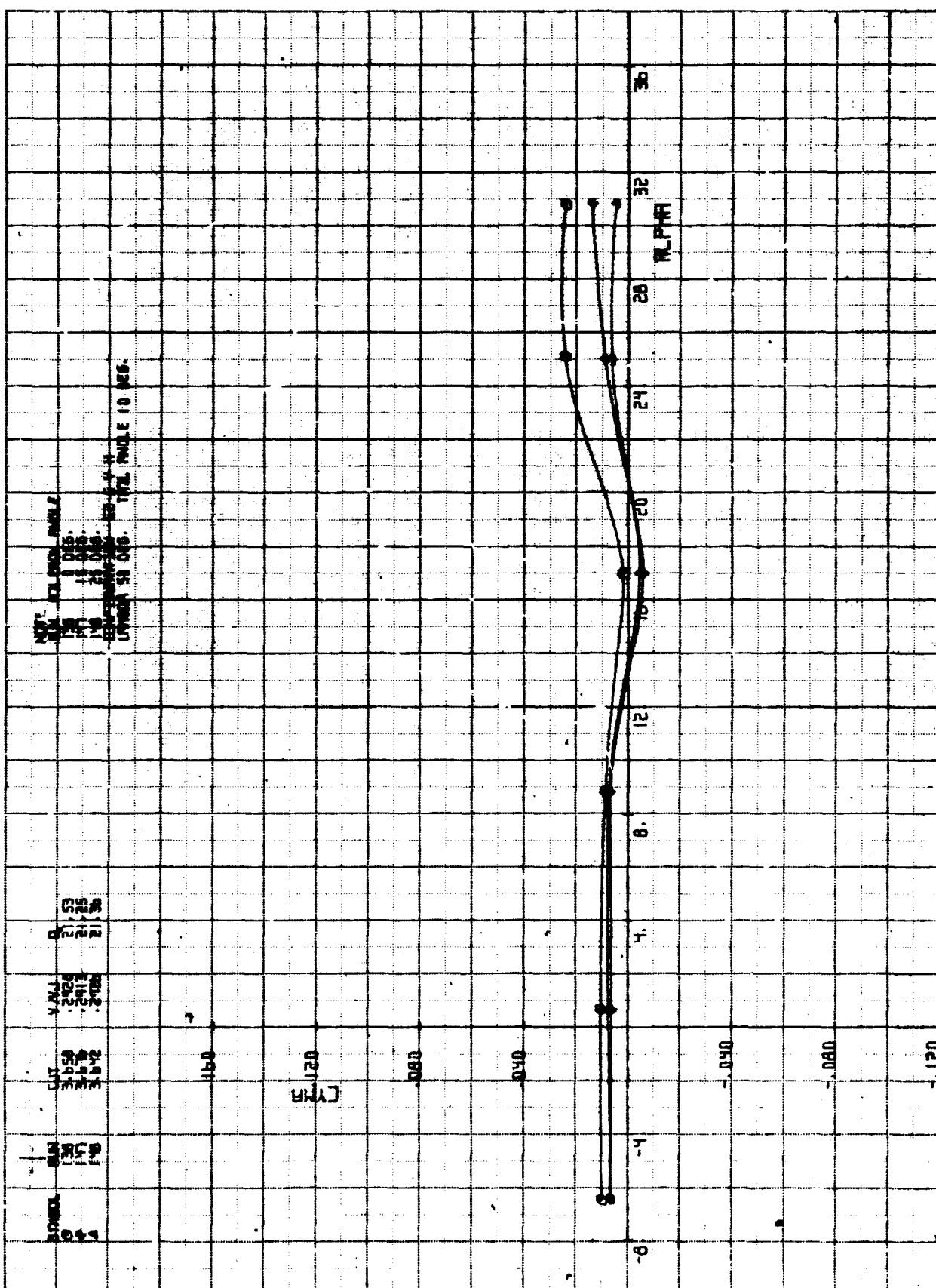


CALC		REVISED	DATE
CHECK			
APR			
APR			

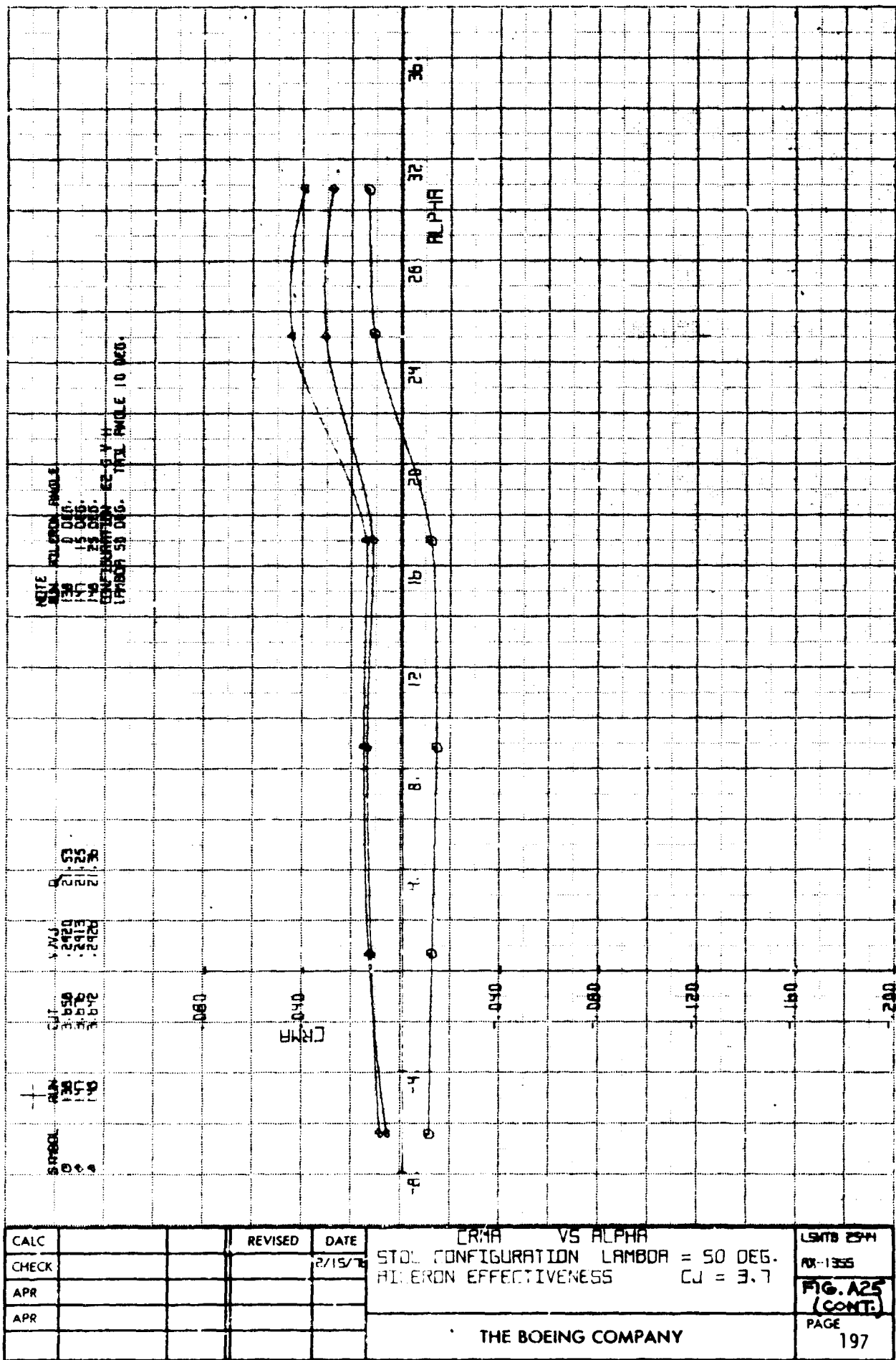
CPMA VS ALPHA
STOL CONFIGURATION $\Lambda = 50^\circ$
AILERON EFFECTIVENESS $C_J = 3.7$

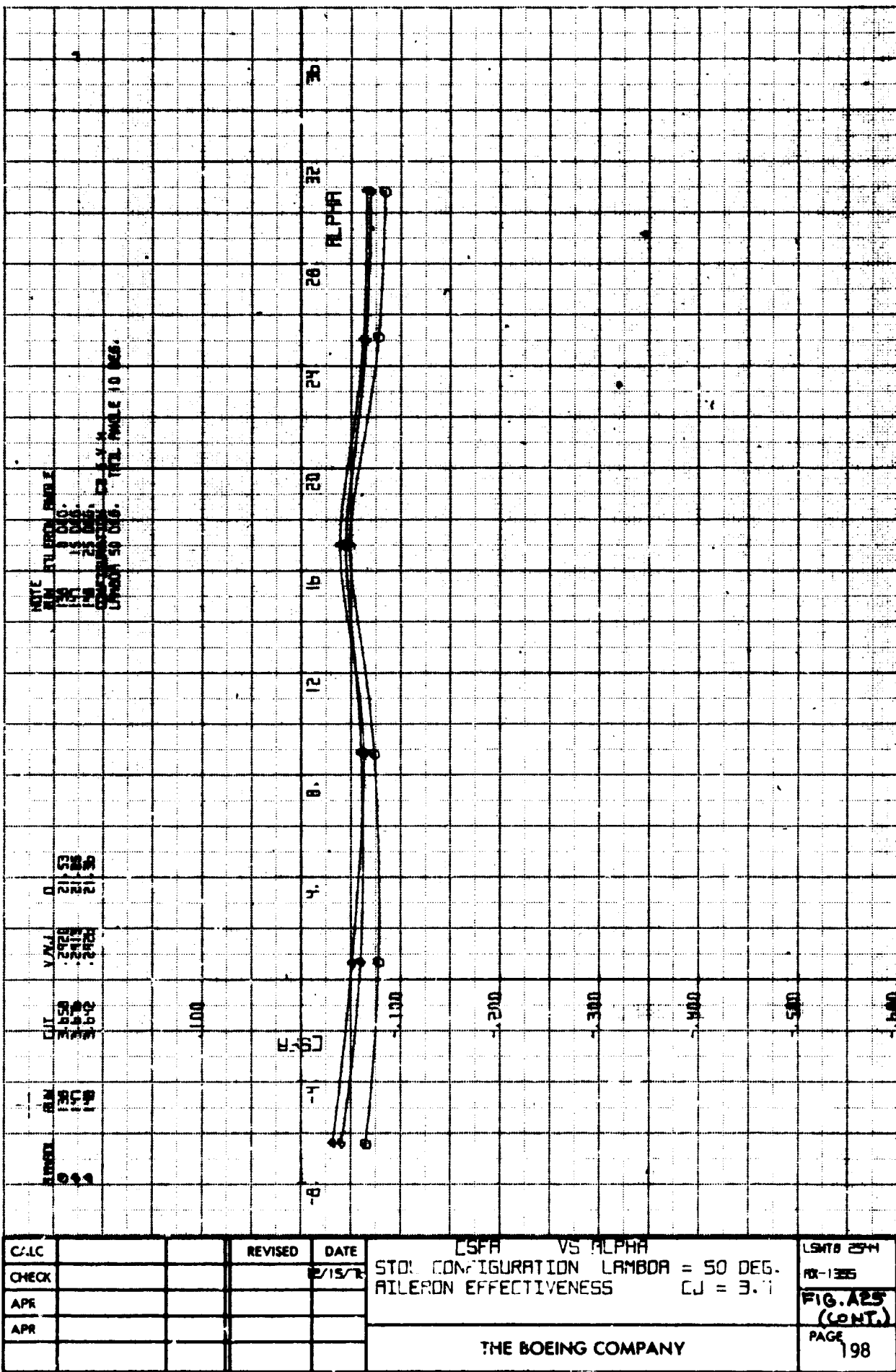
THE BOEING COMPANY

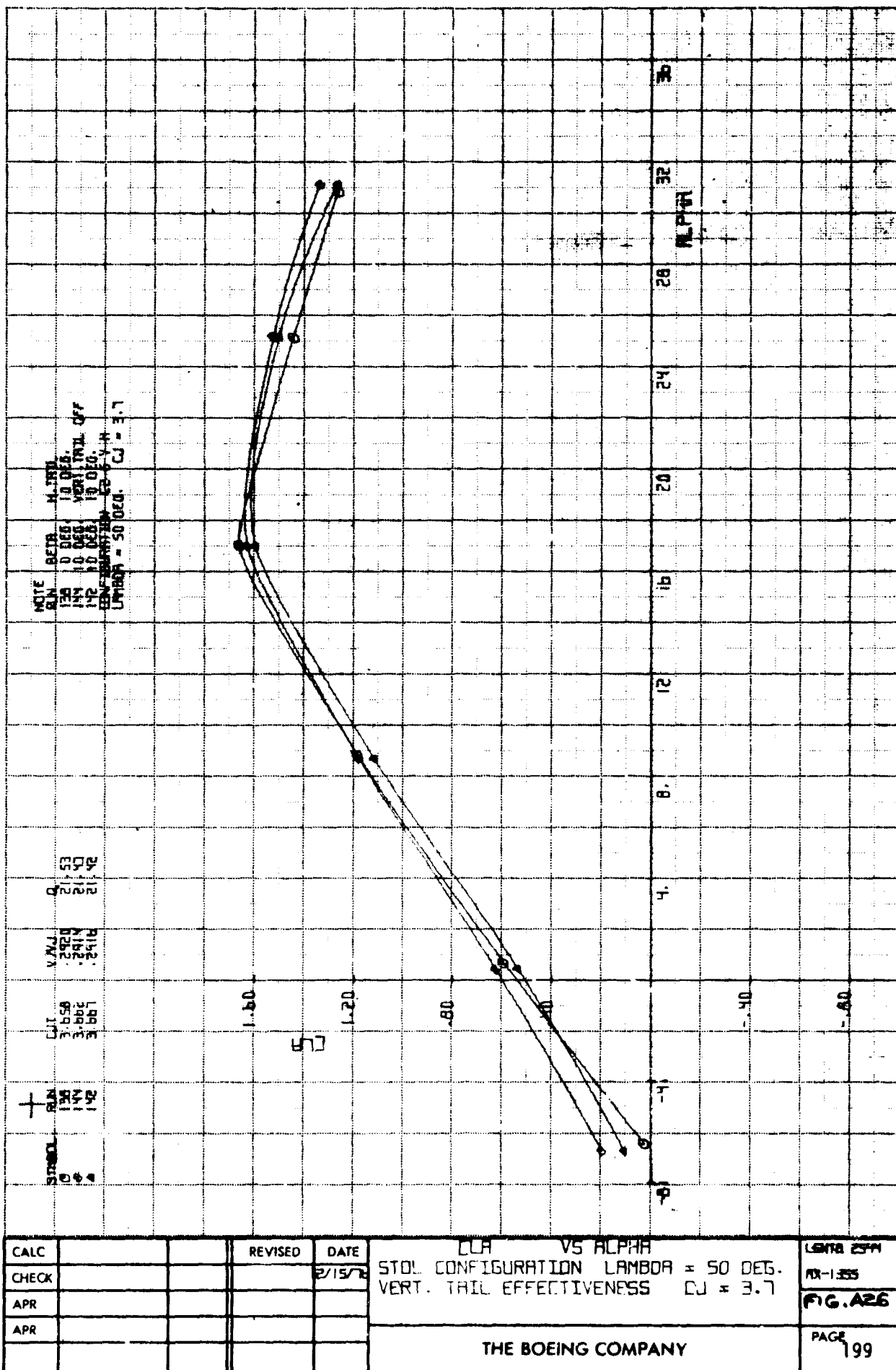
LSWTB
2544
X-1365
FIG. A26
(CONT.)
PAGE
195

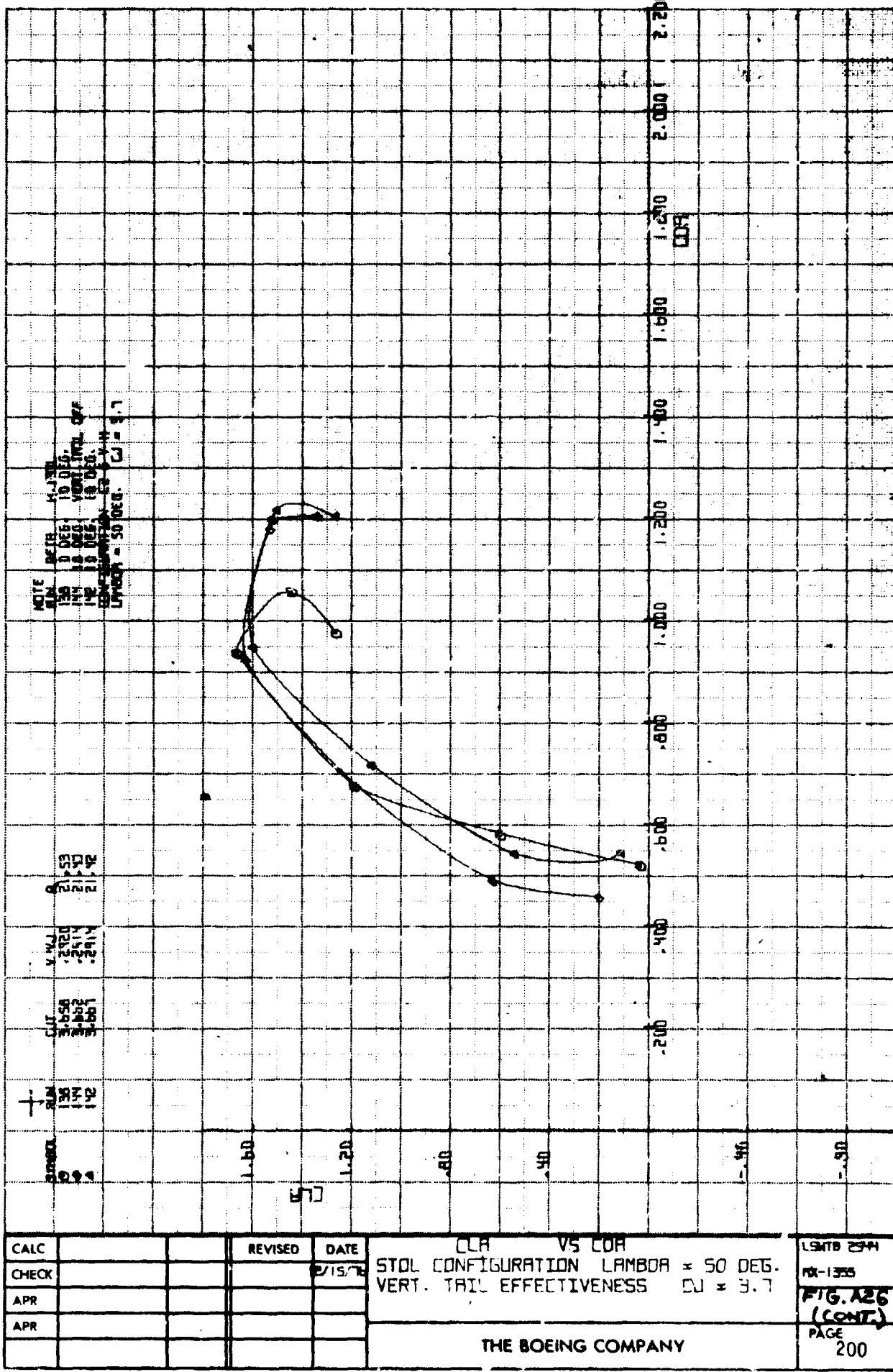


CALC		REVISED	DATE	CYMA VS ALPHA	LMTD 2544
CHECK			2/15/67	STOL CONFIGURATION LAMBDA = 50 DEG.	MX-1355
APR				RILERON EFFECTIVENESS $\epsilon_J = 3.7$	
APR					
				THE BOEING COMPANY	PAGE 196

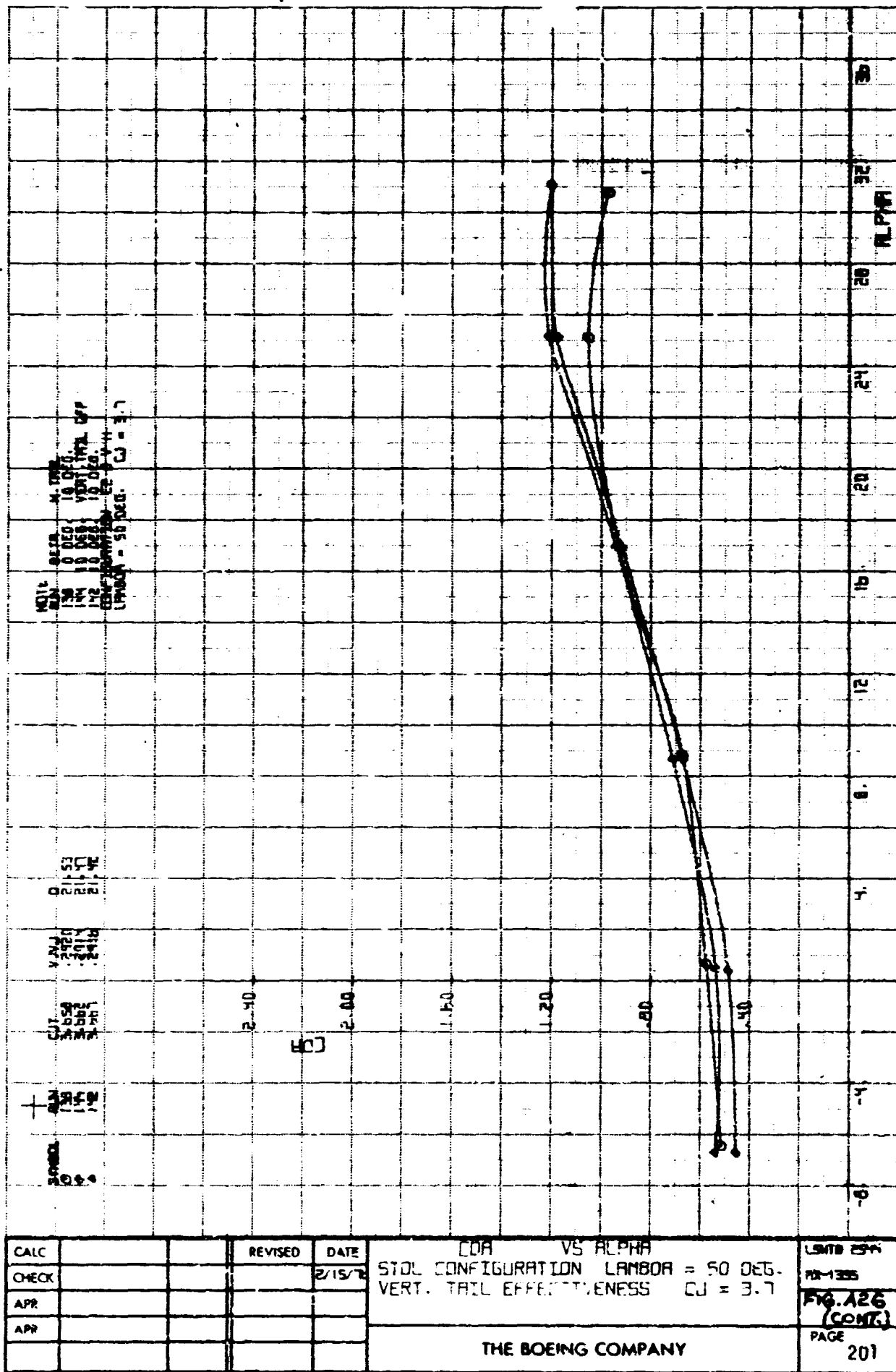








TD 461 D

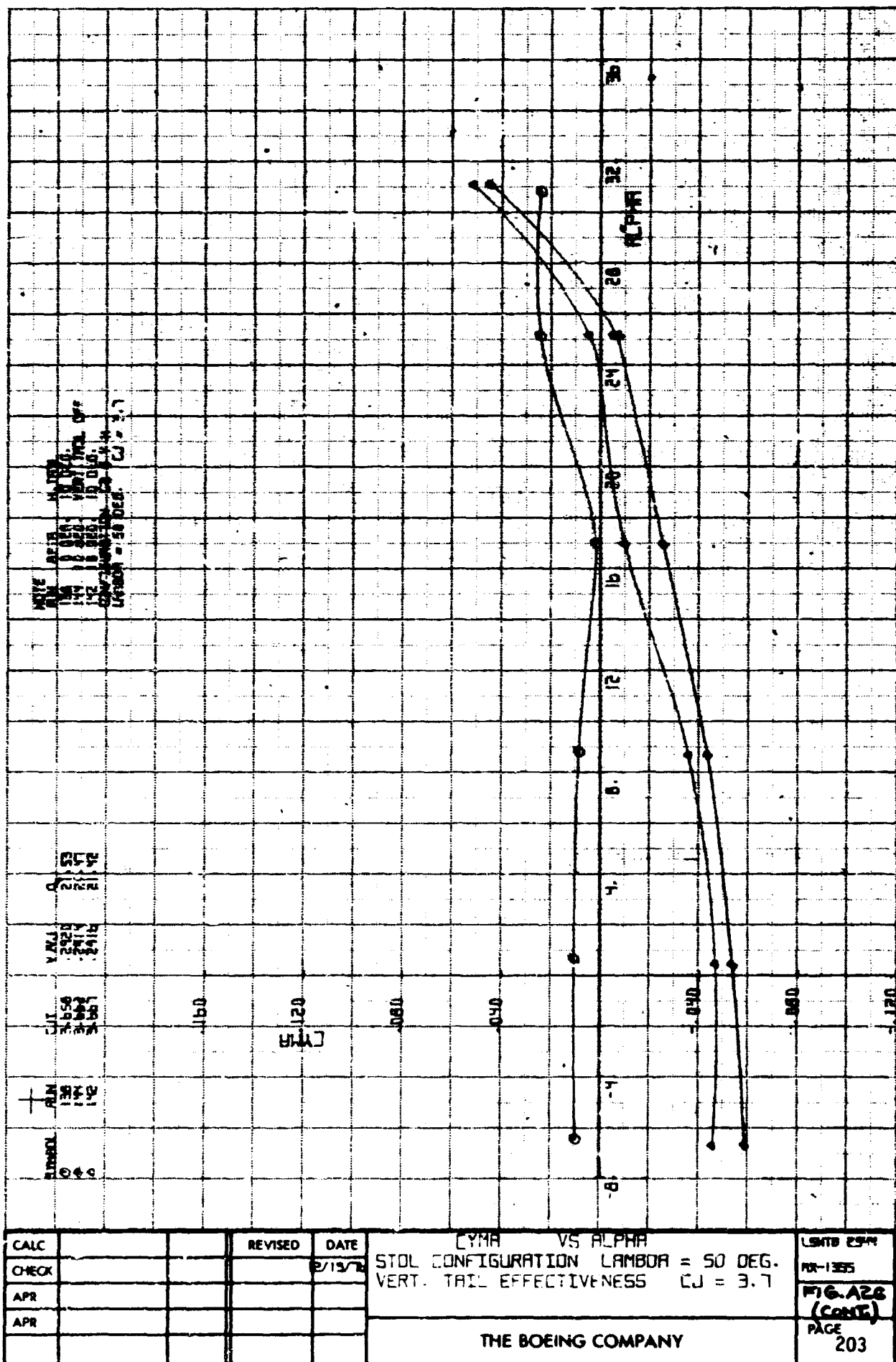


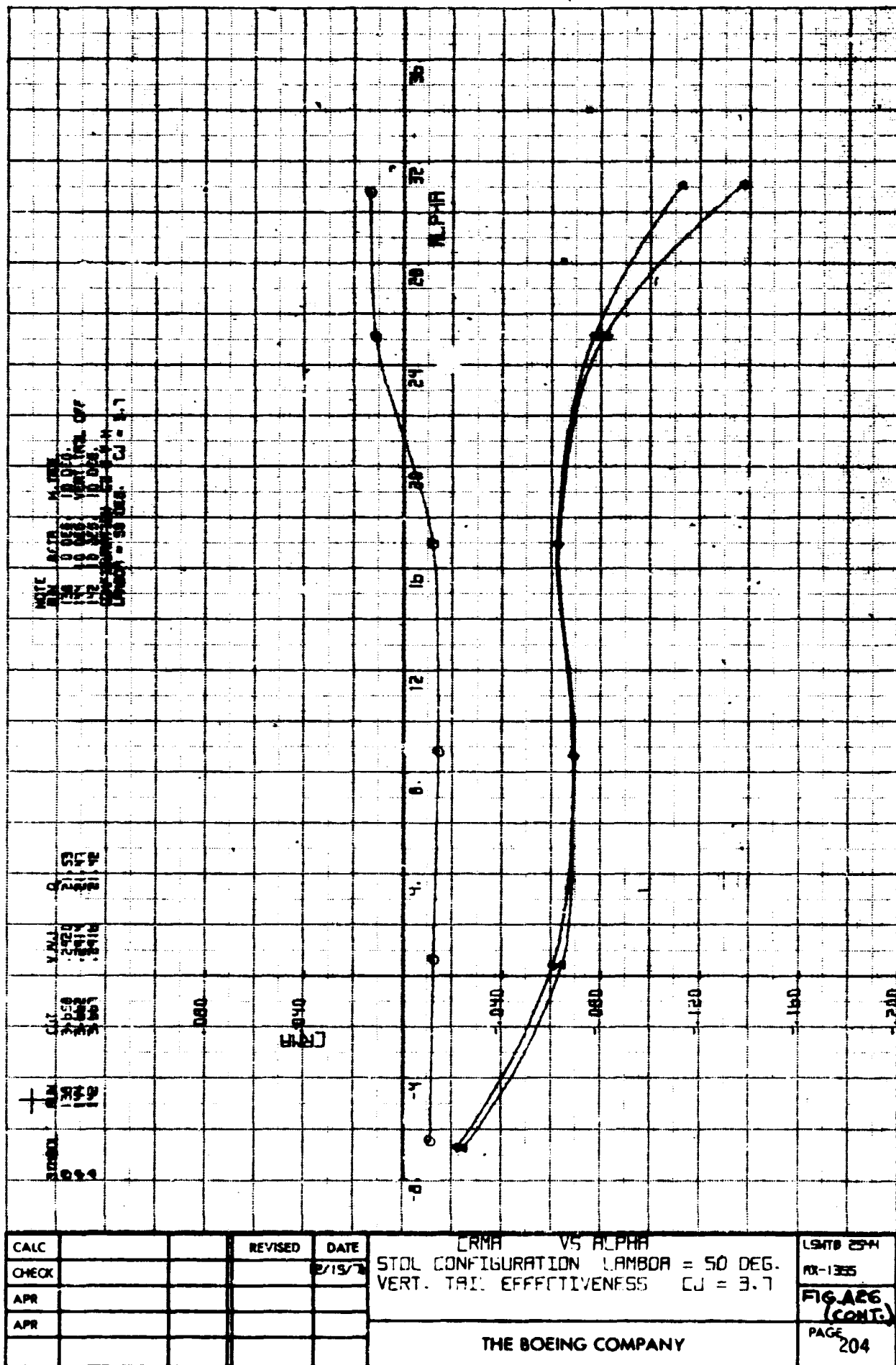


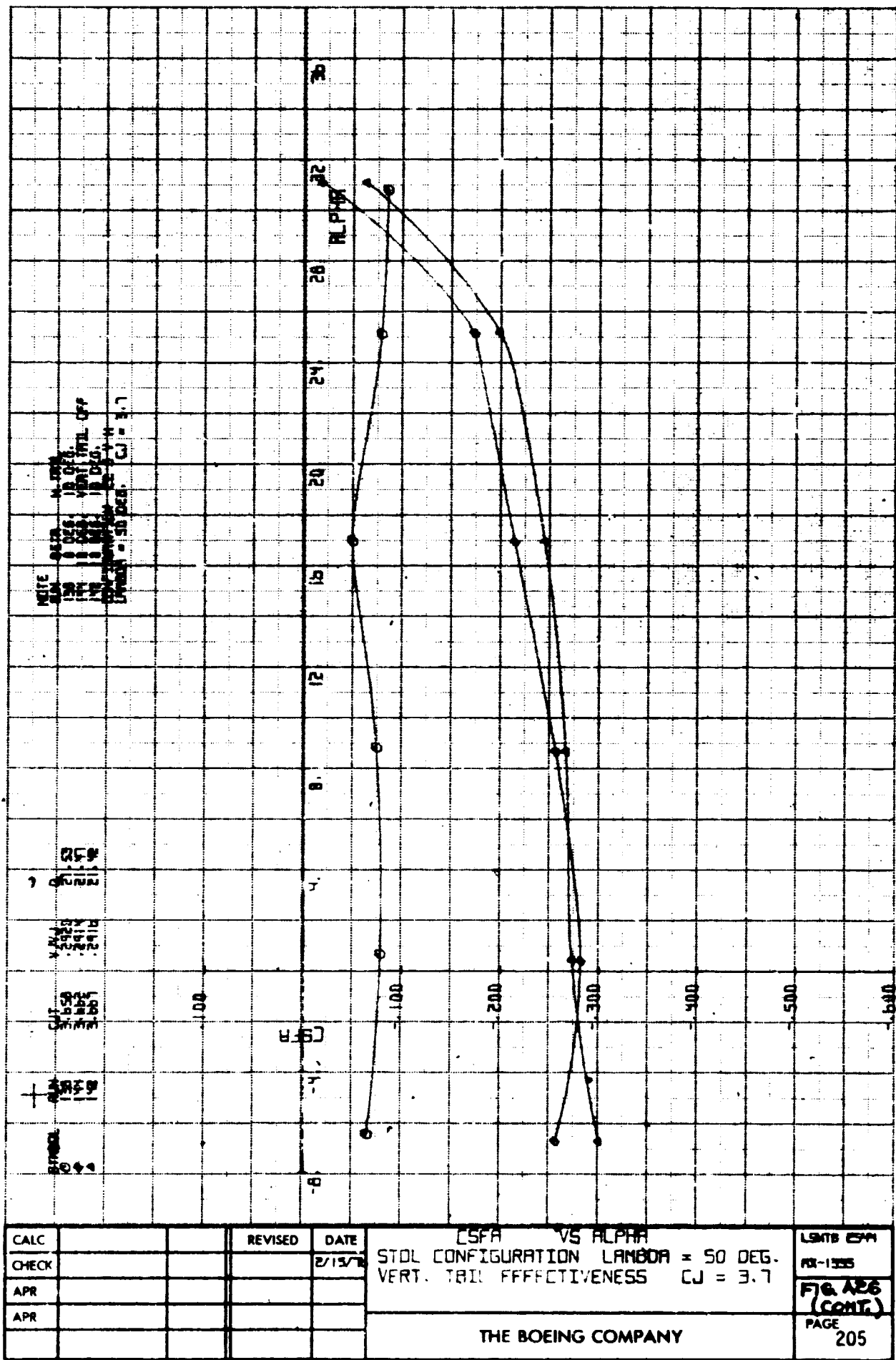
CALC		REVISED	DATE
CHECK			
APR			
APB			

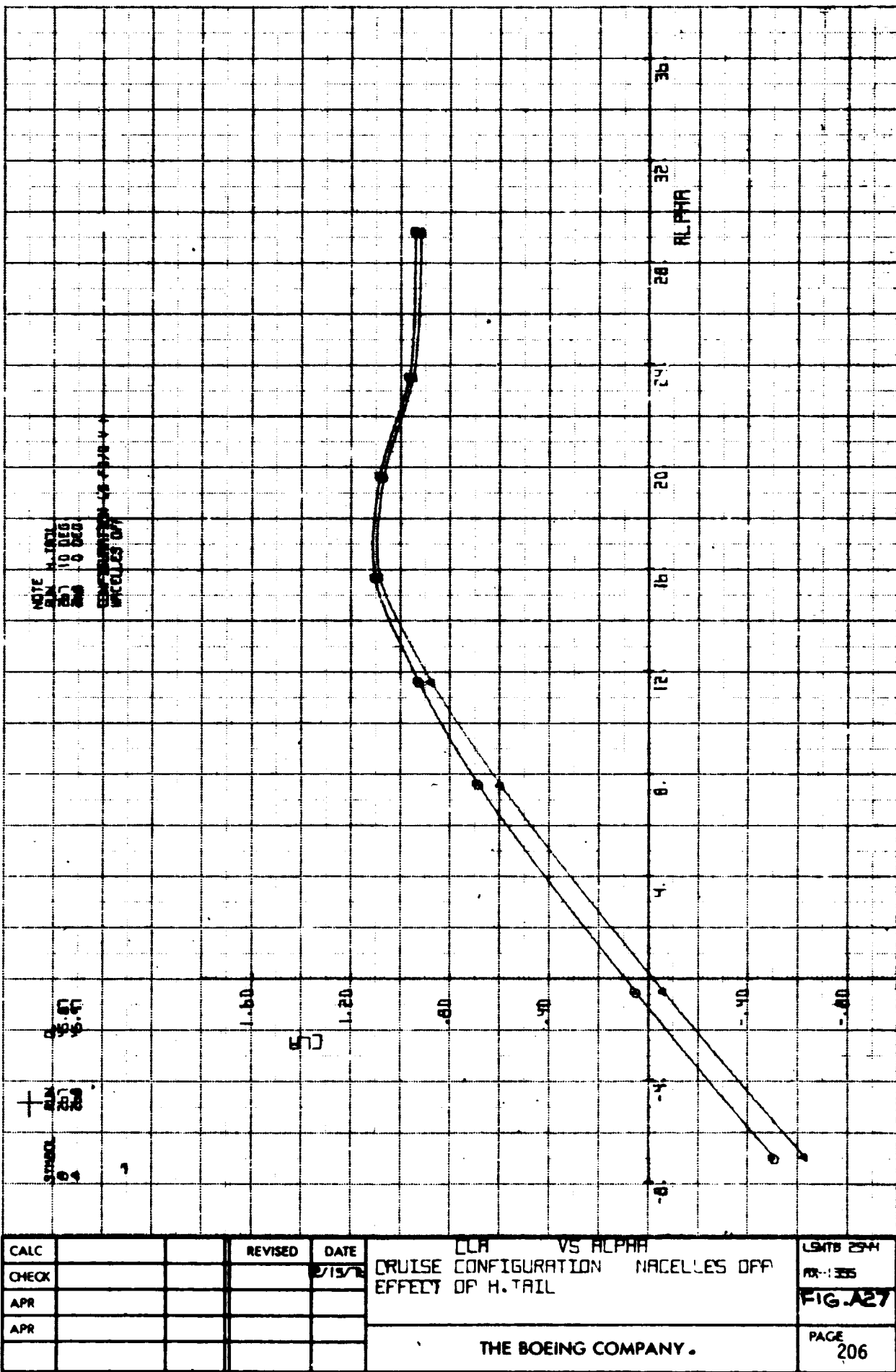
CPMA VS ALPHA
 STOL CONFIGURATION $\lambda = 50$ DEG
 VERT. TAIL EFFECTIVENESS C.J.3.7
 THE BOEING COMPANY

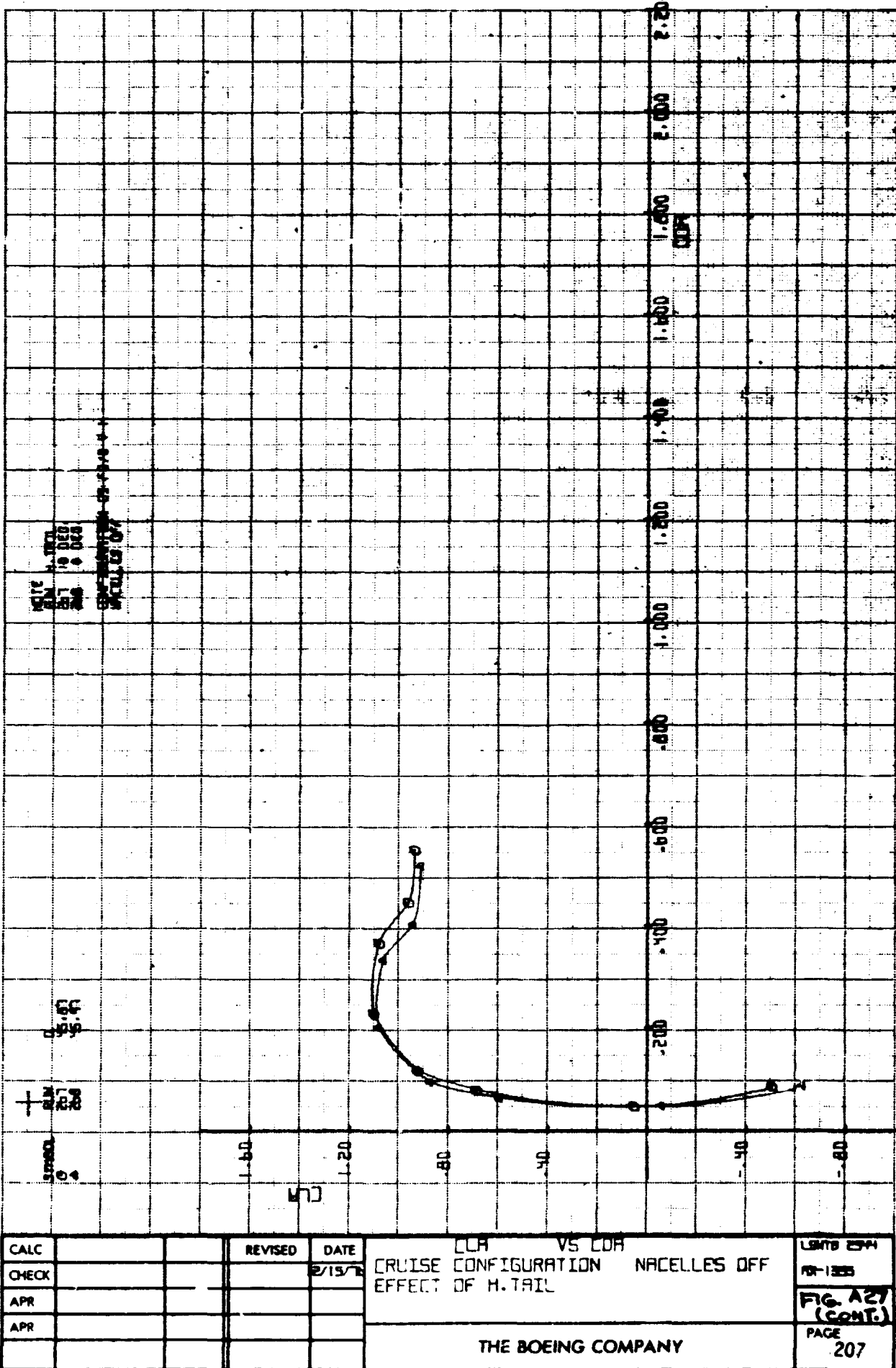
ISWFB
 2004-9
 AX-1253
 FIG. A.BS
 (CONT'D)
 PAGE
 202

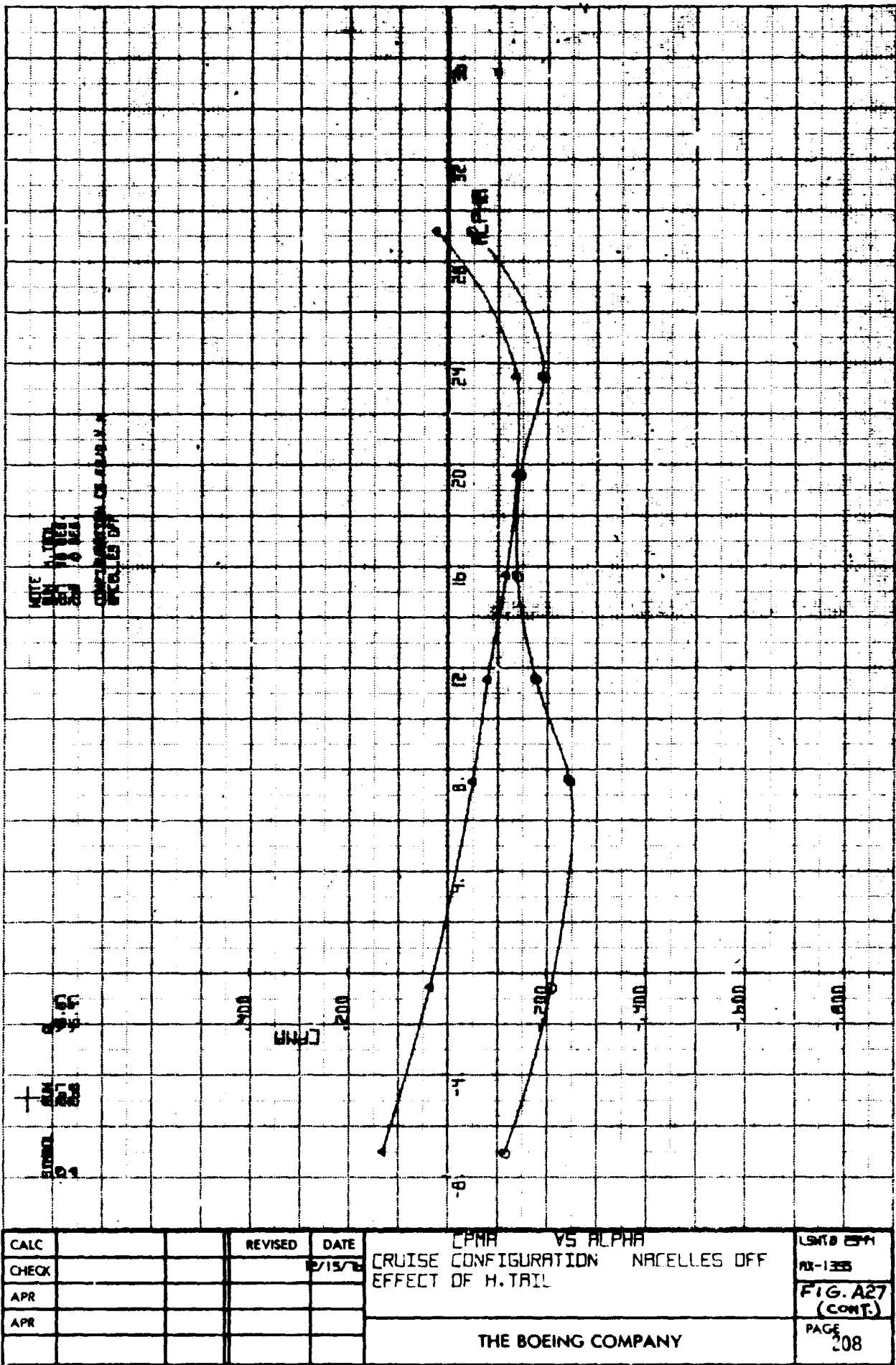


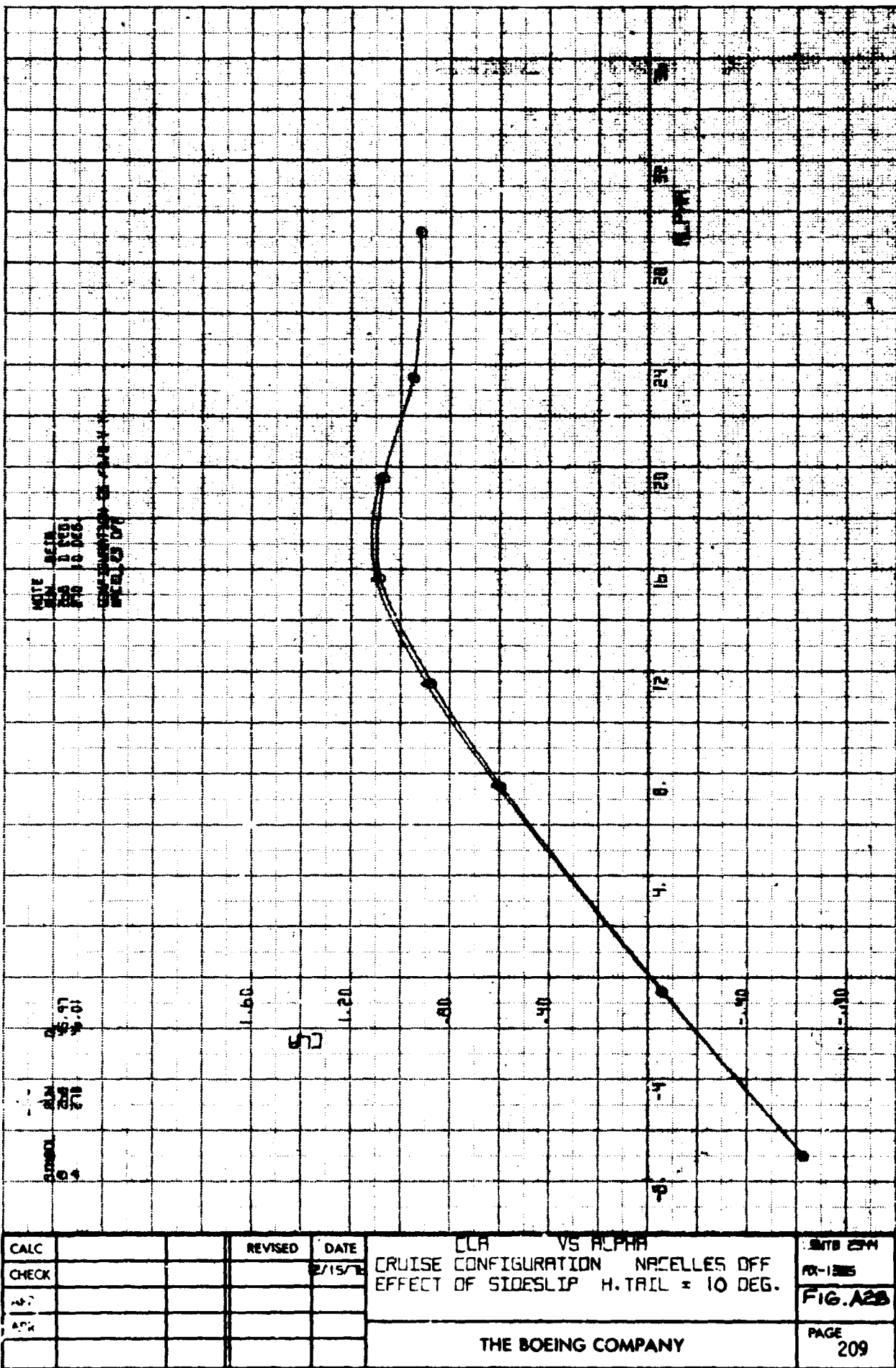


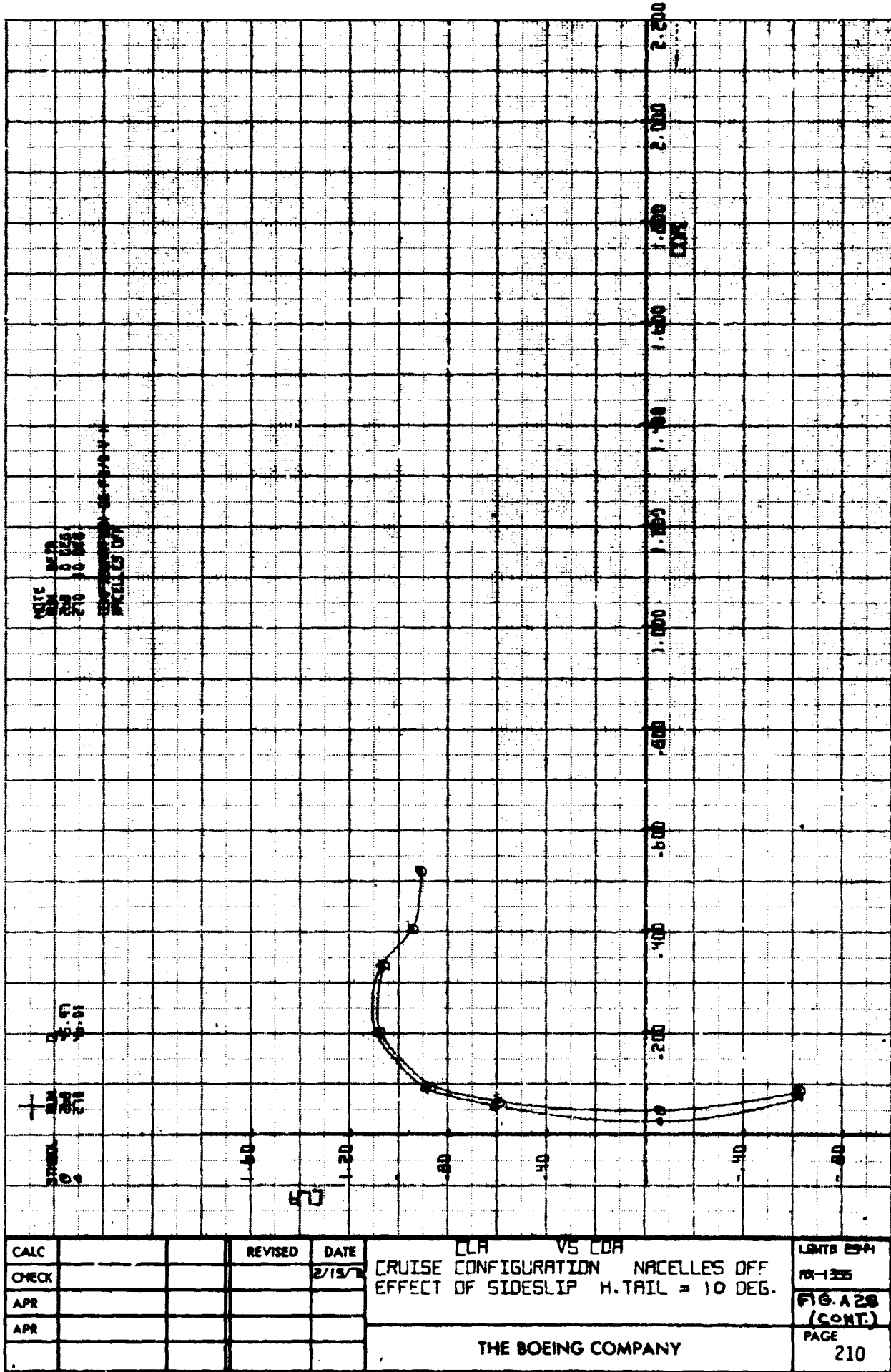


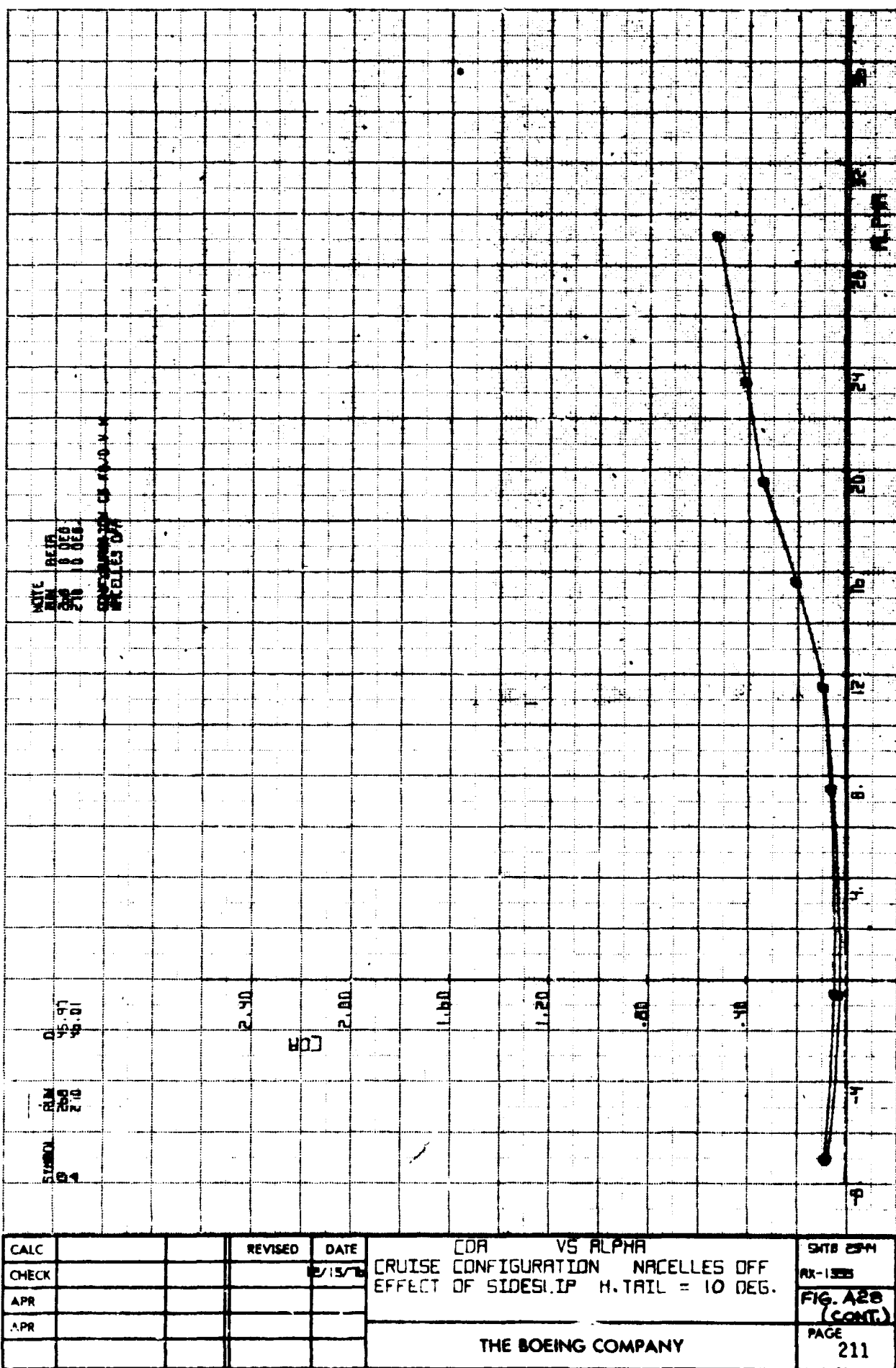


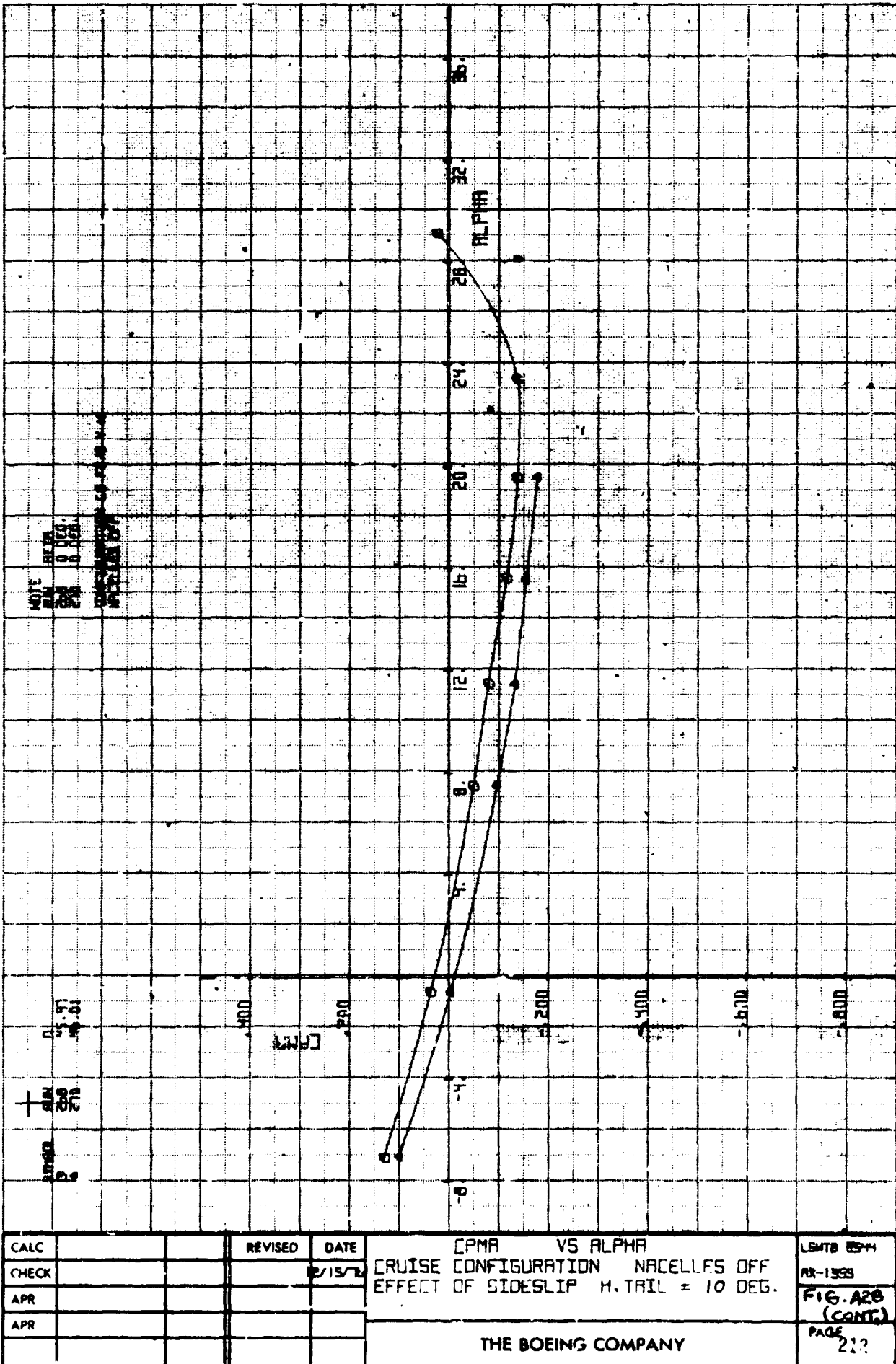


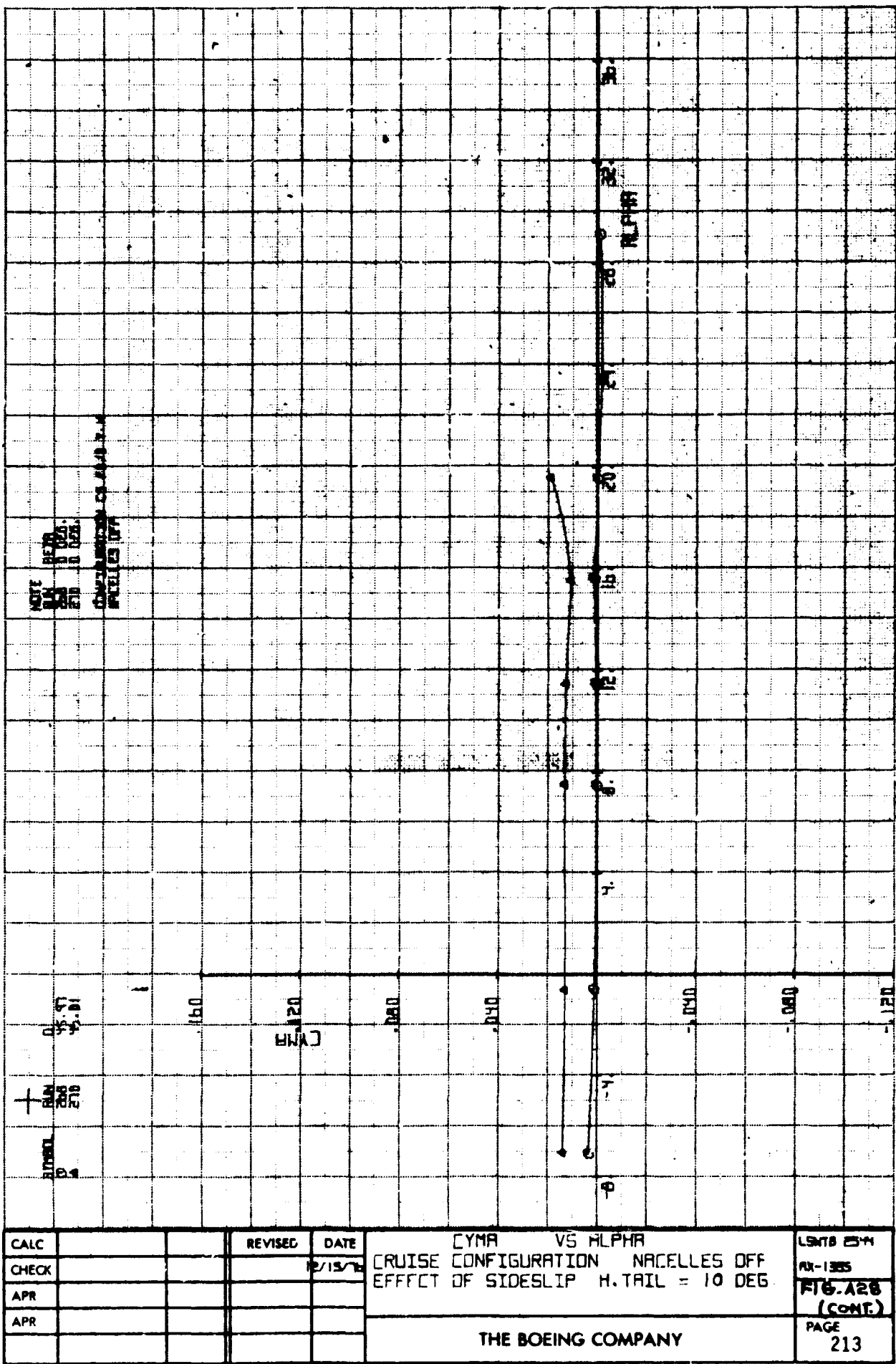












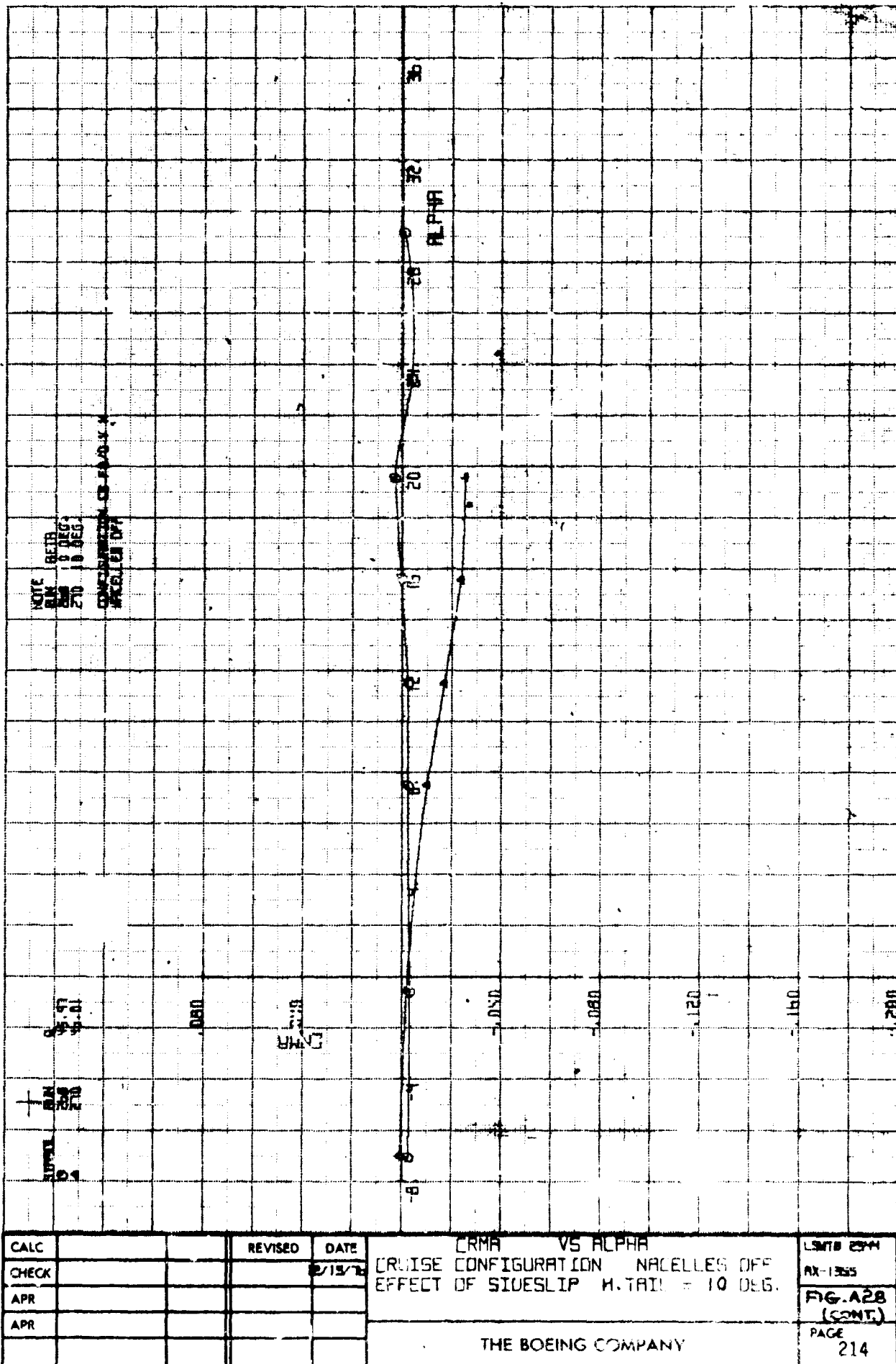


FIG. 35

4.

